This study aims to develop a robust, efficient and versatile structural identification and damage detection framework based on optimization algorithms to be suitable for a wide range of structures. To do so, an improved metaheuristic optimization algorithm is developed based on Harmony Search algorithms that mimic the behavior of musicians to find the best notes to play. Unlike classical methods, which rely on sound mathematical theories, metaheuristic algorithms are gradient-free, do not require good initial guesses and can handle complex structural identification problems with a satisfying level of robustness and accuracy even when incomplete noisy measurements are involved.

The modifications applied to the basic Harmony Search improved its structure and hybridized it with another improved algorithm, thus the Modified Adaptive haRmony SearcH ALgorithm (MARSHAL) has emerged.

MARSHAL is a self-modifying experience-based algorithm that incorporates a smart parameter selection system, allowing it to adapt to the current situation of the optimization problem. Furthermore, MARSHAL exhibits some innovative engineering sense by realizing the coupling effect of stiffness terms in the stiffness matrix. Finally, a two-stage experience-based search guidance utilizing a previously developed reduction scheme is implemented which highlights potential regions within the search space, providing additional information to MARSHAL.

To meet the primary objective of developing a general identification framework, a consistent and unified approach in defining all considered identification problems is adopted, namely: defining the dynamic analysis problem, selecting the structural characteristics to be considered as optimization variables, setting up the search domain and defining the objective function.

Five identification problems are considered, featuring known mass, unknown mass and output-only identification. The considered structures vary in complexity from as simple as numerically modeled two-dimensional shear frames to as complex as experimentally tested tripile structures. Furthermore, incomplete noisy measurements were considered to simulate real data acquisition tools.

MARSHAL's identification capabilities were tested in a comparative study involving a modified version of the well-known Genetic Algorithm optimization technique. The results show the superiority of MARSHAL, encouraging further research of more complex structures, namely: wind turbine supporting structures.

The vibration response required for the identification of offshore wind turbines via MARSHAL was calculated using an open source program called FAST (Fatigue, Aerodynamics, Structures and Turbulence) developed by the National Renewable Energy Laboratory (NREL).

The limitations arising from using FAST were tackled using a reduced model approach. MARSHAL was used to derive, validate and utilize the reduced model in structural identification problems.

No change in MARSHAL's settings was required for all considered identification problems, underlining the versatility of the proposed approach.

To finalize, an experimental study of a tripile supporting structure was considered. Both damaged and undamaged cases were investigated and the results were satisfying, confirming the broad applicability of MARSHAL, thus achieving the primary objective of this research.

The encouraging and satisfying results motivate the involvement of MARSHAL in existing structural health monitoring packages. Another issue for future research is the development of accurate, yet simple, mathematical models that approximate the response of real systems.

ISBN 978-3-935732-42-0

ibnm

A Modified Adaptive Harmony Search Algorithm Approach on Structural Identification and Damage Detection

M. Jahjouh

M. Jahjouh

A

Modified Adaptive Harmony Search Algorithm Approach on Structural Identification and Damage Detection

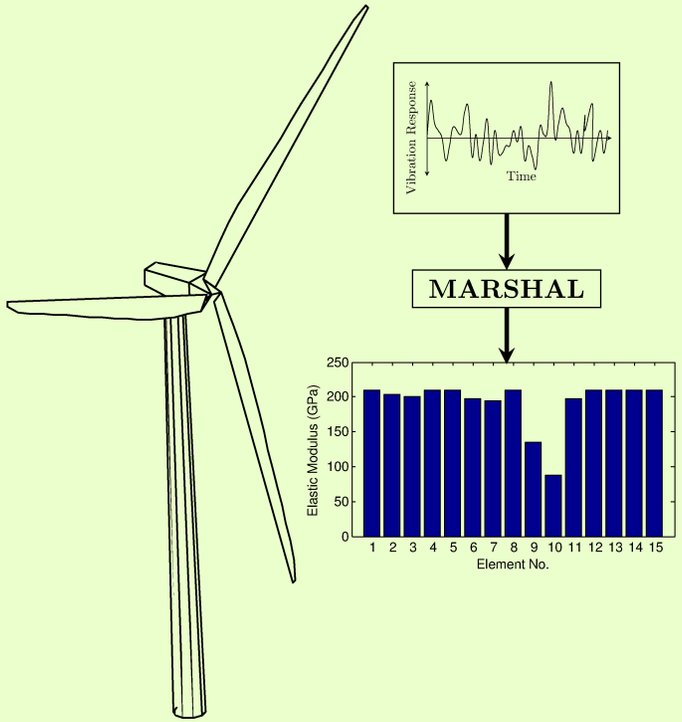

F16/1 F16/1

Institut für Baumechanik
und Numerische Mechanik
Gottfried Wilhelm Leibniz Universität Hannover

ibnm

Hauptreferent:
Prof. Dr.-Ing. U. Nackenhorst

Korreferent:
Prof. Dr.-Ing. habil. R. Rolfes

Doktorand:
M.Sc. Mahmoud M. Jahjouh

A Modified Adaptive Harmony Search Algorithm Approach on Structural Identification and Damage Detection

Von der Fakultät für
Bauingenieurwesen
und Geodäsie der
Gottfried Wilhelm Leibniz
Universität Hannover

zur Erlangung des Grades
eines

Doktor-Ingenieurs

genehmigte Dissertation von

M.Sc. Mahmoud M. Jahjouh

Hannover 2016

Tag der Einreichung:
25.11.2015
Tag der mündl. Prüfung:
18.03.2016

**Institut für
Baumechanik
und Numerische
Mechanik**

Herausgeber:
Prof. Dr.-Ing. U. Nackenhorst

Verwaltung:
Institut für Baumechanik
und Numerische Mechanik
Gottfried Wilhelm Leibniz
Universität Hannover
Appelstr. 9A
30167 Hannover
Tel.: +49 (0)511 / 762-3219
Fax.: +49 (0)511 / 762-19053

Institut für Baumechanik
und Numerische Mechanik
Gottfried Wilhelm Leibniz
Universität Hannover
Appelstr. 9A
30167 Hannover

ISBN 978-3-935732-42-0

Abstract

This study aims to develop a robust, efficient and versatile structural identification and damage detection framework based on optimization algorithms to be suitable for a wide range of structures. To do so, an improved metaheuristic optimization algorithm is developed based on Harmony Search algorithms that mimic the behavior of musicians to find the best notes to play. Unlike classical methods, which rely on sound mathematical theories, metaheuristic algorithms are gradient-free, do not require good initial guesses and can handle complex structural identification problems with a satisfying level of robustness and accuracy even when incomplete noisy measurements are involved.

The modifications applied to the basic Harmony Search improved its structure and hybridized it with another improved algorithm, thus the Modified Adaptive haRmony SearcH ALgorithm (MARSHAL) has emerged.

MARSHAL is a self-modifying experience-based algorithm that incorporates a smart parameter selection system, allowing it to adapt to the current situation of the optimization problem. Furthermore, MARSHAL exhibits some innovative engineering sense by realizing the coupling effect of stiffness terms in the stiffness matrix. Finally, a two-stage experience-based search guidance utilizing a previously developed reduction scheme is implemented which highlights potential regions within the search space, providing additional information to MARSHAL.

To meet the primary objective of developing a general identification framework, a consistent and unified approach in defining all considered identification problems is adopted, namely: defining the dynamic analysis problem, selecting the structural characteristics to be considered as optimization variables, setting up the search domain and defining the objective function.

Five identification problems are considered, featuring known mass, unknown mass and output-only identification. The considered structures vary in complexity from as simple as numerically modeled two-dimensional shear frames to as complex as experimentally tested tripile structures. Furthermore, incomplete noisy measurements were considered to simulate real data acquisition tools.

MARSHAL's identification capabilities were tested in a comparative study involving a modified version of the well-known Genetic Algorithm optimization technique. The results show the superiority of MARSHAL, encouraging further research of more complex structures, namely: wind turbine supporting structures.

The vibration response required for the identification of offshore wind turbines via MARSHAL was calculated using an open source program called FAST (Fatigue, Aerodynamics, Structures and Turbulence) developed by the National Renewable Energy Laboratory (NREL).

The limitations arising from using FAST were tackled using a reduced model approach. MARSHAL was used to derive, validate and utilize the reduced model in structural identification problems.

No change in MARSHAL's settings was required for all considered identification problems, underlining the versatility of the proposed approach.

To finalize, an experimental study of a tripile supporting structure was considered. Both damaged and undamaged cases were investigated and the results were satisfying, confirming the broad applicability of MARSHAL, thus achieving the primary objective of this research.

The encouraging and satisfying results motivate the involvement of MARSHAL in existing structural health monitoring packages. Another issue for future research is the development of accurate, yet simple, mathematical models that approximate the response of real systems.

Keywords:
Optimization Algorithms; Harmony Search; Structural Identification; Damage Detection; Output-Only; Search Space Reduction; FAST; Offshore; Onshore; Wind Turbine Supporting Structures; Model Reduction.

Kurzfassung

Ziel dieser Studie ist es, eine robuste, effiziente und universelle Strukturidentifizierung und Schadensfrüherkennung basierend auf Optimierungsalgorithmen zu entwickeln, die für eine Vielfalt von Strukturen anwendbar ist. Dafür wird ein verbesserter metaheuristischer Optimierungsalgorithmus basierend auf Harmony Search Algorithmen entwickelt. Im Gegensatz zu klassischen Verfahren, die gute Anfangsschätzwerte benötigen, erfordern metaheuristische Algorithmen keine Gradienten-Information und können komplexe Strukturidentifikationsprobleme mit einem befriedigenden Niveau an Robustheit und Genauigkeit lösen, sogar wenn unvollständige und rauschende Messungen gegeben sind.

Der Basis Harmony-Search-Algorithmus wurde verbessert, indem dessen Struktur modifiziert und mit einem weiteren Algorithmus gekoppelt wurde. So entstand der sogenannte Modified Adaptive haRmony SearcH ALgorithm (MARSHAL).

MARSHAL ist ein selbst-modifizierender erfahrungsbasierter Algorithmus, der über ein intelligentes Parameterwahlsystem verfügt, so dass er sich auf die aktuelle Situation des Optimierungsproblems anpasst. Außerdem realisiert MARSHAL den Kopplungseffekt der Steifigkeitsparameter in der Steifigkeitsmatrix. Des weiteren wird eine zweistufige erfahrungsbasierende Suchführung unter Verwendung eines zuvor entwickelten Suchraumreduzierungsalgorithmus implementiert, der die potenzielle Bereiche im Suchraum hervorhebt, was zusätzliche Informationen an MARSHAL weiterleitet.

Um das Ziel der Entwicklung eines allgemeinen Identifikationsrahmens zu erlangen, wird eine einheitliche Definition der Identifikationsprobleme vorangestellt, und zwar: Festlegung der dynamischen Analyse, Auswahl der strukturellen Parameter, Einrichtung des Suchraumes und Definition der Zielfunktion.

Insgesamt wurden 5 Identifikationsprobleme betrachtet, die unter bekannter Masse, unbekannter Masse und Output-Only Identifikationsprobleme identifiziert worden. Die Strukturen unterscheiden sich in Komplexität von einfachen numerisch modellierten zweidimensionalen Scherrahmen bis zu komplexen experimentell-getesteten Tripile Strukturen. Darüber hinaus wurden unvollständige rauschende Messungen benutzt.

MARSHAL's Identifikationsfähigkeiten wurden in einer Vergleichsstudie getestet, wobei zweidimensionale Scherrahmen identifiziert wurden. Die Ergebnisse zeigen die Überlegenheit von MARSHAL, und motivieren die weitergehenden Untersuchungen komplexerer Strukturen, hier Tragstrukturen von Windturbinen.

Das benötigte Schwingungsverhalten für die Identifizierung von Windenergieanlagen mittels MARSHAL wurde durch Verwendung eines Open-Source-Programmes namens FAST (Fatigue, Aerodynamics, Structures und Turbulence), entwickelt von dem National Renewable Energy Laboratory (NREL), berechnet.

Die Einschränkungen, die sich aus FAST ergaben wurden mit einem reduzierten Modell-Ansatz angegangen. MARSHAL wurde verwendet, um das reduzierte Modell abzuleiten, zu validieren und für weitere Strukturidentifikationsprobleme zu nutzen.

Für alle betrachteten Identifikationsprobleme war keine Veränderung der Einstellungen von MARSHAL erforderlich und unterstreicht die Vielseitigkeit des entwickelten Algorithmus.

Abschließend wurde die experimentelle Studie einer Tripile Tragkonstruktion betrachtet. Es wurden die Fälle beschädigt und unbeschädigt untersucht, und die Ergebnisse waren sehr zufriedenstellend. Dies untermauert die breite Anwendbarkeit von MARSHAL.

Die zufriedenstellenden Ergebnisse motivieren die Anwendung von MARSHAL in bestehender Strukturüberwachungssoftware. Ein mögliches Thema für weitergehende Forschungsarbeiten ist die Entwicklung von präzisen, aber dennoch einfachen mathematischen Modellen, mit denen die Systemantwort der realen Systemen mit guter Präzision berechnet werden kann.

Stichworte:
Optimierungsalgorithmen; Harmony Search; Strukturidentifikation; Schadensfrüherkennung; Output-Only; Suchraumreduktion; FAST; Offshore; Onshore; Tragstrukturen von Windturbinen; Modellreduktion.

Dedication

This research is dedicated to my father, Maher, my mother, Reyhan, my wife Hadeel, my children Sewar and Maher and my grandparents Mahmoud and Fatima.

Acknowledgments

This research was performed at the Institute of Mechanics and Computational Mechanics (Institut für Baumechanik und Numerische Mechanik - IBNM) at Leibniz Universität Hannover (LUH) under the direction and guidance of Prof. Dr.-Ing. Udo Nackenhorst, to whom I would like to express my deepest and most sincere gratitude. It has been an honorable and educational experience working under his supervision during my research. He has been more than a supervisor, who always had his office doors open for any discussions that could arise during my three-years stay at IBNM. His expertise, patience, guidance and encouragement were key to the success of this research, and for that I am forever grateful.

I would also like to thank the members of the doctoral committee, Prof. Dr.-Ing. habil. Raimund Rolfes and Prof. Dr.-Ing. Michael Beer, who have enriched this research with their comments and their willingness to dedicate their time to help me improve my research. I would like to extend my thanks and appreciation to Prof. em. Dr.-Ing. Erwin Stein, Prof. Dr.-Ing. Peter Schaumann and Prof. Dr.-Ing. Andreas Reuter for their guidance and support. Special thanks go also to Dr.-Ing. Tanja Grießmann, whose guidance and suggestions were invaluable. The research was enriched with her experience in both practical and numerical aspects.

Special thanks go to my father Maher and my mother Reyhan, who supported me during my entire PhD research and provided me with the necessary perseverance for the completion of this research. I also would like to express my deepest thanks to my family in Hannover, my wife Hadeel, for accompanying me through my highs and lows, for being my motivation and encouragement, and my children, Sewar and Maher, who were a real bless after the tiring daily work. It wouldn't be possible to accomplish this research if it wasn't for their motivation and for that I am thankful. I would like to extend my thanks to my family in Gaza: my grandparents, uncles, brothers, sisters, cousins and relatives who were always supporting me.

Furthermore, I would like to thank my fellow research colleagues, especially my colleague Niraj Kumar Jha, whom I shared the office with, for the collaboration and exchange during my research. He has been a real friend and a well-organized open-minded scientific colleague, who helped me countless times when in need. My thanks go also to Alena Rosenberger, Daniel Ho,

Christine Michitsch and Antje Heidelbeer for their support in IT and management issues. I also would like to thank the team of IBNM for the scientific collaboration and exchange I had during my research: Mainak Bhattacharyya, Dr. Amelie Fau, Mathias Grehn, Oleg Khromov, Ehsan Jamshidi, Sayed Alireza Shirazibeheshtiha, Sebastian Fink, Alexander Sapotnick, Phillip-Paul Jablonski, Andre Hürkamp, Robert Beyer, Maximilian Bittens, Katharina Dees, Robert Gates, Anna Hülsmann, Milena Möhle and Stefanie Tegtmeyer. Furthermore, I'm sincerely grateful to my friends in the Institute of Structural Analysis (Institut für Statik und Dynamik - ISD) for providing me with the necessary experimental data used in this research, especially to Karsten Schröder, Jan Häfele and Andreas Ehrmann for the scientific exchange on the analysis of wind turbines.

Last but not least, I would like to thank the German Academic Exchange Service (Deutscher Akademischer Austauschdienst - DAAD) for funding my research. This research would not be possible if it wasn't for their generous support.

Contents

List of Figures

List of Tables

List of Symbols and Abbreviations

α, β	Rayleigh damping coefficients
$\Delta\alpha$	the deviation of α from its originally assumed value
$\Delta\beta$	the deviation of β from its originally assumed value
Δk_i	the deviation of the i-th DOF stiffness from its originally assumed value
Δm_i	the deviation of the i-th DOF mass from its originally assumed value
Δt	time increment for each time step
ϵ_α	Error in identified damping coefficient α
ϵ_β	Error in identified damping coefficient β
ϵ_k	Average error in identified stiffness
ϵ_m	Average error in identified mass
γ	Learning rate of AHS
λ_i	i-th modification factor required for model reduction
$\mathbf{C}$	Damping matrix
$\mathbf{C}^*$	Damping matrix of reduced model
$\mathbf{C}^e$	Local damping matrix for element e
$\mathbf{F}$	Applied excitation history
$\mathbf{F}_k^u$	Unknown excitation at time step k
$\mathbf{F}_k^{kn}$	Known excitation at time step k

$\mathbf{K}$ Stiffness matrix

$\mathbf{K}^*$ Stiffness matrix of reduced model

$\mathbf{K}^e$ Local stiffness matrix for element e

$\mathbf{M}$ Mass matrix

$\mathbf{M}^*$ Mass matrix of reduced model

$\mathbf{M}^e$ Local mass matrix for element e

$\mathbf{X}$ The solution vector

$\mathbf{X}_\mu$ The average optimum solution

$\mathbf{X}_i$ i-th solution vector stored in the HM

$\mathbf{X}_S$ A storage matrix containing the optimum solution of all previous sub-runs

$\mathbf{X}_{new}$ Newly assumed solution vector for each iteration

$\mathbf{X}_{opt}$ Optimum or best solution vector / Matrix storing all best solution vectors obtained during an optimization run

$\mathbf{X}_{worst}$ Worst solution vector stored in the HM

$\ddot{\mathbf{x}}_\mathbf{p}(i,t)$ Predicted response of the i-th DOF at time t resulting from a trial solution $\mathbf{X}$

$\ddot{\mathbf{x}}_\mathbf{r}(i,t)$ Real or measured response of the i-th DOF at time t

$\ddot{\mathbf{x}}$ Acceleration response

$\ddot{\mathbf{x}}^*$ Measured acceleration response

$\dot{\mathbf{x}}$ Velocity response

$\mathbf{CP}_i$ The vector of control parameters corresponding to the i-th solution stored in HM

$\mathbf{x}$ Displacement response

HMCR^k Assumed value of HMCR for the k-th iteration

HMCR_i HMCR corresponding to the i-th solution stored in HM

LER^k Assumed value of LER for the k-th iteration

LER_i LER corresponding to the i-th solution stored in HM

PAR^k Assumed value of PAR for the k-th iteration

PAR_i PAR corresponding to the i-th solution stored in HM

μ_i Average value of the i-th optimization variable of all solutions stored in the HM

$\overline{\mathrm{HMCR}}$ Average of HMCR values for solution vectors stored in HM

$\overline{\mathrm{LER}}$ Average of LER values for solution vectors stored in HM

$\overline{\mathrm{PAR}}$ Average of PAR values for solution vectors stored in HM

ρ Density of element

σ_i Standard deviation of the i-th optimization variable of all solutions stored in the HM

ζ_1 Stage 1 damping ratio

ζ_2 Stage 2 damping ratio

A Cross sectional area of element

bw Bandwidth of pitch adjustment modification

C_R Added rotational damping at tower top

C_T Added translational damping at tower top

C_t Uncoupled tower damping matrix terms

$C^*_{(\phi_n,\phi_n)}$ Modified damping matrix entry of tower top rotation DOF

$C_{(d_i,\phi_j)}$ Damping matrix term for the i-th displacement and j-th rotation

$C^*_{(d_n,d_n)}$ Modified damping matrix entry of tower top displacement DOF

C_{RNAt}, C_{tRNA} coupled damping matrix terms

C_{RNA} Uncoupled RNA damping matrix terms

DI Vector of damage indices

DI_j Damage index of the j-th DOF

E Elastic (Young's) modulus

e	The exponential function
EI_i	Stiffness of the i-th element/DOF which corresponds to $E_i \times I_i$
$F(\mathbf{X})$	Objective function value of $\mathbf{X}$
F_i	Objective function value of $\mathbf{X}_i$
F_{new}	Objective function of $\mathbf{X}_{new}$
G	Shear modulus
h	time increment for each time step
I	Current iteration / second moment of area
$i, j, ...$	counters and indices for loops and vectors
I_S	A predetermined number of required iterations before reducing the search space
I_y	Second moment of area around local y-axis
I_z	Second moment of area around local z-axis
$I_{(y,i)}$	The second moment of area of the i-th element around local y-axis
$I_{(z,i)}$	The second moment of area of the i-th element around local z-axis
I_{max}	Maximum number of iterations per run or sub-run
J	Polar moment of inertia
k_i	Stiffness of i-th DOF
k_j^0	Originally assumed stiffness of the j-th DOF
k_j^d	Damaged or identified stiffness of the j-th DOF
K_R	Added rotational stiffness at tower top
K_T	Added translational stiffness at tower top
K_t	Uncoupled tower stiffness matrix terms
$K^*_{(\phi_n,\phi_n)}$	Modified stiffness matrix entry of tower top rotation DOF
$K_{(d_i,\phi_j)}$	Stiffness matrix term for the i-th displacement and j-th rotation
$K^*_{(d_n,d_n)}$	Modified stiffness matrix entry of tower top displacement DOF

$k_{i,real}$ Real value of the i-th DOF stiffness

K_{RNAt}, K_{tRNA} coupled stiffness matrix terms

K_{RNA} Uncoupled RNA stiffness matrix terms

L Length of element

m_i Mass of i-th DOF

m_j^0 Originally assumed mass of the j-th DOF

M_R Added rotational mass at tower top

M_T Added translational mass at tower top

M_t Uncoupled tower mass matrix terms

$M^*_{(\phi_n,\phi_n)}$ Modified mass matrix entry of tower top rotation DOF

$M_{(d_i,\phi_j)}$ Mass matrix term for the i-th displacement and j-th rotation

$M^*_{(d_n,d_n)}$ Modified mass matrix entry of tower top displacement DOF

M_{RNAt}, M_{tRNA} coupled mass matrix terms

M_{RNA} Uncoupled RNA mass matrix terms

n Number of DOF / Number of entries in $\mathbf{X}$

$N(0,1)$ Normally distributed random number

N_S Number of Sensors

N_{SS} Search space size

$NVAR$ Number of variables in solution vector

p Penalty factor

r number of sub-runs / sub-run counter

r_S A predetermined number of required sub-runs before reducing the search space

$rand_i$ a random variable between 0 and 1. The index i denotes the independency between the random variables

t time

T_p Average period of vibration for trial solution vector $\mathbf{X}$

T_r Average period of vibration resulting from measured data

w Constant representing a window for reduction

w_{min} Constant representing minimum window between x_i^u and x_i^l

x_i i-th optimization variable in $\mathbf{X}$

x_i^l The lower bound for x_i

x_i^u The upper bound for x_i

x_i^{l0} Initially assumed lower bound for x_i

x_i^{ss} The step size for x_i

x_i^{u0} Initially assumed upper bound for x_i

$x_{(j,i)}$ i-th optimization variable in j-th solution vector stored in HM

ABC Artificial Bee Colony

AHS Adaptive Harmony Search

ANN Artificial Neural Network

AR Auto-Regressive

ARMAV Auto-Regressive Moving Average Vector

ASCE American Society of Civil Engineers

Avg. Average

Ch. Chapter

DOF Degree Of Freedom

EKF Extended Kalman Filter

EMD Empirical Mode Decomposition

FAST Fatigue, Aerodynamics, Structures and Turbulence

Fig. Figure

FRF Frequency Response Function

GA Genetic Algorithm

HHT Hilbert-Huang Transformation

HM Harmony Memory

HMCR Harmony Momory Considering Rate

HMS Harmony Memory Size

I/O Input/Output

IASC International Association for Structural Control

IMF Intrinsic Mode Functions

KM Known Mass

LER Local Effect Ratio

LSS Low Speed Shaft

MA Moving Average

MAC Modal Assurance Criterion

MARSHAL Modified Adaptive Harmony Search Algorithm

MDLAC Multiple Damage Location Assurance Criterion

MDOF Multi Degree Of Freedom

MSE Modal Strain Energy

MSL Mean Sea Level

No. Number

NREL National Renewable Energy Laboratory

OO Output-only

PAR Pitch Adjusting Rate

PSO Particle Swarm Optimization

RMS Root Mean Square

RNA Rotor-Nacelle Assembly

RPM Revolutions Per Minute

SA Simulated Annealing

SDOF Single Degree Of Freedom

Sec. Section

SHM Structural Health Monitoring

SI Structural Identification (and damage detection)

SSE Sum of Squared Error

SSI Stochastic Subspace Identification

SSRM Search Space Reduction Method

UKM Unknown Mass

VBAR Vector Backward Auto-Regressive

WGN White Gaussian Noise

WT Wind Turbine

Chapter 1

Introduction

Structural identification and damage detection is an important component of a structural health monitoring scheme and has become a growing research and development area, as witnessed by the increasing number of relevant journal and conference papers. To this end, a crucial challenge is the development of robust and efficient structural identification methods that can be used to identify key parameters and hence, uncover the causes that change the structural state.

1.1 Motivation

Despite the fact that numerous methods for structural identification have been proposed and developed, most of these are problem specific and cannot be applied on a broad variety of structures. Furthermore, most of the proposed methods are classical approaches relying on sound mathematical theories, which have limitations in one way or another. Some require gradient information to guide their search in a point-to-point basis, which also relies on a relatively good initial guess, something that becomes unpractical as the complexity of the problem increases. Other require special conditions to be applied in identification problems, such as assuming a certain noise or excitation pattern, assuming that all components of vibration response (acceleration, velocity and displacements) are measured and/or that an extensive array of sensors is implemented. In their best performance, they still obtain near optimal, i.e. close to real values, structural parameters.

Metaheuristic algorithms, although being powerful computational methods, are relatively uncommon in structural identification problems when compared to classical approaches. Numerous new and promising metaheuristic

algorithms were proposed recently and were successfully applied on a variety of problems, namely: economy, production, resource allocation, management, design optimization and even more. Thus motivating the research community to tap into their potential in complex structural identification problems. In this context, structural identification problems are treated as optimization problems with the objective to minimize errors between measured and predicted data.

A quick glimpse on the current literature, as presented in Sec. 1.2, shows that the structural identification of two-dimensional shear frames has been extensively studied due to their simplicity, and present an adequate problem for comparative studies. On the other hand, the structural identification of wind turbines pose a challenging and active field of research.

Wind turbines have gained an increasing attention over the years motivated by the increasing numbers of such turbines, their various installation locations, foundation types, as well as the fact that such structures are subjected to fluctuating wind loads, making them prone to damage, as well as the continuously increasing size and production capabilities of such turbines.

The measurement of applied excitations is another challenging issue, as such cannot be always feasible especially outside a controlled laboratory environment, thus triggering the need to ensure that the developed scheme can tackle such output-only problems.

Motivated by the challenges posed by the drawbacks and limitations of classical identification schemes, the need for further research in the field of damage detection of wind turbines via non-classical techniques and the need for a reliable and versatile structural identification scheme, this research proposes a structural identification scheme based on metaheuristic optimization algorithms.

1.2 State of the Art

An introduction to structural health monitoring and structural identification is presented in this section, followed by a review of the related literature. Due to the large amount of research on structural health monitoring techniques applied on a variety of structures, the review presented here shall focus on the topics related to the research work of this dissertation, namely:

- Structural identification and damage detection methods involving optimization algorithms.

- Global structural identification and damage detection of frames, with special emphasis on two-dimensional shear frames.

- Structural identification and damage detection of wind turbines, with special emphasis on vibration-based global detection methods

An outlook presenting the most important findings and critical issues encountered during the review is presented at the end of this section, to summarize the current "state of the art" and further motivate the need for the proposed identification algorithm.

1.2.1 An Introduction to Structural Health Monitoring

Structural Health Monitoring (SHM) is the process of implementing a structural identification and damage detection technique to assess the current state of a structure [27] and, if possible, determine its deviation from an initial undamaged, or sound, state, in order to detect any changes that adversely affect the performance of the structure currently or in the future [27, 82], thus assessing its health.

The importance of SHM lies within its ability to track down the changes of the current "health" of the structure via predefined indices, acting as an early warning system that detects the progressive degradation of the structure's condition due to its operation and gradual aging as well as the sudden degradation due to damaging events such as earthquakes [75, 91]. A visualization of such health degradation is shown in Fig. 1.1, where it is evident that a structure with an implemented SHM would have a prolonged service life since failing to identify the health degradation could lead to the point where the structure becomes "beyond repair".

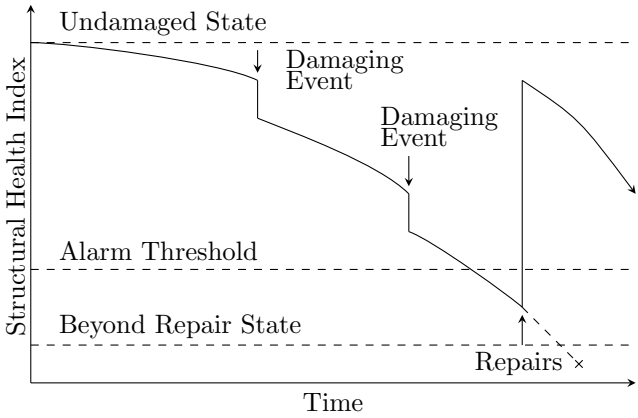

Figure 1.1: Degradation of structural health with time.

Depending on the type and importance of the structure, a suitable SHM scheme can be "tailored" [1, 93] to provide an efficient and cost effective operation, on time maintenance, better safety and longer service life of the structure.

Decision making is further enhanced by the information provided from SHM [39, 53, 68], helping in:

1. determining the suitability and safety of a structure,
2. deciding if protective repairs are necessary to prolong the service life of a structure,
3. estimating of the remaining service life of a structure, and/or
4. deciding to dismantle or dispose of a structure, if it is beyond repair.

SHM is considered an inverse problem in structural dynamics and vibration analysis [15, 52, 53] in which it is required to identify the structure and, if required, the input excitation that led to the given output vibration signal. Both forward analysis and inverse problem analysis in structural dynamics are illustrated in Fig. 1.2.

Classification of Structural Health Monitoring

SHM problems can be classified based on the frequency of application [82], the utilization of a structural model [48, 83], the effects of damage on the structural behavior [22], the scope of damage detection [66], its learning scheme [48] and the method used, as summarized in Fig. 1.3 and detailed as follows:

- **Based on the frequency of application [82]:** i.e. the frequency at which SHM collects and processes data, which is directly proportional to the required computational cost.
  - **Real-time or continuous SHM:** in which data is collected, assessed and processed continuously.
  - **Discrete SHM:** here the data is collected less frequently and the structural degradation is detectable.
  - **Reactive SHM:** the application of SHM on structure occurs in response to a certain event, especially after the occurrence of a damaging effect such as hurricanes, earthquakes and so on.
- **Based on the utilization of a structural model [48, 83]:** SHM could be performed on the collected data whether a model is present or not.

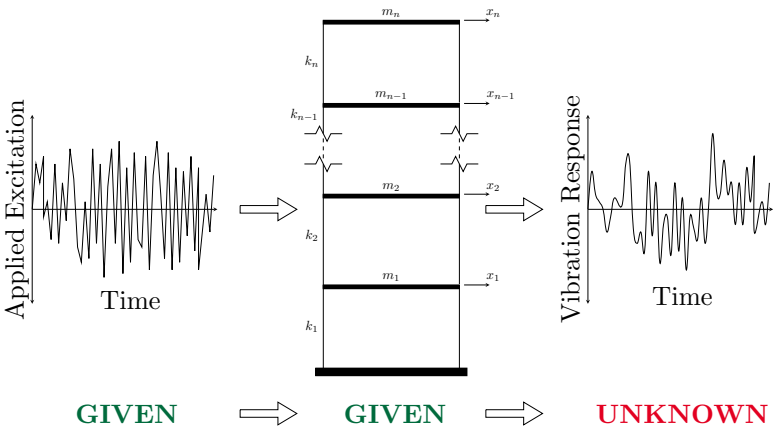

(a) A forward problem.

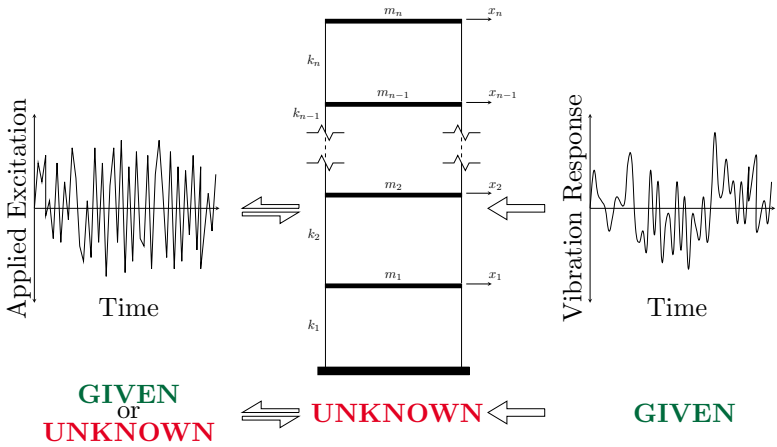

(b) An inverse problem.

Figure 1.2: Structural dynamics and vibration problems.

– **Model based SHM:** SHM in this case utilizes a structural model to update its characteristics, thus providing an easy interpretation of signals, support decision making and supports rehabilitation and repair planning. However, it is computational expensive in both

Figure 1.3: Classification of structural health monitoring problems.

time and effort.

  - **Model free SHM:** SHM could utilize, for example, incremental training and comparative studies on the collected data to track damage accumulation. However, such approach also lacks physical interpretation of signals and has a weak decision support.

- **Based on the damage effect [22]:** i.e. the behavior of the structure after the occurrence of damage.

  - **Linear damage:** the structural behavior remains linear elastic after the occurrence of damage. The majority of research addresses such damage situation [22].

  - **Nonlinear damage:** the structural behavior changes significantly after the occurrence of damage.

- **Based on the scope of damage detection [66]:** i.e. the detail, region and level of damage detection, further illustrated in Fig. 1.4.

– **Local SHM:** which detects damage at component level using local measurements such as, but not limited to, ultrasound, acoustic emissions and so on. Inherited in such detection is the fact that the location of damage is known a priori.
– **Global SHM:** damage detection is performed at region level or element level utilizing measurements from an array of well-placed sensors, thus obtaining global information about the structure's condition.

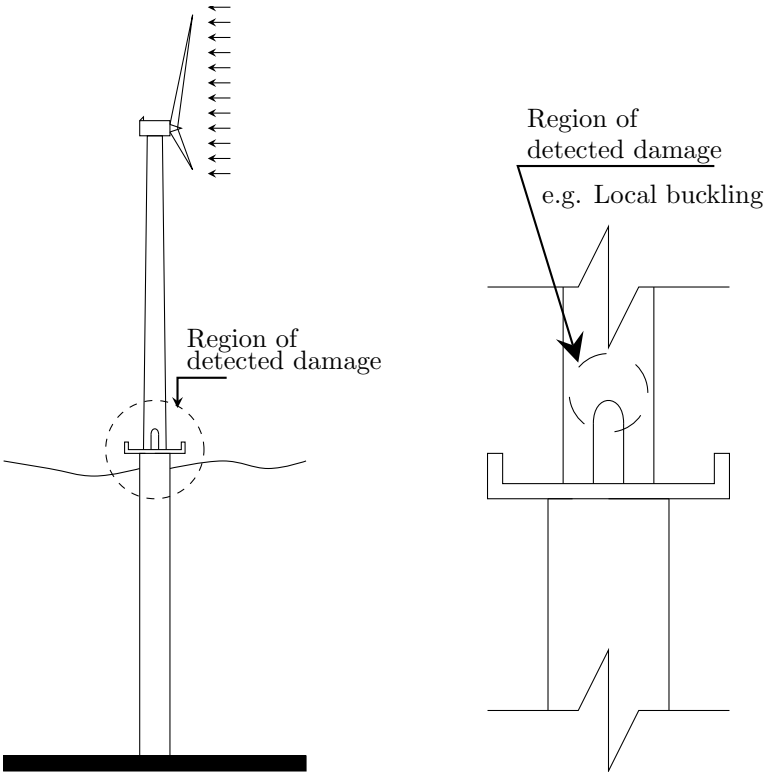

(a) Global structural health monitoring. (b) Local structural health monitoring.

Figure 1.4: Global vs local structural health monitoring.

Global and local schemes are complementary to each other, as global damage detection schemes pinpoint the proximity of damage, providing

local schemes with the location of potential damage points for further investigation.

- **Based on its learning scheme [48]:** i.e. based on the availability of data from both damaged and undamaged states of the structure.
  - **Supervised learning:** in such cases, data from both undamaged and damaged structures is available.
  - **Unsupervised learning:** where data is available only for the undamaged case and outlier or novelty detection techniques are utilized for damage detection.
- **Based on the method used for structural identification:** which shall be discussed later on in this section.

Components of Structural Health Monitoring

The SHM problem could be described as a problem in statistical pattern recognition [26] as shown in Fig. 1.5, which is a four-part process [82]:

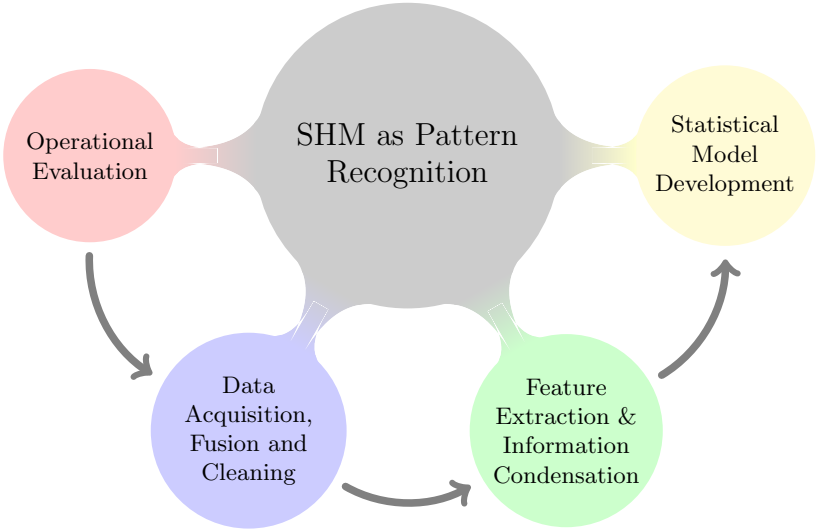

Figure 1.5: Structural health monitoring as statistical pattern recognition.

- **Operational Evaluation:**
  The motives of performing SHM are identified and the framework of

monitoring is set in terms of damage definition, data measurements and measurement limiting factors such as the operational environment.

- **Data Acquisition, Fusion and Cleansing:**
  Which is basically the transformation of raw unfiltered sensor data into useful data arrays. An example is shown in Fig. 1.6, where raw data is filtered, shifted and trimmed. This will be further detailed in Ch. 5.

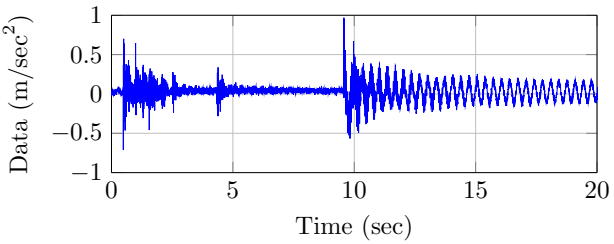

(a) Raw data.

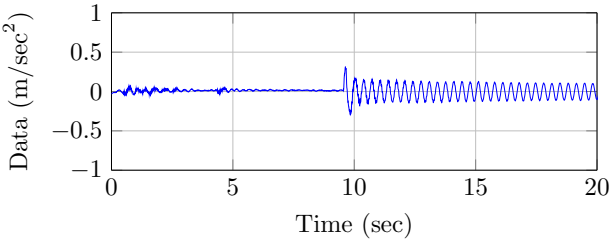

(b) Data filtering and shifting.

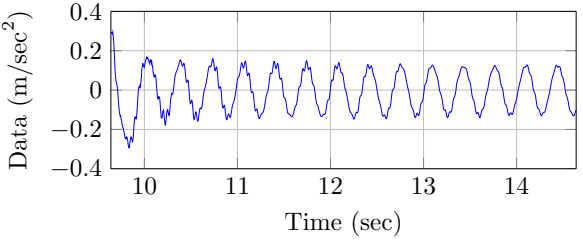

(c) Data Trimming.

Figure 1.6: Data processing.

- **Feature Extraction and Information Condensation:**
  The damage sensitive properties derived from the measured response are identified, enabling the comparison between the damaged and undamaged states. One possibility for feature extraction is to use an optimization algorithm within the context of system identification. Before this is performed, however, a data classification is required to distinguish between the effects of environmental and operational conditions and the effects of actual damage. Typically, the amount of information generated from SHM is large, and extracted key features are selectively chosen.

- **Statistical Model Development for Feature Discrimination:**
  These methods are used to assess if the changes in the selected features are statistically significant, for example, affects the probability of failure, which could happen in case of an overload coupled with a simultaneously occurring understrength.

1.2.2 An Introduction to Structural Identification and Damage Detection

Generally speaking, Structural Identification (SI) is analogous to system identification in which the outputs and, optionally, the inputs are known, and it is required to determine the set of processes, equations, functions, ...etc that relate these inputs and outputs.

In this context, structural Identification is the process of determining the dynamic structural parameters, namely: mass, stiffness and/or damping of a structure utilizing vibration-based measurements, in order to identify the existence, location and extent of damage and provide necessary information for the supervising SHM.

Generally, damage is a change introduced to any structural characteristic that adversely affects the current or future performance of the structure [82]. More specifically, in this research, the structural characteristics of interest are the three dynamic parameters of the structure, namely: mass, stiffness and/or damping, where reduction in stiffness is treated as damage.

Implicitly included in this definition is the concept of comparison [34, 105], i.e. to compare the current state of a structure to an undamaged or initial state of the structure. Furthermore, it is clear that damage cannot be assessed from vibration measurements alone without a structural identification technique, which is also stated in Axiom IV established by Worden et al. [93].

Both structural identification and damage detection methods used within the SHM are of significant importance, since structural identification extracts structural features from measured data, which are passed to damage detection

to assess the existence, location and extent of damage. For a satisfying and reliable performance, the SI method should be:

- Precise and accurate, i.e. as close as possible to the correct structural characteristics.
- Robust, i.e. produces satisfying results even with the presence of some error, e.g. measurement noise.
- Versatile, i.e. capable of solving various identification problems without significant change in its algorithm.

When detecting damage, 4 levels of detection exist based on the information that was provided about the structural damage [76]:

- Level 1: Detection. Is there damage in the structure?
- Level 2: Location. Where is the damage?
- Level 3: Quantity. How severe is the damage?
- Level 4: Prediction. What is the remaining service life of the structure?

Although it is sought to achieve a perfect identification, errors still exist due to systematic or non-systematic sources. Two types of errors may occur [26, 82]:

- **False positives:** Here, the structural identification and damage detection scheme senses damage at locations where, in fact, no damage is present. This reduces the trust in the identification method.
- **False negatives:** Considered a more serious case than false positives, the identification scheme fails to indicate damage at damaged locations. This is a detrimental problem and can have serious implications. Thus, it must be minimized.

With the advances in sensor technology and computational power, interest in structural identification has grown significantly in recent literature. This can be noticed in the number of contributions that are presented in general review papers such as [22, 82, 81]. The review presented in this dissertation is, however, limited to the problems directly related to the research work.

One possible method of structural identification and damage localization and quantification is to rely on an optimization algorithm in the context of structural identification and to utilize the identified structure to assess its damage by comparison with an undamaged or sound structure.

With that regard, structural identification and damage detection methods can be classified into classical and non-classical methods, i.e. methods based on metaheuristic optimization algorithms [53].

Classical methods are derived from sound mathematical theories. Generally, they perform an iterative search advancing from one point to the other and require sometimes gradient information for guidance [53].

On the other end, non-classical methods rely on optimization algorithms and metaheuristic, or soft, concepts rather than hard mathematical principles and do not require a good initial guess for convergence. These methods convert the identification problem into an optimization problem with the objective of finding the best structure that minimizes the difference between the predicted response and the measured/actual response [53].

1.2.3 Structural Identification and Damage Detection using Non-Classical Optimization Algorithms

With the growing potential and efficiency of optimization algorithms, the interest in structural identification and damage detection using non-classical optimization algorithms has increased significantly. Famous in this field are the Genetic Algorithms (GAs) and Artificial Neural Networks (ANNs), as evident by the amount research utilizing these two algorithms.

Masri et al. [65] based their damage detection scheme on neural networks. In their study, the network was trained using a healthy structure and then used to identify a damaged structure. Noisy readings were also studied. The structure itself is of unknown topology. However, the study was limited to the detection of damage, whereas locating and quantifying the damage is not done. The authors state that their scheme would be successful in detecting, locating and quantifying the damage if the structure is given. Nevertheless, the usage of ANNs requires the availability of a large amount of data for the purpose of training the ANN. Other applications of the ANN in the structural identification and damage detection can be found in Zhao et al. [105], Bani-Hani et al. [5], Yun and Bahng [101] and Xu et al. [95].

Besides frames, Masri et al. [66] applied ANNs in non-parametric structural damage identification. ANNs were also applied in identifying a theoretical model of the behavior of fibrous composites under cyclic loading in Lefik and Schrefler [60], and in identifying the dynamic characteristics of an existing concrete gravity dam as in Karimi et al. [49].

Franco et al. [28] used an evolutionary strategy to identify structural dynamic parameters, namely: mass, stiffness and damping. The method was tested on a 10-story shear frame under various levels of noise. The effect of full and partial output readings was addressed, too. Other studies on evolution

strategies can be found in Tang et al. [88].

GAs found a wide range of application in SI. A modified GA coupled with a search space reduction scheme was studied by Perry et al. [71]. The method was applied on two-dimensional shear frames with various levels of noise. Excellent results were obtained when identifying stiffness and mass while damping coefficients were identified at a lower level of accuracy.

An output-only structural identification method was presented in Perry and Koh [70]. The force was identified via a predictor-corrector scheme and was applied to a seismic two-dimensional shear frame and an experimental example. Satisfying results were obtained, even at higher noise levels. Mass was considered known to obtain a unique solution for the structure. Other studies utilizing GAs can be found in Raich and Liszkai [72], Na et al. [69], Marano et al. [64], Zhang et al. [104], and Koh and Trinh [55].

GAs were successfully applied for the identification of elastic constants in composite materials from dynamic tests as in Cunha et al. [19], in the identification of trusses and beams subjected to noise by Chou and Ghaboussi [15] and in the identification of beams and portal frames via mode shapes and frequency changes by Hao and Xia [37] and Li et al. [63].

GAs were also hybridized with other local search schemes and used in SI as in Koh et al. [51] based on Koh et al. [52], and in Zhang et al. [103]. Hybridized GAs were also used in Wang et al. [91], Zhang et al. [102] and Wang [90].

A dynamic quantum-behaved Particle Swarm Optimization (PSO) algorithm is presented in Rao et al. [73] and used in the structural identification of a simply supported beam, a 50-DOF shear building model and a truss. In this study, it was assumed that the mass properties, load history and initial conditions are known a priori. Various degrees of noise were considered too and results were compared with other optimization algorithms.

Another study for the identification of linear and nonlinear two-dimensional shear frames was done by Sun et al. [85]. Multiple degrees of noise were introduced and the problem was solved using a modified artificial bee colony algorithm. Simulation results show excellent parameter estimation, even with few measurements and high noise corruptions. A hybridized Artificial Bee Colony (ABC) algorithm coupled with a local search operator was investigated by Sun and Betti [84].

Bayissa and Haritos [6] used the Simulated Annealing (SA) method as a global optimization technique in the SI of beams.

PSO was successfully used in Charalampakis and Dimou [12] in the identification of Bouc-Wen hysteretic systems.

Miguel et al. [67] used harmony search algorithm in detecting structural damage to a beam under ambient vibration. An experimental study was

performed. However, only stiffness parameters were identified.

1.2.4 Structural Identification and Damage Detection of Frames via Classical Methods

Because of their simplicity, frames lend themselves well to SI techniques. This can be easily realized when comparing the large number of research in SI of frames with other structures, allowing a broad classification of classical methods as follows:

1) Auto-Regressive Moving Average Vector (ARMAV) Models: ARMAV models can be implemented in the analysis of ambient excited multi degree of freedom (MDOF) structures [9].

Although being able to perform structural identification and damage detection even in the absence of input excitations, ARMAV models still have some significant drawbacks [9]:

- The input excitations are assumed to be WGN of zero RMS.
- The best ARMAV model order is not known a priori and requires identification.
- Since the natural eigenfrequencies f_r and damping ratios ζ_r are extracted from the eigenvalues τ_r of the AR coefficient matrix, and due to the fact that the ARMAV model order and the resulting eigenvalues are in general larger than the number of eigenvalues of the structure, it is required to develop a distinction between the physical and non-physical modes via, for example, a dispersion analysis.
- Another method, such as the Kalman filter, has to be coupled to perform the parameter estimation of the ARMAV model.
- The model sometimes can exhibit undesired local minima, requiring more effort on producing good initial values for the iterative procedure.

Bodeux and Golinval [9] utilized an ARMAV model to identify the structure and detect damage within a numerically modeled simply supported beam and an experimental benchmark one-bay two-story steel frame. For the ARMAV model parameter estimation, a Kalman filter is used. The method identified frequencies and mode shapes of both undamaged and damaged cases of the structure. The problem of investigation is, however, limited to damage detection, i.e. damage localization was not implemented.

Hung et al. [40] extended the method applied in Hung and Ko [41] based on a vector backward auto regressive (VBAR) method, which was capable of distinguishing between the correct eigenvalues and vectors. The method was applied on a numerical 3 degree-of-freedom (DOF) spring structure and an experimental five-story single-bay steel structure in order to extract the modal characteristics and damping ratio. The identification was performed to an undamaged structure only.

2) Least Squares Methods:

The least squares identifies structures by minimizing the sum-of-squared errors between the measured response and what is predicted by the mathematical model [53].

The damage detection of a one-bay one-story braced frame and a cantilever plate was investigated by Friswell et al. [29]. Damage was considered as a reduction in the stiffness of an element and was introduced by saw cuts. The algorithm, based on a generalized least squares theory, fits the measured data to each predefined damage case. The most likely damage case is then the one that has the best fit. The method achieved reasonable success: it was capable of finding the damage, but sometimes gave false-positive detections with regard to non-damaged locations.

An iterative least squares identification technique and modification process based on output-only readings was studied by Chen and Li [13] and applied on various undamaged structures: a 4-DOF spring mass damper structure, a 15-story shear frame and a truss. Both noise-free and noise-polluted signals as well as incomplete measurements were considered and the structure was excited by a sinusoidal force. Stiffness identification was satisfactorily whereas damping was identified at a lower accuracy as the noise increases. Furthermore, identification accuracy depended on the initial values used for the iterative search.

An adaptive least mean square filtering theory was used in the direct identification of structural stiffness of 4- and 12-DOF benchmark structures by Goeffrey Chase et al. [31]. The study investigated the effect of measurement noise and applied a sinusoidal excitation to the structure. Damage was considered as a change in the structural stiffness only, and the undamaged structural characteristics were known and used as initial values for the iterative search. The results showed that the proposed method is effective in identifying damage, but has some implementation issues affected by the sampling rate of the data acquisition sensors. Furthermore, the method assumes that the acceleration, velocity and displacements are measured at each DOF, requiring extensive instrumentation.

Classical least squares method was utilized by Zhao et al. [107, 106]

for the identification of an undamaged seismically loaded 3-story shear frame. The method was tested using different values of noise and different number of sensors, yet filtering the noise out using a low pass filter. Mass was assumed known and the number of DOFs considered in this study is rather low. Furthermore, the method requires all response components of all DOFs to be known, i.e. acceleration, velocity and displacement. To do so, the measured acceleration was numerically integrated which could accumulate error due to measurement noise.

3) Kalman Filter Methods:

The Kalman filter [47] is a recursive method to estimate a state vector via minimizing the mean square error.

A possible improvement of the linear Kalman filter is the Extended Kalman Filter (EKF) that is used in non-linear systems by linearizing the basic Kalman filter about the current operating point [54]. This important modification allowed the utilization of the Kalman filter in identification and control problems.

Toki et al. [89] used the Kalman filter to identify structural parameters and input ground motions from measured responses only by applying ground accelerations to the structure and allowing it to vibrate freely afterwards. The structural parameters of an undamaged 3-DOF two-dimensional shear frame were first identified by a free vibration state then used to identify the response using output-only signals. However, all numerical tests were performed in a noise-free environment and assuming that the structural characteristics remained the same before and after the ground motion excitation is inaccurate, as damage is most likely to take place during these motions.

Koh et al. [54] studied the identification of multistory frame building damage in terms of change in story stiffness using an improved condensation method coupled with an EKF. A numerically simulated 12-story frame and an experimental 6-story laboratory model were identified. Several levels of Input/Output (I/O) noise were studied. The mass matrix was, however, assumed known.

An extended Kalman approach was applied in Lei et al. [61] for the structural identification of a numerical 5-DOF and an experimental 4-DOF shear building excited by unknown earthquake excitations. The recursive solution for the structural parameters above the first story were estimated by an extended Kalman estimator followed by the estimation of unknown input excitation at the first story via a least squares estimation. Finally, the first floor parameters are estimated using an eigenvalue analysis. Response measurements were considered at parts of the structure and noise was also considered. Although a rather simple structure with only 5-DOFs was consid-

ered, the results showed a false-positive damage of nearly 5%. Furthermore, mass and damping were not identified and only undamaged structures were considered.

4) Bayesian Analysis Methods:

It is a probabilistic approach in which the most probable damage scenario is obtained of some previously assumed damage scenarios [83]. By identifying the modal parameters based on measured data, the probability of each damage scenario can be calculated based on the difference between the identified modal parameters and their theoretical counterpart. Once these relative posterior probabilities are formulated, a branch-and-bound search is applied to identify the most likely damage scenario.

A Bayesian probabilistic approach was applied by Sohn and Law [83] to identify the most probable damage scenario in a structure, where damage is introduced as a reduction in structural stiffness of a member. Both two-dimensional and three-dimensional numerical frame models were studied under a variety of noise percentages. With sufficient data sets and several fundamental modes of vibration being estimated, the method was capable of identifying both damage location and extent. However, the computational effort required increases exponentially with the number of predefined damage scenarios. Also, false damage scenarios may be highlighted since the method relies on modal parameters, which could be similar for different damage scenarios. Furthermore, the selection of the assumed damage states as well as accuracy of the numerically assumed model (when applied in the laboratory) would play a significant role in the outcomes of this method.

Ching and Beck [14] used a two step probabilistic Bayesian approach in the structural identification and damage detection of the IASC-ASCE (International Association for Structural Control - American Society of Civil Engineers) benchmark frame. Both brace damage and connection damage were studied while the structure was excited by either hammer or ambient excitations. For braced cases, the damage can be detected reliably for hammer and ambient excitations. However, for the unbraced cases, reliable damage detection was not achieved.

Bayesian updating utilizing a Markov chain Monte Carlo simulation was used to tackle the numerical integration required in the Bayesian updating scheme in Yuen et al. [100]. The approach was applied to the 4-DOF simplified IASC-ASCE benchmark structure. It requires the identification of the first 4 modal frequencies, otherwise the problem becomes unidentifiable. The approach showed that there is insufficient data in the unidentifiable case to successfully assess damage location and severity.

5) Empirical Mode Decomposition and Hilbert-Huang Transformation Methods:

In the Empirical Mode Decomposition (EMD), the data is decomposed into several intrinsic mode functions (IMFs) by a sifting process, which continues to extract IMFs until the residue of the signal becomes sufficiently small. Decomposing the signal in the time domain allows the identification of the occurrence time of the damaging event or damage spike, and the damage location can be determined by the spatial distribution of these damage spikes. The Hilbert-Huang transformation (HHT) is simply an empirical mode decomposition combined with a Hilbert spectral analysis [98, 96].

The drawback of this method is that it requires a continuous SHM which is, of course, computationally expensive. The need for the continuous SHM comes from the fact that the data provided to the HHT must contain the time instance of damage occurrence for it to work. Furthermore, the damage detection accuracy depends on the sampling frequency, noise contamination and severity of damage [98, 96].

Xu and Chen [96] presented the applicability of the EMD to identify damage in an experimental 3-story shear building model subjected to damage in the form sudden change in structural stiffness via releasing two pretensioned springs. The structure was studied while in free vibration, random vibration and earthquake vibration. The damage location was identified by analyzing the spatial distribution of the damage spikes along the building heights. A similar study using the HHT is presented in Yang et al. [98] and was applied on the 4-DOF simplified IASC-ASCE benchmark structure.

6) Finite Element Model Updating Methods:

Finite element model updating is a method based on the modification of the structural properties, namely mass, stiffness and damping to represent, as accurate as possible, the response obtained from the measured data [11]. Although the research work presented in this dissertation is somehow related to this method, it is still treated as an independent category and only classical methods used in model updating are listed below.

It is also noted that a significant amount of research has applied model updating in the structural identification of trusses and beams when compared to the frame and more complicated bridge counterparts.

A detection method based on minimizing the difference between analytical and experimental identified modal frequencies was presented in Capecchi and Vestroni [11]. The study investigated the damage detection of a numerically modeled beam and ten-story shear frame as well as an experimental cantilever beam. Damage was in the form of stiffness reduction and only changes in stiffness were identified. The location was accurate but some error

was in the quantification of damage.

Xia et al. [94] identified the probability of structural damage in elements in cantilever beams and frame structures by comparing the frequencies and mode shapes before and after damage. Damage was modeled by saw cuts in the structure and only stiffness was detected and located but not quantified. However, it requires a certain procedure when exciting the structure. All the 29 nodes of the frame were impacted by a hammer rather than utilizing ambient or random excitation signals and sometimes gave false-positive results.

Damage, in the form of stiffness reduction, in a simple numerical two-story frame structure was identified in Fanning and Carden [24] using a single-input and single-output measurement and a correlated numerical model of the structure. The undamaged structure is tested and the numerical model is calibrated first, followed by the identification of the damaged structure by exciting the structures using a sinusoidal excitation signal without considering any input or output noise. The algorithm was successful as long as the number of damaged members is limited to two.

The IASC-ASCE benchmark shear frame was also identified in Lam et al. [56] via an output-only vibration-based statistical model updating methodology. The statistical model updating is based on a Bayesian modal identification studied in Katafygiotis and Yuen [50]. In case of zero noise and modeling error, the method identified the location and extent of damage successfully. In the presence of noise, however, the damage was identified successfully but the extent was overestimated and some secondary false-positive damage was detected.

7) Modal Identification Methods:

These methods rely on the fact that changes in mass, stiffness and/or damping produces a change in the modal parameters of the structure. However, it was debated that damage identification using modal parameters alone is sufficient [25, 53].

Methods relying on the change of natural frequencies only in detecting damage were reviewed in Salawu [77].

A detection routine to identify the correct damage state from six possible predefined damage states was studied in Lam et al. [57]. His mode shape based detection routine was applied to a one-bay two-story steel frame and utilizes a Modal Assurance Criterion (MAC) for the prediction of the correct damage case.

Frequency response functions (FRFs) were investigated by Choudhury and He [16] in the identification of a planar frame structure damaged by saw cuts. The damage was successfully located using this method in conjunction

with a dynamic expansion procedure.

Bicanic and Chen [7] developed a damage detection methodology based on modal information and applied it on two-dimensional frames as well as other structures. Damage was modeled as a reduction in structural stiffness. However, no noise was considered and some significant false-positive damage was detected.

FRFs and an analytical model were presented in Wang [92] in the damage detection two-dimensional frame structure. The algorithm identified the location and magnitude of damage even when at 5% measurement error. In the experimental investigation, however, the method was less successful.

Zhu and Lu [108] developed a sensitivity-based method for damage localization and quantification utilizing the slopes and curvature of mode shapes for damage localization and the natural frequencies for damage quantification. The approach was applied on 10-DOF and 20-DOF spring-mass-damper structures and a 3-DOF experimental shear building. Damage was considered as a reduction in stiffness and no damping or mass was identified.

The Modal Strain Energy (MSE) approach, developed by Shi et al. [79], relies on the changes of the MSE before and after the occurrence of damage to find its location. The elemental MSE requires the components of the mode shapes, which are - in practice - incomplete, thus requiring a mode expansion technique, discussed in Law et al. [58]. An improved MSE approach using incomplete mode shapes directly, called the Multiple Damage Location Assurance Criterion (MDLAC) was developed in Shi et al. [80]. In his research, a two-step approach was used. The damage location was preliminarily located using incomplete measured mode shapes. The suspected damaged elements were reassessed using more accurate data to determine the exact location and extent of damage.

Shi et al. [79] used the MSE approach in the structural identification and damage detection of a plane truss and an experimental two-story frame. Damage was modeled by releasing the restraint at the joints. The method was successful in locating damage as long as the measurement noise is low, as measurement noise and incompleteness of measured modes greatly affect the damage location result.

Li et al. [62] developed a new MSE method based on the decomposition of the modal strain energy into an axial and transverse part. The developed method is then used to perform numerical studies on three-dimensional five-story frame structure and an offshore template platform based on data generated by a finite element model. Damage was in the form of stiffness reduction, and no noise was considered. The proposed method located the damage, but was less successful in predicting the extent of damage.

1.2.5 Structural Identification of Horizontal Axis Wind Turbines

The structural identification and damage detection of Wind Turbines (WTs) is an active research field, especially after the rapid increase in the numbers of WTs due to the urge to produce energy from clean renewable resources. Although a significant number of research papers has been published recently, the number of general review papers still remain few.

Ciang et al. [17] provided a review to damage detection techniques in WTs as a part of the implemented SHM, with special emphasis on blades and towers. Another review to condition monitoring and fault detection of WTs is presented in Hameed et al. [36]. Rolfes et al. [74] presented and extensive review of SHM applied on support structures and rotor blades with special emphasis on sensor technology.

Current SHM practice can be found in Butterfield et al. [10], whereas a survey of commercially available condition monitoring systems is presented in Crabtree et al. [18]

Although the structural identification and damage detection technique developed in this dissertation is a global vibration-based method investigating the turbine supporting structure, it is still beneficiary to provide a brief overview of various local and global SI methods, as this research area is still relatively new when compared to the SI of two-dimensional shear frames. Some of the SI methods are listed below [17]:

- **Acoustic emission based detection methods:** Damage - in form of cracks, debonding ...etc - produces a change in the stored elastic energy at the point of damage which can be captured by acoustic emission monitoring, e.g. Sutherland et al. [86] and Anastassopoulos et al. [3].

- **Thermal imaging method:** These methods rely on spotting a temperature difference on a surface to indicate damage. This difference is a result of the change in thermal diffusivity between the damaged and undamaged part, thus indicating material irregularity or damage, e.g. Dutton [23].

- **Ultrasonic methods:** The basic idea behind ultrasonic methods is to pass an ultrasonic wave through the material, which will get reflected and/or mode altered when passing through a defect, e.g. Lee et al. [59].

- **Fiber optics method:** The fibers are attached to the blade to measure loads, as the optical power of a light source reduces when it passes

through an optical fiber depending on the strain of that fiber. An implementation in damage detection can be found in Dutton [23]

- **Vibration-based approaches:** Being considered amongst the most common damage detection methods used, these approaches rely on the measurement of the response of structures from ambient or other types of excitation, and the extraction of structural features from those to determine structural parameters, and ultimately, structural damage.

  Gross et al. [34] studied the structural identification and damage detection of rotor blades subjected to hammer input forces and natural wind excitation from their modal characteristics. Damage to rotors was simulated by loosening the bolts at the root of one blade. Three damage detection techniques were used, namely: the Rational Polynomial Curve Fit, the Eigensystem Realization Algorithm and the Ritz vector extraction method. However, damage identification was inconclusive. This was attributed to the noise pollution in the signals, manual triggering process and/or inadequate sensor placement.

  Structural identification based on vibration response of blades when excited using piezoceramic actuators was studied by Ghoshal et al. [32]. Four different algorithms were used: transmittance function, resonant comparison, operational deflection shape and wave propagation function. This still remains a laboratory technique as it required extensive use of actuators and sensors. The indication of the presence of damage was clear, but the location was not always correct and the authors suggest an even finer resolution grid for damage localization. Furthermore, no damage quantification was performed.

  Rolfes et al. [75] investigated the components of an automated structural identification system for the early detection of damage in WTs utilizing smart wireless sensors. The system was divided into modules: each of these having a specific task to be completed. Module 3, i.e. the damage identification module, requires highly resolved eigenfrequencies and a validated structural model. The system was applied to obtain a numerical model of the NEG-MICON 250 WT, but still requires further improvements to be applied on the Vestas V-80 WT due to the presence of a tuned mass damper that reduces the first mode vibration amplitude.

  The structural monitoring of WTs using wireless sensor networks was investigated by Swartz et al. [87]. In this study, the utility of wireless sensors is illustrated and output-only modal analysis of three operational turbines has been performed using DIAMOND modal analysis software package.

Adams et al. [1] studied the SHM of WT blades as a process in statistical pattern recognition. The MAC was used for the analysis of changes in modal deflections. Damage was detected and located via a damage index approach. The study also shows that a change of 4% in natural frequencies corresponded to a 25% reduction in stiffness at the root of one blade.

Multiple stationary and non-stationary methods using non-parametric and parametric representations were investigated in the online output-only identification of a NEG MICON NM52/900 WT by Avendavo-Valencia and Fassois [4]. It was concluded that stationary analysis is unable of capturing the dynamics of the turbine. Non-parametric non-stationary methods were capable of capturing the dynamics, but with limited accuracy. Finally, parametric non-stationary, although being more complex, lead to a more accurate model.

The SI of damage to monopile foundation of offshore WTs from scour was studied by Gomez et al. [33]. Vibration response was recorded at tower top and bottom flange and the natural frequencies and mode shapes were extracted via a Frequency Domain Decomposition technique.

Monitoring of an offshore WT using vibration response to ambient excitation was studied by Häckell and Rolfes [35]. The study investigates the classification of a large database of readings, structural identification via driven stochastic subspace identification, extraction of modal parameters via an automated triangulation based approach, and extraction of condition parameters via AR models.

Coupling both local and global SHM for offshore WT was presented by Schröder et al. [78]. The considered structure is a laboratory model of a tripile offshore WT's supporting structure and vibration was induced by releasing the structure from an initial displaced state. Global SHM was performed based on modal parameters extracted using data driven Stochastic Subspace Identification (SSI) from an array of sensors distributed on the structure, whereas local SHM was performed using data gathered from local displacement measurement data. Finally, the MAC was used for comparison between the damaged and undamaged structural states.

1.2.6 Outlook and Critical Issues

A quick glimpse on the reviewed literature reveals that the structural identification of two-dimensional shear frames has been extensively studied due

to their simplicity, and present an adequate problem for comparative studies. On the other hand, structural identification of wind turbines is still an active field of research.

Thus, the capabilities of the proposed identification scheme are assessed first by a comparative study performed on two-dimensional shear frames. Then, the complex problem of wind turbine damage detection is investigated.

One of the most important findings obtained from reviewing various identification techniques is that structural identification based on modal characteristics and frequency changes is not always advantageous. Structural frequency variation due to changes in environmental and operational conditions could exceed that of structural damage, as reported by Farrar and Doebling [25]. This underlines the importance of incorporating a data classification scheme before measured data is passed to the identification algorithm.

Another problem in frequency domain methods is their low sensitivity to structural damage. Furthermore, damage in some elements may lead to a larger change in frequencies than in other elements [70].

In general, classical approaches relying on sound mathematical theories have limitations in one way or another. Some require gradient information to guide their search in a point-to-point basis, which also relies on a relatively good initial guess, something that becomes unpractical as the complexity of the problem increases. Other methods require special conditions to be applied on identification problems, such as assuming a certain noise or excitation pattern, assuming that all components of vibration response (acceleration, velocity and displacements) are measured and/or that an extensive array of sensors is implemented. In their best performance, they still obtain near optimal, i.e. close to real values, structural parameters [53].

Versatility becomes another issue, as structural identification schemes applied on a certain type of structures may require extensive modifications to work on other structures, or are even not applicable at all to any other structure.

Another important issue is the fact that data from real acquisition tools is polluted by noise. A general case of noise corruption is the I/O noise, in which both excitations and vibration response are polluted by a randomly generated noise. I/O noise present a more challenging identification problem than output-only noise as the sources of error are increased.

Motivated by the challenges posed by the drawbacks and limitations of classical identification schemes, the need for further research in the field of damage detection of wind turbines via non-classical techniques and the need for a reliable and versatile structural identification scheme, a modified hybridized metaheuristic structural identification and damage detection technique is developed in this research, compared to the well-known Genetic Al-

gorithm optimization technique and applied on a variety of identification problems from two-dimensional shear frames, through wind turbines, finalized by an experimental investigation.

To meet these challenges, it is required that the developed structural identification and damage detection techniques is:

- Precise and accurate, identifying the structural characteristics with minimum error and deviation and avoiding errors, especially false-negative identification errors.
- Capable of handling noise corrupted signals in both input excitations and output response, i.e. robust.
- Expandable, requiring minimum modifications for improvements, e.g. easy to convert it from being a normal identification scheme into an output-only scheme.
- Versatile, handling different structural systems with minimum modification needs.
- Unaffected by the initial guess. In fact, it is found out later that the developed algorithm finds the structural characteristics even if initialized randomly.
- Computationally efficient.

1.3 Problem Statement

Although structural identification and damage detection methods are an important component in structural health monitoring, the developed methods so far lack versatility, utilize classical methods which have some limitations as previously mentioned, and usually rely on modal characteristics which are not always advantageous, as structural frequency variation due to changes in environmental and operational conditions could exceed that of structural damage, affecting the accuracy of the detection scheme. Furthermore, the development of a structural identification and damage detection scheme for wind turbine supporting structures is still an active research and development field and is not yet fully researched.

1.4 Research Aim and Objectives

This research aims to develop a vibration-based global structural identification and damage detection numerical framework that is applicable on a broad

variety of structures with minimum modifications provided that an accurate dynamic analysis method is "plugged-into" the framework. The framework is based on a modified and hybridized metaheuristic optimization algorithm and identifies the structural properties, namely mass-, damping- and stiffness-distribution to assess the current state of the structure and detect damage.

To achieve such aim, following objectives are established:

- The development of a modified hybridized metaheuristic algorithm.
- The formulation of the optimization problem for each studied identification problem.
- The implementation of comparative studies with other well-known optimization algorithms.
- The continuous introduction of further modifications and improvements to the developed optimization algorithm, e.g. to be capable of performing output-only identification.
- The investigation of both numerical and laboratory identification problems to demonstrate the applicability of the developed numerical identification scheme.

1.5 Methodology

To achieve the aim and objectives of this research, following tasks were executed:

1. A continuous review of literature on optimization techniques, dynamic response calculation methods, classical structural identification methods and recent non-classical identification methods.
2. Developing and coding a structural identification model utilizing a metaheuristic algorithm. In contrast to multi-purpose commercial codes, the specialized code enables an easier and straight forward access to data structures for an efficient implementation of the approach.
3. Benchmarking the developed scheme on examples presented in recent literature, namely: two-dimensional shear frames, investigated using the Genetic Algorithm optimization technique.
4. Incorporate experience-based improvements to the algorithm, e.g. fine-tuning of the algorithm's main control parameters.

5. Considering more challenging problems such as offshore and onshore wind turbine supporting structures, both numerically and experimentally.

1.6 Contents of this Dissertation

The chapters of this dissertation are organized in conformance with the methodology of solving an optimization problem. An introduction to this study, its current state of the art, motivations, aims and objectives as well as undertaken methodology is presented in the first chapter.

The development of the proposed optimization algorithm is the subject of the second chapter. The basic algorithm is explained first, followed by a variety of improvements and modifications that were implemented, eventually leading to the algorithm used in this study.

The third chapter is dedicated to the preparation of the various identification problems to be solved using an optimization algorithm. The optimization problems are constructed and the search space and objective function involved in these problems are described.

Once the optimization algorithm is developed and the problems are formulated, the numerical investigation follows. This is the subject of the fourth chapter in which the results obtained from numerical study cases are detailed, analyzed and commented on. Each problem starts by stating the structural related information, the excitation related information, the search space, the time history properties and the studied identification cases. Then, the results are obtained, tabulated, summarized in illustrative figures and commented on.

To prove the applicability of the developed optimization algorithm on data obtained from real acquisition tools, an experimental tripile supporting structure is investigated in the fifth chapter. The laboratory tests were conducted at the Institute of Structural Analysis (Institut für Statik und Dynamik - ISD) at Leibniz Universität Hannover (LUH), with aim to identify damage via changes in the modal parameters by comparing damaged and undamaged structural states using the Modal Assurance Criterion (MAC).

To finalize the study, a summary and concluding remarks as well as the areas of future research are detailed in the sixth chapter, to give a broad view of the results, and motivate future investigations of the remaining issues.

Chapter 2

The Development of MARSHAL

Despite being a promising optimization algorithm, Harmony Search algorithms still require some improvements to tackle problems as complex as structural identification, model reduction, damage detection and output-only identification.

In this chapter, a brief introduction to the concepts of optimization are given, followed by a detailed explanation of the basic Harmony Search algorithm. After performing modification and hybridization, the final algorithm used in this research is presented, namely: The Modified Adaptive haRmony SearcH ALgorithm (MARSHAL).

2.1 Introduction to Optimization

Principally, an optimization algorithm aims to select the optimum solution within a predefined population of possible solutions that best achieves a certain objective. In its simplest cases, optimization algorithms may search for a solution vector that maximizes or minimizes a certain function called "The Objective Function". Thus, for an optimization algorithm to solve structural identification and damage detection problems, such objective function must be determined.

When solving an optimization problem, a systematic guided search within a predefined search space is performed to obtain the optimal solution. It is this systematic iterative mechanism that differentiates one optimization algorithm from another.

Due to their versatility, simplicity and flexibility, optimization algorithms were applied in various fields of research: economy, production, resource allocation, management, design optimization and even more. Thus motivating

the research community to tap into their potential in complex structural identification problems.

Conceptually, Harmony Search (HS) is considered a metaheuristic algorithm. Such class of algorithms is adequate for the application to combinatorial optimization problems, as they provide effective strategies that guide the search process, thus solving optimization problems with satisfying results [8]. Metaheuristic algorithms were defined as "*high level strategies for exploring search spaces by using different methods*" [8]. Another definition is provided by Yagiura and Ibraki [97] and defines metaheuristic algorithms as "*the collection of ideas of how to use the search history to generate new solutions and how to extract the necessary information from the generated solutions*".

Amongst the well-known broadly applied metaheuristic algorithms are: simulated annealing, particle swarm optimization, genetic algorithms (and all other evolutionary algorithms), scatter search, tabu search and the harmony search algorithm.

The identification problems considered in this research are formulated as discrete, or combinatorial, optimization problems, i.e. the variables are selected from a defined pool of discrete values, which is the reason why a metaheuristic algorithm was used in this research. HS was chosen as it is a powerful and promising algorithm that has emerged recently.

2.2 The Basic Harmony Search Algorithm

HS is a recently developed metaheuristic algorithm presented in Geem et al. [30], which emerged as a powerful and promising optimization algorithm. HS is more efficient, faster and easier in implementation than other well-known metaheuristic algorithms such as the Genetic Algorithms (GAs) [99]. Recent optimization studies such as Degertekin [20] and Degertekin et al. [21] show that HS is a superior optimization algorithm with promising potential.

The gradient-free nature of the HS algorithm enabled it to achieve satisfying results even for the most complex optimization problems, such as structural identification and damage detection [67]. Classical gradient-based methods, on the other hand, get trapped in local optimums due to the complexity of the considered optimization problem.

Due to its simplicity, HS can be easily improved to further enhance its capabilities. A recent overview of well-known improvements made to the HS is presented in Alia and Mandava [2]. From an algorithmic point of view, modifications/improvements could be introduced in two ways:

1. Improvements on features and additional search parameters within the

algorithm's own structure, or

2. Hybridizing it with other algorithms.

MARSHAL is an enhanced HS algorithm that resulted from both improving the basic algorithm's structure as well as hybridizing it with another algorithm. The development of MARSHAL is presented in Sec. 2.3.

The iterative scheme of the basic HS in searching for the optimum solution consists of four steps, namely: (1)- Initialization, (2)- Improvising a new harmony, (3)- Updating, and (4)- Termination. These steps are detailed below.

(1)- Initialization

During this phase, the control parameters of the HS are initialized. These control parameters are:

- The Harmony Memory Size (HMS), which controls the number of solution vectors stored in the memory of the harmony search.
- The Harmony Memory Considering Rate (HMCR $\in [0, 1]$), which represents the probability that the elements of a new trial solution vector are chosen from within the harmony memory.
- The Pitch Adjusting Rate (PAR $\in [0, 1]$), which guides the local search of HS, i.e. the probability that the value of an element in the solution vector gets slightly changed.
- The termination criteria, e.g. the maximum number of iterations.

After initializing the control parameters, the Harmony Memory (HM) gets filled with initial solution vectors. The assumption of solution vectors could be random or set to a predetermined value. Once these vectors are assumed, the objective function of each vector is calculated and stored in the HM. Generally, the solution vector $\mathbf{X}$ of an optimization problem takes the form,

$$\mathbf{X} = \{x_1, x_2, \ldots, x_n\} \ , \tag{2.1}$$

where each entry $x_i \in \mathbf{X}$ is chosen from a predetermined pool of values called "The Search Space".

At the end of the initialization step, the objective function value F_i of each

solution is evaluated and stored as follows:

$$\mathrm{HM} = \left[\begin{array}{c|c} \mathbf{X_1} & F_1 \\ \mathbf{X_2} & F_2 \\ \vdots & \vdots \\ \mathbf{X}_{\mathrm{HMS}} & F_{\mathrm{HMS}} \end{array}\right] = \left[\begin{array}{cccc|c} x_{(1,1)} & x_{(1,2)} & \cdots & x_{(1,n)} & F_1 \\ x_{(2,1)} & x_{(2,2)} & \cdots & x_{(2,n)} & F_2 \\ \vdots & \vdots & \vdots & \vdots & \vdots \\ x_{(\mathrm{HMS},1)} & x_{(\mathrm{HMS},2)} & \cdots & x_{(\mathrm{HMS},n)} & F_{\mathrm{HMS}} \end{array}\right] . \tag{2.2}$$

(2)- Improvising a new harmony

As long as no termination criteria is met, a new solution vector is derived for each iteration. When HS derives the new solution vector $\mathbf{X_{new}}$, it follows an element-by-element basis, in which it is decided whether element x_i is derived from a randomly chosen solution vector inside HM or is randomly selected from the search space, and whether a slight modification is done to this element via pitch adjustment.

The probability of an element x_i to be derived from HM is HMCR, thus,

$$x_i = \left\{\begin{array}{ll} x_i \in \{x_{(1,i)}, x_{(2,i)}, \ldots, x_{(\mathrm{HMS},i)}\} & \text{if} \quad rand_1 \leq \mathrm{HMCR} \\ x_i \in \{x_i^l\,,\, x_i^l + x_i^{ss}\,,\, x_i^l + 2x_i^{ss}\,,\, \ldots\,,\, x_i^u\} & \text{if} \quad rand_1 > \mathrm{HMCR} \end{array}\right. , \tag{2.3}$$

where $rand_1 \in [0,1]$, x_i^l, x_i^{ss} and x_i^u are the lower bound, step size and upper bound of element x_i in solution vector $\mathbf{X_{new}}$, respectively.

Furthermore, if an element x_i is selected from inside HM, i.e. if $rand_1 \leq$ HMCR, then a local search may be performed by slightly modifying the variable x_i. The probability that such local search is performed is PAR, thus,

$$x_i = \left\{\begin{array}{ll} x_i \pm round(rand_3 \times bw)\, x_i^{ss} & \text{if} \quad rand_2 \leq \mathrm{PAR} \\ x_i & \text{if} \quad rand_2 > \mathrm{PAR} \end{array}\right. , \tag{2.4}$$

where $rand_2 \in [0,1]$, $rand_3 \in [0,1]$, $rand_2 \neq rand_3$ and bw is the bandwidth of modification, i.e. the number of steps the element x_i is modified.

(3)- Updating

Once all element of $\mathbf{X_{new}}$ are derived, the objective function $F_{new} = F(\mathbf{X_{new}})$ is evaluated. Assuming that the minimization of F is required, the worst solution $\mathbf{X_{worst}}$ stored in HM is selected, which satisfies,

$$F_{worst} = F(\mathbf{X_{worst}}) = max(F_1, F_2, \ldots, F_{\mathrm{HMS}}) \; . \tag{2.5}$$

The worst solution $\mathbf{X_{worst}}$ in HM is replaced by $\mathbf{X_{new}}$ if $F_{new} < F_{worst}$.

(4)- Termination

The HS algorithm continues to the next iteration unless the maximum number of iterations is reached or any other predefined termination criteria is met.

A flowchart of the basic HS algorithm is shown in Fig. 2.1 and 2.2.

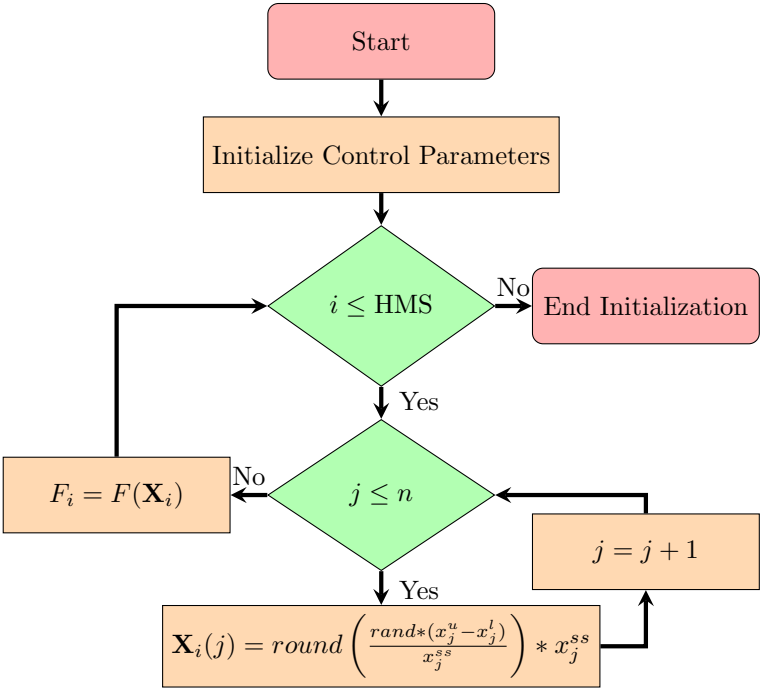

Figure 2.1: Original harmony search initialization step.

2.3 MARSHAL

A basic HS, although being a promising algorithm, was still no match for the complexity involved in structural identification and damage detection problems, which lead to the development of the more advanced Modified Adaptive haRmony SearcH ALgorithm (MARSHAL).

The modifications made to the basic HS were:

1. An experience-based control parameter selection system developed by

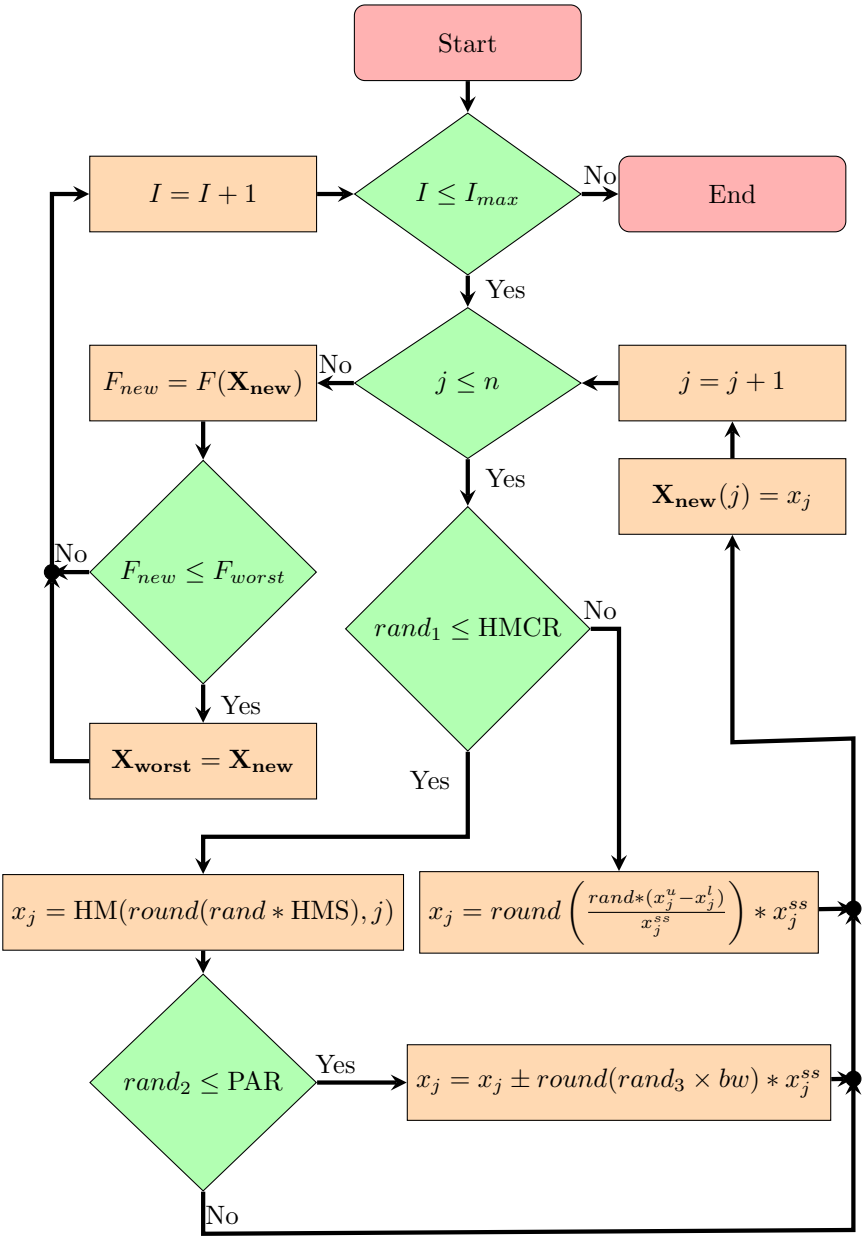

Figure 2.2: Original harmony search iterative steps.

Hasancebi et al. [38], explained in Sec. 2.3.1.

2. The addition of a local effect, developed by Jahjouh and Nackenhorst [42], explained in Sec. 2.3.2.

3. A two-level experience-based search space reduction method developed by Jahjouh and Nackenhorst [42], explained in Sec. 2.3.3.

2.3.1 An Adaptive Harmony Search Algorithm

One of the drawbacks of metaheuristic optimization algorithms is the fine-tuning of control parameters, i.e. the selection of control parameter values is problem-dependent, requiring preliminary optimization runs to be performed for fine-tuning. This led to the development of a new HS called the Adaptive Harmony Search (AHS) algorithm by Hasancebi et al. [38].

In the AHS, the control parameters (HMCR and PAR) are adaptively determined in each iteration utilizing the experience gathered so far in the HM. This eliminates the need to fine-tune these variables. For each iteration,

$$\mathrm{HMCR}^k = \left(1 + \frac{1 - \overline{\mathrm{HMCR}}}{\overline{\mathrm{HMCR}}} \cdot e^{-\gamma \,.\, N(0,1)}\right)^{-1} , \tag{2.6}$$

and

$$\mathrm{PAR}^k = \left(1 + \frac{1 - \overline{\mathrm{PAR}}}{\overline{\mathrm{PAR}}} \cdot e^{-\gamma \,.\, N(0,1)}\right)^{-1} , \tag{2.7}$$

where HMCR^k and PAR^k are the AHS control parameters for iteration k, e is the exponential function, $N(0,1)$ is a normally distributed random number that adds a dispersion effect on the newly selected control parameters around their corresponding average values, γ is the learning rate of the adapted parameters, recommended to be $\gamma \in [0.25, 0.50]$ [38] and $\overline{\mathrm{HMCR}}$ and $\overline{\mathrm{PAR}}$ are the average values of the control parameters for every solution vector in HM, which are calculated as follows:

$$\overline{\mathrm{HMCR}} = \frac{\sum_{i=1}^{i=\mathrm{HMS}} \mathrm{HMCR}_i}{\mathrm{HMS}} , \tag{2.8}$$

and

$$\overline{\mathrm{PAR}} = \frac{\sum_{i=1}^{i=\mathrm{HMS}} \mathrm{PAR}_i}{\mathrm{PAR}} . \tag{2.9}$$

Thus, during initialization of the AHS, the values of HMCR and PAR must be initialized with the solution vectors. Furthermore, when $\mathbf{X_{new}}$ replaces $\mathbf{X_{worst}}$, then both HMCR and PAR associated with (having the same index

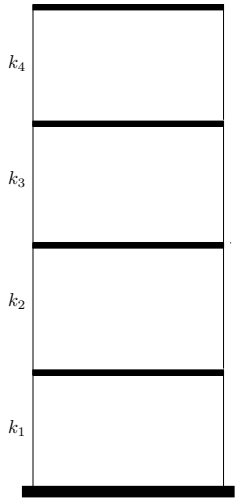

Figure 2.3: A sample 4-DOF shear building.

as) $\mathbf{X_{worst}}$ must be replaced by HMCR^k and PAR^k, respectively. This leads to an expanded storage system for HM as follows:

$$\mathrm{HM} = \left[\begin{array}{cccc:ccc} x_{(1,1)} & x_{(1,2)} & \dots & x_{(1,n)} & F_1 & \mathrm{HMCR}_1 & \mathrm{PAR}_1 \\ x_{(2,1)} & x_{(2,2)} & \dots & x_{(2,n)} & F_2 & \mathrm{HMCR}_2 & \mathrm{PAR}_2 \\ \vdots & \vdots & \vdots & \vdots & \vdots & \vdots & \vdots \\ x_{(\mathrm{HMS},1)} & x_{(\mathrm{HMS},2)} & \dots & x_{(\mathrm{HMS},n)} & F_{\mathrm{HMS}} & \mathrm{HMCR}_{\mathrm{HMS}} & \mathrm{PAR}_{\mathrm{HMS}} \end{array}\right]. \tag{2.10}$$

2.3.2 Introducing the Local Effect

An additional modification presented in Jahjouh and Nackenhorst [42] in the form of a so-called "local effect" is implemented in this research. The introduction of the local effect was motivated by the fact that stiffness variables of structures are coupled with each other. To illustrate this coupling effect, a 4-DOF shear building, shown in Fig. 2.3, is considered.

Following the general assumptions of shear buildings, i.e. beams being considered rigid, columns being flexible and neglecting axial compressibility,

the stiffness matrix of such a structure is assembled as follows:

$$\mathbf{K} = \begin{bmatrix} k_1 + k_2 & -k_2 & 0 & 0 \\ -k_2 & k_2 + k_3 & -k_3 & 0 \\ 0 & -k_3 & k_3 + k_4 & -k_4 \\ 0 & 0 & -k_4 & k_4 \end{bmatrix} . \tag{2.11}$$

When identifying the solution vector $\mathbf{X} = \{k_1, k_2, k_3, k_4\}$ using the AHS, inaccurate results were obtained. The source of error was in the form of an error in neighboring stiffness entries of same magnitude but opposite sign, e.g. $k_2 = k_{2,\text{real}} + error$ and $k_3 = k_{3,\text{real}} - error$. Such error cancels out in $diag(\mathbf{K})$, creating a near optimum solution in the vicinity of the real solution due to the fact that the $diag(\mathbf{K})$ assembled from the near optimum solution has the same numerical value as that assembled from the real solution. To tackle this problem, the concept of local effect was developed.

This new feature has a probability of occurrence defined as the Local Effect Rate (LER). If it is triggered, a pitch adjustment is performed in the neighboring elements when the currently considered element has undergone pitch adjustment. Mathematically speaking, assuming that an element x_i has undergone pitch adjustment, then,

$$x_{i-1} = \begin{cases} x_{i-1} \pm round(rand_5 \times bw)\, x^{ss}_{i-1} & \text{if} \quad rand_4 \leq \text{LER} \\ x_{i-1} & \text{if} \quad rand_4 > \text{LER} \end{cases} , \tag{2.12}$$

and

$$x_{i+1} = \begin{cases} x_{i+1} \pm round(rand_7 \times bw)\, x^{ss}_{i+1} & \text{if} \quad rand_6 \leq \text{LER} \\ x_{i+1} & \text{if} \quad rand_6 > \text{LER} \end{cases} , \tag{2.13}$$

where x_{i-1} and x_{i+1} are the neighboring elements of x_i in the solution vector $\mathbf{X_{new}}$. The LER is calculated adaptively, similar to the other control parameters,

$$\text{LER}^k = \left(1 + \frac{1 - \overline{\text{LER}}}{\overline{\text{LER}}} \cdot e^{-\gamma \cdot N(0,1)}\right)^{-1} . \tag{2.14}$$

Thus, the HM expands once more as follows:

$$\text{HM} = \left[\begin{array}{cccc:cc} x_{(1,1)} & x_{(1,2)} & \cdots & x_{(1,n)} & F_1 & \mathbf{CP}_1 \\ x_{(2,1)} & x_{(2,2)} & \cdots & x_{(2,n)} & F_2 & \mathbf{CP}_2 \\ \vdots & \vdots & \vdots & \vdots & \vdots & \vdots \\ x_{(\text{HMS},1)} & x_{(\text{HMS},2)} & \cdots & x_{(\text{HMS},n)} & F_{\text{HMS}} & \mathbf{CP}_{\text{HMS}} \end{array}\right] , \tag{2.15}$$

where $\mathbf{CP}_i = \{\text{HMCR}_i, \text{PAR}_i, \text{LER}_i\}$, i.e. the vector of control parameters for solution $\mathbf{X}_i$.

A flowchart of the resulting algorithm's iterative search is presented in Fig. 2.4. It shall be mentioned that the initialization phase is similar to that illustrated in Fig. 2.1, but include now the initialization of the control parameters as well.

2.3.3 Search Space Reduction Scheme

In discrete combinatorial optimization problems, the optimum solution lies within a pool of solutions that is defined by the search space. The larger the search space, the more calculation time and effort is required to obtain the optimum solution and the less effective the algorithm becomes. The limits of any optimization algorithm can be easily reached with the simplest increase in the complexity of the structure in the form of, for example, increase in design variables.

For an optimization algorithm to cope with the changes in problem complexity, an experience-based dynamic reduction of the search space boundaries has to be implemented. Search space reduction, however, has to be applied mindfully. A smart reduction scheme is carried out on the right time and with the right size. On one hand, a well-designed search space reduction scheme could significantly improve the capabilities of the optimization algorithm. On the other hand, narrowing the search space too much could lead the search away from the region where the optimum solution is located to regions where only low quality solutions exist. Furthermore, an earlier implementation of the search space reduction scheme could lead the algorithm to premature convergence, i.e. to local optimum solutions of less quality.

Most of the metaheuristic optimization algorithms have some sort of "storage system" that stores a chosen population of good solution vectors so far tested during the optimization run to assist in improving the assumption of solution vectors for the next iterations. In HS based algorithms, it is the Harmony Memory (HM). This particular storage system also contains the "experience" of the algorithm gathered from all the iterations so far performed.

Smart search space reduction methods tap into the potential of this experience to redefine the boundaries based on the solutions obtained so far.

A simple and easy Search Space Reduction Method (SSRM) was investigated by Koh and Perry [53] and applied to Genetic Algorithms (GAs) as an improved way to invest iterations in an optimization run.

Assuming that a generic solution vector has the form

$$\mathbf{X} = \{x_1, x_2, \ldots, x_i, \ldots, x_n\} \,, \tag{2.16}$$

for which each element x_i has a lower bound x_i^l, upper limit x_i^u and step size x_i^{ss}. Furthermore, assuming that it is required to find $\mathbf{X}$ that minimizes some

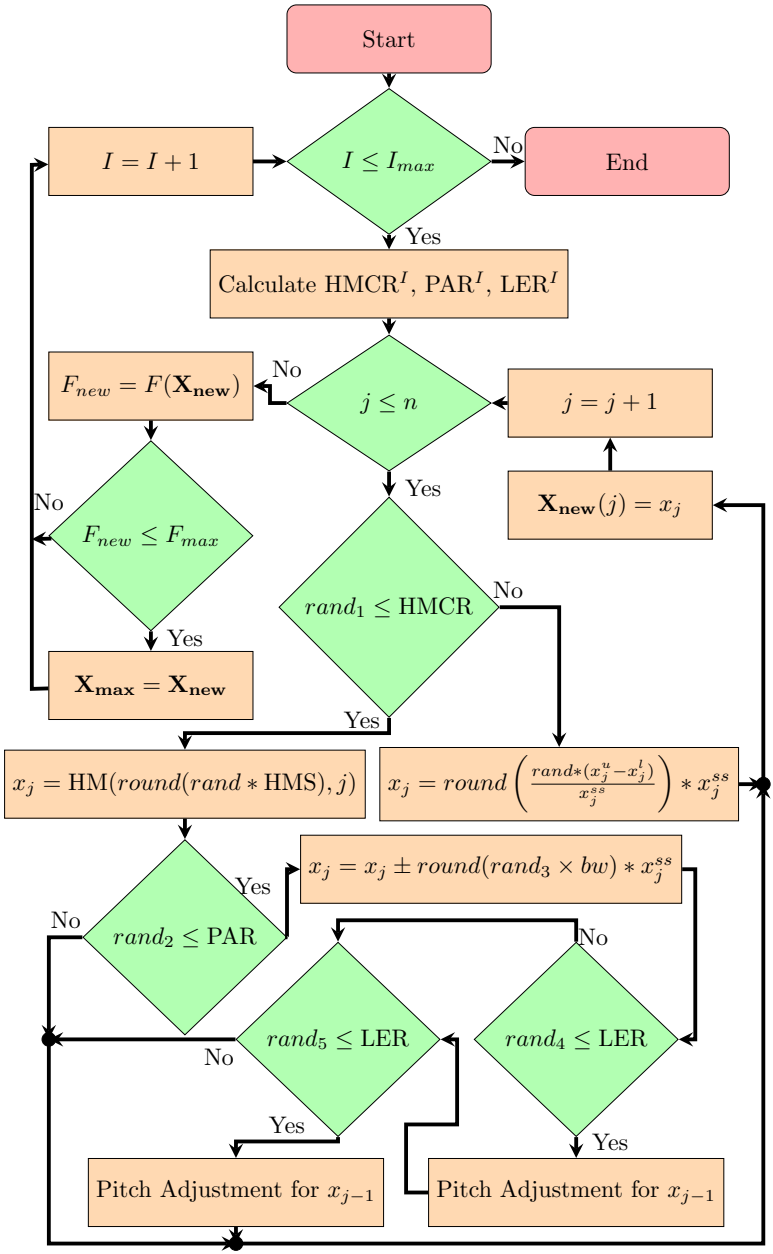

Figure 2.4: Adaptive harmony search with modifications: Iterative search.

objective function $F(\mathbf{X})$, then a simple way to do so is to allow a metaheuristic iterative algorithm to perform an optimization run with I_{max} number of iterations. In other words, a calculation effort of I_{max} is invested in the mentioned optimization problem. The next steps are quite straightforward: the algorithm would perform its iterative search until it reaches its maximum predefined number of iterations, then report the final result $\mathbf{X}_{opt}$ as output.

The SSRM suggest a more intelligent way to invest the calculation effort I_{max}. Instead of performing all of the iterations in a single optimization run, the optimization run is subdivided into r number of sub-runs. Each of these sub-runs would have I_{max}/r maximum number of iterations. Yet, the calculation effort invested in a single run, now being a collective term representing all sub-runs, remains unchanged.

Once a number of predetermined sub-runs have passed, the optimum solutions obtained from each sub-run is utilized in redefining the search space. Mathematically speaking, assuming that a predetermined number of runs r_S have passed, a corresponding number of optimum solutions resulting from each sub-run would have been obtained. These can be sorted as rows in a "storage matrix" as follows:

$$\mathbf{X}_S = \begin{bmatrix} x_{1,1} & x_{1,2} & \dots & x_{1,n} \\ x_{2,1} & x_{2,2} & \dots & x_{2,n} \\ \vdots & \vdots & \vdots & \vdots \\ x_{S,1} & x_{S,2} & \dots & x_{S,n} \end{bmatrix} . \tag{2.17}$$

The solutions stored in $\mathbf{X}_S$ are used to redefine the search space as follows:

$$x_i^u = \mu_i + w \times \sigma_i \leq x_i^{u_0} , \tag{2.18}$$

and

$$x_i^l = \mu_i - w \times \sigma_i \geq x_i^{l_0} , \tag{2.19}$$

where μ_i and σ_i are the average value and standard deviation of the $i-$th column in $\mathbf{X_S}$, $x_i^{u_0}$ and $x_i^{l_0}$ are the initial upper and lower bounds, respectively, and w is a predetermined window. To assure, statistically, a high probability that the optimum value is still within the defined bounds and to prevent premature convergence, the value was set to be $w = 4$.

Hence, the experience obtained from a predetermined number of sub-runs is utilized in redefining the search space of the problem as explained above. To summarize, a schematic is shown in Fig. 2.5.

Although the previous reduction scheme worked well with GAs, it had some shortcomings in HS related algorithms. During this research, it was found that the search space tends to get too small or even collapse as the stored

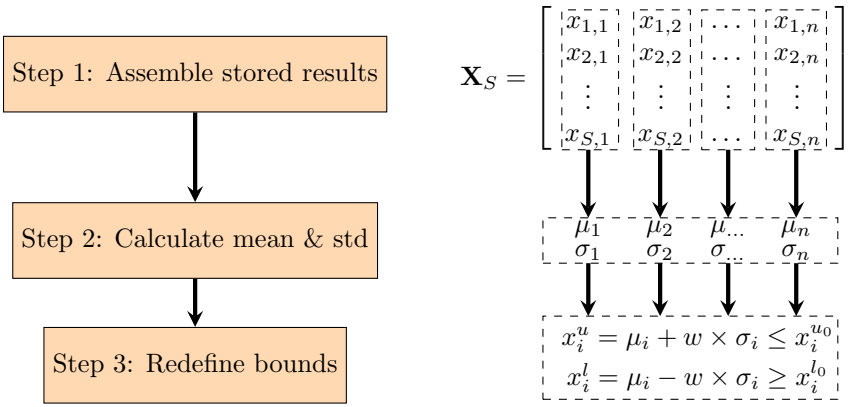

Figure 2.5: Sub-run level search space reduction.

solutions become more and more identical. A modification implemented to the reduction method is the addition of a minimum search space size as follows:

$$\text{if } (x_i^u - x_i^l) < (w_{min} \,.\, x_i^{ss}) \text{ then } \begin{cases} x_i^u = x_i^u + round(\frac{1}{2}(w_{min} - \frac{x_i^u - x_i^l}{x_i^{ss}})) \,.\, x_i^{ss} \\ x_i^l = x_i^l - round(\frac{1}{2}(w_{min} - \frac{x_i^u - x_i^l}{x_i^{ss}})) \,.\, x_i^{ss} \end{cases}, \tag{2.20}$$

where w_{min} is the minimum window to be kept between x_i^u and x_i^l.

To further utilize the experience gained in the solutions stored in the HM, another level of reduction is implemented [42]. The second level reduces the search space during a sub-run, i.e. an iteration level reduction scheme in addition to the reduction on a sub-run level. Hence, after a predetermined number of iterations I_S, the search space is reduced using the results stored so far in the HM. The equations to calculate the upper and lower bounds for each iteration are similar to equations (2.18) and (2.19), but now μ_i and σ_i are calculated from the solution in the HM. The reduced space is checked again to ensure it is large enough and did not collapse.

Implementing these modification resulted in the development of MARSHAL, which is a self-learning, experience-based, adaptive optimization algorithm capable of coping with the variation of the optimization problem's size via its built-in improved search space reduction scheme. MARSHAL's flowchart is shown in Fig. 2.6.

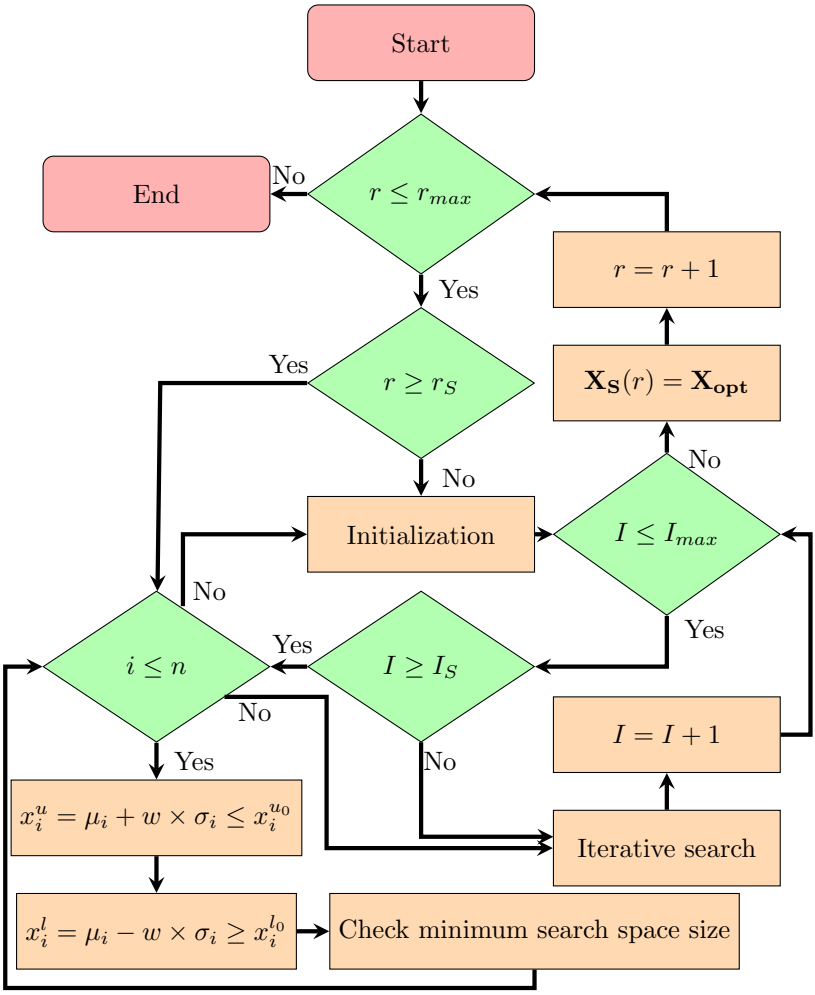

Figure 2.6: MARSHAL's flowchart.

2.4 Summary and Conclusions

Despite the fact that the basic HS achieved promising results in various optimization problems considered in the literature, it still was not powerful enough to tackle the complexity of identification problems, motivating the development of the global vibration-based structural identification framework:

MARSHAL.

MARSHAL (Modified Adaptive haRmony SearcH ALgorithm) is a self-modifying experience-based algorithm that incorporates a smart parameter selection system, allowing it to adapt to the current situation of the optimization problem. Furthermore, it exhibits some innovative engineering sense by realizing the coupling effect of stiffness terms in the stiffness matrix. Finally, a two-stage experience-based search guidance utilizing a previously developed reduction scheme is implemented which highlights potential regions within the search space, providing additional information to MARSHAL.

The automatic control parameter selection system solved one of the most common drawbacks of metaheuristic optimization, i.e. the fine-tuning of control parameters. Furthermore, the added local modification effect allowed MARSHAL to realize the coupling effect of adjacent DOF stiffness terms, aiding it in escaping near optimum solutions. Finally, search space reduction utilizes the "experience" gathered by the algorithm during its iterations and sub-runs to further pinpoint the potential location of optimum solution.

An important issue in search space reduction is, however, the careful application of such reduction, as a mistimed or narrowly designed search space reduction would mislead MARSHAL or even cause premature convergence.

To utilize MARSHAL, it is necessary to define the optimization problem aspects on which it is applied. The formulation of identification problems as optimization problems is subject of Ch. 3. Whereas the results obtained from the application of MARSHAL on the defined optimization problems are discussed in Ch. 4 and 5 for numerical and experimental cases, respectively.

Chapter 3

Formulation of Optimization Problems

MARSHAL, with all the improvements it got enhanced with, is still a mere minimization/maximization strategy that can only work as good as the optimization problem's aspects are defined. It is the researcher who defines the optimization problem, objective function, solution vector and search space in order to put this algorithm into proper use.

The formulation of the structural identification and damage detection problems as optimization problems is investigated in this chapter. For each identification problem, the solution vector and dynamic analysis concepts are presented followed by the description of search spaces and objective functions.

3.1 Considered Structural Identification Problems

To test the capabilities of MARSHAL, several identification problems with ascending complexity have been considered.

The structural identification and damage detection in two-dimensional shear frames has been considered first. Due to their simple dynamics, these structures were considered using a variety of optimization algorithms such a modified GA, as in Koh and Perry [53]. Although simple in nature, these structures are a good starting point to test the capabilities of MARSHAL when compared with other advanced optimization algorithms such as GAs. The experience and promising results obtained encouraged further investigation of more complex structures.

Once sufficient experience has been obtained from two-dimensional shear frames, more complex structures are numerically investigated, namely: Offshore Wind Turbines (WTs). Initially, the dynamic analysis of these structure

was performed by an open source software package.

The idea of using structural identification as means of model reduction of WTs was motivated by the complexity of such structures and the drawbacks that resulted from utilizing an open source software package. The objective was to first establish a reduced numerical model that approximates, as accurately as possible, the dynamic behavior of parked WTs subjected to inflow wind, then use this reduced model to numerically investigate structural identification and damage detection under a variety of noise magnitudes, sensor configuration and damage extents.

To assess the applicability of MARSHAL to more realistic data, an experimental test model of a scaled WT tower supported by a tripile foundation was considered. The laboratory tests were conducted at the Institute of Structural Analysis (Institut für Statik und Dynamik - ISD) at Leibniz Universität Hannover (LUH), with aim to identify damage via changes in the modal parameters by comparing damaged and undamaged structural states using the MAC as reported by Schröder et al. [78].

3.2 Two-Dimensional Shear Frames

Generally, one-bay multi-story two-dimensional shear frames, illustrated in Fig. 3.1, are simplified by assuming that they consist of relatively rigid beams and flexible columns, with the story mass being lumped at the story level and the axial compressibility being neglected, resulting in a single translational DOF at every story level.

3.2.1 Dynamic Analysis

Based on the assumptions mentioned above, the vibration response of such structures can be calculated by solving the second order differential equation

$$\mathbf{M}\ddot{\mathbf{x}} + \mathbf{C}\dot{\mathbf{x}} + \mathbf{K}\mathbf{x} = \mathbf{F} \ , \tag{3.1}$$

where $\mathbf{M}$,$\mathbf{C}$ and $\mathbf{K}$ are the mass, damping and stiffness matrices of the structure and $\mathbf{F}$ is the applied excitation.

For the simplification mentioned above, the mass matrix $\mathbf{M}$ takes the form of a diagonal matrix,

$$\mathbf{M} = \begin{bmatrix} m_1 & & & 0 \\ & m_2 & & \\ & & \ddots & \\ 0 & & & m_n \end{bmatrix} , \tag{3.2}$$

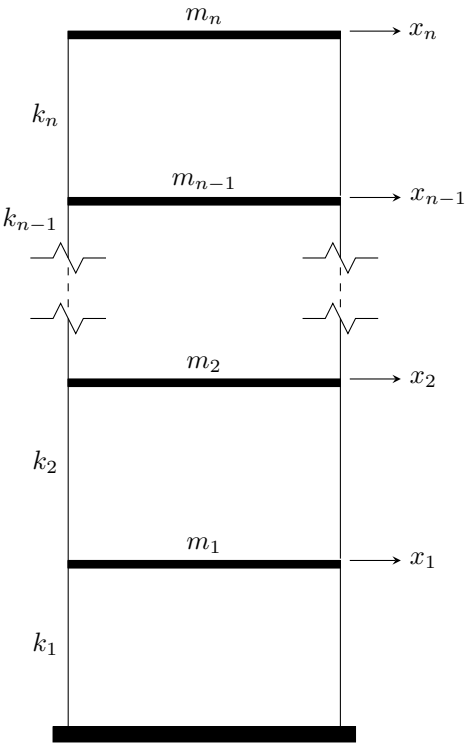

Figure 3.1: Two-dimensional shear frame model.

and the stiffness matrix $\mathbf{K}$ takes the form of a banded matrix,

$$\mathbf{K} = \begin{bmatrix} k_1 + k_2 & -k_2 & & & 0 \\ -k_2 & k_2 + k_3 & -k_3 & & \\ & -k_3 & \ddots & \ddots & \\ & & \ddots & k_{n-1} + k_n & -k_n \\ 0 & & & -k_n & k_n \end{bmatrix} . \tag{3.3}$$

Rayleigh damping is assumed for the structure, thus the damping matrix $\mathbf{C}$ is calculated as follows:

$$\mathbf{C} = \alpha \mathbf{M} + \beta \mathbf{K} , \tag{3.4}$$

where α and β are the Rayleigh coefficients. For the solution of equation (3.1), a time domain analysis is performed using Newmark's constant average

acceleration integration scheme.

3.2.2 The Solution Vector

For an optimization algorithm to perform structural identification and damage detection to a two-dimensional shear frame, it has to extract the structural characteristics from the measured vibration response. To do so, these characteristics must be included in the solution vector.

Assuming that it is intended to perform a structural identification to an n-DOF two-dimensional shear frame, the generic solution vector in equation (2.1) would take the form

$$\mathbf{X} = \{m_1, m_2, \ldots, m_n, k_1, k_2, \ldots, k_n, \alpha, \beta\} \ , \tag{3.5}$$

where m_i, k_i are the mass and stiffness of the $i-$th degree of freedom, respectively.

The solution vector presented in equation (3.5) represents the more general and complex case of unknown mass identification. If the mass of the structure is known or can be easily calculated, a simpler solution vector can be used as follows:

$$\mathbf{X} = \{k_1, k_2, \ldots, k_n, \alpha, \beta\} \ . \tag{3.6}$$

3.2.3 The Output-Only Identification Problem

Identification of structural parameters using output vibration response without the knowledge of the input excitations is within the scope of output-only identification. Output-only identification is an important class of structural identification as the measurement of input forces is not always possible outside a controlled laboratory environment.

When identifying a structure using output-only identification, equation (3.1) can no longer be solved for a trial structure since excitations $\mathbf{F}$ are unknown. Thus a predictor-corrector scheme based on Koh and Perry [53] is used to identify the excitations along with the structural characteristics. It shall be noted that these excitations are treated as terms to ensure the consistency of the equations of motion, rather than variables in the solution vector.

The Predictor Step:

At each time step k, the displacement $\mathbf{x}$ and velocity $\dot{\mathbf{x}}$ of the next time step $k+1$ are predicted using the measured acceleration $\ddot{\mathbf{x}}^*$ at time step $k+1$

(provided from the structure subjected to identification) and the acceleration so far obtained from the trial solution vector at time step k. Thus,

$$\dot{\mathbf{x}}_{k+1} = \dot{\mathbf{x}}_k + \frac{h}{2}(\ddot{\mathbf{x}}_k + \ddot{\mathbf{x}}^*_{k+1}) \tag{3.7}$$

and

$$\mathbf{x}_{k+1} = \mathbf{x}_k + \frac{h}{2}(\dot{\mathbf{x}}_k + \dot{\mathbf{x}}_{k+1}) \ . \tag{3.8}$$

Once the vibration response is determined for time step $k+1$, a prediction of the unknown excitation $\mathbf{F}^u$ is calculated considering any known excitations $\mathbf{F}^{kn}$ as follows:

$$\mathbf{F}^u_{k+1} = \mathbf{M}\ddot{\mathbf{x}}_{k+1} + \mathbf{C}\dot{\mathbf{x}}_{k+1} + \mathbf{K}\mathbf{x}_{k+1} - \mathbf{F}^{kn}_{k+1} \ . \tag{3.9}$$

The Corrector Step:

After predicting $\mathbf{F}^u_{k+1}$, the response of the trial structure at time step $k+1$ is calculated from equation (3.1) using Newmark's constant average acceleration scheme, resulting in a corrected response. This response is passed to the next time step, and the process is repeated for the whole time history. A flowchart for the predictor-corrector scheme is shown in Fig. 3.2.

3.3 Offshore Wind Turbines

Once the identification of two-dimensional shear frames is successfully implemented, the challenging problem of identification and damage detection of an offshore WT is considered. The complexity of this problem lies in the modeling of the vibration response of such a structure.

3.3.1 Dynamic Analysis

Modeling a full-scale wind turbine, illustrated in Fig. 3.3, requires the modeling of several sub systems that interact simultaneously when subjected to inflow wind. Thus, a dynamic analysis of a full-scale WT performs a so-called aero-hydro-servo-elasto analysis, which considers:

1. The aerodynamic analysis of wind and blades,
2. The hydrodynamic analysis of waves and currents,
3. The input from several control systems of the wind turbine (pitch, yaw, ...etc) and

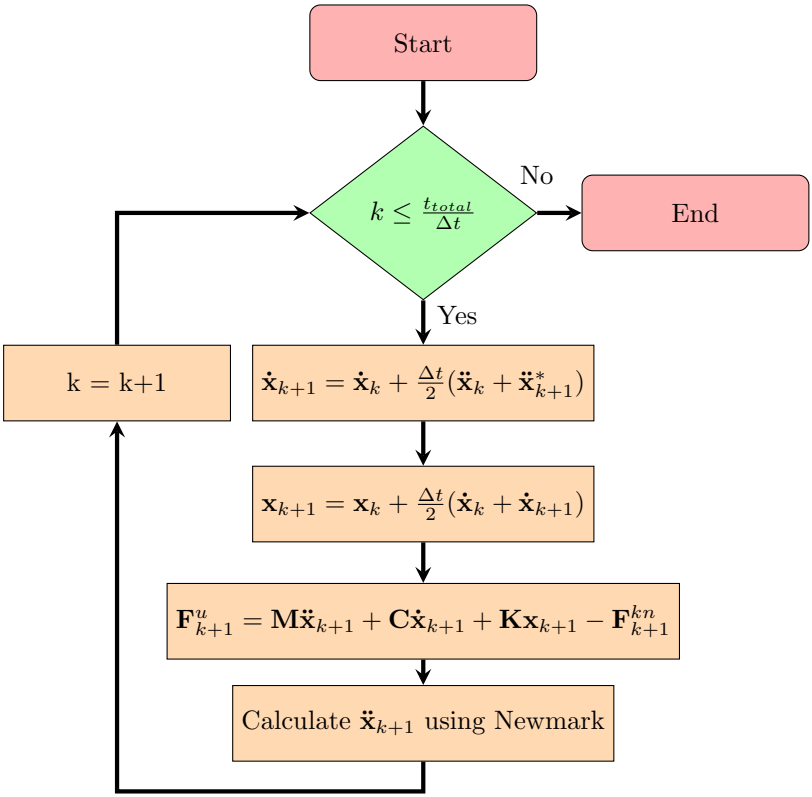

Figure 3.2: Predictor-Corrector scheme.

4. The structural response of the full-scale WT structure to the excitations resulting from the aero-hydro-servo analysis, taking into consideration possible soil-structure interactions.

Since the identification scheme used in this research is a vibration- and model-based method, it is required to either develop or use an analysis code that converts the various inputs of a WT (aerodynamics, control systems, geometry, hydrodynamics, ...etc) into vibration response signals.

Thus, an open source code called FAST (Fatigue, Aerodynamics, Structures and Turbulence) developed by the National Renewable Energy Laboratory (NREL) [46] is used to perform the multi-body simulation of the WT and provide MARSHAL with the necessary vibration response. The accuracy of FAST was verified in an offshore code comparison collaboration (OC3) [44]

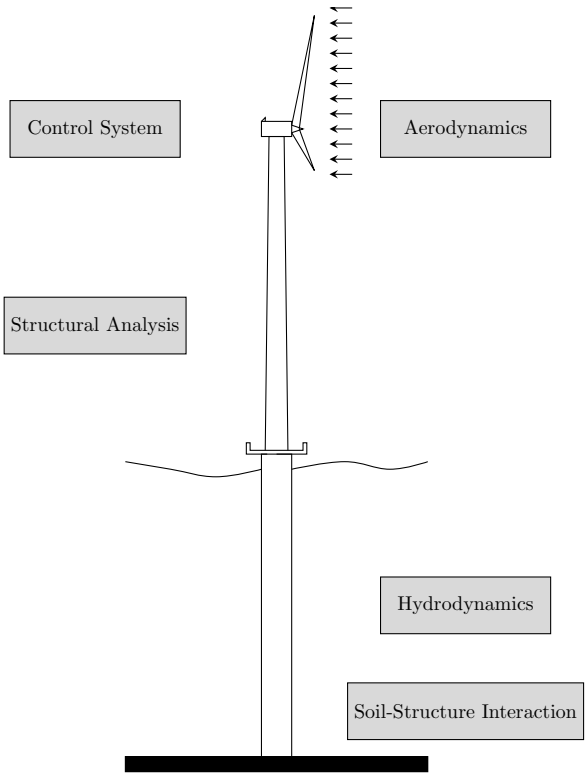

Figure 3.3: Offshore wind turbine schematic.

and (OC4) [45].

3.3.2 The Solution Vector

The identification and damage detection scheme developed in this research is applied on the turbine supporting structure without considering the identification of other components such as blades or mechanical parts inside the rotor nacelle assembly. Due to the complexity of the full-scale model, the identification is limited to the stiffness terms of the turbine supporting structure.

When using FAST, the characteristics of the supporting structure are provided via a so-called "tower file", which contains a table that defines its flexural, torsional and axial stiffness as well as the corresponding mass terms. An example of such file is provided in Appendix A.

To simplify the problem, it is assumed that the turbine is idling and faces wind directly. Thus the fore-after vibrations are dominant. Since only stiffness terms are to be identified, the generic solution vector in equation (2.1) would only contain terms related to the fore-after stiffness parameters, thus,

$$\mathbf{X} = \{k_1, k_2, \ldots, k_n\} \ , \tag{3.10}$$

where k_i is the fore-after stiffness of the i-th input station in the tower file and n is the number of input stations used to define the tower in FAST.

3.3.3 Critical Aspects

The identification problem defined for offshore WTs has both its advantages and disadvantages, despite the fact that it performs its identification task successfully, as detailed in Sec. 4.2.

On one hand, utilizing an open source ready-to-use and tested code provides a full-scale wind turbine model that is accurately modeled by FAST, which models the full aero-hydro-servo-elasto simulation of a wind turbine and allows hydrodynamic loads to be calculated.

On the other hand, it is model specific, i.e. for any wind turbine to be identified, the FAST settings, control systems,...etc must be known a priori. Furthermore, it requires a full wind profile input, i.e. the wind speed of each point within the swept area of the turbine blades needs to be provided as input to FAST. However, wind speeds are measured only at the nacelle, thus such wind field can only be approximated or numerically generated and is too complicated, prohibiting the development of an effective output-only identification scheme.

3.4 Onshore Wind Turbines: Development of a Reduced Model

As previously mentioned, modeling the vibration response of a full-scale WT is challenging, and has its advantages and disadvantages. Since the structural identification and damage detection scheme is applied on the turbine tower, it could be beneficiary to consider a reduced, yet accurate, model that simulates the dynamics of the turbine tower effectively.

For that purpose, a reduced model for the dynamic analysis of onshore WT towers is presented in this section, in an effort to overcome the disadvantages of using FAST as the main structural modeling code, especially the disadvantage that FAST requires a detailed input for the WT as well as its incompatibility with the output-only identification scheme utilized in this research.

Onshore WTs were selected for the model reduction scheme since their simulation does not include any hydrodynamic effects, which allows them to be reduced effectively.

Although a reduced model would, at its best, only approximate the vibration response of the turbine supporting structure without the rest of the turbine's components, it is still this particular response that is of interest. Amongst other motivations, following advantages are achieved when using a reduced model:

- Reduction in the complexity of the problem.
- Reduction in computational cost.
- Independence of inflow wind measurements, by either measuring forces at tower top or performing an output-only identification.
- Compatibility with the output-only approach used in this research.

3.4.1 Definition of the Reduced Model

The reduced model, shown in Fig. 3.4, is a discretized beam fixed at bottom and modified at top. As a replacement for the idling rotor nacelle assembly, artificial masses, stiffnesses and damping were attached to the tower top. The turbine is assumed to be idling and facing wind directly, thus fore-after motion is dominant.

The structural properties of a full-scale WT model, i.e. mass **M**, stiffness **K** and damping **C** are composed of the properties of the WT tower coupled with the rotor nacelle assembly, as follows:

$$\mathbf{M} = \begin{bmatrix} M_t & M_{tRNA} \\ M_{RNAt} & M_{RNA} \end{bmatrix} , \tag{3.11}$$

$$\mathbf{K} = \begin{bmatrix} K_t & K_{tRNA} \\ K_{RNAt} & K_{RNA} \end{bmatrix} \tag{3.12}$$

and

$$\mathbf{C} = \begin{bmatrix} C_t & C_{tRNA} \\ C_{RNAt} & C_{RNA} \end{bmatrix} . \tag{3.13}$$

where M_t , K_t , C_t are tower characteristics, M_{tRNA} , M_{RNAt} , K_{tRNA} , K_{RNAt} , C_{tRNA} , C_{RNAt} are the coupled characteristics, and M_{RNA} , K_{RNA} , C_{RNA} are the rotor nacelle assembly characteristics.

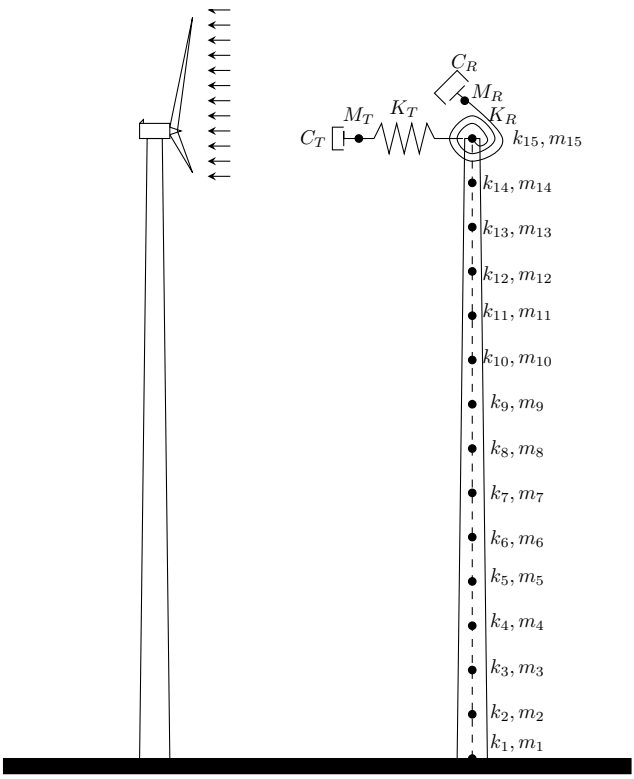

Figure 3.4: Onshore wind turbine model reduction.

The reduced model has its corresponding mass $\mathbf{M}^*$, stiffness $\mathbf{K}^*$, and damping $\mathbf{C}^*$ matrices. For the mass matrix,

$$\mathbf{M}^* = \begin{bmatrix} M_{d_1,d_1} & M_{d_1,\phi_1} & \dots & M_{d_1,d_n} & M_{d_1,\phi_n} \\ M_{\phi_1,d_1} & M_{\phi_1,\phi_1} & \dots & M_{\phi_1,d_n} & M_{\phi_1,\phi_n} \\ \vdots & \vdots & \vdots & \vdots & \vdots \\ M_{d_n,d_1} & M_{d_n,\phi_1} & \dots & M^*_{d_n,d_n} & M_{d_n,\phi_n} \\ M_{\phi_n,d_1} & M_{\phi_n,\phi_1} & \dots & M_{\phi_n,d_n} & M^*_{\phi_n,\phi_n} \end{bmatrix}, \tag{3.14}$$

where d_i,ϕ_i are the displacement and rotation DOFs of node i, and $M^*_{d_n,d_n}$ and $M^*_{\phi_n,\phi_n}$ are the modified mass entries of the reduced model.

Similarly, the reduced stiffness matrix $\mathbf{K}^*$ is

$$\mathbf{K}^* = \begin{bmatrix} K_{d_1,d_1} & K_{d_1,\phi_1} & \dots & K_{d_1,d_n} & K_{d_1,\phi_n} \\ K_{\phi_1,d_1} & K_{\phi_1,\phi_1} & \dots & K_{\phi_1,d_n} & K_{\phi_1,\phi_n} \\ \vdots & \vdots & \vdots & \vdots & \vdots \\ K_{d_n,d_1} & K_{d_n,\phi_1} & \dots & K^*_{d_n,d_n} & K_{d_n,\phi_n} \\ K_{\phi_n,d_1} & K_{\phi_n,\phi_1} & \dots & K_{\phi_n,d_n} & K^*_{\phi_n,\phi_n} \end{bmatrix} . \tag{3.15}$$

The damping matrix of the turbine tower is calculated first using equation (3.4), then modified similarly to the mass and stiffness matrix to result in

$$\mathbf{C}^* = \begin{bmatrix} C_{d_1,d_1} & C_{d_1,\phi_1} & \dots & C_{d_1,d_n} & C_{d_1,\phi_n} \\ C_{\phi_1,d_1} & C_{\phi_1,\phi_1} & \dots & C_{\phi_1,d_n} & C_{\phi_1,\phi_n} \\ \vdots & \vdots & \vdots & \vdots & \vdots \\ C_{d_n,d_1} & C_{d_n,\phi_1} & \dots & C^*_{d_n,d_n} & C_{d_n,\phi_n} \\ C_{\phi_n,d_1} & C_{\phi_n,\phi_1} & \dots & C_{\phi_n,d_n} & C^*_{\phi_n,\phi_n} \end{bmatrix} . \tag{3.16}$$

Thus, to derive the reduced model that closely approximates the vibration response of an idling full-scale turbine, $M^*_{d_n,d_n}$,$M^*_{\phi_n,\phi_n}$, $K^*_{d_n,d_n}$,$K^*_{\phi_n,\phi_n}$ and $C^*_{d_n,d_n}$,$C^*_{\phi_n,\phi_n}$ as well as the Rayleigh damping coefficients α and β are required to be estimated.

Since the modifications, as illustrated in Fig. 3.4, are in the form of an added artificial mass, stiffness and damping, the following equations could be used to estimate the required terms to derive the reduced model:

$$M^*_{d_n,d_n} = M_{d_n,d_n} + M_T = \lambda_1 * M_{d_n,d_n} \ , \tag{3.17}$$

$$M^*_{\phi_n,\phi_n} = M_{\phi_n,\phi_n} + M_R = \lambda_2 * M_{\phi_n,\phi_n} \ , \tag{3.18}$$

$$K^*_{d_n,d_n} = K_{d_n,d_n} + K_T = \lambda_3 * K_{d_n,d_n} \ , \tag{3.19}$$

$$K^*_{\phi_n,\phi_n} = K_{\phi_n,\phi_n} + K_R = \lambda_4 * K_{\phi_n,\phi_n} \ , \tag{3.20}$$

$$C^*_{d_n,d_n} = C_{d_n,d_n} + C_T = \lambda_5 * C_{d_n,d_n} \tag{3.21}$$

and

$$C^*_{\phi_n,\phi_n} = C_{\phi_n,\phi_n} + C_R = \lambda_6 * C_{\phi_n,\phi_n} \ . \tag{3.22}$$

where M_T, M_R, K_T, K_R, C_T and C_R are the artificial structural parameters added to the turbine tower as illustrated in Fig. 3.4, and $\lambda_1 \dots \lambda_6$ are the modification factors.

3.4.2 The Solution Vector

In case of model reduction, an optimization algorithm has to obtain the best reduced structure that approximates, as accurate as possible, the vibration response of the full-scale structure. The representation of other characteristics is of secondary importance, since the reduced model is developed for the purpose of structural identification and damage detection using a vibration-based method. Thus, the algorithm must optimize the solution vector

$$\mathbf{X} = \left\{ \begin{array}{cccccccc} \lambda_1 & \lambda_2 & \lambda_3 & \lambda_4 & \lambda_5 & \lambda_6 & \alpha & \beta \end{array} \right\} \tag{3.23}$$

to get an approximation of the full-scale model's vibration response.

3.5 Onshore Wind Turbines: Identification using a Reduced Model

Once the reduced model is obtained, it is put to use in structural identification and damage detection. The reduced model lends itself well to the identification scheme proposed in this research, enabling the identification of stiffness, mass and damping simultaneously.

3.5.1 Dynamic Analysis

Since the reduced model is essentially a beam model, equation (3.1) can be easily used to determine its vibration response.

When calculating the stiffness matrix of the reduced model, the following stiffness matrix for a simple beam element is used

$$\mathbf{K^e} = \frac{EI}{L^3} \begin{bmatrix} 12 & 6L & -12 & 6L \\ 6L & 4L^2 & -6L & 2L^2 \\ -12 & -6L & 12 & -6L \\ 6L & 2L^2 & -6L & 4L^2 \end{bmatrix}, \tag{3.24}$$

where $\mathbf{K^e}$ is the local stiffness matrix of a beam element, E is the elastic modulus, I is the moment of inertia, L is the element's length.

For the mass matrix, a consistent mass matrix is used, thus,

$$\mathbf{M^e} = \frac{\rho AL}{420} \begin{bmatrix} 156 & 22L & 54 & -13L \\ 22L & 4L^2 & 13L & -3L^2 \\ 54 & 13L & 156 & -22L \\ -13L & -3L^2 & -22L & 4L^2 \end{bmatrix}, \tag{3.25}$$

where $\mathbf{M^e}$ is the consistent mass matrix of a beam element, ρ is the mass density of the beam's material.

For the damping matrix, Rayleigh damping is assumed, thus it is calculated as equation (3.4).

Once the mass, stiffness and damping matrices for the turbine tower are calculated and assembled, they are modified based on the modification factors $\lambda_1 \dots \lambda_6$ as explained in Sec. 3.4.1.

The vibration response can then be calculated using Newmark's constant average acceleration integration scheme.

3.5.2 The Solution Vector

When performing structural identification and damage detection using a reduced model, it is sought to identify the structural properties of the turbine tower. Assuming that the tower is discretized using n equally spaced nodes, then n stiffness and n mass parameters have to be identified. Furthermore, if Rayleigh damping is assumed, another 2 damping variables α and β have to be considered.

When the optimization algorithm identifies onshore WT towers using a reduced model, the reduced model must be established a priori. That is, the 6 modification factors should be known. The optimization algorithm then assumes a turbine tower, assembles its structural matrices, applies the modification factors (as explained in Sec. 3.4.1) and obtains the vibration response required for optimization.

With that being said, the solution vector of such identification problems would have the form

$$\mathbf{X} = \{EI_1, EI_2, \dots, EI_n, \rho_1, \rho_2, \dots, \rho_n, \alpha, \beta\} \ , \tag{3.26}$$

where EI_i and ρ_i are, respectively, the fore-after stiffness and mass density of the i-th node in the reduced structure.

Similar to Sec. 3.2.2, one could simplify the identification problem by assuming that the mass is known or can be accurately approximated, an assumption that is valid in most engineering structures. When such assumption is made, the problem becomes a "known mass identification" problem and the solution vector is simplified to,

$$\mathbf{X} = \{EI_1, EI_2, \dots, EI_n, \alpha, \beta\} \ . \tag{3.27}$$

3.5.3 The Output-Only Identification Problem

In the case of WTs, measuring the inflow wind accurately is quite difficult, which led to the development of the reduced model in the first place. The re-

duced model enables an easy output-only identification scheme that is similar to the method explained in Sec. 3.2.3. Thus, the excitations are determined using a predictor-corrector scheme, with equations identical to equations (3.7) through (3.9).

3.6 Experimental Tripile Structure

To illustrate the capabilities of MARSHAL outside a numerical framework, an experimental study is considered. The laboratory tests were conducted at the Institute of Structural Analysis (Institut für Statik und Dynamik - ISD) at Leibniz Universität Hannover (LUH) and results were reported in Schröder et al. [78].

The tested structure is a turbine tower supported by a tripile foundation, illustrated in Fig. 3.5 and further detailed in Ch. 5.

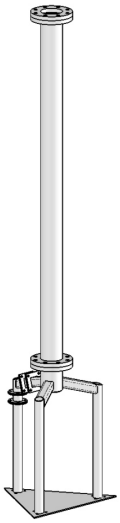

Figure 3.5: Schematic of the experimental model [78].

3.6.1 Dynamic Analysis

Since a tripile is essentially a three-dimensional model, 3-D Bernoulli beam elements were used in the construction of a numerical model corresponding to the experimental structure.

Once the dynamic characteristics of the tripile are calculated, the vibration response of the structure is determined using equation (3.1).

For a 3-D Bernoulli beam, the following stiffness matrix is used:

$$\mathbf{K^e} = \begin{bmatrix}
\frac{AE}{L} & 0 & 0 & 0 & 0 & 0 & -\frac{AE}{L} & 0 & 0 & 0 & 0 & 0 \\
0 & 12\frac{EI_z}{L^3} & 0 & 0 & 0 & 6\frac{EI_z}{L^2} & 0 & -12\frac{EI_z}{L^3} & 0 & 0 & 0 & 6\frac{EI_z}{L^2} \\
0 & 0 & 12\frac{EI_y}{L^3} & 0 & -6\frac{EI_y}{L^2} & 0 & 0 & 0 & -12\frac{EI_y}{L^3} & 0 & -6\frac{EI_y}{L^2} & 0 \\
0 & 0 & 0 & \frac{GJ}{L} & 0 & 0 & 0 & 0 & 0 & -\frac{GJ}{L} & 0 & 0 \\
0 & 0 & -6\frac{EI_y}{L^2} & 0 & 4\frac{EI_y}{L} & 0 & 0 & 0 & 6\frac{EI_y}{L^2} & 0 & 2\frac{EI_y}{L} & 0 \\
0 & 6\frac{EI_z}{L^2} & 0 & 0 & 0 & 4\frac{EI_z}{L} & 0 & -6\frac{EI_z}{L^2} & 0 & 0 & 0 & 2\frac{EI_z}{L} \\
-\frac{AE}{L} & 0 & 0 & 0 & 0 & 0 & \frac{AE}{L} & 0 & 0 & 0 & 0 & 0 \\
0 & -12\frac{EI_z}{L^3} & 0 & 0 & 0 & -6\frac{EI_z}{L^2} & 0 & 12\frac{EI_z}{L^3} & 0 & 0 & 0 & -6\frac{EI_z}{L^2} \\
0 & 0 & -12\frac{EI_y}{L^3} & 0 & 6\frac{EI_y}{L^2} & 0 & 0 & 0 & 12\frac{EI_y}{L^3} & 0 & 6\frac{EI_y}{L^2} & 0 \\
0 & 0 & 0 & -\frac{GJ}{L} & 0 & 0 & 0 & 0 & 0 & \frac{GJ}{L} & 0 & 0 \\
0 & 0 & -6\frac{EI_y}{L^2} & 0 & 2\frac{EI_y}{L} & 0 & 0 & 0 & 6\frac{EI_y}{L^2} & 0 & 4\frac{EI_y}{L} & 0 \\
0 & 6\frac{EI_z}{L^2} & 0 & 0 & 0 & 2\frac{EI_z}{L} & 0 & -6\frac{EI_z}{L^2} & 0 & 0 & 0 & 4\frac{EI_z}{L}
\end{bmatrix}, \tag{3.28}$$

where $\mathbf{K^e}$ is the local stiffness matrix of a beam element, E is the elastic modulus, I_y is the moment of inertia around the y axis, I_z is the moment of inertia around the z axis, G is the shear modulus, J is the polar moment of inertia, A is the cross sectional area and L is the element's length.

The consistent mass matrix for a 3-D element is,

$$\mathbf{M^e} = \rho AL \begin{bmatrix}
\frac{1}{3} & 0 & 0 & 0 & 0 & 0 & \frac{1}{6} & 0 & 0 & 0 & 0 & 0 \\
0 & \frac{13}{35} & 0 & 0 & 0 & \frac{11L}{210} & 0 & \frac{9}{70} & 0 & 0 & 0 & \frac{-13}{420} \\
0 & 0 & \frac{13}{35} & 0 & \frac{-11L}{210} & 0 & 0 & 0 & \frac{9}{70} & 0 & \frac{13}{420} & 0 \\
0 & 0 & 0 & \frac{I_y+I_z}{3A} & 0 & 0 & 0 & 0 & 0 & \frac{I_y+I_z}{6A} & 0 & 0 \\
0 & 0 & \frac{-11L}{210} & 0 & \frac{L^2}{105} & 0 & 0 & 0 & \frac{-13L}{420} & 0 & \frac{-L^2}{140} & 0 \\
0 & \frac{11L}{210} & 0 & 0 & 0 & \frac{L^2}{105} & 0 & \frac{13L}{420} & 0 & 0 & 0 & \frac{-L^2}{140} \\
\frac{1}{6} & 0 & 0 & 0 & 0 & 0 & \frac{1}{3} & 0 & 0 & 0 & 0 & 0 \\
0 & \frac{9}{70} & 0 & 0 & 0 & \frac{13L}{420} & 0 & \frac{13}{35} & 0 & 0 & 0 & \frac{-11L}{210} \\
0 & 0 & \frac{9}{70} & 0 & \frac{-13L}{420} & 0 & 0 & 0 & \frac{13}{35} & 0 & \frac{11L}{210} & 0 \\
0 & 0 & 0 & \frac{I_y+I_z}{6A} & 0 & 0 & 0 & 0 & 0 & \frac{I_y+I_z}{3A} & 0 & 0 \\
0 & 0 & \frac{13L}{420} & 0 & \frac{-L^2}{140} & 0 & 0 & 0 & \frac{11L}{210} & 0 & \frac{L^2}{105} & 0 \\
0 & \frac{-13L}{420} & 0 & 0 & 0 & \frac{-L^2}{140} & 0 & \frac{-11L}{210} & 0 & 0 & 0 & \frac{L^2}{105}
\end{bmatrix}, \tag{3.29}$$

where $\mathbf{M^e}$ is the consistent mass matrix of a beam element and ρ is the mass density of the beam's material.

For the damping matrix, a two-stage Rayleigh damping scheme is adopted for reasons explained later on in Ch. 5. In the two-stage damping scheme, the damping matrix is calculated twice using equation (3.4). A damping ratio ζ_1 is assumed for $0 \leq t \leq t_1$ and another damping ratio ζ_2 is assumed for $t > t_1$.

3.6.2 The Solution Vector

Assuming that the mass density is known, the solution vector would contain elements related to the stiffness and two damping stages.

Stiffness, as evident from equation (3.28), is expressed in numerous products, e.g. EI_y, EI_z, EA, and GJ. Thus, if it is required to identify stiffness parameters, a general approach is to include all these variables for each element in the solution vector, thus taking the form of

$$\mathbf{X} = \{E_1, G_1, J_1, I_{(y,1)}, I_{(z,1)}, A_1, \ldots, E_n, G_n, J_n, I_{(y,n)}, I_{(z,n)}, A_n, \zeta_1, \zeta_2\} \ . \tag{3.30}$$

However, adopting such expanded approach leads to an overcomplicated problem, as the number of elements in the solution vector $\mathbf{X}$ would be prohibitively large due to the fact that each element is defined using 6 variables, so if the tripile would be modeled using 15 elements, a total number of 92 variables are required to be identified in $\mathbf{X}$.

A reduction in stiffness, i.e. damage, results from the reduction in the elastic modulus and/or geometric properties. It could be argued that such damage would be detected by a reduction in the elastic modulus E even if it was actually caused by a reduction in geometric properties.

Nevertheless, such argument has its shortcomings: It assumes a homogeneous damage effect, as such approach identifies damage in the elastic modulus, leading to a decrease in EI_z EI_y and EA of same magnitude. Such approach could be inaccurate when identifying inhomogeneous damage patterns. Theoretically, this would be the case when the axial stiffness is reduced whilst the bending stiffnesses remain unchanged. Yet, WT supporting structures resist loads mainly in the form of bending moments and shear forces, thus the terms EI_z and EI_y are dominant and can, fortunately, be assumed to decrease and increase homogeneously. Furthermore, utilizing 6 variables per element would be too detailed for a global identification approach.

With that being discussed, the solution vector used in the identification of the experimental tripile supporting structure is

$$\mathbf{X} = \{E_1, E_2, \ldots, E_{15}, G_1, G_2, \ldots, G_{15}, \zeta_1, \zeta_2\} \ . \tag{3.31}$$

3.7 The Search Space

Metaheuristic optimization algorithms are searching tools, simply searching a predefined domain, called “Search Space”, to obtain the best solution according to a criteria, called “Objective Function”.

Recalling the generic solution vector $\mathbf{X}$, defined in equation (2.1) and repeated here for convenience,

$$\mathbf{X} = \{x_1, x_2, \ldots, x_n\} \ . \tag{3.32}$$

The search space is set by defining the maximum value, called "upper bound", minimum value, or "lower bound" and an increment, or "step size" for each entry x_i in the solution vector $\mathbf{X}$. These bounds and step sizes combined create the search space in which the algorithm must now explore to obtain the optimum solution.

Thus, for each entry x_i the following holds true:

$$x_i \in \{x_i^l \, , \, x_i^l + x_i^{ss} \, , \, x_i^l + 2x_i^{ss} \, , \, \ldots \, , \, x_i^u\} \ . \tag{3.33}$$

The search space must be predefined with care, it should not be too large to reduce the efficiency of the algorithm, nor too small to prevent the optimum solution from ever being reached. In the context of structural identification, however, this task is quite simple. One can simply assume the search space to be defined in a region around the expected values of the structural parameters.

Once these bounds are defined, a measurement of the overall complexity of the optimization problem, namely: The search space size (N_{SS}) can be calculated as follows:

$$N_{SS} = \prod_{i=1}^{n} \left(\frac{x_i^u - x_i^l}{x_i^{ss}} \right) \ , \tag{3.34}$$

where n is the number of entries within the solution vector $\mathbf{X}$, i.e. the length of $\mathbf{X}$.

3.8 The Objective Function

Whether structural identification, damage detection, output-only identification or model reduction, all these implementations can be treated as optimization problems with the objective to minimize errors between the predicted response $\ddot{\mathbf{x}}_\mathbf{p}$ from a trial solution vector $\mathbf{X}$ and the measured/real response $\ddot{\mathbf{x}}_\mathbf{r}$ obtained from the structure being identified.

Mathematically, the objective is to find $\mathbf{X}$ that minimizes $F(\mathbf{X})$ where,

$$\mathbf{X} \in \text{Search Space} \tag{3.35}$$

and

$$F(\mathbf{X}) = \frac{1}{t_{total}} \frac{1}{n} \sum_{t=0}^{t_{total}} \sum_{i=1}^{n} \sqrt{\left[\ddot{\mathbf{x}}_\mathbf{p}(i,t) - \ddot{\mathbf{x}}_\mathbf{r}(i,t)\right]^2} \ , \tag{3.36}$$

where t_{total} is the total time history and n is the number of acceleration measurement locations.

The objective function presented in equation (3.36) was generally applied to all problems considered in the research work of this dissertation, with the exception of the model reduction of onshore WTs and the experimental identification and damage detection of the WT tripile supporting structure.

For the model reduction of onshore WTs, following modifications were implemented:

- **Extensive Vibration Measurements:**
  All three response components are provided to the reduction, i.e. $\ddot{\mathbf{x}}$, $\dot{\mathbf{x}}$ and $\mathbf{x}$ at tower top in addition to the acceleration measurements obtained at all other sensor locations.

- **Normalization:**
  The vibration response obtained from various sensors was normalized, i.e. the signal obtained from each sensor was divided by its RMS. Reason for such normalization is the fact that the recorded vibration response from the tower top is significantly larger than those obtained from the tower bottom, which means that the response of the tower top has a larger "weight" in the objective function. Normalization remedies such issue.

In the experimental study of tripile supporting structures, following modifications were implemented:

- **Normalization:**
  As previously explained.

- **Addition of Penalty Factor:**
  To further assist MARSHAL in its optimization task, a penalty factor was introduced to the objective function to account for the difference in the average period of vibration response as follows:

$$p = |T_p - T_r| \ , \tag{3.37}$$

  where p is the penalty factor, T_p is the average vibration period of the trial solution vector $\mathbf{X}$ and T_r is the average vibration period from the measured response.

  The objective function in equation (3.36) is then modified to a penalized/constrained objective function which replaces the objective function in MARSHAL. The penalized objective function is calculated as follows:

$$F_p(\mathbf{X}) = (1 + p)\, F(\mathbf{X}) \ . \tag{3.38}$$

3.9 Summary and Conclusions

As an optimization algorithm, the performance of MARSHAL can only be as good as the defined optimization problem, underlining the importance of a proper optimization problem formulation.

To achieve the primary objective of developing a general identification framework, a unified and consistent approach in the formulation of structural identification and damage detection problems as optimization problems was presented in this chapter. For each considered problem, the dynamic analysis, solution vector, search space and objective function were established.

As a good basis for comparative studies, various identification problems applied on two-dimensional shear frames were established, namely: known mass, unknown mass and output-only identification problems.

The experience gained from such comparative studies motivated the investigation of structural identification and damage detection problems involving offshore WTs.

The challenging task of modeling such full-scale structures was tackled using an open source software called FAST. However, the utilization of FAST had some drawbacks, namely: being problem specific, and requiring detailed full wind inflow information, making it incompatible with the adopted output-only approach.

Thus, model reduction of onshore WTs was considered. The optimization problems with regard to deriving and utilizing such reduced model were discussed in this chapter.

To assess the applicability of MARSHAL to more realistic data, the formulation of the optimization problem corresponding to an experimental tripile supporting structure was discussed.

The previously developed MARSHAL in Ch. 2 and the formulated optimization problems in this chapter are put to use in Ch. 4 in a numerical investigation, followed by an experimental investigation in Ch. 5.

Chapter 4

Numerical Study Cases

After presenting MARSHAL in Ch. 2 and formulating the required optimization problems in Ch. 3, the results obtained from various numerical studies investigated in the research work of this dissertation are presented in this chapter.

The general procedure when numerically applying the proposed identification scheme is to assume the target structure as well as the excitations, followed by the calculation of its vibration response in the time domain, which serves as the original/measured vibration response provided to the identification scheme. Once evaluated, the measured vibration signals and excitations are infused with noise. Finally, the noisy vibration response and excitations (if not a case of output-only identification) are passed to MARSHAL to get an estimate of the structural characteristics, which is compared to the initially assumed structural characteristics. This procedure is illustrated in Fig. 4.1 and 4.2 for structural identification problems and model reduction problems, respectively.

MARSHAL's control parameters for all problems considered in this chapter were as follows: initial HMCR = 0.50, initial PAR = 0.35 and initial LER = 0.30. Furthermore, the HMS was 10 and γ was 0.35. The sub-run level reduction starts after 4 sub-runs, whereas the iteration level reduction starts after 5% of the iterations per sub-run were evaluated. These values were selected based on a preliminary study that involved variations of these control parameters for optimum convergence.

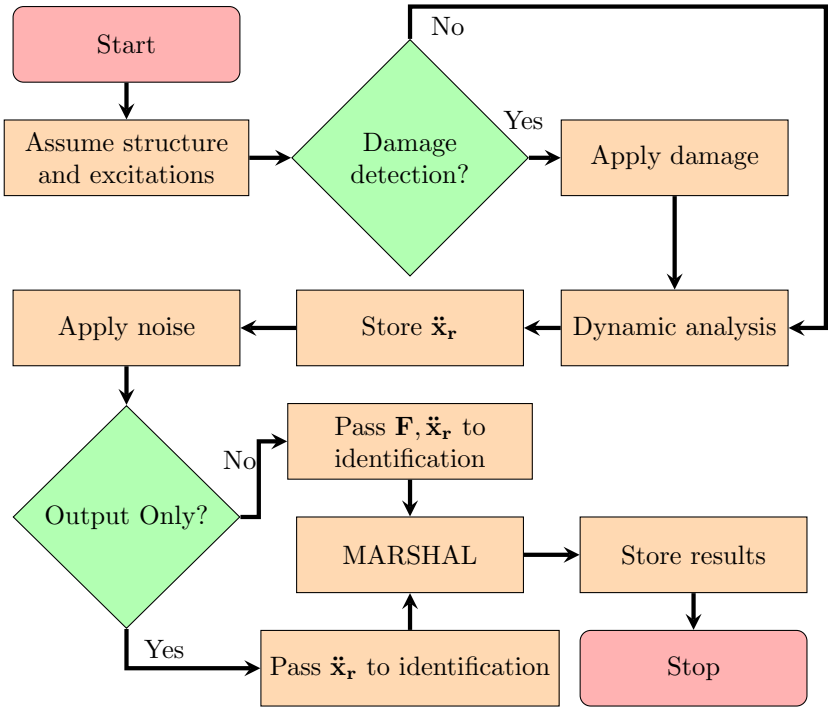

Figure 4.1: Structural identification and damage detection procedure.

4.1 Two-Dimensional Shear Frames

To start with, the structural identification of simple structures, namely: two-dimensional shear frames, is considered. Due to their simplicity and availability in literature, such structures were extensively studied, thus providing a suitable example for comparative studies.

The schematics of the investigated two-dimensional shear frames are shown in Fig. 4.3, 4.4 and 4.5 along with their structural characteristics, excitation application DOFs, and measurement locations for the case of Known Mass (KM), Unknown Mass (UKM) and Output-Only (OO) structural identification problems. These frames, as well as all other settings with regard to the time history, excitations,...etc, were identical to those presented in Koh and Perry [53] for comparison purposes.

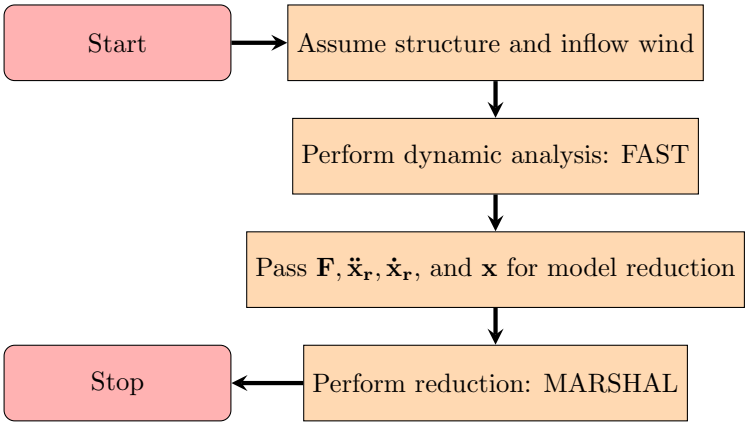

Figure 4.2: Model reduction of onshore wind turbines procedure.

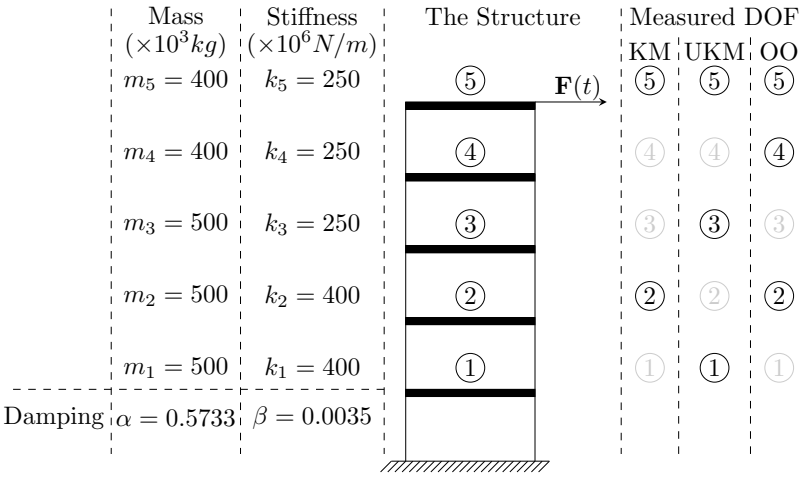

Figure 4.3: 5-DOF shear frame identification problem.

When defining the search space boundaries, the upper bound, lower bound and step size of each $x_i \in \mathbf{X}$ were taken as 200%, 50% and 1% of the assumed values shown in Fig. 4.3, 4.4 and 4.5, respectively, thus generating 151 possible values per x_i. Unless mentioned otherwise, excitations were provided as a WGN, having a RMS of 1000 Newtons.

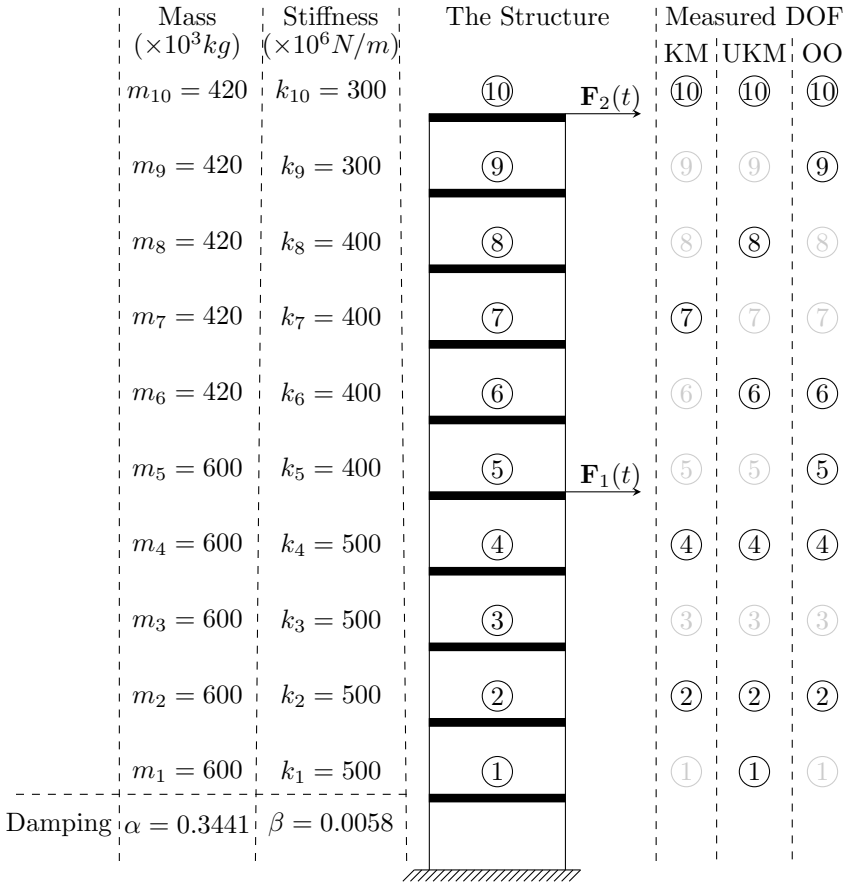

Figure 4.4: 10-DOF shear frame identification problem.

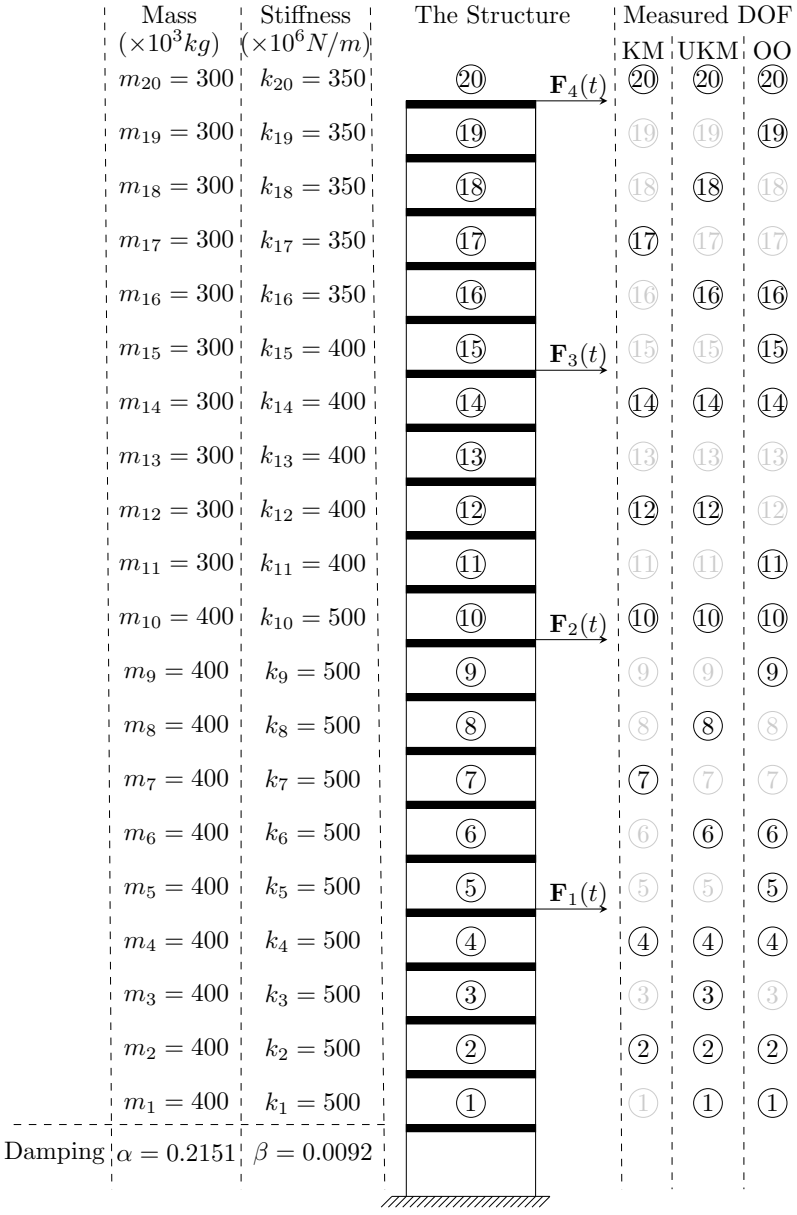

Figure 4.5: 20-DOF shear frame identification problem.

4.1.1 Structural Identification

The structural identification of the previously presented structures is investigated in this section. Various time history lengths were considered, namely: 0.50, 1, 2, 5 and 10 seconds discretized into increments of 0.01 seconds. To simulate response measurements from real data acquisition tools, noise is applied to the original vibration response and applied excitation as a percentage of the RMS, namely: 0%, 5% and 10%. Noisy vibration and excitations irregularly deviate from their corresponding noise-free values, as shown in Fig. 4.6 and 4.7. Such deviation has a negative impact on the identification accuracy by misleading the optimization algorithm into identifying a structure that best fits inaccurate vibration measurements using inaccurate excitation inputs, as illustrated in the flowchart shown in Fig. 4.8.

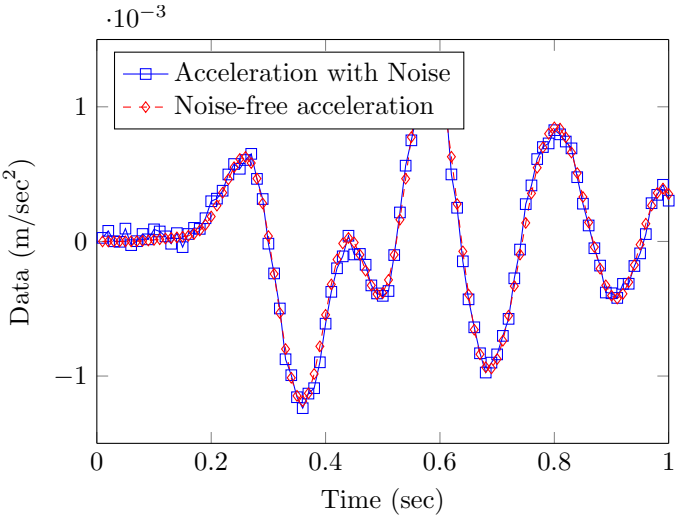

Figure 4.6: Effect of noise on acceleration: 5-DOF, 1st story, 10% noise.

For each identification problem, 10 optimization runs are performed. Each of these 10 runs is further divided into 10 sub-runs, that are used for the sub-run level search space reduction scheme. One result per optimization run is reported from all of its 10 sub-runs, namely: the best result which corresponds to the lowest objective function value.

The complexity of the considered identification problems could be represented via the problem's search space size, illustrated in Fig. 4.9. The invested calculation effort to solve these problems, i.e. the number of iterations per

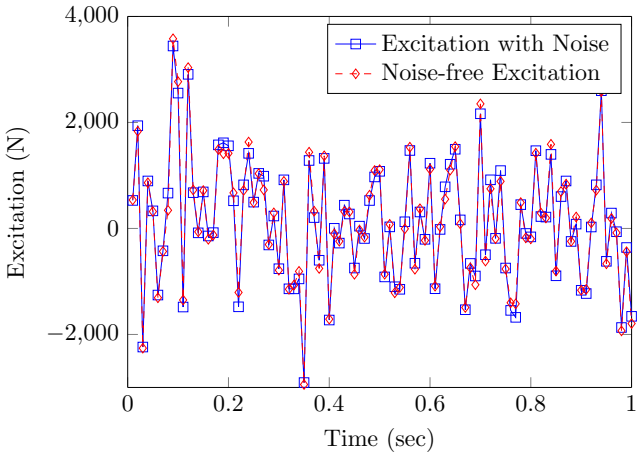

Figure 4.7: Effect of noise on excitation: 5-DOF, 5th story, 10% noise.

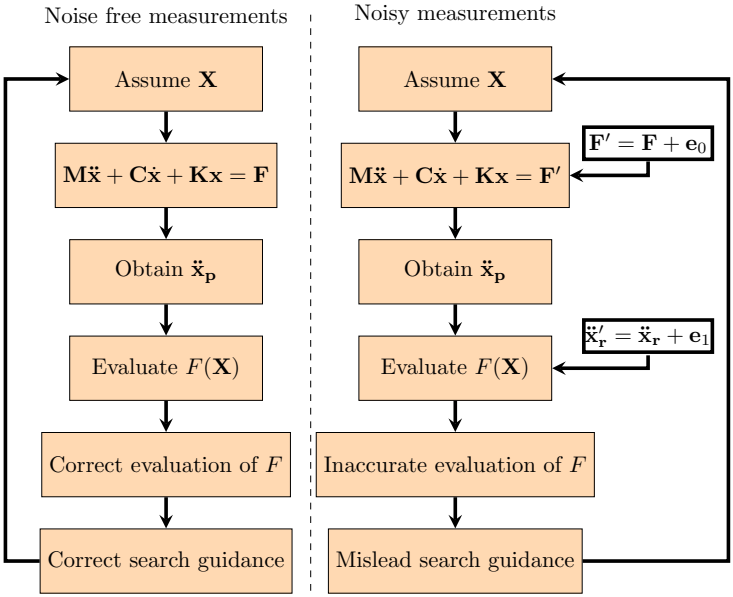

Figure 4.8: Effect of noise on identification accuracy.

optimization run, was taken identical to Koh and Perry [53] and is shown in Fig. 4.10.

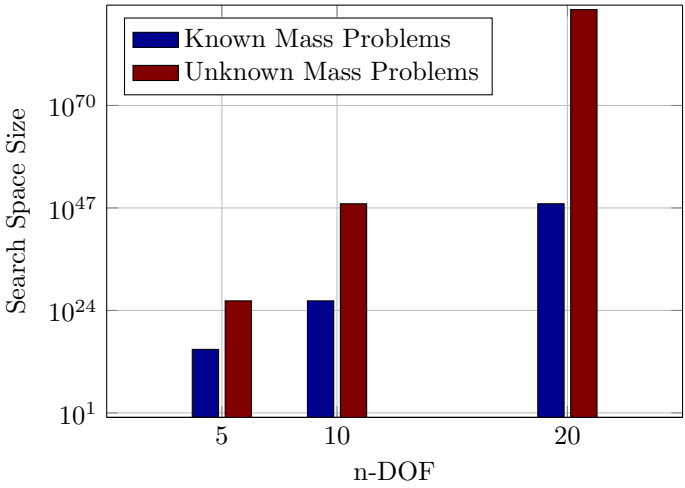

Figure 4.9: Search space size for various identification problems.

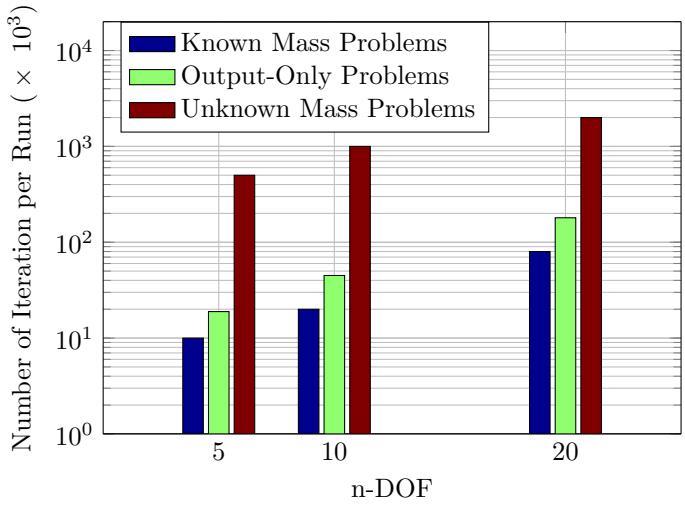

Figure 4.10: Number of iterations used for various identification problems.

Comparing the complexity of the problem with the invested calculation effort, it can be concluded that MARSHAL only requires a small fraction of the search space to converge to the optimum solution vector.

Results of Identification

The convergence of MARSHAL, i.e. the variation of the objective function value corresponding to the best solution stored in the HM during an optimization run, is plotted for a 20-DOF known mass identification subjected to 0% noise in Fig. 4.11. The second level (iteration level) search space reduction, which starts at the 400th iteration, has a significant positive effect on the convergence rate after some iterations, which is evident by the increase in slope. The reduction of the search space is shown in Fig. 4.12 for one of the stiffness parameters in the solution vector of a 5-DOF known mass identification problem.

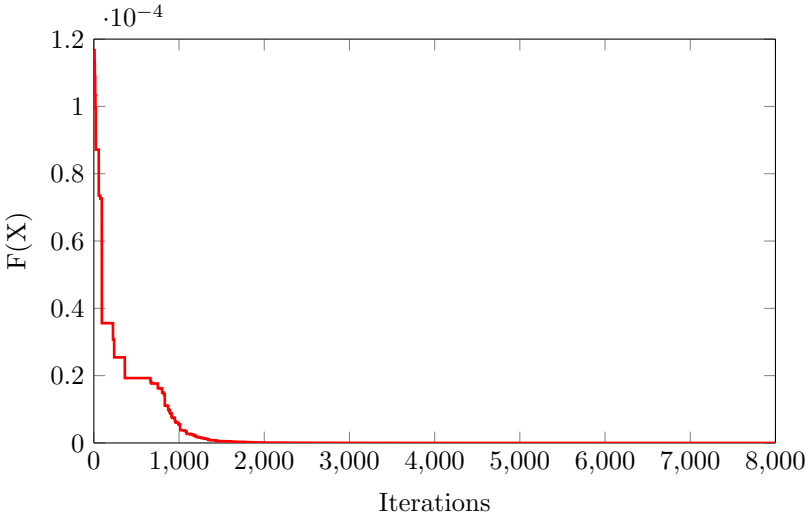

Figure 4.11: Convergence of identification run.

To demonstrate the behavior of the adapting control parameters (HMCR, PAR and LER) of MARSHAL, Fig. 4.13, 4.14 and 4.15 are presented.

The increase in HMCR is due to the increase in quality of the solutions inside the HM as the algorithm progresses through its iterations, thus a higher chance of obtaining an optimum solution is possible if the new solutions are derived from inside HM.

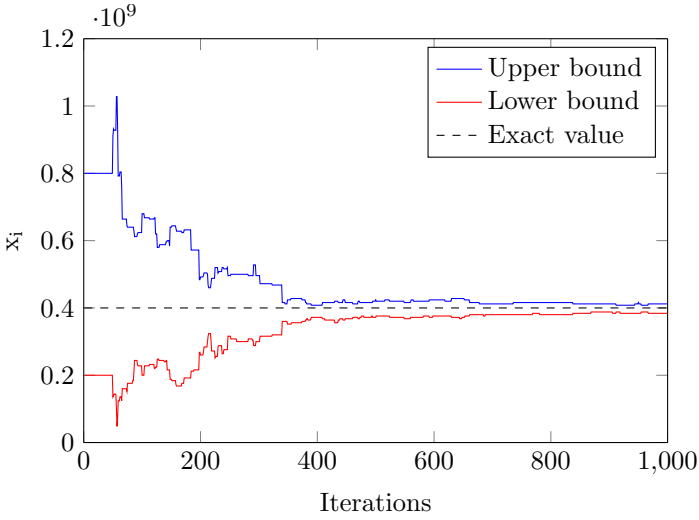

Figure 4.12: Iteration-level search space reduction: 5-DOF, variable k_1.

The PAR, however, decreases since the optimum solution at late stages could be a mere combination of the elements inside HM without the requirement of adjusting the pitch.

For the LER, a slightly increasing trend is noted. It was observed that the optimum solution was obtained by shifting two neighboring stiffness terms in opposite directions, which was the reason why the "local effect" was introduced in the first place. This was explained in detail in Sec. 2.3.2.

Since MARSHAL is a metaheuristic algorithm, the optimum results obtained from performing identical runs is not always identical. Thus it is necessary to perform averaging to obtain a representative result and get its scatter.

Once all 10 optimization runs are performed, the results are stored in a matrix, where each solution occupies a row, as follows:

$$\mathbf{X}_{opt} = \begin{bmatrix} k_{1,1} & k_{1,2} & \dots & k_{1,n} & m_{1,1} & m_{1,2} & \dots & m_{1,n} & \alpha_1 & \beta_1 \\ k_{2,1} & k_{2,2} & \dots & k_{2,n} & m_{2,1} & m_{2,2} & \dots & m_{2,n} & \alpha_2 & \beta_2 \\ \vdots & \vdots & \vdots & \vdots & \vdots & \vdots & \vdots & \vdots & \vdots & \vdots \\ k_{10,1} & k_{10,2} & \dots & k_{10,n} & m_{10,1} & m_{10,2} & \dots & m_{10,n} & \alpha_{10} & \beta_{10} \end{bmatrix}. \tag{4.1}$$

The results stored in $\mathbf{X}_{opt}$ are averaged to get a single representative structure per identification case, namely: the average optimum solution ($\mathbf{X}_{\mu}$).

An example of storing results in $\mathbf{X}_{opt}$ and averaging these results to get $\mathbf{X}_{\mu}$

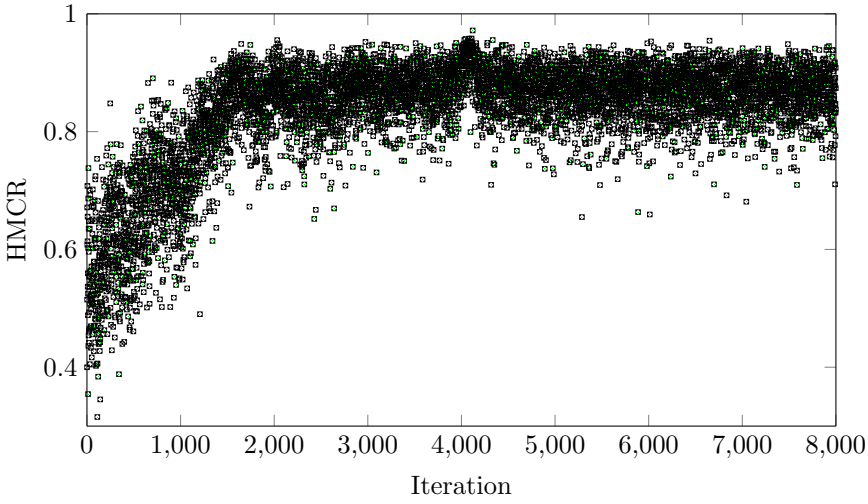

Figure 4.13: Variation of HMCR: 20-DOF, noise 0%.

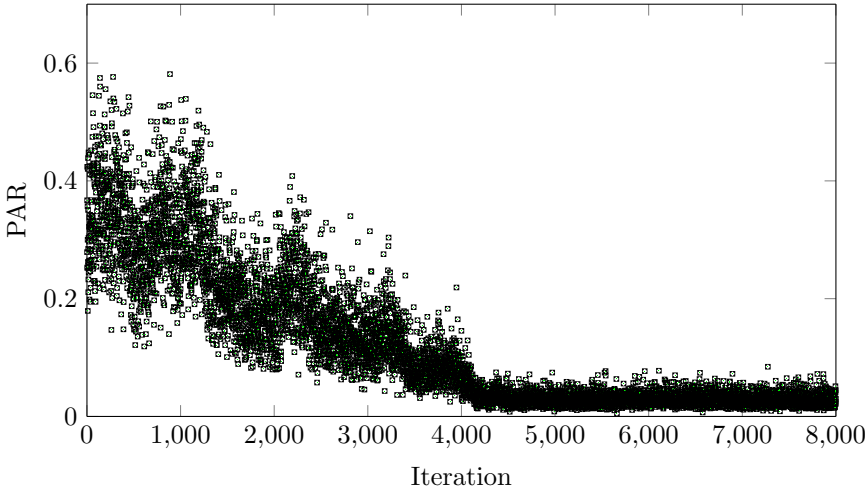

Figure 4.14: Variation of PAR: 20-DOF, noise 0%.

is shown in Table B.1. Furthermore, the scatter in the results is also evident in B.1. Such scatter is proportional to the step size being used. Thus, using

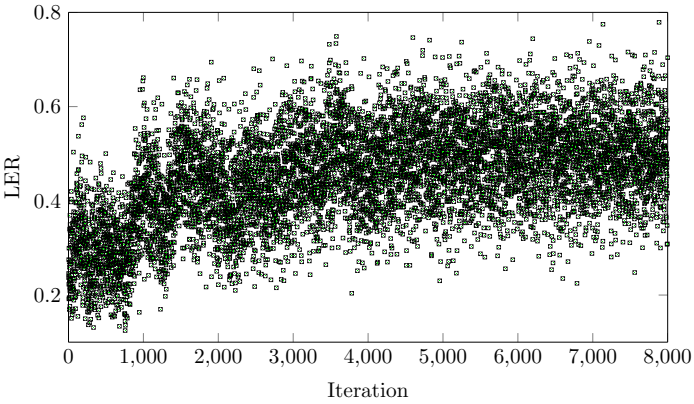

Figure 4.15: Variation of LER: 20-DOF, noise 0%.

a finer step size resolution improves the results, but comes with a price in the form of an increase in search space size. Additionally, $\mathbf{X}_\mu$ for all identification cases is detailed in Appendix B.

As evident from Appendix B, an abstract representation of obtained results should be adopted. Thus, for each average optimum result $\mathbf{X}_\mu$, 4 representative values corresponding to the average error in the identified stiffness ϵ_k, mass ϵ_m and damping ϵ_α and ϵ_β are defined as follows:

$$\epsilon_k = \frac{1}{n}\sum_{j=1}^{j=n}\frac{|k_j - k_j^0|}{k_j^0} \times 100\% \ , \tag{4.2}$$

where n is the number of DOFs, k_j is the $j-$th DOF stiffness stored in $\mathbf{X}_\mu$, k_j^0 is the $j-$th DOF stiffness of the original structure.

Similarly,

$$\epsilon_m = \frac{1}{n}\sum_{j=1}^{j=n}\frac{|m_j - m_j^0|}{m_j^0} \times 100\% \ , \tag{4.3}$$

$$\epsilon_\alpha = \frac{|\alpha - \alpha^0|}{\alpha^0} \times 100\% \tag{4.4}$$

and

$$\epsilon_\beta = \frac{|\beta - \beta^0|}{\beta^0} \times 100\% \ . \tag{4.5}$$

A comparison of the identification results obtained by MARSHAL and SSRM, in terms of the average stiffness error ϵ_k, is summarized in Fig. 4.16

through 4.21 for the case of known mass and unknown mass identification of the 20-,10- and 5-DOF structures, respectively. Detailed results can be found in Table 4.1 and 4.2. For each noise level and time history, the average error is calculated as per equation (4.2) through (4.5) and compared to the results obtained by Koh and Perry's modified Genetic Algorithm (SSRM) approach [53].

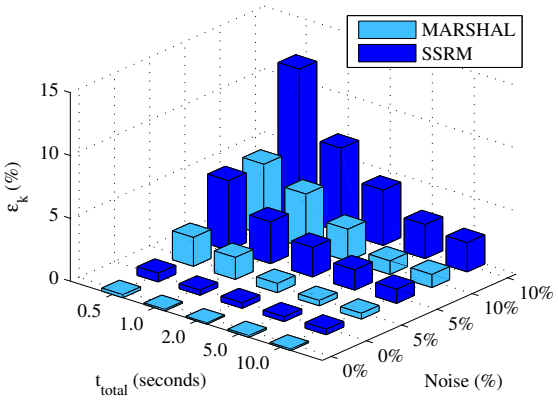

Figure 4.16: 20-DOF known mass identification results summary.

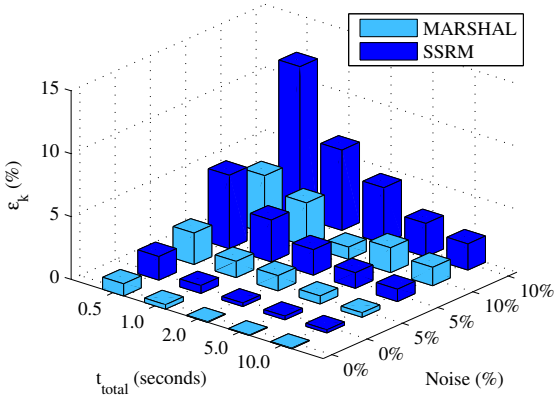

Figure 4.17: 20-DOF unknown mass identification results summary.

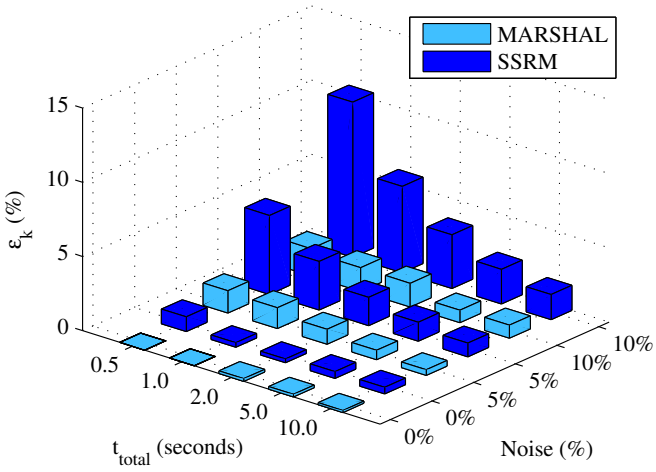

Figure 4.18: 10-DOF known mass identification results summary.

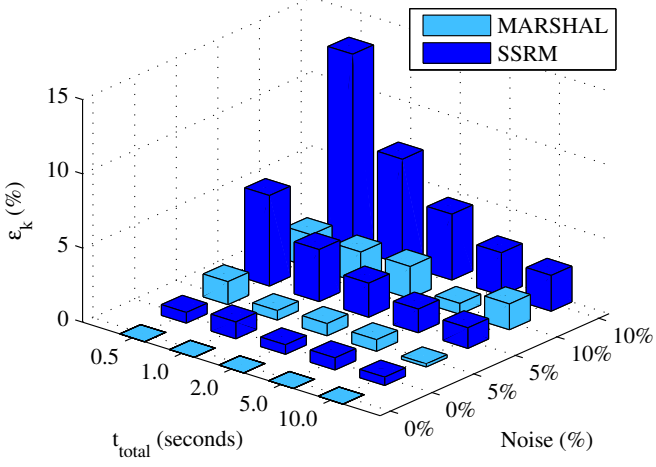

Figure 4.19: 10-DOF unknown mass identification results summary.

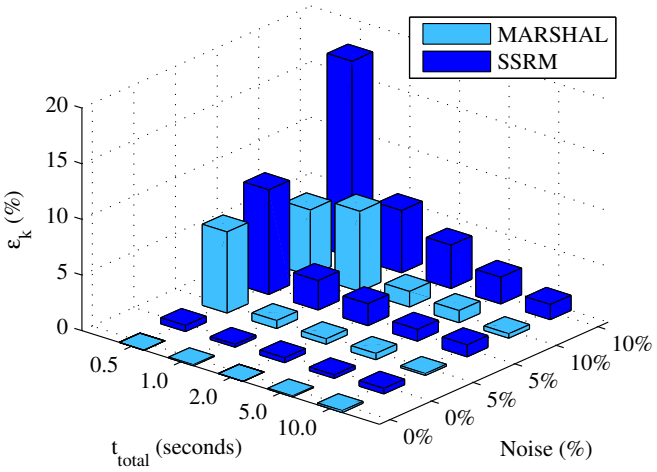

Figure 4.20: 5-DOF known mass identification results summary.

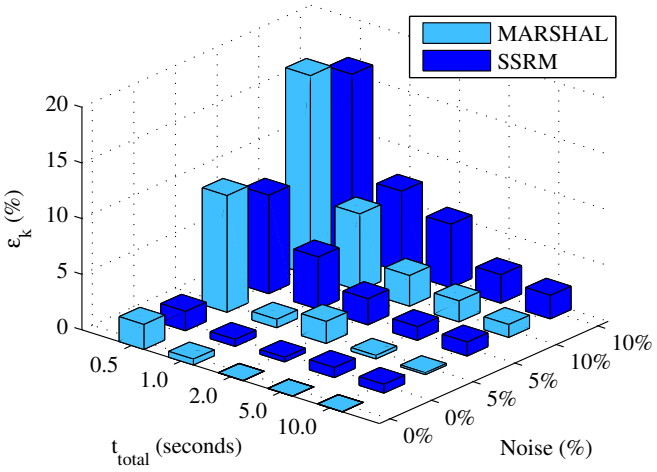

Figure 4.21: 5-DOF unknown mass identification results summary.

Table 4.1: Known mass identification results.

Noise (%)	t_{total} (seconds)	Structure 5-DOF ϵ_k	5-DOF ϵ_α	5-DOF ϵ_β	10-DOF ϵ_k	10-DOF ϵ_α	10-DOF ϵ_β	20-DOF ϵ_k	20-DOF ϵ_α	20-DOF ϵ_β
0	0.50	0.00	1.20	0.20	0.00	3.00	0.00	0.24	0.20	0.00
		[0.54]*	[—]**	[—]	[0.99]	[—]	[—]	[0.69]	[—]	[—]
	1.00	0.08	0.40	0.20	0.00	1.40	0.00	0.11	0.80	0.00
		[0.25]	[—]	[—]	[0.30]	[—]	[—]	[0.39]	[—]	[—]
	2.00	0.00	0.20	0.20	0.18	0.20	0.00	0.09	0.20	0.00
		[0.44]	[—]	[—]	[0.26]	[—]	[—]	[0.44]	[—]	[—]
	5.00	0.08	0.60	0.20	0.18	0.00	0.20	0.13	0.00	0.00
		[0.31]	[—]	[—]	[0.45]	[—]	[—]	[0.38]	[—]	[—]
	10.00	0.16	0.40	0.40	0.14	0.40	0.00	0.11	0.20	0.00
		[0.50]	[—]	[—]	[0.45]	[—]	[—]	[0.44]	[—]	[—]
5	0.50	7.28	21.20	12.60	1.50	12.20	0.20	2.29	62.20	0.40
		[9.40]	[—]	[—]	[5.32]	[—]	[—]	[5.55]	[—]	[—]
	1.00	0.72	2.00	0.60	1.40	9.40	0.40	1.75	13.60	0.20
		[2.64]	[—]	[—]	[3.27]	[—]	[—]	[3.33]	[—]	[—]
	2.00	0.48	3.40	1.20	1.00	1.80	1.60	0.73	5.00	0.40
		[1.96]	[—]	[—]	[1.90]	[—]	[—]	[2.34]	[—]	[—]
	5.00	0.56	2.40	1.40	0.64	4.00	0.20	0.42	6.60	0.60
		[1.06]	[—]	[—]	[1.28]	[—]	[—]	[1.61]	[—]	[—]
	10.00	0.16	1.60	0.60	0.38	2.60	0.80	0.46	0.40	0.20
		[1.07]	[—]	[—]	[0.92]	[—]	[—]	[1.11]	[—]	[—]
10	0.50	5.92	122.40	39.80	1.84	3.00	1.20	5.61	149.00	5.60
		[17.61]	[—]	[—]	[10.45]	[—]	[—]	[11.92]	[—]	[—]
	1.00	7.20	23.00	3.80	1.60	5.60	1.00	4.29	28.20	1.40
		[5.59]	[—]	[—]	[5.82]	[—]	[—]	[6.68]	[—]	[—]
	2.00	1.40	12.60	17.00	1.60	14.80	0.40	2.54	10.20	1.00
		[3.88]	[—]	[—]	[3.61]	[—]	[—]	[4.40]	[—]	[—]
	5.00	1.08	1.40	4.00	0.84	10.20	0.40	1.07	33.60	0.60
		[2.40]	[—]	[—]	[2.34]	[—]	[—]	[2.70]	[—]	[—]
	10.00	0.40	7.80	0.40	0.88	12.00	1.80	1.04	6.60	0.20
		[1.36]	[—]	[—]	[1.69]	[—]	[—]	[2.32]	[—]	[—]

* Bracketed results represent those obtained by Koh and Perry [53].

** No results were reported.

Table 4.2: Unknown mass identification results.

Noise (%)	t_{total} (seconds)	Structure 5-DOF ϵ_k	5-DOF ϵ_m	5-DOF ϵ_α	5-DOF ϵ_β	10-DOF ϵ_k	10-DOF ϵ_m	10-DOF ϵ_α	10-DOF ϵ_β	20-DOF ϵ_k	20-DOF ϵ_m	20-DOF ϵ_α	20-DOF ϵ_β
0	0.50	2.24	1.72	11.60	0.20	0.00	0.00	0.00	0.00	0.96	0.62	11.80	0.00
		[1.74]*	[—]**	[—]	[—]	[0.72]	[—]	[—]	[—]	[1.88]	[—]	[—]	[—]
	1.00	0.52	0.44	4.00	0.20	0.00	0.00	0.00	0.00	0.35	0.40	3.00	0.00
		[0.62]	[—]	[—]	[—]	[1.13]	[—]	[—]	[—]	[0.62]	[—]	[—]	[—]
	2.00	0.00	0.00	0.00	0.00	0.00	0.00	0.00	0.00	0.04	0.06	0.20	0.00
		[0.41]	[0.40]	[—]	[—]	[0.64]	[0.56]	[—]	[—]	[0.28]	[0.32]	[—]	[—]
	5.00	0.00	0.00	0.40	0.20	0.00	0.00	0.00	0.00	0.04	0.02	0.00	0.00
		[0.90]	[—]	[—]	[—]	[0.81]	[—]	[—]	[—]	[0.29]	[—]	[—]	[—]
	10.00	0.00	0.00	0.00	0.00	0.00	0.00	0.00	0.00	0.04	0.04	0.00	0.00
		[0.78]	[—]	[—]	[—]	[0.56]	[—]	[—]	[—]	[0.25]	[—]	[—]	[—]
5	0.50	10.48	9.08	81.40	6.80	1.54	1.20	19.00	1.60	2.49	2.40	113.60	0.00
		[8.83]	[—]	[—]	[—]	[6.09]	[—]	[—]	[—]	[5.84]	[—]	[—]	[—]
	1.00	0.76	1.44	17.20	3.00	0.64	0.80	22.80	1.80	1.29	1.85	10.00	0.20
		[4.68]	[—]	[—]	[—]	[3.50]	[—]	[—]	[—]	[3.33]	[—]	[—]	[—]
	2.00	1.96	1.08	3.20	3.00	0.82	0.74	2.80	0.40	1.21	0.90	16.60	0.40
		[2.34]	[—]	[—]	[—]	[2.29]	[—]	[—]	[—]	[2.02]	[—]	[—]	[—]
	5.00	0.32	0.44	0.40	0.80	0.78	0.62	4.00	0.60	0.64	0.56	10.00	0.40
		[1.23]	[—]	[—]	[—]	[1.59]	[—]	[—]	[—]	[1.24]	[—]	[—]	[—]
	10.00	0.16	0.20	0.60	0.40	0.20	0.24	1.00	0.20	0.35	0.37	0.60	0.20
		[1.25]	[—]	[—]	[—]	[1.38]	[—]	[—]	[—]	[0.98]	[—]	[—]	[—]
10	0.50	17.92	13.68	42.80	19.60	2.20	2.08	31.00	1.20	4.56	4.82	40.40	4.60
		[16.36]	[—]	[—]	[—]	[13.11]	[—]	[—]	[—]	[11.98]	[—]	[—]	[—]
	1.00	6.88	11.52	57.80	6.00	2.08	1.56	7.00	3.80	3.44	3.53	75.80	1.00
		[7.25]	[—]	[—]	[—]	[7.09]	[—]	[—]	[—]	[6.39]	[—]	[—]	[—]
	2.00	2.76	2.32	13.80	2.00	2.16	2.42	2.20	0.00	0.97	1.21	5.80	0.00
		[5.69]	[—]	[—]	[—]	[4.43]	[—]	[—]	[—]	[4.44]	[—]	[—]	[—]
	5.00	1.88	2.00	2.00	1.20	0.72	1.14	10.40	2.20	1.97	1.80	5.40	1.00
		[2.55]	[—]	[—]	[—]	[2.88]	[—]	[—]	[—]	[2.65]	[—]	[—]	—
	10.00	1.16	1.12	7.00	0.40	1.74	1.54	1.60	0.80	1.47	1.32	4.60	0.20
		[2.11]	[—]	[—]	[—]	[2.41]	[—]	[—]	[—]	[2.08]	[—]	[—]	[—]

* Bracketed results represent those obtained by Koh and Perry [53].

** No results were reported.

Considering the results obtained in Table 4.1 and 4.2, it can be noted that:

- MARSHAL approach was superior to the modified hybrid GA based approach, as it was capable of identifying the considered structures in almost all identification cases with less error while using the same calculation effort as in [53].
- At 0% noise, the algorithm was sometimes capable of obtaining the target structure exactly (error = 0%).
- The adverse effect of noise can be decreased by considering longer time histories, as such help averaging the noise out. This can be concluded when comparing the results obtained using shorter time histories with those of longer time histories.
- Even at extreme noise values (10%), the algorithm provided satisfying results. For instance, the 10-DOF shear frame at 10% noise and 10 seconds long time history was identified with an average stiffness error of 0.88% for the known mass identification, and an average error of 1.74% and 2.02% for stiffness and mass for the unknown mass identification, respectively.
- The identification of damping is very sensitive to noise. Furthermore, it was noticed that the identification of damping parameter α was less accurate than β, which is due to the fact that the contribution of structural stiffness in the damping matrix is significantly larger than that of mass, resulting in the identification of β being more accurate than α.

4.1.2 Output-Only Structural Identification

Since the measurement of excitations is not always possible or feasible outside the laboratory, an advanced structural identification scheme, namely: the output-only identification scheme becomes necessary. In output-only identification, input excitations are predicted since these are not given. The theoretical and mathematical formulation of an output-only identification problem as an optimization problem was discussed in Sec. 3.2.3.

Since the results obtained are compared with Koh and Perry [53], a similar method of generating a smoothed, yet random, excitation history was used. That is, random excitation points were generated every 20 time increments using a WGN with RMS of 1000 Newtons, then, the intermediate points are filled using interpolation functions to obtain a smoothed excitation history. Such a smoothed random excitation is presented in Fig. 4.22.

The structural characteristics, excitation application DOFs and measured DOFs are provided in Fig. 4.3 through 4.5.

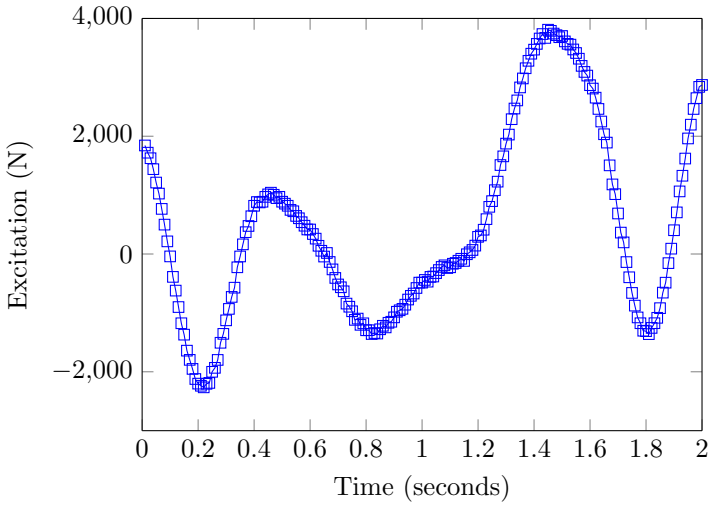

Figure 4.22: Smoothed random generated excitation.

It shall be mentioned that output-only problems are essentially known mass identification problems. The requirement of mass being known a priori ensures the uniqueness of the solution. Such assumption can be justified as, in most engineering structures, it is possible to accurately approximate structural mass.

It is assumed that the structure is initially at rest and that the location of excitations are known. Mass is assumed to be known and damping is assumed to be of Rayleigh damping. It is also important that the vibration response is available for the DOF at which excitation is applied as well as the adjacent DOFs. Other DOFs may or may not be available.

The search space size for output-only problems is identical to those of the known mass identification since the unknown force is not included in the solution vector, but is approximated, as explained in Sec. 3.2.3. The invested calculation effort, in the form of the number of iterations per run, is shown in Fig. 4.10. Once again, the invested effort is only a fraction of the problem's search space.

For each output-only identification case, 10 optimization runs, consisting of 15 sub-runs, were performed, with the same results extraction methodology as in Sec. 4.1.1. Detailed results can also be found in Appendix B.

For comparison purposes, a data reduction scheme identical to that implemented in Koh and Perry [53] is used. That is, the length of time history

is reduced to 40% after 50% of iterations are evaluated. The aim of such reduction is to decrease the calculation effort. Initial time history lengths of 0.5 and 1.0 second discretized into 0.001 second increments were used. Although apparently looking short, these time histories are consisted of 500 and 1000 data points, which are, quantitatively speaking, as much as a 5 and 10 second time history discretized into 0.01 seconds. Furthermore, noise percentages of 0%, 2%, 5% and 10% were tested. It is noted that a finer time increment is used in output-only problems than that used in normal identification problems, which was recommended by a preliminary study performed by Koh and Perry [53].

Results of Identification

Since the convergence rate, behavior of the adapting control parameters and the reduction of the search space were similar to those in Sec. 4.1.1, these issues will not be addressed again in future structural identification problems.

Satisfying results were obtained, as summarized in Fig. 4.23 and detailed in Table 4.3. A comparison between the identified force and the actual applied force is shown in Fig. 4.24, 4.25 and 4.26 for a 5-, 10- and 20-DOF structure at 10% noise, respectively.

With regard to these results, following conclusions could be drawn:

- MARSHAL proved to be a versatile identification algorithm, as it was modified to investigate output-only problems with minimum effort and no compatibility issues what so ever.
- The predictor-corrector scheme implemented in MARSHAL approximated the applied excitations on the structure satisfactorily. Even at extreme noises of 10%, little deviation was found in the identified forces.
- In most of the cases, MARSHAL was capable of competing and even surpassing the SSRM, proving once again that it is a promising algorithm to be used in structural identification problems.
- MARSHAL's results improved as the length of the time history increases. Furthermore, obtaining an error of less than 1% at noise levels as high as 10% is quite satisfying.

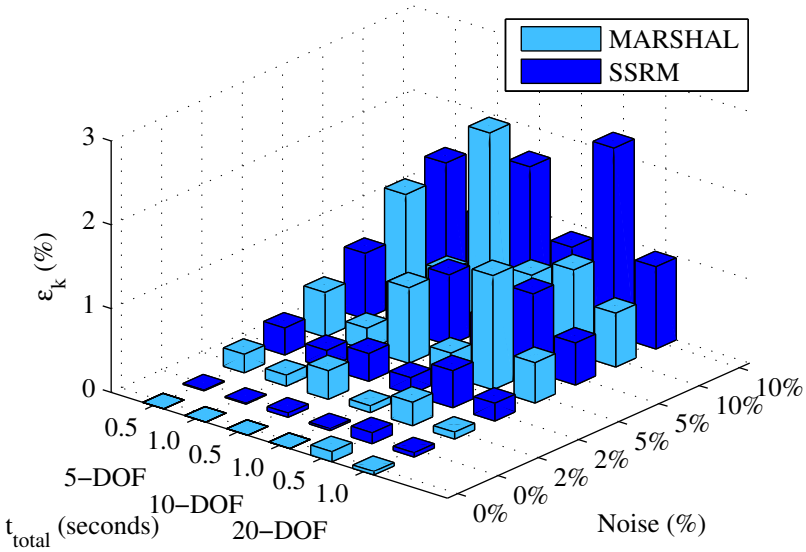

Figure 4.23: Output-only identification results summary.

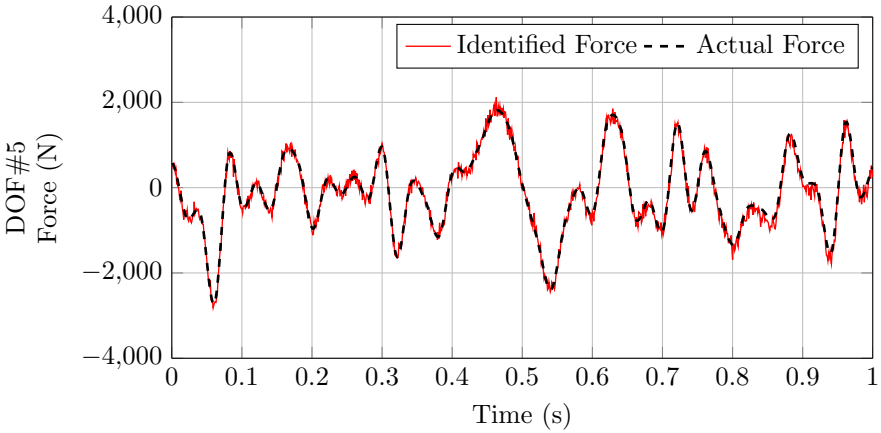

Figure 4.24: Identified vs. actual force: 5-DOF, noise 10%.

Table 4.3: Output-only identification results.

Noise (%)	t_{total} (seconds)	Structure 5-DOF ϵ_k	5-DOF ϵ_α	5-DOF ϵ_β	10-DOF ϵ_k	10-DOF ϵ_α	10-DOF ϵ_β	20-DOF ϵ_k	20-DOF ϵ_α	20-DOF ϵ_β
0	0.50/0.20	0.12	3.60	0.20	0.00	0.00	0.00	0.00	0.00	0.00
		[0.13]*	[—]**	[—]	[0.05]	[—]	[—]	[0.01]	[—]	[—]
	1.00/0.40	0.04	0.00	0.00	0.00	0.00	0.00	0.00	0.00	0.00
		[0.05]	[—]	[—]	[0.02]	[—]	[—]	[0.01]	[—]	[—]
2	0.50/0.20	0.28	6.00	0.60	0.34	14.60	0.40	0.22	16.40	0.20
		[0.44]	[—]	[—]	[0.33]	[—]	[—]	[0.32]	[—]	[—]
	1.00/0.40	0.08	9.80	1.00	0.08	3.60	0.00	0.13	5.20	0.00
		[0.21]	[—]	[—]	[0.20]	[—]	[—]	[0.21]	[—]	[—]
5	0.50/0.20	1.36	31.40	7.60	0.90	45.40	0.80	0.53	46.80	0.40
		[0.93]	[—]	[—]	[0.84]	[—]	[—]	[0.78]	[—]	—
	1.00/0.40	0.48	5.80	1.00	0.28	1.20	0.40	0.26	15.20	0.00
		[0.50]	[—]	[—]	[0.47]	[—]	[—]	[0.52]	[—]	[—]
10	0.50/0.20	1.00	25.60	1.00	2.32	31.60	2.80	1.27	28.00	1.40
		[2.24]	[—]	[—]	[1.70]	[—]	[—]	[1.43]	[—]	[—]
	1.00/0.40	0.64	9.80	2.20	0.78	0.40	0.60	0.51	36.20	0.00
		[0.98]	[—]	[—]	[0.90]	[—]	[—]	[0.93]	[—]	[—]

* Bracketed results represent those obtained by Koh and Perry [53].
** No results were reported.

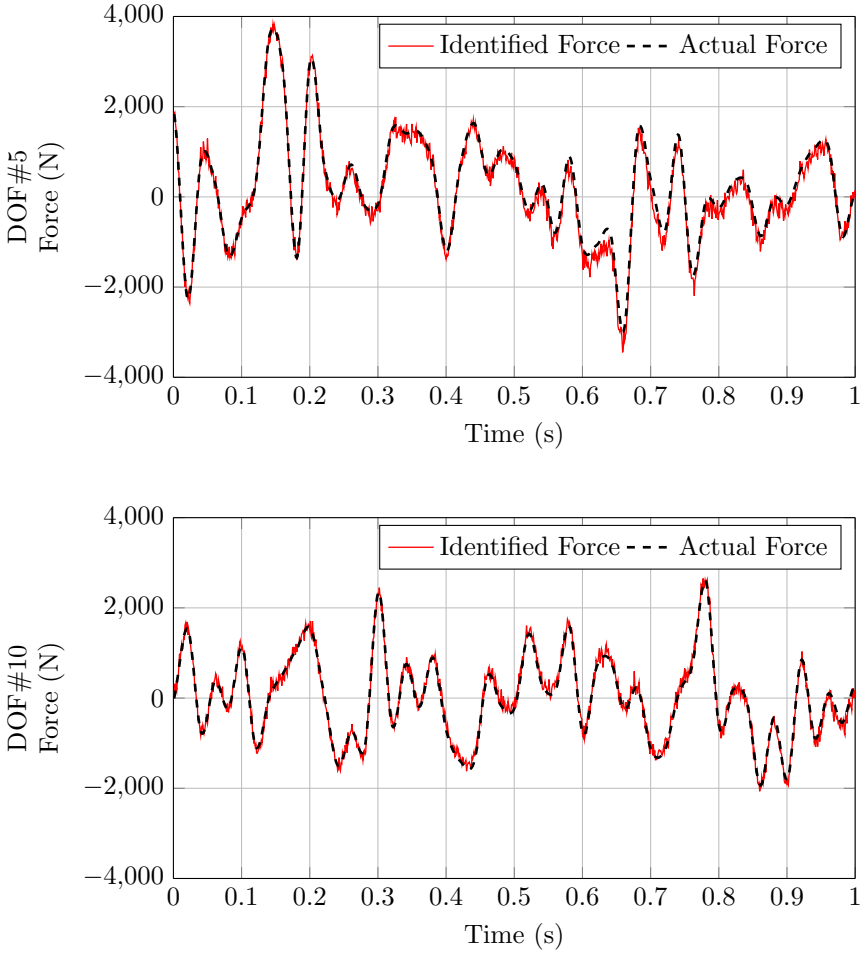

Figure 4.25: Identified vs. actual force: 10-DOF, noise 10%.

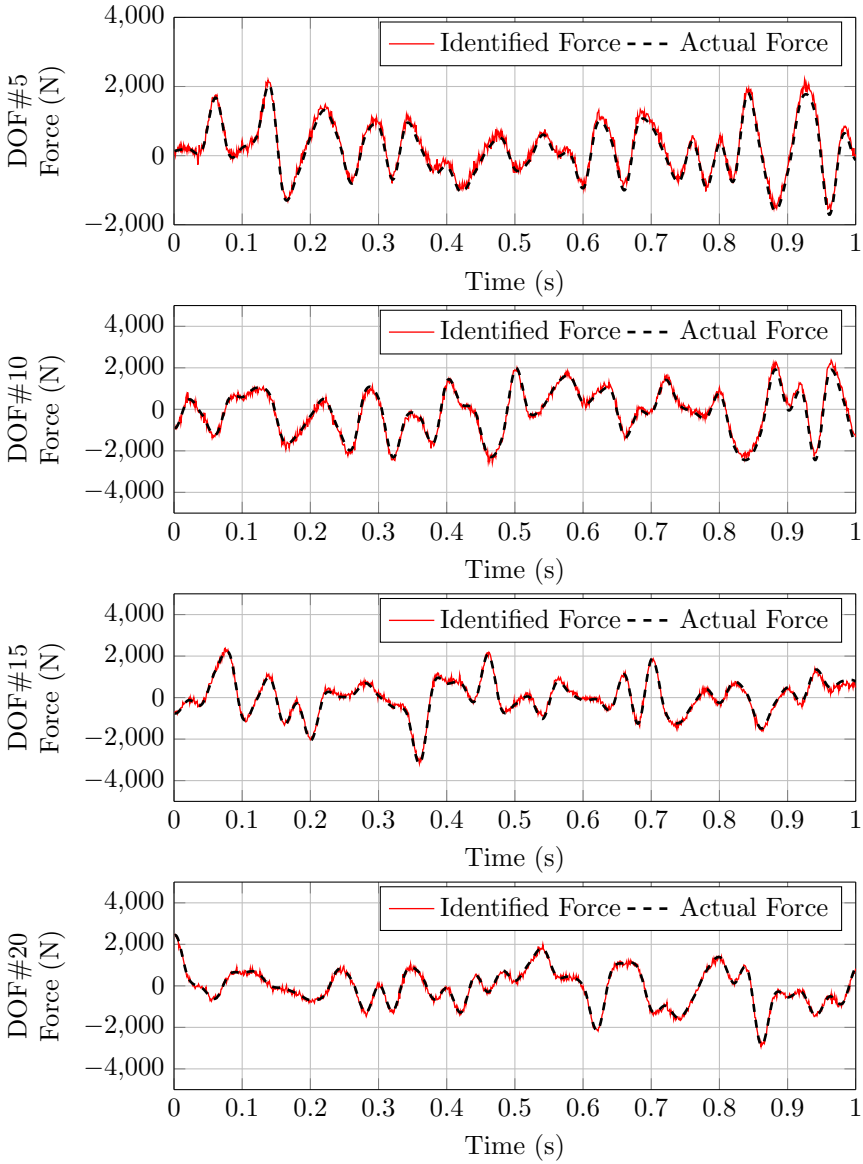

Figure 4.26: Identified vs. actual force: 20-DOF, noise 10%.

4.2 Structural Identification of Offshore Wind Turbines

Motivated by the promising results obtained for two-dimensional shear frames, the challenging problem of offshore wind turbines (WTs) is considered.

A 5-MW reference wind turbine for offshore system development, defined by Jonkman et al. of the National Renewable Energy Laboratory (NREL) [43], is considered. The geometry and structural characteristics of the Rotor Nacelle Assembly (RNA) and blades as well as the control systems of the considered turbine are taken "as is" from Jonkman et al. [43]. For the turbine tower and monopile supporting structure, the values used in the OC3 final report by Jonkman and Musial [44] are adopted. The structural characteristics of the turbine supporting structure define a monopile of 30m height (+10 m above the MSL) having an outer diameter of 6m and a wall thickness of 0.06m followed by a tower of 77.6m height having a tapering cross section which starts at +10m MSL with a diameter of 6m and wall thickness of 0.027m, and ends at +87.6m MSL with a diameter of 3.87m and wall thickness of 0.019m. These characteristics are summarized in Fig. 4.27 and detailed in the "tower file" provided in Appendix A.

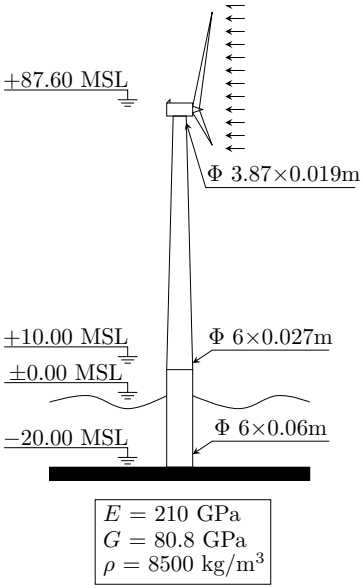

Figure 4.27: Structural characteristics of considered offshore wind turbine.

The turbine's supporting structure, i.e. tower and monopile, are defined using 16 input stations. It is assumed that the turbine blades are facing wind directly, thus fore-after accelerations are dominant. A turbulent inflow wind was generated using an open source software called TurbSim, also provided by NREL. The generated inflow wind has a characteristic wind speed of 10 m/s. To limit the influence of RNA dynamics, the turbine was set to idling, i.e. its RPM ≈ 0.

Due to the complexity of the problem, only stiffness parameters are identified and a rather narrower search space than that used in two-dimensional shear frames is assumed. That is, the upper bounds, lower bounds and step sizes for all elements in the solution vector are 100%, 50% and 1%, of the undamaged fore-after stiffness values respectively, creating a search space of $N_{SS} = 2.0947 \times 10^{27}$ possible solutions. Implicitly assumed in these bounds is that damage results in the decrease of the stiffness of a structure.

A variety of identification and damage detection cases, summarized in Table 4.4, were considered to study the effect of the number of sensors, sensor location, damage magnitude and noise percentage. The sensors are applied at locations that are above the MSL for practical considerations. In all cases damage is applied to the 6th input station of the supporting structure in the form of a reduction in the fore-after stiffness. This input station corresponds to the location that is just above the transition piece, which connects the monopile with the turbine tower. The tower is grouted to such transition piece, creating a potential location for damage propagation. The magnitude of damage can be represented by a Damage Index (DI), defined as follows:

$$DI = \{DI_1, DI_2, \ldots, DI_{NVAR}\} \ , \tag{4.6}$$

where $NVAR$ is the number of variables in the solution vector, i.e. $length(\mathbf{X})$, and

$$DI_j = \frac{k_j^0 - k_j^d}{k_j^0} \times 100\% \ , \tag{4.7}$$

where k_j^0 and k_j^d are the undamaged and damaged stiffness values of the $j-$th input station.

To start with, the performance of MARSHAL is first tested for different damage magnitudes while using a constant number of 10 sensors and a 0% noise value. The results, as will be detailed later on in this section, show that MARSHAL is unaffected by the damage magnitude, i.e. has approximately the same identification accuracy regardless of the damage magnitude. Thus, to finalize, the performance of MARSHAL is then tested using a variety of sensor and noise scenarios while keeping the damage magnitude at a constant 10%.

Table 4.4: Offshore wind turbine identification cases.

Number of Sensors (N_S)	Sensor Location	Noise (%)	DI_6 (%)
10	Station No. 4, 5, 6, 7, 8, 9, 11, 13, 14, 16	0	10
6	Station No. 5, 6, 8, 10, 12, 16	2	5
1	Station No. 16	5	3
		10	0

Significant effort was required for coupling FAST with MARSHAL, as MARSHAL was programmed in MatLab whilst FAST uses Fortran. This required an interface routine that generates a "tower file" for FAST from MARSHAL's assumed solution vector, calculates the required mode shape characteristics via an open source program called BMODES, then passes it to FAST, commands FAST to perform its aero-elasto-hydro-servo analysis, and extracts the required vibration data from FAST's output file to pass it back to MARSHAL.

For each identification case, 10 optimization runs were performed, having a total of 16,000 iterations, and subdivided into 8 sub-runs of 2,000 iterations each. Once all runs are performed, the results are stored in $\mathbf{X}_{opt}$ and averaged to obtain the representative average optimum solution $\mathbf{X}_{\mu}$. Once $\mathbf{X}_{\mu}$ is obtained, the damage index for each input station DI_j is calculated according to equation (4.7). Furthermore, the average error in the identified stiffness ϵ_k of $\mathbf{X}_{\mu}$ is calculated in accordance with equation (4.2). Detailed results showing the damage index for all considered identification cases are reported in Appendix C.

A time history of 2 seconds discretized into 0.01 second increments is used for noise free signals, and is increased to 10 seconds with a finer discretization of 0.001 seconds when identifying damage using noisy signals.

Results of Identification

A convergence history similar to that shown in Fig. 4.11 was obtained. As the algorithm progresses, the average of the structures stored within the Harmony Memory (HM) as well as the best structure, corresponding to the lowest objective function, converge to the real/correct structure. This is shown in Fig. 4.28, 4.29 and 4.30, for three different stages, namely: early stage (shortly after beginning the sub-run), middle stage (at around 50% of iterations) and final stage (near end of sub-run), respectively.

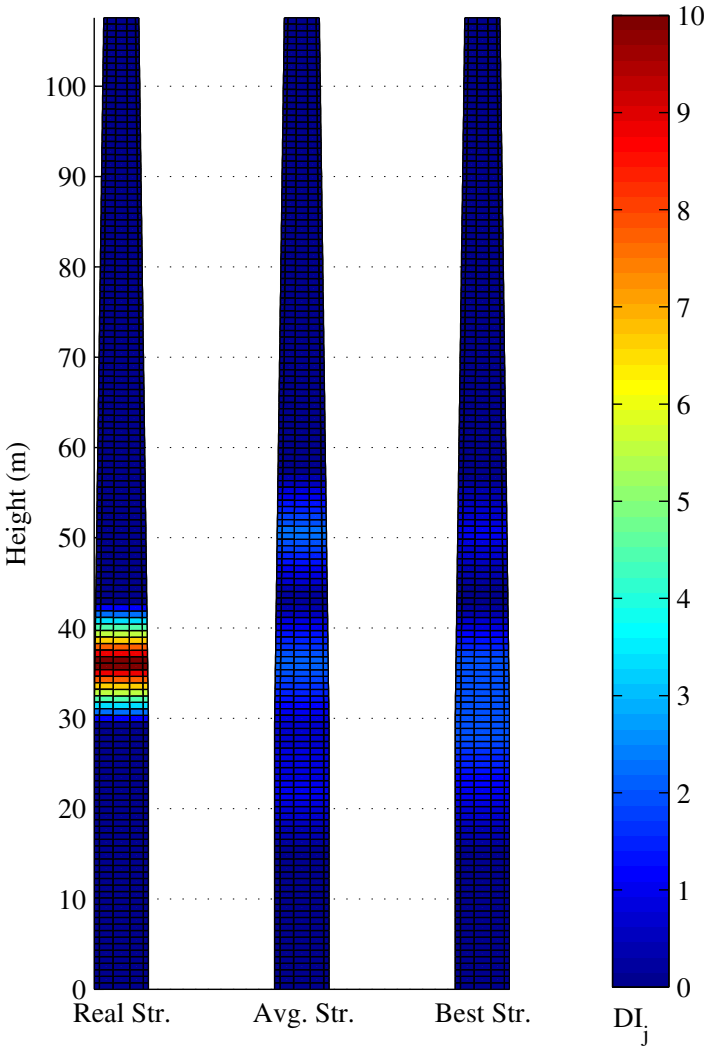

Figure 4.28: Early stage identified structures.

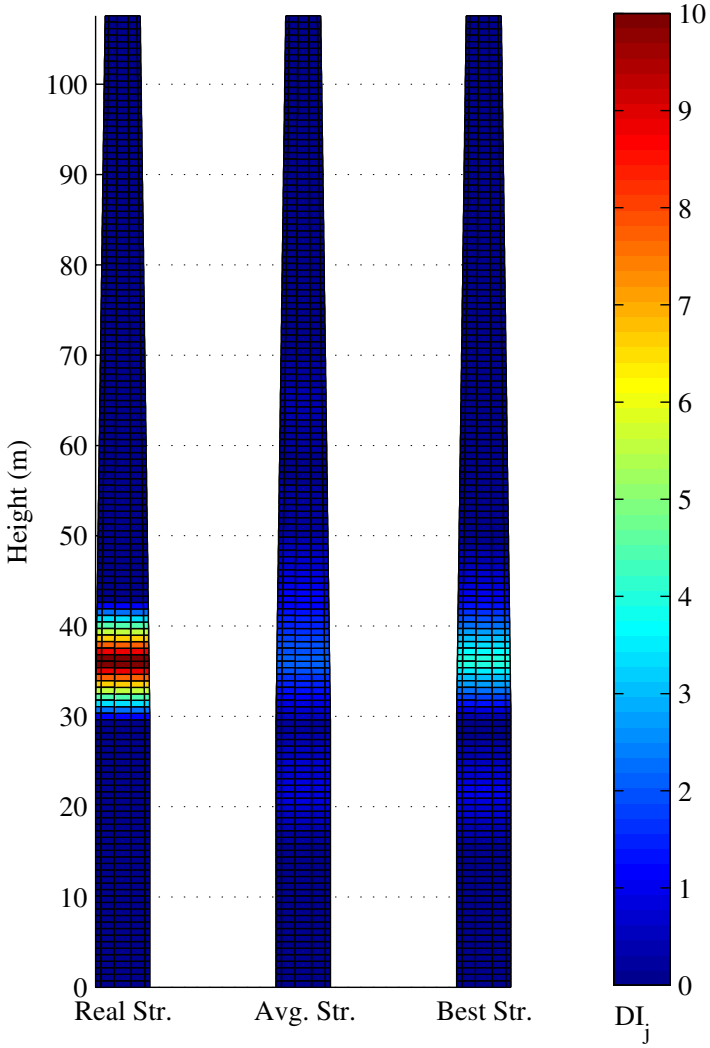

Figure 4.29: Middle stage identified structures.

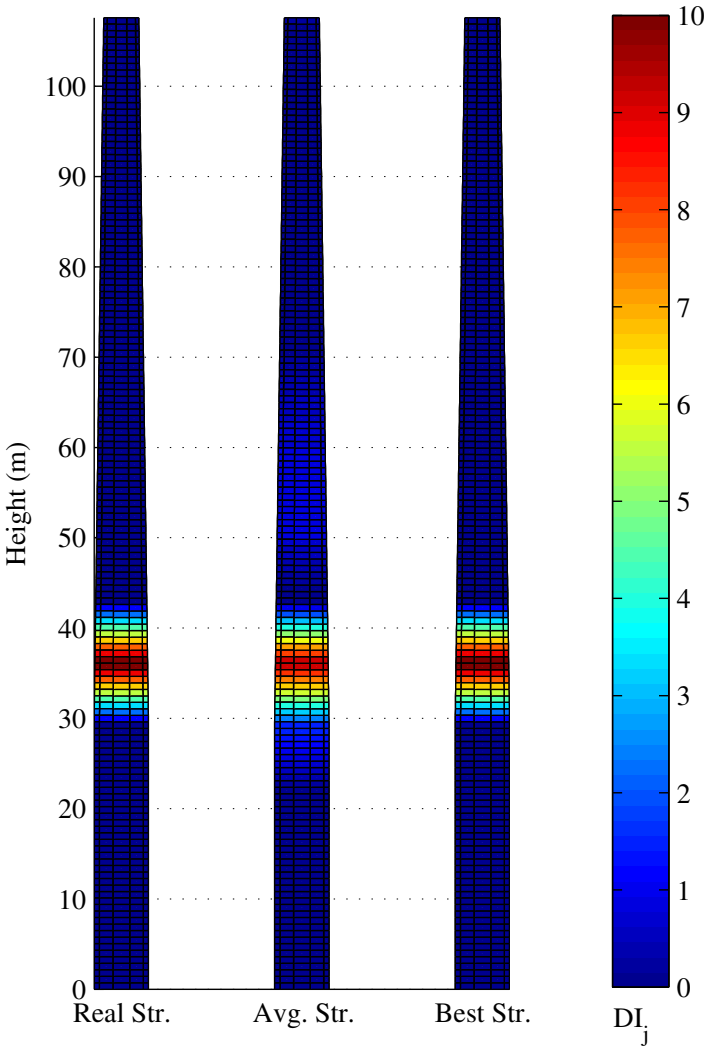

Figure 4.30: Final stage identified structures.

To assess the effect of damage magnitude on the accuracy of the algorithm, a variety of damage values for station No. 6 were tested, namely: 10%, 5%, 3% and 0% . Here, the number of sensors was set to 10 and no noise was considered. Results obtained from these setups are detailed in Table 4.5.

Furthermore, the influence of various sensor scenarios is considered for a variety of noise percentages. These results are detailed in Table 4.6 and further summarized in Fig. 4.31, 4.32 and 4.33.

Table 4.5: Identification results: Damage magnitude effect.

DI (%)	ϵ_k (%)	Identified DI (%) at station No. 1	2	3	4	5	6	7	8	9	10	11	12	13	14	15	16
10	0.0063	0	0	0	0	0	10.1	0	0	0	0	0	0	0	0	0	0
5	0.0000	0	0	0	0	0	5	0	0	0	0	0	0	0	0	0	0
3	0.0000	0	0	0	0	0	3	0	0	0	0	0	0	0	0	0	0
0	0.0125	0	0	0	0	0.1	0	0	0.1	0	0	0	0	0	0	0	0

Table 4.6: Identification results: Sensor effect.

N_S	Noise (%)	ϵ_k (%)	Identified DI (%) at station No. 1	2	3	4	5	6	7	8	9	10	11	12	13	14	15	16
10	0	0.00	0	0	0	0	0	10.0	0	0	0	0	0	0	0	0	0	0
	2	0.04	0	0	0	0	0.1	9.6	0.1	0	0	0	0	0	0	0	0	0
	5	0.14	0	0	0	0.2	0.4	8.8	0.4	0	0	0	0	0	0	0	0	0
	10	0.18	0	0	0	0.1	0.1	8.7	0.3	0.9	0.1	0	0	0	0	0.1	0	0
6	0	0.06	0	0	0	0.1	0.2	9.3	0	0	0	0	0	0	0	0	0	0
	2	0.14	0	0	0	0.2	0.4	8.9	0.5	0	0	0	0	0	0	0	0	0
	5	0.31	0	0	0	0.5	0.6	7.6	0.9	0.3	0	0	0	0	0	0	0	0.2
	10	0.36	0	0	0	0.3	0.3	6.3	0.2	1.0	0	0	0	0	0	0.3	0	0
1	0	0.27	0	0	0	0.5	1.2	9.2	0.6	0.7	0	0.2	0	0	0	0	0	0.2
	2	0.26	0	0	0	0.4	0.8	8.1	0	0.4	0	0	0	0	0	0	0	0.6
	5	0.70	0	0	0	1.2	0.8	3.2	0.4	1.6	0	0	0	0	0	0	0	0.4
	10	0.60	0	0	0	0.6	2.0	4.8	0.4	0.2	0.4	0.4	0	0	0	0.2	0	0.2

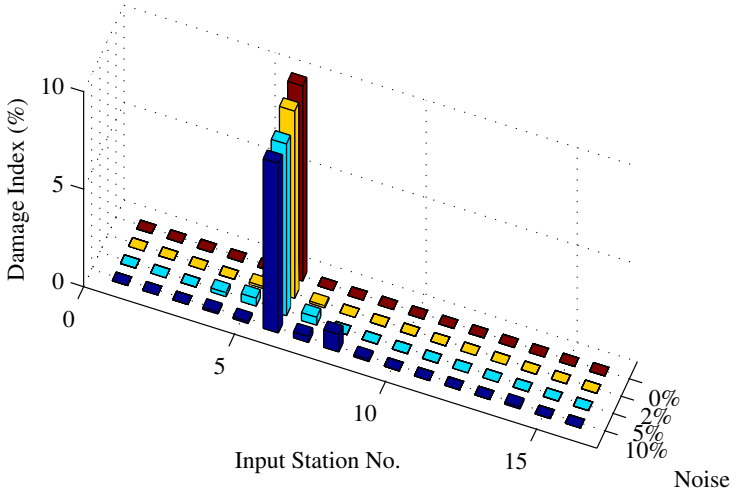

Figure 4.31: Identification results: 10 Sensors.

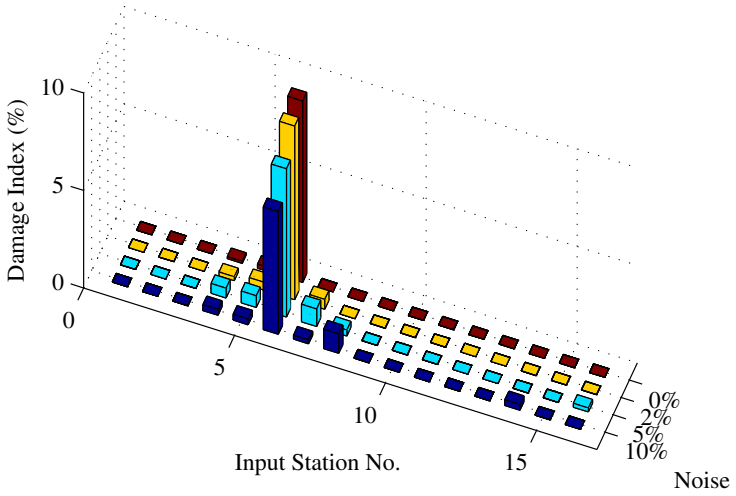

Figure 4.32: Identification results: 6 Sensors.

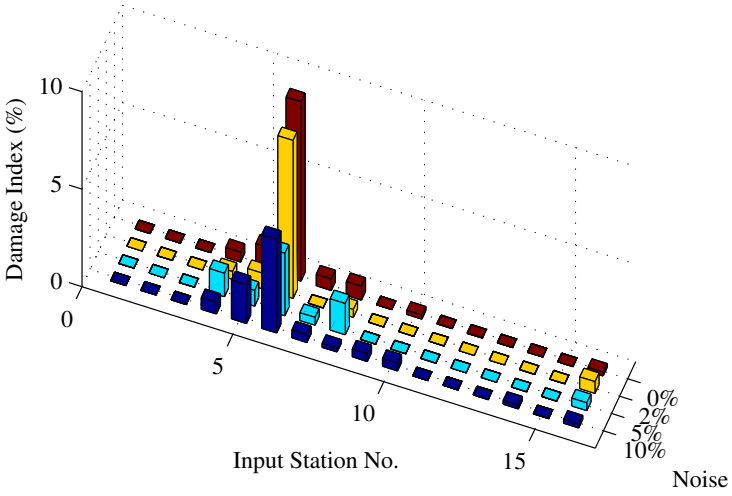

Figure 4.33: Identification results: 1 Sensor.

Based on the results in Table 4.5 and 4.6, following conclusions could be drawn:

- The results obtained for various damage magnitudes show that MARSHAL's identification and detection capabilities are unaffected by the severity of damage.
- In the case of damage detection, limited instrumentation could compromise the accuracy of detection at high noise values. For example, only the existence and location of damage could be concluded from the results obtained using a single sensor at the top of the tower under 10% noise, thus achieving only a Level II damage detection.
- As the number of sensors increase, better detection levels are achieved, as the existence, location and severity of damage can be concluded from these results, achieving a Level III detection.
- Despite being a challenging problem, satisfying results were obtained even at high noise values, except for the 1-sensor scenario.
- The practical problem that arises is the fact that most WTs have a limited number of sensors installed near the rotor-nacelle assembly (around

the top of the tower). To improve the results obtained for such limited instrumentation, it becomes necessary to include a data filtering subroutine before passing the measured vibration data to MARSHAL. It is noteworthy that no filtering subroutine was used in any of the numerical study cases, as it was sought to test MARSHAL's limits whilst exposing it to the full noise magnitude.

Although satisfying results were obtained when identifying offshore WTs using a full-scale model simulated by FAST, some disadvantages still arise. Mainly, the identification scheme presented in this section is problem/model specific, meaning that a full-scale model, compatible with FAST, has to be developed for the WT that is intended to be identified. Such full-scale modeling is not always available. Also, requiring a full inflow wind profile is prohibitive, and can only be approximated. Finally, it is incompatible with the output-only identification scheme, presented in Sec. 3.5.3, that is used in this research.

4.3 Model Reduction of Onshore Wind Turbines

Motivated by the drawbacks of using FAST as an analysis routine, the idea of model reduction arose. The reduction problem considers a 5-MW reference onshore WT developed by the National Renewable Energy Laboratory (NREL), which is the land-based version of the NREL offshore 5-MW baseline turbine documented in Jonkman et al. [43].

For deriving the reduced model, a full-scale analysis of the onshore WT is performed using FAST. The resulting vibration response of the tower as well as the excitations applied at the tower top are stored and passed to the identification/reduction routine which determines the best reduction vector which produces a vibration response as close as possible to that produced by the full-scale analysis conducted by FAST. A detailed description for this procedure was provided in Sec. 3.4 and Fig. 4.2.

Both geometry and structural characteristics were adopted from Jonkman et al. [43] and are illustrated in Fig. 4.34. An idling turbine is assumed to simplify the analysis. The turbine tower is 87.6m high, starts with a diameter of 6 meter and a thickness of 0.0351 meter at its bottom, and ends with a diameter of 3.87 meter and a thickness of 0.0247 meter at top. The elasticity of the tower material is 210 GPa with a density of 8500 kg/m^3. The tower is defined using 15 equally spaced input stations. The mass of the rotor-nacelle-blades assembly is 360×10^3 kg.

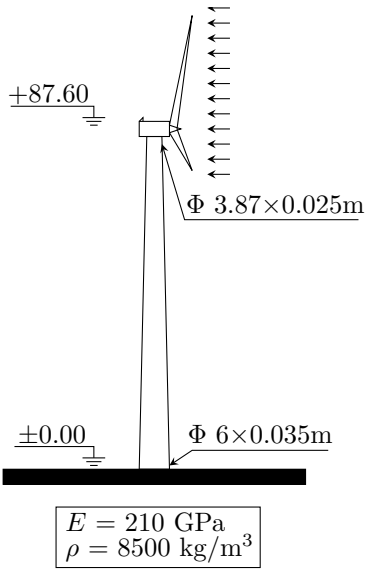

Figure 4.34: Structural characteristics of considered onshore wind turbine.

Deep thought was put into the selection of the excitation that shall be applied on the tower top as FAST is capable of providing the excitations applied on virtually any point on the structure. For the sake of model reduction, two possible excitation locations, illustrated in Fig. 4.35, could be considered. These are:

- The rotor thrust, designated in FAST as (RotThrust) coupled with the bending moment on the low speed shaft (LSS), designated as (LSSTipMys).
- The shear force and bending moments applied on the yaw bearing, i.e. tower top, designated in FAST as (YawBrFxp) and (YawBrMyp), respectively.

The aim of the reduced model is, however, to replace the whole RNA with equivalent forces and stiffnesses, thus using RotThrust and LLSTipMys does not serve that purpose and both YawBrMyp and YawBrFxp were used instead for the following reasons:

- As evident from Fig. 4.35a, the actual moment applied on the tower top is a summation of the contributions of RotThrust, LSSTipMys and the

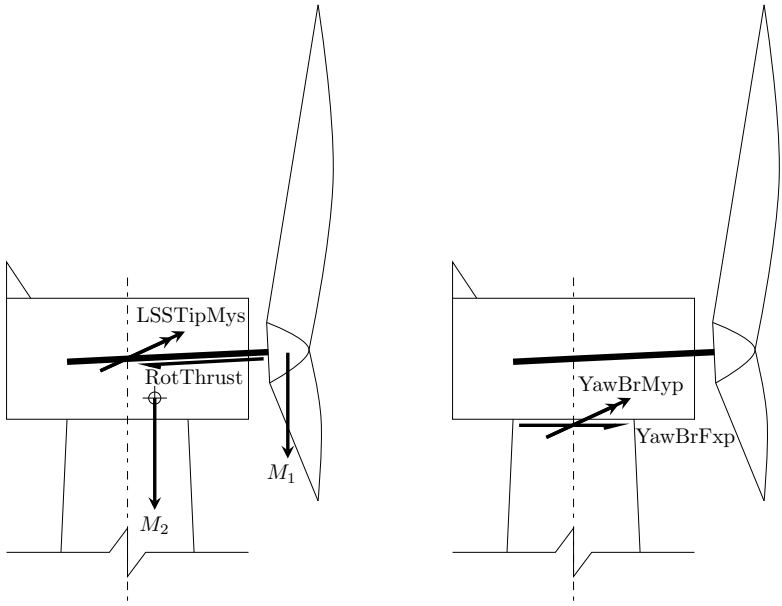

(a) External excitations on LSS. (b) Internal excitation on tower top.

Figure 4.35: Possible excitation scenarios.

masses of different components of the RNA. These masses are coupled with the vibration response of the RNA, creating additional complexities and preventing the replacement of these dynamics via the reduced model.

- Due to the fact that YawBrFxp and YawBrMyp are applied at a predetermined joint, it becomes easier to measure such excitations rather than the thrust and corresponding moment, as these are also dependent on the current blade configuration.
- The blade configuration and motions affects RotThrust and LSSTipMys. It can be argued that the turbine is idling, thus such influence is minimum. However, although the turbine was set to idling via pitching the blades out of the wind, some "pendulum" movement still occurred in FAST, which - due to the huge size of blades - has a significant effect.

For generating the vibration response, a 10 m/s turbulent inflow wind, generated via TurbSim, is used.

Defining the search space is another issue that has to be considered carefully, because the entries within the stiffness matrix are of much higher magnitude than those in the mass matrix, as E is of order $\times 10^{11}\, Pa$ whilst ρ is of $\times 10^{3}\, kg/m^{3}$. Meaning that a smaller search domain with a finer step size should be established for the stiffness modification factors when compared to the mass modification factors. Furthermore, the damping matrix is of similar magnitude as the stiffness matrix ($C = \alpha M + \beta K$), hence the same discussion applies. The upper bounds, lower bounds and step sizes are shown in Table 4.7 which define a search space of $N_{SS} = 6.6148 \times 10^{17}$ possible solution vectors.

Table 4.7: Search space definition for model reduction.

x_i	x_i^l	x_i^u	x_i^{ss}
$\lambda_1, \lambda_2, \lambda_5$, and λ_6	0.99	1.01	0.0001
λ_3 and λ_4	0.80	1.20	0.01
α	0.0115	0.5770	0.0012
β	0.0010	0.0475	0.0001

The vibration response of the full-scale model simulated in FAST is obtained at 9 nodes and stored along with the shear force and bending moments at tower top. The nodes that were measured are: 2, 3, 4, 5, 6, 8, 10, 12, and 15.

Once again, 10 optimization runs of 8 sub-runs with 2000 iterations per sub-run were performed. The configurations of MARSHAL remained unchanged. A total time history of 30 seconds at an increment of 0.01 second was considered when generating and validating the reduced model.

The best reduction vector obtained was

$$\mathbf{X} = \left\{ \begin{array}{cccccccc} 1.0000 & 1.0003 & 0.80 & 1.20 & 1.0000 & 1.0100 & 0.1200 & 0.0123 \end{array} \right\} . \tag{4.8}$$

Since the obtained vector should produce a reduced structure that, as accurately as possible, represents the vibration response of the full-scale structure, it should be expected for the vibration response of both full-scale and reduced structures to be as close as possible to each other. This can be seen when comparing the vibration response of the tower top as shown in Fig. 4.36, 4.37 and 4.38. Some differences still exist, since it is impossible for a reduced structure to completely capture the dynamic behavior of a full-scale structure.

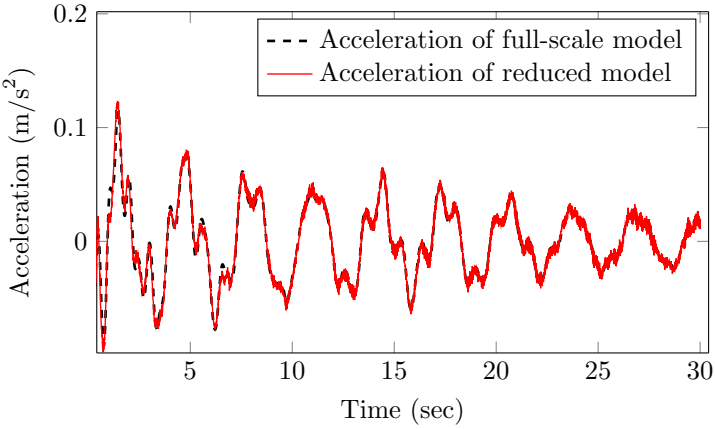

Figure 4.36: Acceleration comparison: 10 m/s characteristic wind speed.

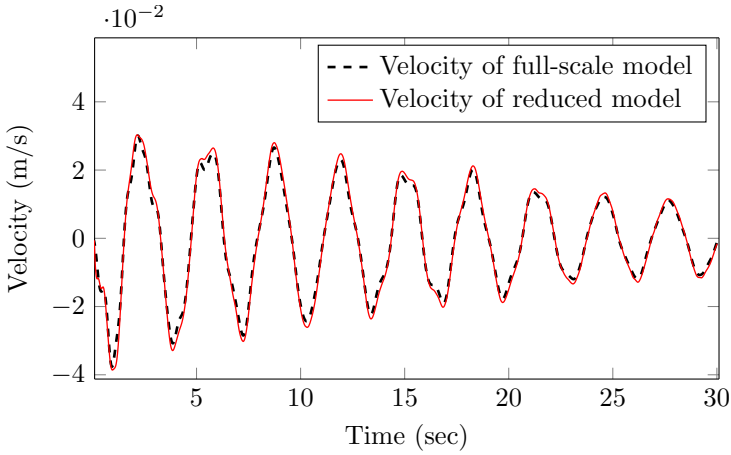

Figure 4.37: Velocity comparison: 10 m/s characteristic wind speed.

4.4 Verification of Reduced Model

Since the reduced model was derived using a full-scale model subjected to a turbulent inflow wind having a characteristic wind speed of 10 m/s, it should work best for this particular model subjected to this particular wind speed.

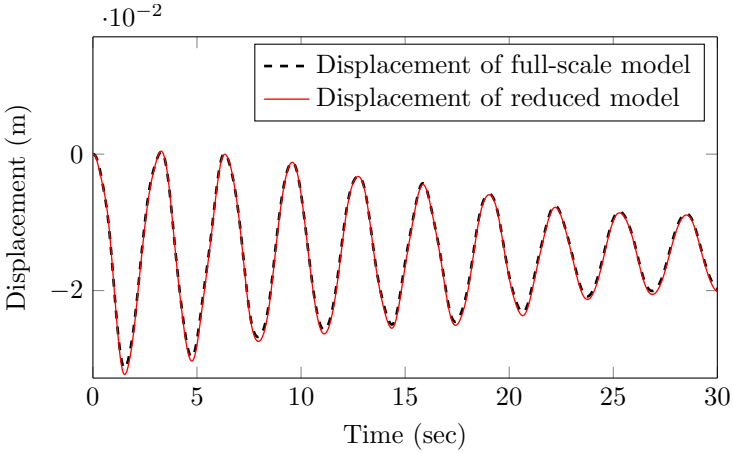

Figure 4.38: Displacement comparison: 10 m/s characteristic wind speed.

Nevertheless, it was found that the reduced model still satisfactorily approximates the structural response for the same structure under different wind speeds. This is illustrated in Fig. 4.39 through 4.42. However, the larger the difference between the characteristic wind speed used in deriving the reduced model and that used in the full-scale analysis conducted in FAST, the less accurate the approximation becomes.

Furthermore, it is necessary to verify the suitability of the reduced model for damage detection. To do so, it must be compared with FAST. That is, FAST is used to generate the vibration response of an undamaged and damaged WT, and it is required from the reduced model, without any further modification, to identify these structures correctly. It shall be mentioned that none of the settings with regard to MARSHAL, sensor locations, wind speeds,...etc. are changed, but these are taken to be identical to what was assumed during the derivation of the reduced model.

To start with, an undamaged structure is considered first. The vibration response is generated using FAST first, followed by the identification of the stiffness terms EI using the reduced model. 10 Optimization runs are performed and are detailed in Appendix D. The identified Damage Index (DI) obtained from the average optimum result $\mathbf{X}_\mu$ is

$$DI = \{0, 0, 0, 0, 0, 0, 0, 0, 0, 0, 0, 0, 0, 0, 0\} \ , \tag{4.9}$$

i.e. no damage was detected, which is true since an undamaged structure was provided to FAST while generating the original response vibration.

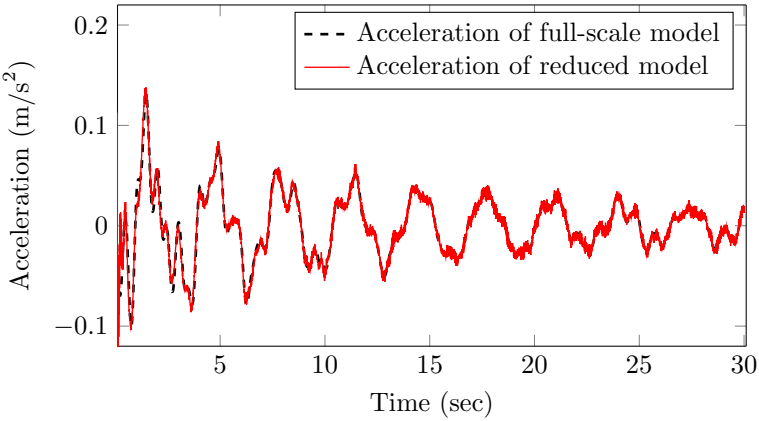

Figure 4.39: Acceleration comparison: 15 m/s characteristic wind speed.

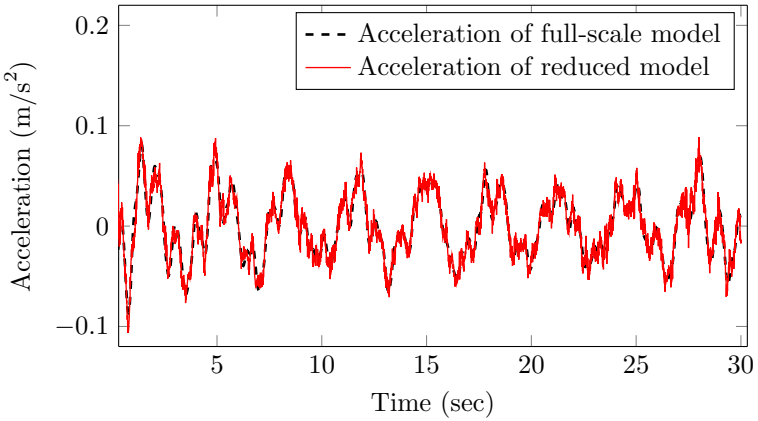

Figure 4.40: Acceleration comparison: 20 m/s characteristic wind speed.

To finalize, a damaged case is identified. Damage was applied at node No. 5, 6, and 7 by reducing EI by 10%, i.e. DI_5, DI_6, and DI_7 are equal to 10%. FAST is used to obtain the vibration response, then the reduced model is used for identification and damage detection, resulting in

$$DI = \{0, 0, 0, 0, 10.3, 11.2, 11.3, 0, 0, 0, 0, 0, 0, 0, 0\} \ . \tag{4.10}$$

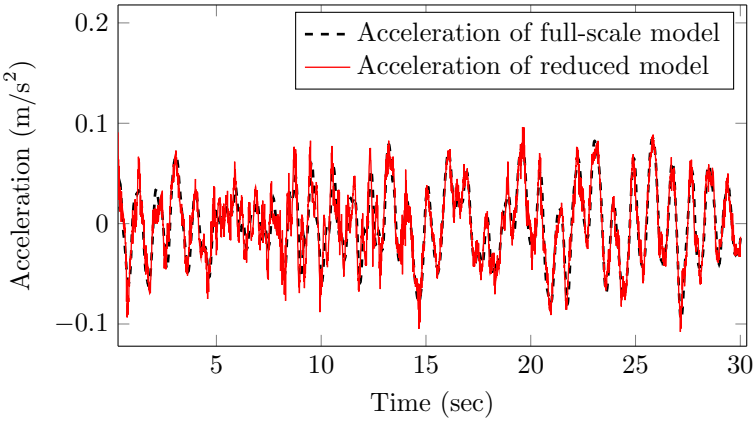

Figure 4.41: Acceleration comparison: 25 m/s characteristic wind speed.

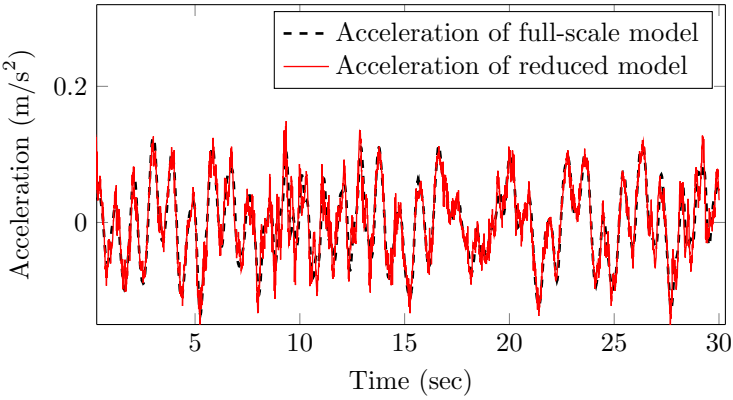

Figure 4.42: Acceleration comparison: 30 m/s characteristic wind speed.

The identified damage in both undamaged and damaged validation tests is satisfyingly accurate, as such results identify no false-positive damage in the case of undamaged structures, and detect the presence, location and obtain a good approximation of the magnitude of damage in the damaged case. These results allow the use of the derived reduced model in further numerical investigations. Further detailed results can be found in Appendix D.

4.5 Structural identification and damage detection using reduced models

The reduced model derived in Sec. 4.3 and verified in Sec. 4.4 is put to use in the structural identification and damage detection of onshore WT towers. The optimization problem involved in doing so was discussed in Sec. 3.5.

The excitations could be assumed using its statistical characteristics and general pattern. For all input/output identification problems, the used time history is 5 seconds long, discretized into 0.01 seconds increments. For output-only problems, a smaller and finer discretized time history is used following the recommendation of Koh and Perry [53]. That is, the time history is 1 second long discretized into 0.001 second increments.

Since the tower is discretized using 15 equally spaced nodes, it is represented using 15 stiffness, 15 density and 2 damping parameters, as follows:

$$\mathbf{X} = \{EI_1, EI_2, \ldots, EI_{15}, \rho_1, \rho_2, \ldots, \rho_{15}, \alpha, \beta\} \ . \tag{4.11}$$

For the simpler case of known mass identification, it becomes,

$$\mathbf{X} = \{EI_1, EI_2, \ldots, EI_{15}, \alpha, \beta\} \ . \tag{4.12}$$

For all structural identification, damage detection and output-only identification cases investigated, following settings were adopted:

- The structural characteristics of the turbine tower shown in Fig. 4.34 were used.
- 10 Optimization runs consisted of 8 sub-runs of 5,000 iterations each are performed. The results extraction scheme remains unchanged, and further details are provided in Appendix D.
- The upper bound, lower bound and step size for this optimization problem are taken as 100%, 50% and 0.1% of the values of the reduced structure for the stiffness and mass terms, whereas these are taken as 200%, 50% and 1% for the damping terms. This results in a search space of $N_{SS} = 7.1700 \times 10^{44}$ and $N_{SS} = 2.2547 \times 10^{85}$ for the cases of known mass and unknown mass, respectively.

4.5.1 The Structural Identification Problem

To start with, various cases of an undamaged reduced turbine tower, as summarized in Table 4.8, are considered.

Table 4.8: Cases studied in structural identification problems.

Mass	Number of Sensors (N_S)	Sensor Location	Noise (%)
Known	14	Node No. 2 to 15	0
Unknown	7	Node No. 2,4,6,8,10,12,15	2
	4	Node No. 4,8,12,15	5
			10

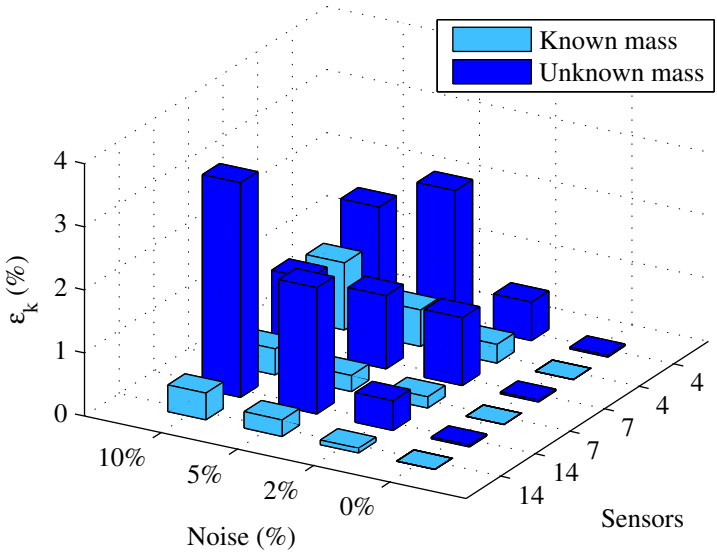

Figure 4.43: Identification using reduced model: results summary.

Detailed results for each identification case are shown in Table 4.9. These results are further visualized in Fig. 4.43.

Based on the results in Table 4.9, following conclusions could be drawn:

- The results obtained for both known and unknown mass identification are quite satisfying. For known mass identification at maximum noise (10%) and lowest number of sensors (only 4), the average error was around 1.1% and 1.6% for the case of known and unknown identification,

Table 4.9: Identification results.

N_S	Noise (%)	Known mass error (%)			Unknown mass error (%)			
		ϵ_k	ϵ_α	ϵ_β	ϵ_k	ϵ_m	ϵ_α	ϵ_β
14	0	0.0000	0.0000	0.0000	0.0275	0.7388	0.0100	0.0000
	2	0.0731	0.1000	0.2400	0.4694	1.8813	0.1400	0.0800
	5	0.2606	0.1600	0.9700	1.9975	2.8281	1.8700	0.3000
	10	0.4231	4.6400	3.9400	3.3994	4.0581	0.7500	0.7500
7	0	0.0000	0.0000	0.0000	0.0269	1.0088	0.0400	0.0000
	2	0.1769	2.8600	0.2400	1.0725	1.9631	0.1900	0.0100
	5	0.2519	2.9700	0.5400	1.1619	2.2975	0.7900	0.1600
	10	0.4131	4.3700	0.6800	1.1744	4.6200	2.1900	3.4100
4	0	0.0000	0.0000	0.0000	0.0281	0.8381	0.0000	0.0000
	2	0.2938	2.9100	0.4000	0.6088	1.7375	0.1300	0.1000
	5	0.5794	5.1900	1.8400	2.1138	3.3569	0.4800	0.4900
	10	1.0656	6.5200	2.3700	1.5944	2.5406	1.8800	0.2700

respectively.

- Similar conclusions with regard to the effect of noise can be drawn when compared to the results of previous investigated numerical study cases.

- Logically, the identification of known mass systems is more accurate than their unknown mass counterparts, as the number of variables decreases, improving MARSHAL's performance. Thus, such results encourage to perform known mass identification of structures whenever it is possible to accurately estimate its mass, as the extra calculation effort to do so does improve the accuracy of identification.

- Surprisingly, the identification cases utilizing 7 sensors obtained the best results at high noise values. This is expected when compared against the identification using 4 sensors, but was unexpected when competing with 14 sensors. This suggests that using an extensive number of sensors only "confuses" the identification algorithm, as all of these sensors are subjected to noise, increasing the overall error in the vibration signal. So a balance must be found between the number of sensors required to perform an accurate identification, and the fact that every sensor comes with its error inherited from noise.

4.5.2 The Damage Detection Problem

Damage could occur as a homogeneously dispersed reduction of the structural stiffness, or, at its worst cases, concentrated at a single node. Damage identified in this research is assumed to be concentrated, which is harder to be identified since it represents an abrupt change within the solution vector. As will be seen later, the identification scheme sometimes disperses damage within the damaged node and its neighboring nodes. Nevertheless, a strategy of obtaining the correct damage is explained later on. In all cases, damage was applied to the 6th DOF in the form of a stiffness reduction, having a DI_6 of 10%.

It was already established that the magnitude of damage has no effect on the accuracy of identification. Thus only the number of sensors and noise percentages are considered. A known mass damage detection problem is assumed, with similar sensor and noise configurations as in Table 4.8.

The damage detection results obtained are detailed in Table 4.10 and further summarized in Fig. 4.44, 4.45 and 4.46 for 14, 7 and 4 sensors, respectively.

Table 4.10: Damage detection using reduced model.

Sensor Number	Noise (%)	Identified DI (%) at node No.															Error (%)	
		1	2	3	4	5	6	7	8	9	10	11	12	13	14	15	ϵ_α	ϵ_β
14	0	0.02	0.01	0.00	0.04	1.20	7.88	0.79	0.02	0.00	0.00	0.00	0.00	0.02	0.00	0.00	0.01	0.00
	2	0.69	0.08	0.11	0.20	3.03	7.73	1.36	0.02	0.02	0.01	0.16	0.52	0.52	0.44	0.00	1.22	0.38
	5	0.70	0.45	0.71	0.01	2.81	7.61	2.70	0.01	0.00	0.02	0.52	1.22	0.58	0.79	0.00	2.38	1.46
	10	2.16	0.81	0.31	0.34	2.14	7.20	2.29	0.17	0.00	0.13	0.30	0.55	0.31	0.57	0.00	3.01	0.81
7	0	0.01	0.00	0.00	0.02	1.32	7.73	0.87	0.02	0.00	0.00	0.02	0.01	0.01	0.02	0.00	0.06	0.00
	2	0.45	0.57	0.82	0.15	2.30	7.23	1.33	0.01	0.01	0.01	0.11	0.58	0.15	0.27	0.00	2.32	0.10
	5	1.39	0.40	0.42	0.48	4.12	7.02	1.65	0.00	0.00	0.03	0.35	0.84	0.06	0.45	0.00	3.73	0.55
	10	0.41	0.46	0.44	0.14	2.05	5.63	1.34	0.30	0.08	0.16	0.98	0.42	0.39	0.45	0.00	7.52	0.51
4	0	0.06	0.00	0.00	0.06	1.56	7.20	1.06	0.02	0.00	0.01	0.00	0.02	0.00	0.01	0.03	0.11	0.00
	2	1.20	0.71	0.47	0.28	1.90	7.75	0.50	0.00	0.01	0.15	0.15	0.21	0.06	0.93	0.00	1.50	0.13
	5	1.57	0.50	0.58	0.80	1.01	5.23	0.25	0.00	0.00	0.00	0.64	0.59	0.17	0.35	0.00	6.20	1.14
	10	0.08	0.79	0.01	0.69	5.46	1.43	0.01	0.02	0.34	0.04	0.85	0.19	0.44	0.76	0.00	6.02	4.21

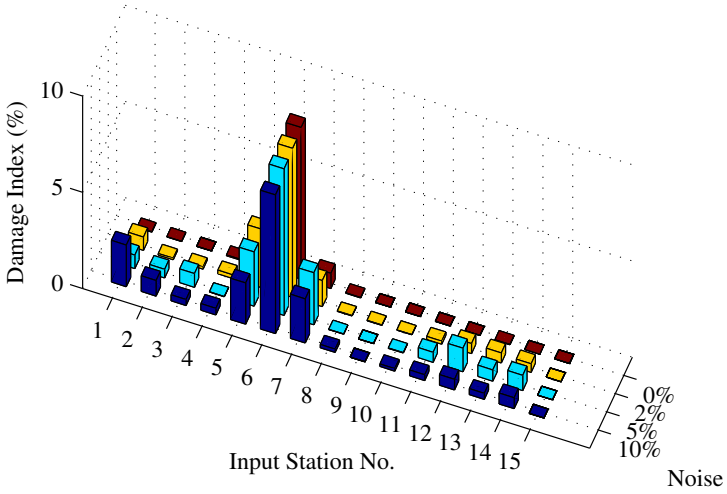

Figure 4.44: Identification results: 14 sensors.

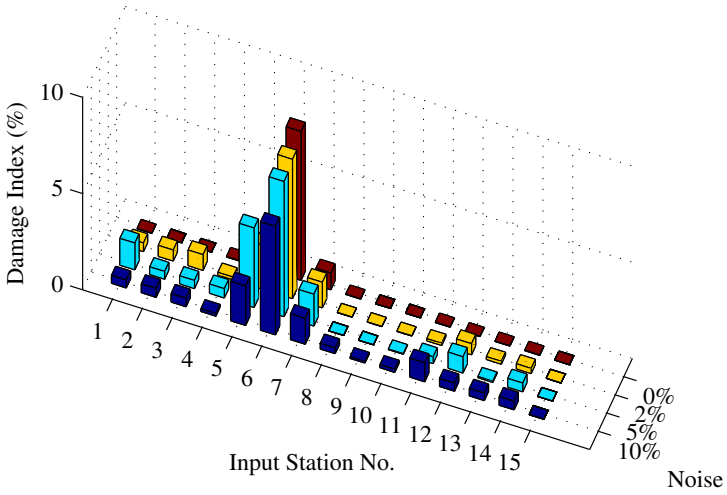

Figure 4.45: Identification results: 7 sensors.

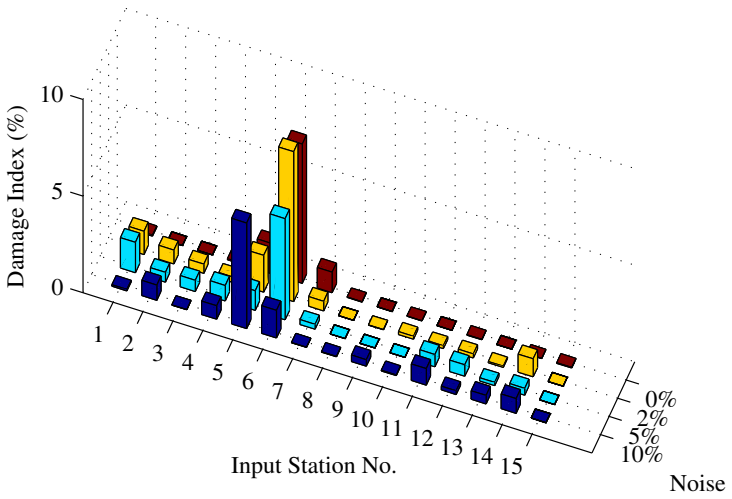

Figure 4.46: Identification results: 4 sensors.

Analyzing the obtained results, following conclusions can be drawn:

- It was noted that MARSHAL identifies a rather dispersed pattern of damage, namely: the damage is distributed on the damaged node as well as its neighboring nodes. In fact, the defined damage is challenging as it represents an abrupt change in the stiffness of the structure. Furthermore, although structural characteristics identified from MARSHAL are defined at nodes, the structural parameters of the beam elements used in the vibration analysis is, as a matter of fact, the average value of the defined structural characteristics at the nodes, thus dispersing the damage amongst two beam elements.

- As evident in Fig. 4.44, 4.45 and 4.46, the presence, location and magnitude of damage can be interpreted via sound engineering judgement. In most cases, the location of damage is established via the highest DI in the solution vector, whilst its severity is calculated by summing up the DI of in the vicinity of that location.

- For the identification cases utilizing 4 sensors at a noise level of 10%, the accuracy of identification is compromised. As damage is only identified in the vicinity of the actual damage location.

4.5.3 The Output-Only Identification Problem

Similar to Sec. 4.1.2, the output-only identification problem for an onshore WT reduced model is considered. The optimization problem involved in doing so is explained in detail in Sec. 3.5.3 and the excitations were generated as explained in Sec. 4.5.

An important difference between the output-only problem studied for reduced onshore models and all other SI problems considered so far lies in the fact that the excitations applied on the structure are both forces and moments. For the purpose of identifying forces, it was already shown that linear accelerometers were sufficient. For moments, however, additional angular accelerometers must be installed near the point of excitation application. The sensor configuration along with the noise percentages is shown in Table 4.11. The designation n^r denote a sensor installed at the $n-$th node and measure angular accelerations while an l superscript stands for linear accelerometers.

Table 4.11: Sensor configurations and noise values.

Number of Sensors (l+r)	Sensor Location	Noise (%)
$14+2$	2^l to $15^l, 14^r, 15^r$	0
$8+2$	$2^l, 4^l, 6^l, 8^l, 10^l, 12^l, 14^l, 14^r, 15^l, 15^r$	2
$4+2$	$5^l, 10^l, 14^l, 14^r, 15^l, 15^r$	5
		10

The output-only identification results obtained are detailed in Table 4.12 and further summarized in Fig. 4.47. It was found that, unlike in two-dimensional shear frames, the predicted excitation was inaccurate even when the case of 0% noise was considered. This is attributed to the fact that the applied excitations are both forces and moments, and act on the same spot. Thus creating an indefinite amount of possible force and moment combinations that still generate the same response at that particular DOF. The proposed method, however, still converges to the real structure despite this drawback. To further explain this convergence, it is required to reflect back to the output-only identification scheme adopted in this research, namely: the forces are generated in such a way that the vibration of the DOF at which the forces are applied matches the measured vibration regardless of whether the structure is the correct or incorrect one. It is the other DOFs that provide this distinguishing. Thus, it is vital for the output-only scheme that the vibration response of other DOFs is measured as well.

Table 4.12: Identification results: Output-only.

Sensors	Noise (%)	Error (%) ϵ_k	α	β
14^l+2^r	0	0.0019	-0.5800	0.0000
	2	0.0175	-1.4700	0.0000
	5	0.0313	-1.9200	0.0000
	10	0.1006	-5.0500	0.0000
8^l+2^r	0	0.0031	-0.5700	0.0000
	2	0.0256	-1.6900	-0.0100
	5	0.0488	-1.6000	0.0000
	10	0.0943	-6.6100	-0.0300
4^l+2^r	0	0.0025	-0.3900	0.0000
	2	0.0275	-1.1100	0.0000
	5	0.0606	-2.3600	-0.0100
	10	0.1006	-5.7100	-0.0100

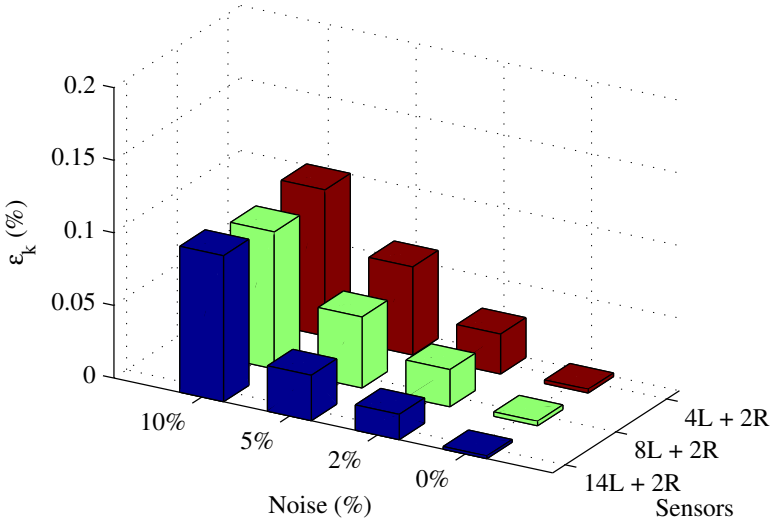

Figure 4.47: Output-only identification results summary.

To conclude, following remarks are made:

- With the accomplishment of output-only identification, the main purpose of developing the reduced model in the first place is fulfilled, remedying the drawbacks of using FAST in the structural identification and damage detection of WTs.
- It was found that the identification results of output-only cases are more accurate for noisy vibration than their input/output counterparts. This is due to the fact that noisy excitations are not provided to MARSHAL, but are rather estimated using the predictor-corrector scheme, thus eliminating one source of noisy error.

4.6 Summary and Conclusions

Four numerical study cases were presented in this chapter, namely: structural identification of two-dimensional shear frames, structural identification and damage detection of offshore WTs, derivation (and verification) of a reduced model for onshore WTs and the structural identification and damage detection of onshore WTs using a reduced model. Various factors affecting the accuracy of identification were investigated: the length of time history, the noise percentage, the damage severity and the number and location of sensors.

To start with, two-dimensional shear frames were considered, featuring known mass, unknown mass and output-only identification, with the results being compared with a previous study utilizing a modified version of the well-known genetic algorithms. To illustrate, the average errors in the case of unknown mass identification of a 20-DOF structure under 10% noise using a 10 seconds long time history was 1.47%, 1.32%, 4.60% and 0.20% for stiffness, mass, α and β, respectively. It shall be noted, however, that the identification of damping coefficients α was less accurate than β. This is due to the fact that α is multiplied by the mass matrix, which has a significantly smaller numerical value than the stiffness matrix, by which β is multiplied.

Even in the absence of excitation information, MARSHAL showed versatility in coping with output-only problems with minimum modification. The results were satisfying, as MARSHAL succeeded not only in surpassing the modified GA approach, but in obtaining accurate stiffness and excitation predictions as well: For the case of 20-DOF structure under 10% noise using an time history of 1 second initial length, the identified average error in stiffness was 0.51%. Furthermore, an extremely accurate prediction of applied excitations was achieved. The damping coefficient α was, however, identified with much less accuracy for reasons previously explained.

Motivated by such promising results, a 5-MW reference wind turbine was considered for identification. Due to the complexity of modeling a full-scale WT, the necessary vibration response was obtained using an open source software called FAST. A variety of identification and damage detection cases were considered to study the effect of the number of sensors, sensor location, damage magnitude and noise percentage.

It was found that MARSHAL is unaffected by the severity of damage. The average error in identified stiffness resulting from identifying offshore WTs under 0% noise and utilizing 10 sensors was 0.0063%, 0.0000%, 0.0000% and 0.0125% for a damage magnitude of 10%, 5%, 3% and 0%, respectively.

The increase in considered number of sensors (up to 10 sensors) had a positive impact on the identification accuracy. Level III detection was achieved using 10 sensors even at 10% noise. On the other end, only Level II detection was achieved when using a single acceleration sensor at 10% noise. In other words, limited instrumentation could compromise the accuracy of detection at high noise values.

Two major drawbacks arise when utilizing FAST as a full-scale modeling routine, namely: being problem/model specific, and requiring a full inflow wind profile. Such drawbacks limit its accuracy in real-life applications and are incompatible with the output-only identification scheme adopted in this research. Thus, a reduced model approach was derived, verified and applied on several identification cases.

Due to the fact that both forces and moments act on the same spot in the output-only identification problem, an infinite amount of possible force and moment combination would yield the same response. Thus, the prediction of excitations was, unlike in two-dimensional shear frames, inaccurate. The structural identification was, however, satisfying. For instance, the average error in identified stiffness under 10% noise was 0.1006%, 0.0943% and 0.1006% for a total of 16, 10 and 6 sensors, respectively.

Reconsidering the results obtained from the identification of reduced models, an interesting conclusion about the number of sensors could be drawn, namely: using an extensive number of sensors only "confuses" the identification algorithm, as all of these sensors have inherent noise.

Despite the fact that satisfying results were obtained in numerical study cases, it is still necessary to test MARSHAL in an experimental study case, which is done in Ch. 5.

Chapter 5

Experimental Study Case

To assess the applicability of the proposed identification scheme to more realistic data, a laboratory test model of a scaled wind turbine tower supported by a tripile foundation was considered. The laboratory tests were conducted at the Institute of Structural Analysis (Institut für Statik und Dynamik - ISD) at Leibniz Universität Hannover (LUH), with aim to identify damage via changes in the modal parameters by comparing damaged and undamaged structural states using the Modal Assurance Criterion (MAC) as presented by Schröder et al. [78].

5.1 Description of Laboratory Test Model

The considered scaled laboratory wind turbine model is shown in Fig. 5.1. The model is made of structural steel having an elastic modulus of 210 GPa, shear modulus of 80.8 GPa, and mass density 7850 kg/m^3.

The tower has a circular cross section having an outer diameter of 114.3mm and wall thickness of 3.2mm. It is 2m long and the rotor nacelle assembly was substituted by a concentrated mass at the tower top.

Three inclined rectangular cross sections (50mm $\times$ 50mm and 3mm thickness) support the tower and transfer the loads to three piles. These piles have a circular cross section (outer diameter 48.3mm, thickness 3.2mm) and are 0.6m long.

To simulate damage, two flange connections were added to one of the three supporting legs of the tripile. When testing a damaged structure, the bolts of these flanges were unscrewed and completely loosened, creating a more complicated and challenging type of damage than the usual approach used in damaging a structure, namely by introducing saw cuts in the cross sections.

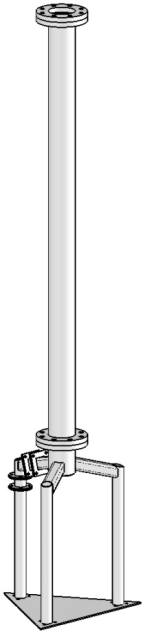

Figure 5.1: Schematic of laboratory model [78].

The reason behind this added complexity is that loosening the bolts does not only affect the stiffness of the structure, but the damping behavior as well. This is witnessed in a sudden and significant increase in the damping properties of the structure when damaged.

Such increase in damping could be due to the occurrence of relative sliding in the flange connection at high vibration amplitudes of the structure. Such sliding generates additional energy dissipating mechanisms, thus increasing the damping properties. Following such reasoning, damping would be amplitude dependent. This issue was, however, tackled with a two-stage damping scheme introduced later on in this chapter.

When performing the laboratory test, the structure was released from an initial displacement caused by a 100 N force applied at the tower top in a direction parallel to the leg that has the installed flanges.

Data acquisition was done via 4 accelerometers, 3 of which are installed at the third, two thirds and top of the tower, whilst the last one is installed near the damage-inducing flange.

5.2 The Corresponding Numerical Model

Based on the geometry and structural characteristics provided by SCHRÖDER ET AL. [78], a three dimensional numerical model was assembled as shown in Fig. 5.2. Beam elements were used in the assembly of the numerical model, with their mass, stiffness and damping matrices calculated in accordance with Sec. 3.6.1.

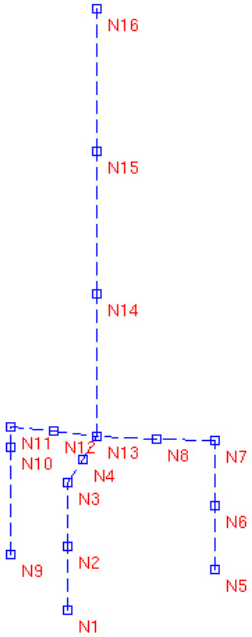

Figure 5.2: Numerical model.

For damping, a Rayleigh type damping was assumed. It is clear that such an assumption is a simplification of the amplitude dependent damping behavior that such a structure is subjected to. Nevertheless, it is out of the scope of this research to further investigate the damping behavior of such a structure as it is believed to be a research topic itself.

For tackling such challenging damping, however, a two-stage damping was considered. To illustrate such two-stage damping, the raw vibration response measured at the tower top of a damaged laboratory model is shown in Fig. 5.3.

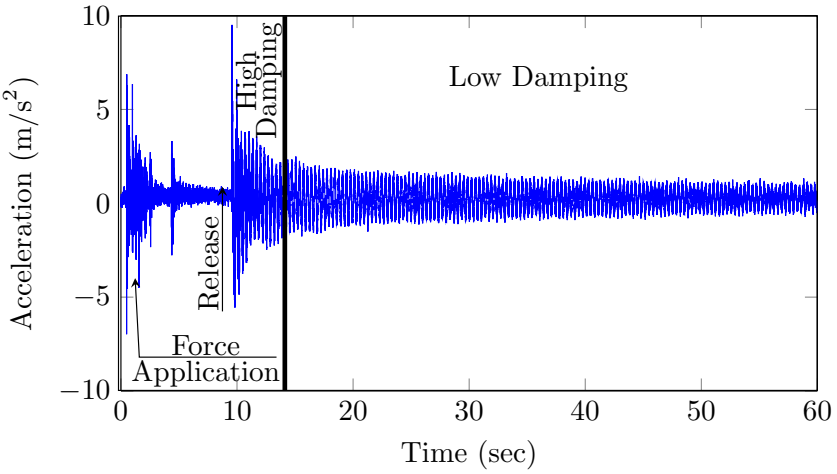

Figure 5.3: Raw acceleration data at tower top for the damaged structure.

It can be seen that during the first moments after releasing the structure, its vibration response is highly damped whereas the rest of the vibration proceeds with a much lower damping.

This previous discussion motivates the two-stage damping approach in which a high damping ratio ζ_1 is assumed for the first t_1 seconds, and a relatively lower damping ratio ζ_2 is assumed for the rest of the time history. Such damping scheme is illustrated in Fig. 5.4a. A possible refinement of such model could be implemented by assuming any function for the variation of damping ratio with time $\zeta(t)$, e.g. a linearly decreasing damping ratio, followed by a constant damping ratio for the rest of the time history. Such refinement is shown in Fig. 5.4b. It shall be mentioned, however, that a two-stage damping scheme using constant damping ratios is implemented in this research. Once the damping ratios are identified, the Rayleigh damping coefficients are calculated.

5.3 Data Pre-processing

As previously mentioned, the vibration response is measured at four points on the structure: three on the tower and one on the damaged supporting pile. The measurements were extremely noisy and required pre-processing before passing them to MARSHAL. The implemented pre-processing scheme,

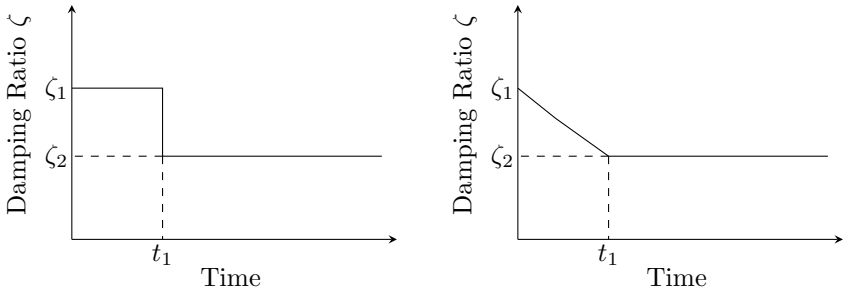

(a) Two-stage damping (b) Refined multi-stage damping

Figure 5.4: Possible damping ratio assumptions.

illustrated in Fig. 5.5 is consisted of:

- Performing noise filtering.
- Resolving any data offset.
- Manual triggering, i.e. determining an accurate time instance at which the force was released.

For filtering the raw data, a 41-term moving average filter was used. The resulting data, shown in Fig. 5.5b is much better when compared to the raw data, shown in Fig. 5.5a.

Fine calibration and data offset correction are inevitable when real data acquisition tools are used. Such offset is treated by shifting the data properly.

Finally, the time instance at which the force was released should be determined and the data shall be trimmed accordingly. Such determination could be done automatically or manually. In the research work of this dissertation, it is done manually via sound engineering judgment. The ready-to-use data is shown in Fig. 5.5c.

Once filtering, shifting and trimming are performed, the data is ready to be used in the structural identification and damage detection of the laboratory structure.

5.4 The Structural Identification Problem

The structural identification of an undamaged structure is performed first, followed by the identification and damage detection of the damaged structure.

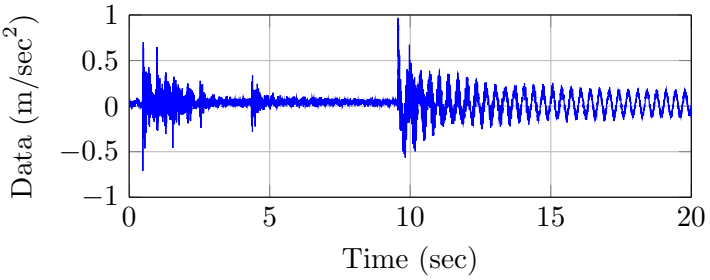

(a) Raw data.

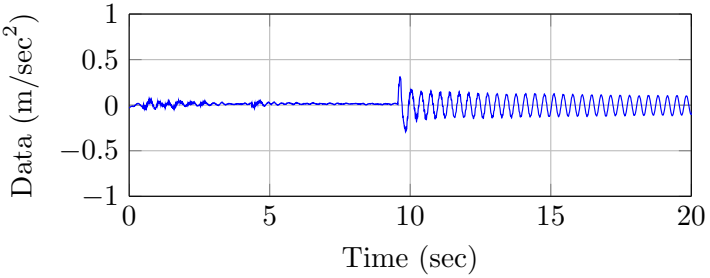

(b) Data filtering and shifting.

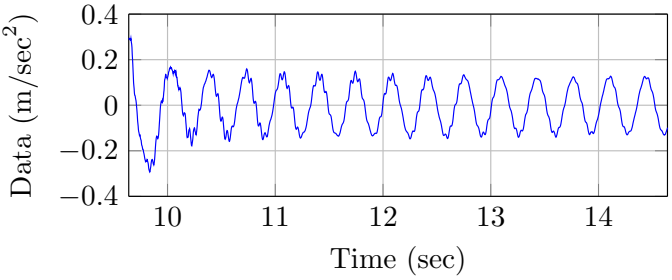

(c) Data Trimming.

Figure 5.5: Data processing.

As detailed previously, the laboratory test model is released from an initial position generated by applying a 100 N force at the tower top. The accelerometers have a sampling frequency of 400 Hz and the length of the considered time history (after releasing the structure) is 5 seconds.

The numerical model of the considered structure is discretized as shown in Fig. 5.2, thus creating 16 nodes, or 15 elements. The mass of the structure was assumed to be known.

The solution vector is defined on an element basis as follows:

$$\mathbf{X} = \{E_1, E_2, \ldots, E_{15}, G_1, G_2, \ldots, G_{15}, \zeta_1, \zeta_2\} \ , \tag{5.1}$$

where E_i and G_i is the elastic and shear modulus of the $i-$th element in the numerical model, ζ_1 is the "Stage 1" high damping ratio and ζ_2 is the "Stage 2" low damping ratio.

The optimization algorithm is run 10 times. Each run has a total of 40,000 iterations and is subdivided into 8 subruns of 5,000 iterations each. Other configurations of MARSHAL remained unchanged and were taken as assumed in Ch. 4.

The upper bounds, lower bounds and step sizes for this optimization problem are shown in Table 5.1, resulting in a search space of $N_{SS} = 7.8020 \times 10^{72}$.

Table 5.1: Search space definition for experimental identification.

x_i	x_i^l	x_i^u	x_i^{ss}
$E_1 \ldots E_{15}$	21 GPa	210 GPa	1.05 GPa
$G_1 \ldots G_{15}$	8.08 GPa	80.8 GPa	0.404 GPa
ζ_1	0.0002	0.0040	1.00×10^{-5}
ζ_2	0.0002	0.0040	1.00×10^{-5}

The optimum results obtained from all 10 optimization runs are stored in $\mathbf{X}_{opt}$ and averaged to obtain the representative $\mathbf{X}_{\mu}$ which is detailed in Table 5.2 and summarized in Fig. 5.6 and 5.7. Further details can be found in Appendix E.

Considering the results obtained from the identification of an undamaged experimental tripile structure, following conclusions could be drawn:

- MARSHAL was capable of identifying the elastic modulus and shear modulus with minimum error.
- Interestingly, the identified damping ratio for both stages was 0.002, meaning that no stage damping is required, as the extra dissipation

Table 5.2: Results for experimental undamaged tripile identification.

Structural Part	Variables E_i	Variables G_i	Value (GPa)	Value (GPa)	DI (%)	DI (%)
Leg 1	E_1	G_1	210.00	80.80	0.00	0.00
	E_2	G_2	210.00	80.80	0.00	0.00
	E_3	G_3	206.01	80.80	1.90	0.00
	E_4	G_4	205.80	80.80	2.00	0.00
Leg 2	E_5	G_5	210.00	80.80	0.00	0.00
	E_6	G_6	210.00	80.80	0.00	0.00
	E_7	G_7	210.00	80.80	0.00	0.00
	E_8	G_8	210.00	80.80	0.00	0.00
Leg 3	E_9	G_9	210.00	79.18	0.00	1.00
(Flanged)	E_{10}	G_{10}	210.00	79.99	0.00	2.00
	E_{11}	G_{11}	210.00	80.80	0.00	0.00
	E_{12}	G_{12}	210.00	80.80	0.00	0.00
Tower	E_{13}	G_{13}	210.00	80.80	0.00	0.00
	E_{14}	G_{14}	210.00	80.80	0.00	0.00
	E_{15}	G_{15}	210.00	80.80	0.00	0.00

Identified damping:
$\zeta_1 = 0.002$ for $t \leq 0.25sec$
$\zeta_2 = 0.002$ for $t > 0.25sec$

mechanism of partial sliding, discussed previously, does not occur when the bolts aren't loosened.

- The results obtained for the shear modulus suggest a slight reduction in the shear modulus of elements 9 and 10. Interesting in that is the fact that elements 9 and 10 are located in the monopile leg that has the installed flanges. Meaning that the algorithm actually succeeded in detecting the presence of the flange.

- It still can be argued that these fluctuations are also inherited in the material characteristics. Practically, these values are not exactly 210 GPa and 80.8 GPa for the elastic and shear modulus, respectively, but fluctuate around that value with some deviation.

- The results are satisfying and encourage further investigation of a damaged case of tripile structure in which the bolts on the installed flanges are loosened.

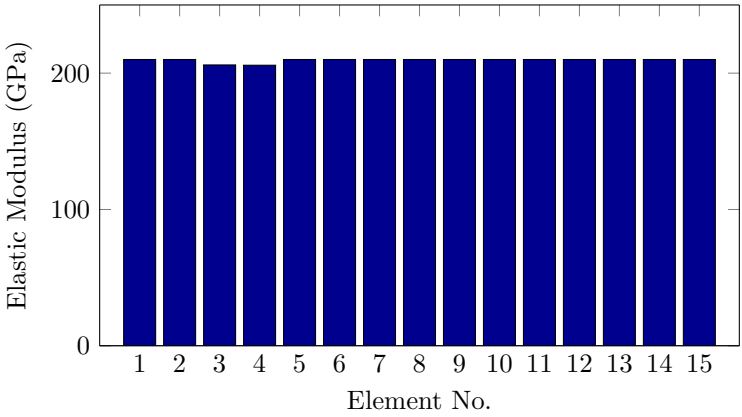

Figure 5.6: Identified elastic modulus: Undamaged case.

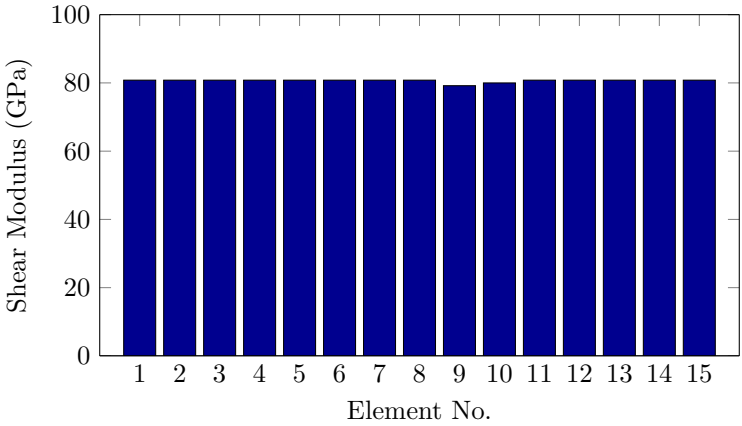

Figure 5.7: Identified shear modulus: Undamaged case.

5.5 The Damage Detection Problem

To follow up, the structural identification and damage detection of a damaged wind turbine model was considered. With the exception of search space definition, all settings with regard to excitations, acceleration measurements, MARSHAL parameters, runs and iterations were identical to those used in the undamaged case.

For defining the search space, the space of variable ζ_1 has been shifted up to search higher values, to meet the significant increase in damping for the damaged experimental case, as previously explained. The upper bounds, lower bounds and step sizes for this optimization problem are shown in Table 5.3, resulting in a search space of $N_{SS} = 7.8020 \times 10^{72}$.

Table 5.3: Search space definition for damage detection

x_i	x_i^l	x_i^u	x_i^{ss}
$E_1 \dots E_{15}$	21 GPa	210 GPa	1.05 GPa
$G_1 \dots G_{15}$	8.08 GPa	80.8 GPa	0.404 GPa
ζ_1	0.0190	0.1900	9.50×10^{-4}
ζ_2	0.0002	0.0040	1.00×10^{-5}

The average optimum solution $\mathbf{X}_\mu$ is detailed in Table 5.4 and illustrated in Fig. 5.8 and 5.9. Details for the optimum solution obtained for each of the 10 optimization runs can be found in Appendix E.

Table 5.4: Results for experimental damaged tripile detection.

Structural	Variables		Value		*DI*	
Part	E_i	G_i	(GPa)	(GPa)	(%)	(%)
Leg 1	E_1	G_1	210.00	80.80	0.00	0.00
	E_2	G_2	203.70	59.15	3.00	26.80
	E_3	G_3	200.97	75.67	4.30	6.35
	E_4	G_4	209.16	69.61	0.40	13.85
Leg 2	E_5	G_5	210.00	80.80	0.00	0.00
	E_6	G_6	197.09	60.12	6.15	25.60
	E_7	G_7	193.73	68.96	7.75	14.65
	E_8	G_8	209.16	71.47	0.40	11.55
Leg 3	E_9	G_9	135.35	38.62	35.55	52.20
(Flanged)	E_{10}	G_{10}	87.89	42.14	58.15	47.85
	E_{11}	G_{11}	197.75	52.20	5.85	35.40
	E_{12}	G_{12}	209.69	54.82	0.15	32.15
Tower	E_{13}	G_{13}	210.00	80.80	0.00	0.00
	E_{14}	G_{14}	210.00	80.80	0.00	0.00
	E_{15}	G_{15}	210.00	80.80	0.00	0.00

Identified damping:
$\zeta_1 = 0.2300$ for $t \leq 0.25sec$
$\zeta_2 = 0.0015$ for $t > 0.25sec$

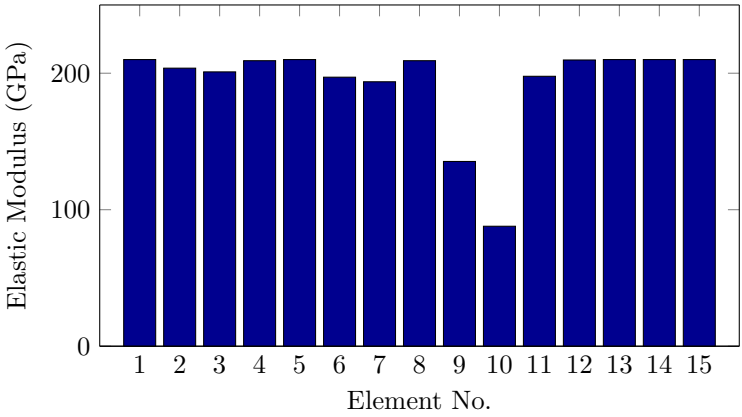

Figure 5.8: Identified elastic modulus: Damaged case.

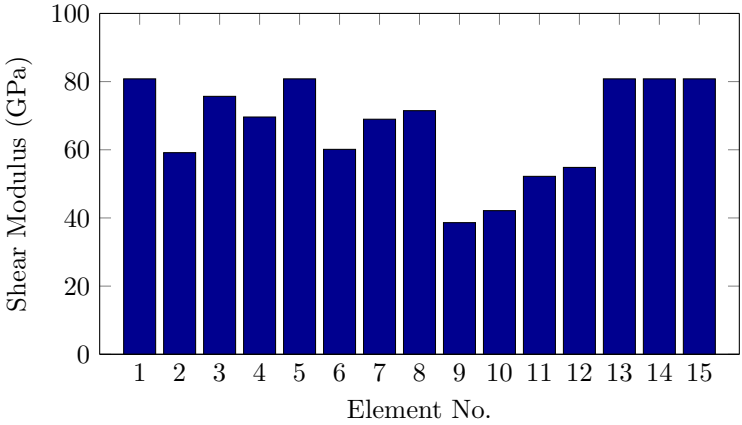

Figure 5.9: Identified shear modulus: Damaged case.

Based on the results of damage detection, as detailed in Table 5.4, following conclusions could be drawn:

- The identified elastic modulus clearly suggests a significant decrease at element 9 and 10, which is the correct location, since these elements have the installed loosened flange connections that are used to induce damage.

- The identified results for the shear modulus are less accurate, as torsional modes were not excited during the test.
- Generally, the damage detection accuracy is considered satisfying.

It is expected for the identified structure to have a vibration response that is as close as possible to the experimental structure. Thus, to conclude the experimental investigation, the acceleration response of both experimental and identified structures is shown in Fig. 5.10 for the damaged case.

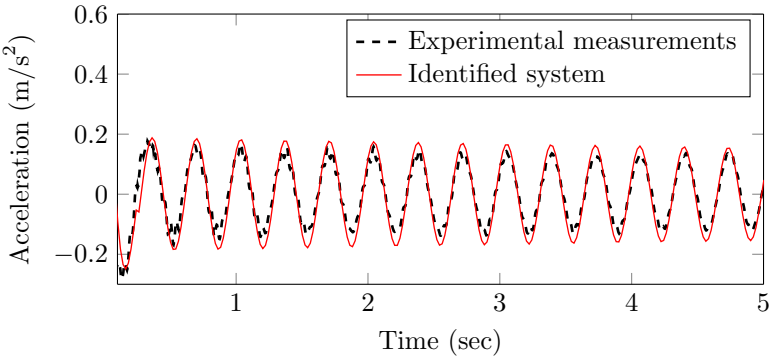

Figure 5.10: Acceleration comparison of identified damaged structure.

The experimental identification and damage detection of a tripile supporting structure has been carried out satisfactorily in this chapter. A simplified representation for the amplitude-dependent damping was presented, which was achieved via a two-stage simplified Rayleigh damping approach. With this success, it can now be established that a new numerical structural identification and damage detection framework has emerged, namely: The Modified Adaptive haRmony SearcH ALgorithm (MARSHAL). MARSHAL's satisfying results and versatility encourages its further utilization in other complicated identification and damage detection problems, as it is now established that MARSHAL requires only a valid analysis routine to be "plugged in" the algorithms structure to work. To prove that, a variety of numerical cases, finalized with an experimental case, were studied and satisfying results were achieved.

5.6 Summary and Conclusions

To confirm the broad applicability of MARSHAL, an experimental study of a tripile supporting structure was considered in this chapter for both damaged

and undamaged cases.

Damage, in the form of flange loosening, represented a more complicated and challenging type of damage as such not only affects the stiffness of the connected members, but the damping behavior as well.

For the case of an undamaged structure, MARSHAL did not identify any significant damage in the structure except for some minor reductions which can be attributed to the fact that such fluctuations are inherent in materials.

For the case of a damaged structure, MARSHAL provided clear indications of a reduction in the elastic modulus at the location of damage. For the elements No. 9 and 10, the identified elastic modulus was $E_9 = 135.35$ GPa and $E_{10} = 87.89$ GPa, which correspond to a reduction of 35.55% and 58.15% in stiffness, respectively. The shear modulus was, however, identified with lower accuracy. Generally, such results are satisfying.

The experimental identification and damage detection of a tripile supporting structure has been carried out satisfactorily in this chapter. A simplified representation for the amplitude-dependent damping was presented, which was achieved via a two-stage simplified Rayleigh damping approach.

The success MARSHAL achieved in numerical and experimental study cases can now establish that a new numerical structural identification and damage detection framework has emerged, namely: The Modified Adaptive haRmony SearcH ALgorithm (MARSHAL).

Chapter 6

Summary, Conclusions and Future Research

This study presented a Modified Adaptive haRmony SearcH ALgorithm (MARSHAL) for the investigation of structural identification and damage detection problems as optimization problems. The experience gained from applying such sophisticated algorithm on both numerical and experimental problems is summarized and concluded in this chapter, setting course for future research to continue from where this research has finished.

6.1 Summary

A variety of structural identification methods have been proposed and developed. Most of these methods are, however, problem specific and utilize classical approaches which rely on sound mathematical theories. Such classical approaches have limitations, such as: requiring gradient information, requiring a relatively good initial guess, assuming a certain noise or excitation pattern, assuming that all components of vibration response (acceleration, velocity and displacements) are measured and/or that an extensive array of sensors is implemented. At their best performance, they still obtain near optimal, i.e. close to real values, structural parameters, motivating the utilization of non-classical approaches based on metaheuristic optimization algorithms.

Thus this study developed a robust, efficient and versatile structural identification and damage detection framework based on a Modified Adaptive haRmony SearcH ALgorithm (MARSHAL).

MARSHAL is a self-modifying experience-based algorithm that incorporates a smart parameter selection system, an innovative engineering sense by realizing the coupling effect of stiffness terms in the stiffness matrix and a

two-stage experience-based search guidance which highlights potential regions within the search space.

To utilize MARSHAL in structural identification and damage detection problems, these problems were formulated as optimization problems with the objective to minimize errors between measured and predicted data.

A unified and consistent approach in the formulation of structural identification and damage detection problems as optimization problems was adopted, namely: establishing the dynamic analysis, solution vector, search space and objective function.

To test MARSHAL in a comparative study with the well-known Genetic Algorithm, the structural identification of two-dimensional shear frames was considered first.

The encouraging results motivated the investigation of structural identification and damage detection problems of offshore wind turbines. Since MARSHAL is a vibration-based identification technique, the vibration response of such turbines must be calculated. Modeling a full-scale wind turbine is challenging, and was achieved by using an open source code called FAST. However, FAST had some drawbacks, namely: it is problem specific, and requires detailed inflow wind information, making it incompatible with the adopted output-only approach.

Thus, to obtain the vibration response of a wind turbine without using FAST, model reduction of onshore wind turbines was considered, where the entire rotor-nacelle assembly was replaced with a much simpler representation. Such simpler representation allowed the direct evaluation of the turbine tower vibration response without the use of sophisticated multi-body analysis packages such as FAST.

To finalize, MARSHAL's applicability on more realistic experimental data was assessed by investigating an undamaged and damaged experimental tripile supporting structure.

6.2 Conclusions

Satisfying results were obtained from the structural identification and damage detection of the various problems considered in this study.

The structural identification of two-dimensional shear frames assuming a known mass, unknown mass and output-only problem was performed successfully. The results were compared to another well-known optimization algorithm, namely: a modified Genetic Algorithm and prove the superiority of MARSHAL. Satisfying results were obtained. To illustrate, the average errors in the case of unknown mass identification of a 20-DOF structure under 10% noise using a 10 seconds long time history was 1.47%, 1.32%, 4.60% and

0.20% for stiffness, mass, α and β, respectively. The identification of damping coefficients α was less accurate than β due to the fact that α is multiplied by the mass matrix, which has a significantly smaller numerical value that the stiffness matrix, by which β is multiplied.

MARSHAL proved its versatility when performing output-only identification, as minimum modifications in the main structure of MARSHAL were required. MARSHAL succeeded in obtaining accurate stiffness and excitation predictions: For the case of 20-DOF structure under 10% noise using an time history of 1 second initial length, the identified average error in stiffness was 0.51%.

The structural identification and damage detection of offshore wind turbines using MARSHAL was performed satisfyingly. Due to the complexity of modeling a full-scale wind turbine, an open source software called FAST was used. The investigated identification and damage detection cases included the effect of noise, number of sensors, sensor location and damage magnitude.

MARSHAL was unaffected by the severity of damage. When identifying offshore wind turbines under 0% noise and utilizing 10 sensors, the average error in stiffness was 0.0063%, 0.0000%, 0.0000% and 0.0125% for a damage magnitude of 10%, 5%, 3% and 0%, respectively. Furthermore, the increase in the number of sensors improved the identification accuracy.

For the case of input-output identification of offshore wind turbines, Level III detection was achieved using 10 sensors even at 10% noise. Whereas a limited instrumentation could compromise the accuracy of detection at high noise values. This was the case when using a single acceleration sensor at 10% noise, where only a Level II identification was achieved.

A reduced model approach, motivated by the drawbacks of using FAST, was derived, validated and applied on several identification cases. The results of identification using the reduced model was satisfying. For the case of an unknown mass identification of an undamaged wind turbine under 10% noise and utilizing 7 sensors, the average error was 1.1744%, 4.6200%, 2.1900% and 3.1400% for stiffness, mass, α and β, respectively.

The results of output-only identification using the reduced model were satisfying: the average error in identified stiffness under 10% noise was 0.1006%, 0.0943% and 0.1006% for a total of 16, 10 and 6 sensors, respectively. Due to the fact that both forces and moments act on the same spot, an infinite amount of possible force and moment combination would yield the same response. Thus, the prediction of excitations was inaccurate.

Surprisingly, it was evident from the results obtained using reduced models that using an extensive number of sensors would "confuse" the identification algorithm, as all of these sensors have inherent noise.

To investigate the applicability of MARSHAL on experimental data, an

experimental study of a tripile supporting structure was considered. Damage was applied by loosening the bolts in installed flanges, which represents a more complicated and challenging type of damage as such not only affects the stiffness of the connected members, but the damping behavior as well.

The results were satisfying: MARSHAL did not identify any damage for the case of undamaged tripile structure. On the other hand, MARSHAL provided clear indications of a reduction in the elastic modulus at the location of damage for the damaged tripile structure. For the elements No. 9 and 10, the identified elastic modulus was $E_9 = 135.35$ GPa and $E_{10} = 87.89$ GPa, which correspond to a reduction of 35.55% and 58.15% in stiffness, respectively. The shear modulus was, however, identified with lower accuracy. Generally, such results are satisfying.

With the success MARSHAL achieved in numerical and experimental study cases the primary objective of this study was fulfilled, i.e. the development of a vibration-based global structural identification and damage detection numerical framework that is applicable on a broad variety of structures with minimum modifications. The framework's official name is now MARSHAL.

6.3 Future Research

MARSHAL was proven to be a powerful and potential algorithm. As a matter of fact, it is this potential that encourages future research work.

Since MARSHAL is a broadly applicable structural identification technique, it is encouraged to consider more complex structural identification problems of wind turbines, involving soil-structure interaction, identification of hydrodynamic loads, on-line structural identification and structural identification with yaw error. Other structures such as bridges, dams and offshore platforms should be investigated, too.

Structural health monitoring is a large system, with MARSHAL being only a part in it. Future research trends should address the inclusion of MARSHAL within existing structural health monitoring packages such as the DIAMOND, developed by Los Alamos National Laboratory.

Despite the fact that MARSHAL provides information about the current state of the structure, it still does not give any information of the effect of such state on the load carrying capacity and long-term behavior of the structure. This could represent an interesting topic to couple MARSHAL with some statistical prediction system.

MARSHAL could perform much better if the location of damage is known a priori. Thus, it could be coupled with an initial Level II detection technique, e.g. relying on modal data.

Application of MARSHAL to real structures requires an accurate mathematical model to be established that reproduces the vibration response of the actual structure. An important balance must be found between accurately modeling the vibration response, yet keeping the model as simple as possible for a feasible search space. Thus, an interesting topic for future research is to test the effect of additional degrees-of-freedom, additional elements and more complex damping behavior on MARSHAL's identification capabilities, performing necessary improvements in the process.

References

[1] Adams, D., White, J., Rumsey, M., and Farrar, C. (2011) Structural health monitoring of wind turbines: method and application to a HAWT. *Wind Energy*, **14**, 603–623.

[2] Alia, O. M. and Mandava, R. (2011) The variants of the harmony search algorithm: an overview. *Artificial Intelligence Review*, **36**, 49–68.

[3] Anastassopoulos, A. A., et al. (2003) Structural integrity evaluation of wind turbine blades using pattern recognition analysis on acoustic emission data. *Journal of Acoustic Emission*, **20**, 229–237.

[4] Avendano-Valencia, L. D. and Fassois, S. D. (2012) In-operation output-only identification of wind turbine structural dynamics: comparison of stationary and non-stationary approaches. *Proceedings of the ISMA 2012*, pp. 4259–4274, Leuven, Belgium.

[5] Bani-Hani, K., Ghaboussi, J., and Schneider, S. P. (1999) Experimental study of identification and control of structures using neural network. Part 1: identification. *Earthquake Engineering & Structural Dynamics*, **28**, 995–1018.

[6] Bayissa, W. L. and Haritos, N. (2009) Structural damage identification using a global optimization technique. *International Journal of Structural Stability and Dynamics*, **9**, 745–763.

[7] Bicanic, N. and Chen, H. (1997) Damage identification in framed structures using natural frequencies. *International Journal for Numerical Methods in Engineering*, **40**, 4451–4468.

[8] Blum, C. and Roli, A. (2003) Metaheuristics in combinatorial optimization: Overview and Conceptual Comparison. *ACM Computing Surveys*, **35**, 268–308.

[9] Bodeux, J. B. and Golinval, J. C. (2001) Application of ARMAV models to the identification and damage detection of mechanical and civil engineering structures. *Smart Materials and Structures*, **10**, 479–489.

[10] Butterfield, S., Sheng, S., and Oyague, F. (2009) Wind Energys New Role in Supplying the Worlds Energy: What Role will Structural Health Monitoring Play? Tech. Rep. December, National Renewable Energy Laboratory, Stanford, USA.

[11] Capecchi, D. and Vestroni, F. (1999) Monitoring of structural systems by using frequency data. *Earthquake Engineering & Structural Dynamics*, **28**, 447–461.

[12] Charalampakis, A. E. and Dimou, C. K. (2010) Identification of BoucWen hysteretic systems using particle swarm optimization. *Computers & Structures*, **88**, 1197–1205.

[13] Chen, J. and Li, J. (2004) Simultaneous identification of structural parameters and input time history from output-only measurements. *Computational Mechanics*, **33**, 365–374.

[14] Ching, J. and Beck, J. L. (2004) Bayesian Analysis of the Phase II IASCASCE Structural Health Monitoring Experimental Benchmark Data. *Journal of Engineering Mechanics*, **130**, 1233–1244.

[15] Chou, J. and Ghaboussi, J. (2001) Genetic algorithm in structural damage detection. *Computers & Structures*, **79**, 1335–1353.

[16] Choudhury, A. R. and He, J. (1996) Structural damage location using expanded measured frequency response function data. *14th International Modal Analysis Conference*, pp. 934–942.

[17] Ciang, C. C., Lee, J., and Bang, H. (2008) Structural health monitoring for a wind turbine system: a review of damage detection methods. *Measurement Science and Technology*, **19**, 122001.

[18] Crabtree, C. J., Zappala, D., and Tavner, P. J. (2014) Survey of commercially available condition monitoring systems for wind turbines. Tech. Rep. May, Durham University School of Engineering and Computing Sciences and the SUPERGEN Wind Energy Technologies Consortium.

[19] Cunha, J., Cogan, S., and Berthod, C. (1999) Application of genetic algorithms for the identification of elastic constants of composite materials from dynamic tests. *International Journal for Numerical Methods in Engineering*, **45**, 891–900.

[20] Degertekin, S. O. (2008) Harmony search algorithm for optimum design of steel frame structures: A comparative study with other optimization methods. *Structural Engineering and Mechanics*, **29**, 391–410.

[21] Degertekin, S. O., Hayalioglu, M. S., and Gorgun, H. (2009) Optimum design of geometrically non-linear steel frames with semi-rigid connections using a harmony search algorithm. *Steel and Composite Structures*, **9**, 535–555.

[22] Doebling, S. W., Farrar, C. R., Prime, M. B., and Shevitz, D. W. (1996) Damage identification and health monitoring of structural and mechanical systems from changes in their vibration characteristics: A literature review. Tech. rep., Los Alamos National Laboratory, Los Alamos, USA.

[23] Dutton, A. G. (2004) Thermoelastic stress measurement and acoustic emission monitoring in wind turbine blade testing. *European Wind Energy Conference*, pp. 1–9, London, UK.

[24] Fanning, P. J. and Carden, E. P. (2003) Damage Detection based on Single-Input-Single-Output Measurements. *Journal of Engineering Mechanics*, **129**, 202–209.

[25] Farrar, C. R. and Doebling, S. W. (1997) Lessons learned from applications of vibration based damage identification methods to large bridge structure. *Structural Health Monitoring: Current Status and Perspectives*, pp. 351–370.

[26] Farrar, C. R., Doebling, S. W., and Nix, D. A. (2001) Vibration-based structural damage identification. *Philosophical Transactions of the Royal Society A: Mathematical, Physical and Engineering Sciences*, **359**, 131–149.

[27] Farrar, C. R. and Worden, K. (2007) An introduction to structural health monitoring. *Philosophical Transactions of the Royal Society of London A: Mathematical, Physical and Engineering Sciences*, **365**, 303–315.

[28] Franco, G., Betti, R., and Lu, H. (2004) Identification of Structural Systems Using an Evolutionary Strategy. *Journal of Engineering Mechanics*, **130**, 1125–1139.

[29] Friswell, M. I., Penny, J. E. T., and Wilson, D. A. L. (1994) Using vibration data and statistical measures to locate damage in structures. *Modal Analysis: The International Journal of Analytical and Experimental Modal Analysis*, **9**, 239–254.

[30] Geem, Z. W., Kim, J. H., and Loganathan, G. V. (2001) A New Heuristic Optimization Algorithm: Harmony Search. *Simulation*, **76**, 60–68.

[31] Geoffrey Chase, J., Leo Hwang, K., Barroso, L. R., and Mander, J. B. (2005) A simple LMS-based approach to the structural health monitoring benchmark problem. *Earthquake Engineering & Structural Dynamics*, **34**, 575–594.

[32] Ghoshal, A., Sundaresan, M. J., Schulz, M. J., and Frank Pai, P. (2000) Structural health monitoring techniques for wind turbine blades. *Journal of Wind Engineering and Industrial Aerodynamics*, **85**, 309–324.

[33] Gomez, H. C., Gur, T., and Dolan, D. (2013) Structural condition assessment of offshore wind turbine monopile foundations using vibration monitoring data. Yu, T. Y., Gyekenyesi, A. L., Shull, P. J., Diaz, A. A., Wu, H. F., and Aktan, A. E. (eds.), *SPIE Smart Structures and Materials+ Nondestructive Evaluation and Health Monitoring*, vol. 8694, pp. 86940B–1–86940B–14, International Society for Optics and Photonics.

[34] Gross, E., Zadoks, R., Simmermacher, T., and Rumsey, M. (1999) Application of damage detection techniques using wind turbine modal data. *37th Aerospace Sciences Meeting and Exhibit*, pp. 1–6, American Institute of Aeronautics and Astronautics, Reston, Virigina.

[35] Häckell, M. W. and Rolfes, R. (2013) Monitoring a 5MW offshore wind energy converterCondition parameters and triangulation based extraction of modal parameters. *Mechanical Systems and Signal Processing*, **40**, 322–343.

[36] Hameed, Z., Hong, Y. S., Cho, Y. M., Ahn, S. H., and Song, C. K. (2009) Condition monitoring and fault detection of wind turbines and related algorithms: A review. *Renewable and Sustainable Energy Reviews*, **13**, 1–39.

[37] Hao, H. and Xia, Y. (2002) Vibration-based Damage Detection of Structures by Genetic Algorithm. *Journal of Computing in Civil Engineering*, **16**, 222–229.

[38] Hasancebi, O., Erdal, F., and Saka, M. P. (2010) An adaptive harmony search method for structural optimization. *Journal of Structural Engineering*, **136**, 419–431.

[39] Hjelmstad, K. D. and Shin, S. (1996) Crack identification in a cantilever beam from modal response. *Journal of Sound and Vibration*, **198**, 527–545.

[40] Hung, C., Ko, W., and Peng, Y. (2004) Identification of modal parameters from measured input and output data using a vector backward auto-regressive with exogeneous model. *Journal of Sound and Vibration*, **276**, 1043–1063.

[41] Hung, C. F. and Ko, W. J. (2002) Identification of modal parameters from measured output data using vector backward autoregressive model. *Journal of Sound and Vibration*, **256**, 249–270.

[42] Jahjouh, M. M. and Nackenhorst, U. (2014) *Structural identification of two dimensional shear buildings using a modified adaptive harmony search algorithm*. CRC Press, London, UK.

[43] Jonkman, J., Butterfield, S., Musial, W., and Scott, G. (2009) Definition of a 5-MW Reference Wind Turbine for Offshore System Development. Tech. Rep. February, National Renewable Energy Laboratory, Colorado, USA.

[44] Jonkman, J. and Musial, W. (2010) Offshore Code Comparison Collaboration (OC3) for IEA Task 23 Offshore Wind Technology and Deployment. Tech. Rep. December, National Renewable Energy Laboratory, Colorado, USA.

[45] Jonkman, J., et al. (2012) Offshore Code Comparison Collaboration Continuation (OC4), Phase I Results of Coupled Simulations of an Offshore Wind Turbine with Jacket Support Structure. Tech. Rep. March, National Renewable Energy Laboratory, Colorado, USA.

[46] Jonkman, J. M. and Buhl Jr., M. L. (2005) FAST user's guide. Tech. rep., National Renewable Energy Laboratory, Colorado, USA.

[47] Kalman, R. E. (1960) A new approach to linear filtering and prediction problems. *Journal of Fluids Engineering*, **82**, 35–45.

[48] Karbhari, V. M. and Ansari, F. (2009) *Structural health monitoring of civil infrastructure systems*. Elsevier.

[49] Karimi, I., Khaji, N., Ahmadi, M. T., and Mirzayee, M. (2010) System identification of concrete gravity dams using artificial neural networks based on a hybrid finite elementboundary element approach. *Engineering Structures*, **32**, 3583–3591.

[50] Katafygiotis, L. S. and Yuen, K. (2001) Bayesian spectral density approach for modal updating using ambient data. *Earthquake Engineering & Structural Dynamics*, **30**, 1103–1123.

[51] Koh, C. G., Chen, Y. F., and Liaw, C. Y. (2003) A hybrid computational strategy for identification of structural parameters. *Computers & Structures*, **81**, 107–117.

[52] Koh, C. G., Hong, B., and Liaw, C. Y. (2000) Parameter Identification of Large Structural Systems in Time Domain. *Journal of Structural Engineering*, **126**, 957–963.

[53] Koh, C. G. and Perry, M. J. (2010) *Structural Identification and Damage Detection using Genetic Algorithms*. CRC Press, London, UK.

[54] Koh, C. G., See, M. S., and Balendra, T. (1995) Damage Detection of Buildings: Numerical and Experimental Studies. *Journal of Structural Engineering*, **121**, 1155–1160.

[55] Koh, C. G. and Trinh, T. N. (2013) *19 An Evolutionary Divide-and-Conquer Strategy for Structural Identification*. Elsevier Inc., first edit edn.

[56] Lam, H. F., Katafygiotis, L. S., and Mickleborough, N. C. (2004) Application of a Statistical Model Updating Approach on Phase I of the IASC-ASCE Structural Health Monitoring Benchmark Study. *Journal of Engineering Mechanics*, **130**, 34–48.

[57] Lam, H. F., Ko, J. M., and Wong, C. W. (1995) Detection of damage locations based on sensitivity analysis. *13th International Modal Analysis Conference*, pp. 1499–1505.

[58] Law, S. S., Shi, Z. Y., and Zhang, L. M. (1998) Structural Damage Detection from Incomplete and Noisy Modal Test Data. *Journal of Engineering Mechanics*, **124**, 1280–1288.

[59] Lee, J., Takatsubo, J., Toyama, N., and Kang, D. (2007) Health monitoring of complex curved structures using an ultrasonic wavefield propagation imaging system. *Measurement Science and Technology*, **18**, 3816–3824.

[60] Lefik, M. and Schrefler, B. A. (2002) Artificial neural network for parameter identifications for an elasto-plastic model of superconducting cable under cyclic loading. *Computers & Structures*, **80**, 1699–1713.

[61] Lei, Y., Liu, C., and Liu, L. J. (2014) Identification of multistory shear buildings under unknown earthquake excitation using partial output measurements: numerical and experimental studies. *Structural Control and Health Monitoring*, **21**, 774–783.

[62] Li, H., Yang, H., and Hu, S.-L. J. (2006) Modal Strain Energy Decomposition Method for Damage Localization in 3D Frame Structures. *Journal of Engineering Mechanics*, **132**, 941–951.

[63] Li, J., Liao, B., and Huang, M. (2010) Structural Damage Identification via Modal Data Based on Genetic Algorithm. *International Conference on Computational Intelligence and Software Engineering*, pp. 1–4, IEEE.

[64] Marano, G. C., Quaranta, G., and Monti, G. (2011) Modified Genetic Algorithm for the Dynamic Identification of Structural Systems Using Incomplete Measurements. *Computer-Aided Civil and Infrastructure Engineering*, **26**, 92–110.

[65] Masri, S. F., Nakamura, M., Chassiakos, A. G., and Caughey, T. K. (1996) Neural Network Approach to Detection of Changes in Structural Parameters. *Journal of Engineering Mechanics*, **122**, 350–360.

[66] Masri, S. F., Smyth, A. W., Chassiakos, A. G., Caughey, T. K., and Hunter, N. F. (2000) Application of Neural Networks for Detection of Changes in Nonlinear Systems. *Journal of Engineering Mechanics*, **126**, 666–676.

[67] Miguel, L. F. F., Miguel, L. F. F., Kaminski Jr., J., and Riera, J. D. (2012) Damage detection under ambient vibration by harmony search algorithm. *Expert Systems with Applications*, **39**, 9704–9714.

[68] Moaveni, B., Stavridis, A., Lombaert, G., Conte, J. P., and Shing, P. B. (2013) Finite-Element Model Updating for Assessment of Progressive Damage in a 3-Story Infilled RC Frame. *Journal of Structural Engineering*, **139**, 1665–1674.

[69] Na, C., Kim, S., and Kwak, H. (2011) Structural damage evaluation using genetic algorithm. *Journal of Sound and Vibration*, **330**, 2772–2783.

[70] Perry, M. J. and Koh, C. G. (2008) Output-only structural identification in time domain: Numerical and experimental studies. *Earthquake Engineering & Structural Dynamics*, **37**, 517–533.

[71] Perry, M. J., Koh, C. G., and Choo, Y. S. (2006) Modified genetic algorithm strategy for structural identification. *Computers & Structures*, **84**, 529–540.

[72] Raich, A. M. and Liszkai, T. R. (2007) Improving the Performance of Structural Damage Detection Methods Using Advanced Genetic Algorithms. *Journal of Structural Engineering*, **133**, 449–461.

[73] Rao, A. R. M., Lakshmi, K., and Ganesan, K. (2013) Structural System Identification Using Quantum behaved Particle Swarm Optimisation Algorithm. *Structural Durability & Health Monitoring*, **9**, 99–128.

[74] Rolfes, R., Tsiapoki, S., and Häckell, M. W. (2014) Sensing solutions for assessing and monitoring wind turbines. *Sensor Technologies for Civil Infrastructure*, chap. 19, pp. 565–604.

[75] Rolfes, R., Zerbst, S., Haake, G., Reetz, J., and Lynch, J. P. (2007) Integral SHM-System for Offshore Wind Turbines Using Smart Wireless Sensors. *6th International Workshop on Structural Health Monitoring*, pp. 1–8, Stanford, USA.

[76] Rytter, A. (1993) *Vibration Based Inspection of Civil Engineering Structures*. Phd thesis, Aalborg University.

[77] Salawu, O. (1997) Detection of structural damage through changes in frequency: a review. *Engineering Structures*, **19**, 718–723.

[78] Schröder, K., Scholle, N., Rolfes, R., and Lohaus, L. (2014) An Approach for Local- Global Structural Health Monitoring for Offshore Wind Energy Converters. *International Wind Engineering Conference*, pp. 318–325, Hanover, Germany.

[79] Shi, Z. Y., Law, S. S., and Zhang, L. M. (1998) Structural damage localization from modal strain energy change. *Journal of Sound and Vibration*, **218**, 825–844.

[80] Shi, Z. Y., Law, S. S., and Zhang, L. M. (2000) Damage Localization by Directly Using Incomplete Mode Shapes. *Journal of Engineering Mechanics*, **126**, 656–660.

[81] Sirca, G. F. and Adeli, H. (2012) System identification in structural engineering. *Scientia Iranica*, **19**, 1355–1364.

[82] Sohn, H., Farrar, C. R., Hemez, F. M., Shunk, D. D., Stinemates, D. W., Nadler, B. R., and Czarnecki, J. J. (2004) A Review of Structural Health Monitoring Literature : 1996-2001. Tech. rep., Los Alamos National Laboratory, Los Alamos, USA.

[83] Sohn, H. and Law, K. H. (1997) A Bayesian probabilistic approach for structure damage detection. *Earthquake Engineering & Structural Dynamics*, **26**, 1259–1281.

[84] Sun, H. and Betti, R. (2014) Simultaneous identification of structural parameters and dynamic input with incomplete output-only measurements. *Structural Control and Health Monitoring*, **21**, 868–889.

[85] Sun, H., Lu, H., and Betti, R. (2013) Identification of structural models using a modified Artificial Bee Colony algorithm. *Computers & Structures*, **116**, 59–74.

[86] Sutherland, H., Beattie, A., Hansche, B., Musial, W., Allread, J., Johnson, J., and Summers, M. (1994) The Application of Non-Destructive Techniques to the Testing of a Wind Turbine Blade. Tech. Rep. June, Sandia National Laboratories, Albuquerque, USA.

[87] Swartz, R. A., Lynch, J. P., Zerbst, S., Sweetman, B., and Rolfes, R. (2010) Structural monitoring of wind turbines using wireless sensor networks. *Smart Structures and Systems*, **6**, 183–196.

[88] Tang, H., Xue, S., and Fan, C. (2008) Differential evolution strategy for structural system identification. *Computers & Structures*, **86**, 2004–2012.

[89] Toki, K., Sato, T., and Kiyono, J. (1989) Identification of structural parameters and input ground motion from response time histories. *Japan Society of Civil Engineers*, **6**, 413–421.

[90] Wang, G. S. (2009) Application of hybrid genetic algorithm to system identification. *Structural Control and Health Monitoring*, **16**, 125–153.

[91] Wang, X. M., Koh, C. G., and Zhang, J. (2014) Substructural identification of jack-up platform in time and frequency domains. *Applied Ocean Research*, **44**, 53–62.

[92] Wang, Z. (1997) Structural damage detection using measured FRF data. *Computer Methods in Applied Mechanics and Engineering*, **147**, 187–197.

[93] Worden, K., Farrar, C. R., Manson, G., and Park, G. (2007) The fundamental axioms of structural health monitoring. *Proceedings of the Royal Society A: Mathematical, Physical and Engineering Sciences*, **463**, 1639–1664.

[94] Xia, Y., Hao, H., Brownjohn, J. M. W., and Xia, P. (2002) Damage identification of structures with uncertain frequency and mode shape data. *Earthquake Engineering & Structural Dynamics*, **31**, 1053–1066.

[95] Xu, B., Wu, Z., Chen, G., and Yokoyama, K. (2004) Direct identification of structural parameters from dynamic responses with neural networks. *Engineering Applications of Artificial Intelligence*, **17**, 931–943.

[96] Xu, Y. L. and Chen, J. (2004) Structural Damage Detection Using Empirical Mode Decomposition: Experimental Investigation. *Journal of Engineering Mechanics*, **130**, 1279–1288.

[97] Yagiura, M. and Ibaraki, T. (2001) On metaheuristic algorithms for combinatorial optimization problems. *Systems and Computers in Japan*, **32**, 33–55.

[98] Yang, J. N., Lei, Y., Lin, S., and Huang, N. (2004) Hilbert-Huang Based Approach for Structural Damage Detection. *Journal of Engineering Mechanics*, **130**, 85–95.

[99] Yang, X. (2008) *Nature-inspired metaheuristic algorithms*. Luniver Press, Cambridge, UK, 2nd editio edn.

[100] Yuen, K., Beck, J. L., and Au, S. K. (2004) Structural damage detection and assessment by adaptive Markov chain Monte Carlo simulation. *Structural Control and Health Monitoring*, **11**, 327–347.

[101] Yun, C. and Bahng, E. Y. (2000) Substructural identification using neural networks. *Computers & Structures*, **77**, 41–52.

[102] Zhang, J., Koh, C. G., Trinh, T. N., Wang, X., and Zhang, Z. (2012) Identification of jack-up spudcan fixity by an output-only substructural strategy. *Marine Structures*, **29**, 71–88.

[103] Zhang, Z., Koh, C. G., and Duan, W. H. (2010) Uniformly sampled genetic algorithm with gradient search for structural identification Part II: Local search. *Computers & Structures*, **88**, 1149–1161.

[104] Zhang, Z., Koh, C. G., and Perry, M. J. (2012) Frequency domain substructural identification for arbitrary excitations. *Earthquake Engineering & Structural Dynamics*, **41**, 605–621.

[105] Zhao, J., Ivan, J. N., and DeWolf, J. T. (1998) Structural damage detection using artificial neural networks. *Journal of Infrastructure Systems*, **4**, 93–101.

[106] Zhao, X., Xu, Y. L., Chen, J., and Li, J. (2005) Hybrid identification method for multi-story buildings with unknown ground motion: Experimental investigation. *Engineering Structures*, **27**, 1234–1247.

[107] Zhao, X., Xu, Y. L., Li, J., and Chen, J. (2006) Hybrid identification method for multi-story buildings with unknown ground motion: theory. *Journal of Sound and Vibration*, **291**, 215–239.

[108] Zhu, H. P. and Xu, Y. L. (2005) Damage detection of mono-coupled periodic structures based on sensitivity analysis of modal parameters. *Journal of Sound and Vibration*, **285**, 365–390.

Appendices

Appendix A

Tower File Example

```
---------------------------------------------------------------------------
---------------------- FAST TOWER FILE ------------------------------------
NREL 5.0 MW offshore baseline monopile tower with rigid foundation input properties.
---------------------- TOWER PARAMETERS -----------------------------------
  13        NTwInpSt    - Number of input stations to specify tower geometry
False       CalcTMode   - Calculate tower mode shapes internally
   1.0      TwrFADmp(1) - Tower 1st fore-aft mode structural damping ratio (%)
   1.0      TwrFADmp(2) - Tower 2nd fore-aft mode structural damping ratio (%)
   1.0      TwrSSDmp(1) - Tower 1st side-to-side mode structural damping ratio (%)
   1.0      TwrSSDmp(2) - Tower 2nd side-to-side mode structural damping ratio (%)
---------------------- TOWER ADJUSTMUNT FACTORS ---------------------------
   1.0      FAStTunr(1) - Tower fore-aft modal stiffness tuner, 1st mode (-)
   1.0      FAStTunr(2) - Tower fore-aft modal stiffness tuner, 2nd mode (-)
   1.0      SSStTunr(1) - Tower side-to-side stiffness tuner, 1st mode (-)
   1.0      SSStTunr(2) - Tower side-to-side stiffness tuner, 2nd mode (-)
   1.0      AdjTwMa     - Factor to adjust tower mass density (-)
   1.0      AdjFASt     - Factor to adjust tower fore-aft stiffness (-)
   1.0      AdjSSSt     - Factor to adjust tower side-to-side stiffness (-)
---------------------- DISTRIBUTED TOWER PROPERTIES -----------------------
HtFract  TMassDen  TwFAStif   TwSSStif   TwGJStif   TwEAStif   TwFAIner  TwSSIner  TwFAcgOf  TwSScgOf
(-)      (kg/m)    (Nm^2)     (Nm^2)     (Nm^2)     (N)        (kg m)    (kg m)    (m)       (m)
0.00000  9517.14   1037.13E9  1037.13E9  798.098E9  235.129E9  41979.2   41979.2   0.0       0.0
0.27881  9517.14   1037.13E9  1037.13E9  798.098E9  235.129E9  41979.2   41979.2   0.0       0.0
0.27882  4306.51    474.49E9   474.49E9  365.133E9  106.396E9  19205.6   19205.6   0.0       0.0
0.35094  4030.44    413.08E9   413.08E9  317.878E9   99.576E9  16720.0   16720.0   0.0       0.0
0.42306  3763.45    357.83E9   357.83E9  275.356E9   92.979E9  14483.4   14483.4   0.0       0.0
```

```
0.49517  3505.52    308.30E9   308.30E9  237.242E9   86.607E9  12478.7   12478.7   0.0       0.0
0.56729  3256.66    264.08E9   264.08E9  203.220E9   80.459E9  10689.2   10689.2   0.0       0.0
0.63941  3016.86    224.80E9   224.80E9  172.987E9   74.534E9   9098.9    9098.9   0.0       0.0
0.71153  2786.13    190.06E9   190.06E9  146.252E9   68.834E9   7692.7    7692.7   0.0       0.0
0.78365  2564.46    159.49E9   159.49E9  122.735E9   63.357E9   6455.7    6455.7   0.0       0.0
0.85576  2351.87    132.77E9   132.77E9  102.167E9   58.105E9   5373.9    5373.9   0.0       0.0
0.92788  2148.34    109.54E9   109.54E9   84.291E9   53.077E9   4433.6    4433.6   0.0       0.0
1.00000  1953.87     89.49E9    89.49E9   68.863E9   48.272E9   3622.1    3622.1   0.0       0.0
---------------------- TOWER FORE-AFT MODE SHAPES -----------------------------
   1.3567   TwFAM1Sh(2) - Mode 1, coefficient of x^2 term
  -3.7853   TwFAM1Sh(3) -       , coefficient of x^3 term
   8.5603   TwFAM1Sh(4) -       , coefficient of x^4 term
  -7.4143   TwFAM1Sh(5) -       , coefficient of x^5 term
   2.2826   TwFAM1Sh(6) -       , coefficient of x^6 term
 -59.6946   TwFAM2Sh(2) - Mode 2, coefficient of x^2 term
  60.4622   TwFAM2Sh(3) -       , coefficient of x^3 term
 -84.6830   TwFAM2Sh(4) -       , coefficient of x^4 term
 182.3303   TwFAM2Sh(5) -       , coefficient of x^5 term
 -97.4148   TwFAM2Sh(6) -       , coefficient of x^6 term
---------------------- TOWER SIDE-TO-SIDE MODE SHAPES -------------------------
   1.3381   TwSSM1Sh(2) - Mode 1, coefficient of x^2 term
  -3.8562   TwSSM1Sh(3) -       , coefficient of x^3 term
   8.8383   TwSSM1Sh(4) -       , coefficient of x^4 term
  -7.5993   TwSSM1Sh(5) -       , coefficient of x^5 term
   2.2791   TwSSM1Sh(6) -       , coefficient of x^6 term
 -79.9756   TwSSM2Sh(2) - Mode 2, coefficient of x^2 term
 114.9671   TwSSM2Sh(3) -       , coefficient of x^3 term
-238.8314   TwSSM2Sh(4) -       , coefficient of x^4 term
 380.7391   TwSSM2Sh(5) -       , coefficient of x^5 term
-175.8991   TwSSM2Sh(6) -       , coefficient of x^6 term
```

Appendix B

Detailed Results for Shear Frames

B.1 Known Mass Results

For the sake of illustration, results from all 10 runs of the known mass identification performed on a 5-DOF structure are presented for the case of 0% noise and a variety of time history lengths. For the sake of abstraction and due to the fact that two-dimensional shear frames are a rather simple problem which does not require such extensive detail, only the average result obtained from all 10 identification results is tabulated for the rest of the identification cases.

For the sake of simplicity and in order to have a unified simple representation of results, the values of structural characteristics in all obtained results in this appendix are shown as the deviation (in %) from the original values. Thus, of it is stated, for example, that $\Delta k_1 = -1\%$, then the identified value of k_1 is 0.99 times its originally assumed value.

Table B.1: Known mass identification detailed results: 5-DOF structure.

Noise (%)	t_{total} (seconds)	Run	Results (%) Δk_1	Δk_2	Δk_3	Δk_4	Δk_5	$\Delta\alpha$	$\Delta\beta$
0	0.5	1	0	0	0	0	0	0	0
		2	0	0	0	0	0	-2	0
		3	0	0	0	0	0	-4	1
		4	0	0	0	0	0	0	0
		5	0	0	0	0	0	0	0
		6	0	0	0	0	0	-1	0
		7	0	0	0	0	0	-1	0
		8	0	0	0	0	0	0	1
		9	0	0	0	0	0	-4	0
		10	0	0	0	0	0	0	0
		$\Delta\mathbf{X}_\mu$	0	0	0	0	0	-1.2	0.2
0	1.0	1	0	0	0	0	0	0	0
		2	0	0	0	0	0	0	0
		3	0	1	-1	0	0	2	1
		4	0	0	0	0	0	0	0
		5	0	0	0	0	0	0	0
		6	0	1	-1	0	0	2	1
		7	0	0	0	0	0	0	0
		8	0	0	0	0	0	0	0
		9	0	0	0	0	0	0	0
		10	0	0	0	0	0	0	0
		$\Delta\mathbf{X}_\mu$	0	0.2	-0.2	0	0	0.4	-0.2
0	2.0	1	0	0	0	0	0	3	0
		2	0	0	0	0	0	-2	1
		3	0	0	0	0	0	0	0
		4	0	0	0	0	0	0	0
		5	0	0	0	0	0	0	0
		6	0	0	0	0	0	1	0
		7	0	0	0	0	0	0	1
		8	0	0	0	0	0	0	0
		9	0	0	0	0	0	0	0
		10	0	0	0	0	0	0	0
		$\Delta\mathbf{X}_\mu$	0	0	0	0	0	0.2	0.2

Table C.1: Cont'd

Noise (%)	t_{total} (seconds)	Run	Results (%) Δk_1	Δk_2	Δk_3	Δk_4	Δk_5	$\Delta\alpha$	$\Delta\beta$
0	5.0	1	0	0	0	0	0	2	0
		2	-1	1	0	0	1	-8	2
		3	0	0	0	0	0	2	0
		4	0	0	0	0	0	0	0
		5	0	-1	0	0	0	1	-1
		6	0	0	0	0	0	0	0
		7	0	1	0	0	1	-4	1
		8	0	-1	0	0	0	0	1
		9	-1	0	0	0	0	0	0
		10	0	0	0	0	0	1	-1
		$\Delta\mathbf{X}_\mu$	-0.2	0	0	0	0.2	-0.6	0.2
0	10.0	1	0	0	0	0	0	0	1
		2	0	0	0	0	0	0	0
		3	-1	1	0	1	0	-2	2
		4	1	-1	0	0	0	-1	0
		5	-1	1	0	0	1	1	-1
		6	-1	1	0	0	0	0	1
		7	1	-1	0	0	0	-2	1
		8	0	0	0	1	0	0	0
		9	0	0	0	0	0	-1	1
		10	-1	1	0	0	1	1	-1
		$\Delta\mathbf{X}_\mu$	-0.2	0.2	0	0.2	0.2	-0.4	0.4

Table B.2: Known mass identification average results: 5-DOF structure.

Noise (%)	t_{total} (seconds)	Results (%) Δk_1	Δk_2	Δk_3	Δk_4	Δk_5	$\Delta\alpha$	$\Delta\beta$
0	0.5	0.0	0.0	0.0	0.0	0.0	-1.2	0.2
	1.0	0.0	0.2	-0.2	0.0	0.0	0.4	-0.2
	2.0	0.0	0.0	0.0	0.0	0.0	0.2	0.2
	5.0	-0.2	0.0	0.0	0.0	0.2	-0.6	0.2
	10.0	-0.2	0.2	0.0	0.2	0.2	-0.4	0.4
5	0.5	11.4	-9.2	4.6	-9.2	-2.0	-21.0	12.6
	1.0	-0.2	-0.8	-0.6	-0.2	1.8	2.0	0.6
	2.0	1.4	-0.2	-0.8	0.0	0.0	-3.4	1.2
	5.0	-0.4	1.2	0.6	0.0	-0.6	2.4	1.4
	10.0	0.2	0.2	0.0	-0.2	0.2	1.6	-0.6
10	0.5	-9.4	-4.8	0.6	10.2	4.6	-122.4	39.8
	1.0	6.0	-8.6	-7.6	7.8	6.0	-23.0	3.8
	2.0	2.6	-1.2	-0.2	-1.6	-1.4	-12.6	17.0
	5.0	1.6	2.0	-1.0	-0.2	0.6	-1.4	4.0
	10.0	-0.4	1.0	0.4	0.2	0.0	7.8	-0.4

Table B.3: Known mass identification average results: 10-DOF structure.

Noise (%)	t_{total} (seconds)	Results (%)											
		Δk_1	Δk_2	Δk_3	Δk_4	Δk_5	Δk_6	Δk_7	Δk_8	Δk_9	Δk_{10}	$\Delta\alpha$	$\Delta\beta$
0	0.5	0.0	0.0	0.0	0.0	0.0	0.0	0.0	0.0	0.0	0.0	3.0	0.0
	1.0	0.0	0.0	0.0	0.0	0.0	0.0	0.0	0.0	0.0	0.0	1.4	0.0
	2.0	-0.4	1.0	0.0	0.4	0.0	0.0	0.0	0.0	0.0	0.0	-0.2	0.0
	5.0	-0.4	0.2	0.0	0.2	0.0	-0.4	0.6	0.0	0.0	0.0	0.0	0.2
	10.0	0.2	-0.4	-0.2	0.0	0.0	0.2	0.2	-0.2	0.0	0.0	0.4	0.0
5	0.5	-2.8	-2.6	0.8	1.4	-0.6	-0.8	3.4	-2.0	0.6	0.0	-12.2	-0.2
	1.0	1.1	-2.2	2.8	1.6	-1.0	-2.0	-1.6	0.7	0.8	0.2	-9.4	0.4
	2.0	1.6	-2.6	-1.2	-0.6	0.8	-0.4	-1.2	0.2	0.8	-0.6	1.8	1.6
	5.0	0.4	0.4	0.2	-1.4	-0.2	1.6	-1.4	0.2	0.4	-0.2	4.0	0.2
	10.0	-0.4	0.4	0.4	-0.2	0.6	-0.6	0.2	-0.4	0.4	0.2	-2.6	0.8
10	0.5	-3.0	-3.0	2.6	2.4	-1.8	-0.2	0.0	-0.8	3.8	-0.8	-3.0	-1.2
	1.0	3.0	-1.2	2.4	1.2	-1.8	1.2	1.6	0.2	2.2	1.2	-5.6	1.0
	2.0	1.8	-1.8	-3.2	2.0	0.8	-2.4	0.6	-0.2	1.0	2.2	14.8	-0.4
	5.0	0.8	0.2	1.0	-1.6	-0.6	1.0	-1.0	-1.8	-0.2	0.2	10.2	-0.4
	10.0	-0.6	4.4	0.4	-0.8	0.0	0.4	0.2	-1.4	-0.6	0.0	-12.0	1.8

Table B.4: Known mass identification average results: 20-DOF structure.

Noise (%)	t_{total} (seconds)	Results (%)										
		Δk_1	Δk_2	Δk_3	Δk_4	Δk_5	Δk_6	Δk_7	Δk_8	Δk_9	Δk_{10}	$\Delta\alpha$
		Δk_{11}	Δk_{12}	Δk_{13}	Δk_{14}	Δk_{15}	Δk_{16}	Δk_{17}	Δk_{18}	Δk_{19}	Δk_{20}	$\Delta\beta$
0	0.5	-0.6	0.6	-0.4	0.6	0.0	-0.6	0.4	0.0	-0.2	0.2	0.2
		-0.2	0.2	-0.2	0.2	0.0	-0.2	0.2	0.0	0.0	0.0	0.0
	1.0	0.0	-0.2	-0.2	0.4	0.0	-0.4	0.4	0.0	0.0	-0.2	-0.8
		0.2	-0.2	0.0	0.0	0.0	0.0	0.0	0.0	0.0	0.0	0.0
	2.0	-0.2	0.2	-0.2	0.2	0	-0.2	0.2	0	0	0.2	-0.2
		-0.2	0.2	0	0	0	0	0	0	0	0	0
	5.0	-0.2	0.2	-0.2	0.2	0	-0.2	0.2	0	0.2	-0.2	0
		0.2	0	0.2	-0.2	0	0.2	-0.2	0	0	0	0
	10.0	0.2	-0.2	0.2	-0.2	0	0.2	-0.2	-0.2	0.2	-0.2	0.2
		0.2	-0.2	0	0	0	0	0	0	0	0	0
5	0.5	5.6	-0.2	5.6	-2	0.2	5.4	-4	-1.6	2.8	4	62.2
		-1.8	2	-1.2	0.2	2	1.8	-0.6	0.4	-3.2	1.2	-0.4
	1.0	1.6	6	3.8	-1	-0.4	1.8	-4	0	-2.6	-0.2	-13.6
		-1	3.4	-2	2.8	-0.6	-1.2	0.8	-0.2	-1	0.6	-0.2
	2.0	0.6	-0.2	0.6	-1.2	-0.2	0.8	-0.8	-0.2	-0.6	-0.6	-5
		-1.2	0.8	-1.6	0.6	-0.4	-1.2	0.8	0.2	1	1	0.4
	5.0	0	-0.2	0	0	-0.4	-0.2	0.4	0.6	0.2	-0.4	-6.6
		1.6	-1.4	-0.2	-0.4	0.2	-0.2	0	-1	0.8	-0.2	0.6
	10.0	0.4	0.4	0.6	0.4	-0.4	0.2	-1	0.4	0	-0.8	0.4
		0.6	-0.4	0.8	-0.2	0.2	0.8	-0.2	0.2	-1	-0.2	0.2
10	0.5	20.4	5.4	17	-3.6	1.8	14.6	-6.4	7.4	-1.2	1	149
		4.2	3.6	-0.6	-1.8	2.2	3.6	-0.6	4.2	-11.8	0.8	-5.6
	1.0	20.2	-1.4	1.2	-2.8	-2.2	7	-6	6.2	-10	-3	28.2
		0.4	7.4	-5.8	3.6	-0.6	-0.8	-3.6	0.8	2.4	0.4	-1.4
	2.0	4.6	-2	1.2	-3	-0.2	1	-0.2	-3.2	10.4	-3.6	-10.2
		3	-5	3.6	-3	-0.6	2.2	-2.2	0	1.8	0	1
	5.0	3.2	1.8	1.2	-1.6	-1	0	-1	2.6	-0.8	-1.4	33.6
		1.2	-0.8	-0.6	0.4	-0.6	-0.6	1.6	0	0.6	-0.4	0.6
	10.0	-2.4	3.4	-0.6	2.8	0	-1.4	0.8	0.8	0	0	6.6
		-0.6	-0.2	1	0.6	-0.4	0.2	1.8	1.6	-1.8	0.4	0.2

B.2 Unknown Mass Results

Table B.5: Unknown mass identification average results: 5-DOF structure.

Noise (%)	t_{total} (seconds)	Results (%) Δm_1	Δm_2	Δm_3	Δm_4	Δm_5	Δk_1	Δk_2	Δk_3	Δk_4	Δk_5	$\Delta\alpha$	$\Delta\beta$
0	0.5	5.4	1.6	1.2	0.4	0	3.4	4.2	2.8	0.8	0	-11.6	0.2
	1.0	0.8	0.6	0.6	0.2	0	0.6	0.8	0.6	0.4	0.2	-4	0.2
	2.0	0	0	0	0	0	0	0	0	0	0	0	0
	5.0	0	0	0	0	0	0	0	0	0	0	-0.4	0.2
	10.0	0	0	0	0	0	0	0	0	0	0	0	0
5	0.5	23.4	9.4	10.8	-1	0.8	16.6	10	20.6	4.2	-1	-81.4	-6.8
	1.0	-2	2.4	0.6	1.8	0.4	0.8	-1.2	0.6	0.8	0.4	-17.2	3
	2.0	3.4	1.6	0	0.4	0	2.2	3	2	1.6	-1	3.2	-3
	5.0	-0.4	-0.4	-0.8	-0.6	0	0	-0.2	-0.6	-0.4	-0.4	0.4	-0.8
	10.0	-0.6	0	0	-0.2	0.2	-0.4	0	0	0.2	-0.2	0.6	-0.4
10	0.5	49.6	3.6	8.8	5.6	0.8	36.6	-2	35.6	7.2	8.2	-42.8	-19.6
	1.0	38.6	2.6	7.6	6.4	2.4	9.2	6.8	5.2	7.8	5.4	-57.8	-6
	2.0	1.8	2.8	3.4	1.2	2.4	2.8	2.4	4.8	2.4	1.4	13.8	-2
	5.0	1.2	1.6	2.6	2.8	1.2	1	2	2.6	3.2	1.2	2	-1.2
	10.0	0.4	1	2	1.2	1	0.8	1	1.6	1	1.4	7	-0.4

Table B.6: Unknown mass identification average results: 10-DOF structure.

Noise (%)	t_{total} (seconds)	Results (%)										
		Δm_1 Δk_1	Δm_2 Δk_2	Δm_3 Δk_3	Δm_4 Δk_4	Δm_5 Δk_5	Δm_6 Δk_6	Δm_7 Δk_7	Δm_8 Δk_8	Δm_9 Δk_9	Δm_{10} Δk_{10}	$\Delta\alpha$ $\Delta\beta$
0	0.5	0	0	0	0	0	0	0	0	0	0	0
		0	0	0	0	0	0	0	0	0	0	0
	1.0	0	0	0	0	0	0	0	0	0	0	0
		0	0	0	0	0	0	0	0	0	0	0
	2.0	0	0	0	0	0	0	0	0	0	0	0
		0	0	0	0	0	0	0	0	0	0	0
	5.0	0	0	0	0	0	0	0	0	0	0	0
		0	0	0	0	0	0	0	0	0	0	0
	10.0	0	0	0	0	0	0	0	0	0	0	0
		0	0	0	0	0	0	0	0	0	0	0
5	0.5	0.2	1.4	3.2	-0.8	1	0.8	1.4	1.8	1.4	0	19
		-0.4	-0.8	3.6	1.2	-1.6	1.8	1.6	2	1.4	1	-1.6
	1.0	-1.2	-0.4	1.8	0.6	-0.4	1	-1	0.6	-0.6	0.4	22.8
		0	-0.2	0	1.4	-1	0.4	2.4	-0.2	0	-0.8	-1.8
	2.0	-1	1	0	0	-0.8	0.2	-0.4	0.6	2.6	0.8	2.8
		-0.2	-2	0.6	0	-0.6	-0.8	-0.2	0.2	1	2.6	0.4
	5.0	-0.8	-0.4	-0.4	0.2	1	1	0.4	0.6	1	0.4	-4
		-1.4	1	-0.6	-0.4	0.6	1.6	0	0.6	0.8	0.8	-0.6
	10.0	-0.2	0.2	-0.4	-0.2	0	0.2	-0.2	-0.6	-0.2	0.2	-1
		0	0.2	-0.4	-0.4	-0.4	0	0	-0.2	-0.4	0	0.2
10	0.5	-4	-3	-2	-3.2	0.2	-2.8	-1.2	1.8	-1.2	1.4	31
		-2.2	-3.4	-2	-2.6	-3.2	-3.4	-0.6	-3.4	0.8	0.4	1.2
	1.0	0.6	-0.4	5	0.8	1	-0.8	1.2	-3.4	1.6	0.8	7
		-0.4	-2.2	9	0.8	0.6	-0.2	-5	1.2	0.4	-1	-3.8
	2.0	1.4	1.8	2.6	3.8	-1	4.2	-0.6	3.6	2.8	2.4	2.2
		2.6	-0.4	3.2	2.8	0.4	2	0.8	1.6	3.8	4	0
	5.0	-0.4	1.6	-0.6	-1.2	1.6	-1.4	-0.2	1	2.2	1.2	10.4
		-1.2	0.2	0.2	0.6	0.8	1	0	-0.8	0.6	1.8	-2.2
	10.0	2	3.2	1.2	1.6	0.4	1	1.2	2.8	1.2	0.8	-1.6
		2.8	2.2	2.4	2.8	1	0.2	2.2	0.2	1.6	2	-0.8

Table B.7: Unknown mass identification average results: 20-DOF structure.

Noise (%)	t_{total} (seconds)	Results (%)										
		Δm_1	Δm_2	Δm_3	Δm_4	Δm_5	Δm_6	Δm_7	Δm_8	Δm_9	Δm_{10}	$\Delta\alpha$
		Δm_{11}	Δm_{12}	Δm_{13}	Δm_{14}	Δm_{15}	Δm_{16}	Δm_{17}	Δm_{18}	Δm_{19}	Δm_{20}	$\Delta\beta$
		Δk_1	Δk_2	Δk_3	Δk_4	Δk_5	Δk_6	Δk_7	Δk_8	Δk_9	Δk_{10}	
		Δk_{11}	Δk_{12}	Δk_{13}	Δk_{14}	Δk_{15}	Δk_{16}	Δk_{17}	Δk_{18}	Δk_{19}	Δk_{20}	
0	0.5	2	2	1.6	1.2	0	-1.2	-1	-0.4	0	0	-11.8
		0.2	0.4	0.4	0.2	0.8	-0.2	0.6	0.2	0	0	0
		2	2	1.8	1.6	1.2	-1.2	-0.8	-1	0.6	-0.8	
		1.2	-0.8	1	-0.4	1	0.6	-0.6	0.6	0	0	
	1.0	0.4	0.6	0.8	-1.2	1.4	-1.2	0.6	-0.4	0.4	0	-3
		-0.2	0.4	0	0.2	0	0.2	0	0	0	0	0
		0.4	0.8	0.6	0.8	0.2	0.2	0.6	0	0.4	-0.6	
		0.6	-0.6	0.2	-0.2	0.2	0.2	-0.2	0.2	0	0	
	2.0	0	0	-0.2	0	0.2	0	0	0.2	-0.2	0	0.2
		0	-0.2	0.2	0	0	0	0	0	0	0	0
		0	0	0	-0.2	0.2	0	0	0	0	0	
		-0.2	0.2	0	0	0	0	0	0	0	0	
	5.0	0	0	0	0	0	0	0	0.2	0	0	0
		0	-0.2	0	0	0	0	0	0	0	0	0
		0	0	0	0	0	0	0	0	-0.2	0.2	
		-0.2	0.2	0	0	0	0	0	0	0	0	
	10.0	0	0	0	-0.2	0.2	-0.2	0	-0.2	0	0	0
		0	0	0	0	0	0	0	0	0	0	0
		0	-0.2	0	0	0	0	0	0	0	-0.2	
		0.2	-0.2	0	0	0	0	0	0	0	0	

Table C.7: Cont'd.

Noise (%)	t_{total} (seconds)	Results (%)										
		Δm_1	Δm_2	Δm_3	Δm_4	Δm_5	Δm_6	Δm_7	Δm_8	Δm_9	Δm_{10}	$\Delta\alpha$
		Δm_{11}	Δm_{12}	Δm_{13}	Δm_{14}	Δm_{15}	Δm_{16}	Δm_{17}	Δm_{18}	Δm_{19}	Δm_{20}	$\Delta\beta$
		Δk_1	Δk_2	Δk_3	Δk_4	Δk_5	Δk_6	Δk_7	Δk_8	Δk_9	Δk_{10}	
		Δk_{11}	Δk_{12}	Δk_{13}	Δk_{14}	Δk_{15}	Δk_{16}	Δk_{17}	Δk_{18}	Δk_{19}	Δk_{20}	
5	0.5	0.8	2	2	4.4	-2.8	2.4	0	8.8	0.8	1.2	-113.6
		7	2.4	1.6	-3.2	1.2	3.5527e-16	0.8	4.8	0.8	1	0
		1.8	0.8	2.2	1.8	-0.8	-3.8	1.6	3.8	5.2	4	
		2.8	7.6	0.6	0.4	-2.6	1.6	4	0.8	-0.4	3.2	
	1.0	-1.6	-1.2	-2	-2.2	0	1.4	0.6	-0.8	3.8	0.6	-10
		-0.6	-1.4	0.8	-1.6	5.6	-3.8	2	-2.8	3.6	0.6	-0.2
		-1.4	-0.6	-0.4	-2.2	-1.8	1.4	0.2	-0.6	4.8	-0.4	
		1.2	0.2	0.8	-1.4	4	1	-2.4	-0.2	0.6	0.2	
	2.0	-0.4	-1.2	-0.4	-1.6	0.2	-0.2	1.8	-0.4	2	0.4	-16.6
		1.2	2	1.4	2.2	0.4	-0.6	0.2	-0.6	-0.4	0.4	0.4
		0.2	-1.6	-1	0	-0.8	0.4	1.4	0.8	2	-0.6	
		3	0.4	3.4	0	2.2	-0.6	-2.2	0.2	-1.4	2	
	5.0	-1.2	0.2	0.2	0	1.6	0.2	1.8	2	0	0.4	-10
		0	0.2	0.4	-0.2	0.6	0	0.4	1	0.4	0.4	-0.4
		-0.8	-1.2	-0.2	-0.2	1.4	1.2	0.8	1.2	1	1.4	
		0.2	-0.2	-0.2	0.4	0.4	0.4	0.6	0.2	0.2	0.6	
	10.0	0.2	-0.4	0.2	0.4	0.2	1	-0.2	-1	0.4	0	0.6
		0	1.4	0.2	-0.4	0.8	-0.2	0.4	0	0	0	-0.2
		-0.2	0.2	0	0.6	0.2	0.6	0.4	-0.4	0.4	-0.6	
		0.8	-0.4	-0.2	0.6	0.2	0.2	0.6	0	0	-0.4	

Table C.7: Cont'd.

Noise (%)	t_{total} (seconds)	Results (%)										
		Δm_1	Δm_2	Δm_3	Δm_4	Δm_5	Δm_6	Δm_7	Δm_8	Δm_9	Δm_{10}	$\Delta\alpha$
		Δm_{11}	Δm_{12}	Δm_{13}	Δm_{14}	Δm_{15}	Δm_{16}	Δm_{17}	Δm_{18}	Δm_{19}	Δm_{20}	$\Delta\beta$
		Δk_1	Δk_2	Δk_3	Δk_4	Δk_5	Δk_6	Δk_7	Δk_8	Δk_9	Δk_{10}	
		Δk_{11}	Δk_{12}	Δk_{13}	Δk_{14}	Δk_{15}	Δk_{16}	Δk_{17}	Δk_{18}	Δk_{19}	Δk_{20}	
10	0.5	8.4	1.4	2.8	12.2	5	6.2	-2	4	1	-0.8	-40.4
		7.6	8.4	2.4	-3	8.2	-2.4	5.6	-8.6	5.2	1.2	-4.6
		10.6	4.4	7.2	4.4	9.6	6.2	8	0.6	0.8	-1.2	
		13.4	5.8	5.2	0	2.8	1.2	2.4	5.4	0.4	1.6	
	1.0	-5.2	-3.8	-5.2	2.4	0.6	3	-1.6	12.2	-2	0.4	75.8
		1.2	-2.6	-2.8	-4.6	6.4	-7.6	-3.8	4	0.2	1	-1
		-4.6	-6	-4	-3.8	1.2	3.2	0.8	1.6	3.8	4.2	
		2	-4.4	-11.8	1.8	1.6	-3.4	-1	-3.6	3.2	2.8	
	2.0	0	-0.6	-0.8	2.4	-1.6	2.4	-0.8	1.4	0.8	0	5.8
		-1.2	3.2	-1.4	0.8	-1	0.6	-1.2	-0.2	2.2	1.6	0
		-0.6	-0.6	-0.6	-0.6	-0.4	-0.2	1	0.8	0.2	-0.2	
		2	-1.6	0.2	2.4	0.2	-1.8	0.8	0.8	2.6	1.8	
	5.0	2	0.6	1.2	-0.8	4.6	1.2	3.6	1.6	1.6	0.8	-5.4
		0.8	3	1.8	4.6	-0.4	2.6	-0.2	-1.4	-1.8	1.4	-1
		2	2	0.4	0.8	2.2	4	3	2	3.4	-0.4	
		4.2	1.4	3	2	2	0.8	0.2	1.4	-2.4	1.8	
	10.0	2.6	2.8	1.4	3	-0.2	1.2	0.2	1	2.4	1	-4.6
		0.2	3.2	0.2	0.8	0.2	0.4	1	2.8	0.6	1.2	-0.2
		3.4	2	2.2	1.6	2.4	0	-0.6	2.2	1.8	1.6	
		1	1	0.4	2.2	1	0.6	1.2	1.6	1.2	1.4	

B.3 Output-Only Results

Table B.8: Output-only identification average results: 5-DOF structure.

Noise (%)	t_{total} (seconds)	Results (%) Δk_1	Δk_2	Δk_3	Δk_4	Δk_5	$\Delta\alpha$	$\Delta\beta$
0	0.5/0.2	0.4	-0.2	0	0	0	3.6	-0.2
	1.0/0.4	0	-0.2	0	0	0	0	0
2	0.5/0.2	0.8	-0.2	0.2	0	-0.2	-6	0.6
	1.0/0.4	0	0.2	0.2	0	0	9.8	-1
5	0.5/0.2	-0.2	-1.8	-0.4	-3.2	-1.2	-31.4	7.6
	1.0/0.4	-1.2	-0.2	0.6	0.2	-0.2	-5.8	1
10	0.5/0.2	-0.8	-1.8	-0.6	-1.4	-0.4	25.6	1
	1.0/0.4	0.6	2.4	-0.2	0	0	-9.8	2.2

Table B.9: Output-only identification average results: 10-DOF structure.

Noise (%)	t_{total} (seconds)	Results (%) Δk_1	Δk_2	Δk_3	Δk_4	Δk_5	$\Delta\alpha$	$\Delta\beta$
		Δk_6	Δk_7	Δk_8	Δk_9	Δk_{10}		
0	0.5/0.2	0	0	0	0	0		
		0	0	0	0	0	0	0
	1.0/0.4	0	0	0	0	0		
		0	0	0	0	0	0	0
2	0.5/0.2	-0.4	0.6	0.4	-1	-0.4		
		0.2	0	-0.2	0	0.2	-14.6	0.4
	1.0/0.4	0	0.2	0	0	0.2		
		0	0	0.2	0.2	0	-3.6	0
5	0.5/0.2	0.4	1.6	2.2	-1.8	0.2		
		0.6	0.6	-0.6	-1	0	45.4	-0.8
	1.0/0.4	0	-1.4	-0.4	0	0.2		
		0.2	-0.2	0.2	-0.2	0	1.2	0.4
10	0.5/0.2	-5.8	-7.4	-1	-0.4	0.2		
		-1.2	-2.6	3	0.8	-0.8	-31.6	2.8
	1.0/0.4	-1	1.4	2.6	-0.2	-1		
		0.2	-0.6	0.4	0.4	0	0.4	-0.6

Table B.10: Output-only identification average results: 20-DOF structure.

Noise (%)	t_{total} (seconds)	Results (%)										
		Δk_1	Δk_2	Δk_3	Δk_4	Δk_5	Δk_6	Δk_7	Δk_8	Δk_9	Δk_{10}	$\Delta\alpha$
		Δk_{11}	Δk_{12}	Δk_{13}	Δk_{14}	Δk_{15}	Δk_{16}	Δk_{17}	Δk_{18}	Δk_{19}	Δk_{20}	$\Delta\beta$
0	0.5/0.2	0	0	0	0	0	0	0	0	0	0	0
		0	0	0	0	0	0	0	0	0	0	0
	1.0/0.4	0	0	0	0	0	0	0	0	0	0	0
		0	0	0	0	0	0	0	0	0	0	0
2	0.5/0.2	0.2	-0.2	0.4	-0.2	-0.2	0	0	0.8	0.2	0	16.4
		0	0.4	0.4	0.2	0	0.2	0.4	0	-0.4	-0.2	-0.2
	1.0/0.4	0.4	0.4	0	-0.4	0	0	0	0	-0.2	0	-5.2
		0	-0.2	0.2	0.4	0	0	0	-0.4	0	0	0
5	0.5/0.2	1.2	0.2	-0.4	-0.6	0.2	-0.6	-0.8	1	-0.2	-0.4	-46.8
		0.4	-0.8	-0.2	-0.8	-0.4	0	-1	-0.8	0.4	-0.2	0.4
	1.0/0.4	-0.2	0	-1	0.2	0	-0.8	0	0.8	-0.2	-0.4	-15.2
		0	-0.2	0	0.2	0.2	0.2	0.2	0.2	-0.2	0.2	0
10	0.5/0.2	0	1	-0.4	2.2	1	1	0.6	-2.6	1.4	0.8	28
		1.8	1.8	-1.2	-1.2	0.2	0.6	0.8	5.2	1.2	-0.4	-1.4
	1.0/0.4	20.2	-1.4	1.2	-2.8	-2.2	7	-6	6.2	-10	-3	28.2
		0.2	0.4	1.4	-0.4	-0.6	0.2	-0.4	-1	0.2	0	0

Appendix C

Detailed Results for Offshore Wind Turbines

C.1 Damage Magnitude Effect

Table C.1: Detailed results: Damage magnitude effect for $DI = 0.0\%$.

Run No.	Identified DI (%) at station No.															
	1	2	3	4	5	6	7	8	9	10	11	12	13	14	15	16
1	0.00	0.00	0.00	0.00	1.00	0.00	0.00	1.00	0.00	0.00	0.00	0.00	0.00	0.00	0.00	0.00
2	0.00	0.00	0.00	0.00	0.00	0.00	0.00	0.00	0.00	0.00	0.00	0.00	0.00	0.00	0.00	0.00
3	0.00	0.00	0.00	0.00	0.00	0.00	0.00	0.00	0.00	0.00	0.00	0.00	0.00	0.00	0.00	0.00
4	0.00	0.00	0.00	0.00	0.00	0.00	0.00	0.00	0.00	0.00	0.00	0.00	0.00	0.00	0.00	0.00
5	0.00	0.00	0.00	0.00	0.00	0.00	0.00	0.00	0.00	0.00	0.00	0.00	0.00	0.00	0.00	0.00
6	0.00	0.00	0.00	0.00	0.00	0.00	0.00	0.00	0.00	0.00	0.00	0.00	0.00	0.00	0.00	0.00
7	0.00	0.00	0.00	0.00	0.00	0.00	0.00	0.00	0.00	0.00	0.00	0.00	0.00	0.00	0.00	0.00
8	0.00	0.00	0.00	0.00	0.00	0.00	0.00	0.00	0.00	0.00	0.00	0.00	0.00	0.00	0.00	0.00
9	0.00	0.00	0.00	0.00	0.00	0.00	0.00	0.00	0.00	0.00	0.00	0.00	0.00	0.00	0.00	0.00
10	0.00	0.00	0.00	0.00	0.00	0.00	0.00	0.00	0.00	0.00	0.00	0.00	0.00	0.00	0.00	0.00
$\mathbf{X}_\mu$	0.00	0.00	0.00	0.00	0.10	0.00	0.00	0.10	0.00	0.00	0.00	0.00	0.00	0.00	0.00	0.00

Table C.2: Detailed results: Damage magnitude effect for $DI = 3.0\%$.

Run No.	Identified DI (%) at station No.															
	1	2	3	4	5	6	7	8	9	10	11	12	13	14	15	16
1	0.00	0.00	0.00	0.00	0.00	3.00	0.00	0.00	0.00	0.00	0.00	0.00	0.00	0.00	0.00	0.00
2	0.00	0.00	0.00	0.00	0.00	3.00	0.00	0.00	0.00	0.00	0.00	0.00	0.00	0.00	0.00	0.00
3	0.00	0.00	0.00	0.00	0.00	3.00	0.00	0.00	0.00	0.00	0.00	0.00	0.00	0.00	0.00	0.00
4	0.00	0.00	0.00	0.00	0.00	3.00	0.00	0.00	0.00	0.00	0.00	0.00	0.00	0.00	0.00	0.00
5	0.00	0.00	0.00	0.00	0.00	3.00	0.00	0.00	0.00	0.00	0.00	0.00	0.00	0.00	0.00	0.00
6	0.00	0.00	0.00	0.00	0.00	3.00	0.00	0.00	0.00	0.00	0.00	0.00	0.00	0.00	0.00	0.00
7	0.00	0.00	0.00	0.00	0.00	3.00	0.00	0.00	0.00	0.00	0.00	0.00	0.00	0.00	0.00	0.00
8	0.00	0.00	0.00	0.00	0.00	3.00	0.00	0.00	0.00	0.00	0.00	0.00	0.00	0.00	0.00	0.00
9	0.00	0.00	0.00	0.00	0.00	3.00	0.00	0.00	0.00	0.00	0.00	0.00	0.00	0.00	0.00	0.00
10	0.00	0.00	0.00	0.00	0.00	3.00	0.00	0.00	0.00	0.00	0.00	0.00	0.00	0.00	0.00	0.00
$\mathbf{X}_\mu$	0.00	0.00	0.00	0.00	0.00	3.00	0.00	0.00	0.00	0.00	0.00	0.00	0.00	0.00	0.00	0.00

Table C.3: Detailed results: Damage magnitude effect for $DI = 5.0\%$.

Run No.	Identified DI (%) at station No.															
	1	2	3	4	5	6	7	8	9	10	11	12	13	14	15	16
1	0.00	0.00	0.00	0.00	0.00	5.00	0.00	0.00	0.00	0.00	0.00	0.00	0.00	0.00	0.00	0.00
2	0.00	0.00	0.00	0.00	0.00	5.00	0.00	0.00	0.00	0.00	0.00	0.00	0.00	0.00	0.00	0.00
3	0.00	0.00	0.00	0.00	0.00	5.00	0.00	0.00	0.00	0.00	0.00	0.00	0.00	0.00	0.00	0.00
4	0.00	0.00	0.00	0.00	0.00	5.00	0.00	0.00	0.00	0.00	0.00	0.00	0.00	0.00	0.00	0.00
5	0.00	0.00	0.00	0.00	0.00	5.00	0.00	0.00	0.00	0.00	0.00	0.00	0.00	0.00	0.00	0.00
6	0.00	0.00	0.00	0.00	0.00	5.00	0.00	0.00	0.00	0.00	0.00	0.00	0.00	0.00	0.00	0.00
7	0.00	0.00	0.00	0.00	0.00	5.00	0.00	0.00	0.00	0.00	0.00	0.00	0.00	0.00	0.00	0.00
8	0.00	0.00	0.00	0.00	0.00	5.00	0.00	0.00	0.00	0.00	0.00	0.00	0.00	0.00	0.00	0.00
9	0.00	0.00	0.00	0.00	0.00	5.00	0.00	0.00	0.00	0.00	0.00	0.00	0.00	0.00	0.00	0.00
10	0.00	0.00	0.00	0.00	0.00	5.00	0.00	0.00	0.00	0.00	0.00	0.00	0.00	0.00	0.00	0.00
$\mathbf{X}_\mu$	0.00	0.00	0.00	0.00	0.00	5.00	0.00	0.00	0.00	0.00	0.00	0.00	0.00	0.00	0.00	0.00

Table C.4: Detailed results: Damage magnitude effect for $DI = 10.0\%$.

Run No.	Identified DI (%) at station No.															
	1	2	3	4	5	6	7	8	9	10	11	12	13	14	15	16
1	0.00	0.00	0.00	0.00	0.00	10.00	0.00	0.00	0.00	0.00	0.00	0.00	0.00	0.00	0.00	0.00
2	0.00	0.00	0.00	0.00	0.00	10.00	0.00	0.00	0.00	0.00	0.00	0.00	0.00	0.00	0.00	0.00
3	0.00	0.00	0.00	0.00	0.00	11.00	0.00	0.00	0.00	0.00	0.00	0.00	0.00	0.00	0.00	0.00
4	0.00	0.00	0.00	0.00	0.00	10.00	0.00	0.00	0.00	0.00	0.00	0.00	0.00	0.00	0.00	0.00
5	0.00	0.00	0.00	0.00	0.00	10.00	0.00	0.00	0.00	0.00	0.00	0.00	0.00	0.00	0.00	0.00
6	0.00	0.00	0.00	0.00	0.00	10.00	0.00	0.00	0.00	0.00	0.00	0.00	0.00	0.00	0.00	0.00
7	0.00	0.00	0.00	0.00	0.00	10.00	0.00	0.00	0.00	0.00	0.00	0.00	0.00	0.00	0.00	0.00
8	0.00	0.00	0.00	0.00	0.00	10.00	0.00	0.00	0.00	0.00	0.00	0.00	0.00	0.00	0.00	0.00
9	0.00	0.00	0.00	0.00	0.00	10.00	0.00	0.00	0.00	0.00	0.00	0.00	0.00	0.00	0.00	0.00
10	0.00	0.00	0.00	0.00	0.00	10.00	0.00	0.00	0.00	0.00	0.00	0.00	0.00	0.00	0.00	0.00
$\mathbf{X}_\mu$	0.00	0.00	0.00	0.00	0.00	10.10	0.00	0.00	0.00	0.00	0.00	0.00	0.00	0.00	0.00	0.00

C.2 Sensor and Noise Effect

Table C.5: Detailed results: Noise = 0.0% and 10 Sensors.

Run No.	Identified DI (%) at station No.															
	1	2	3	4	5	6	7	8	9	10	11	12	13	14	15	16
1	0.00	0.00	0.00	0.00	0.00	10.00	0.00	0.00	0.00	0.00	0.00	0.00	0.00	0.00	0.00	0.00
2	0.00	0.00	0.00	0.00	0.00	10.00	0.00	0.00	0.00	0.00	0.00	0.00	0.00	0.00	0.00	0.00
3	0.00	0.00	0.00	0.00	0.00	10.00	0.00	0.00	0.00	0.00	0.00	0.00	0.00	0.00	0.00	0.00
4	0.00	0.00	0.00	0.00	0.00	10.00	0.00	0.00	0.00	0.00	0.00	0.00	0.00	0.00	0.00	0.00
5	0.00	0.00	0.00	0.00	0.00	10.00	0.00	0.00	0.00	0.00	0.00	0.00	0.00	0.00	0.00	0.00
6	0.00	0.00	0.00	0.00	0.00	10.00	0.00	0.00	0.00	0.00	0.00	0.00	0.00	0.00	0.00	0.00
7	0.00	0.00	0.00	0.00	0.00	10.00	0.00	0.00	0.00	0.00	0.00	0.00	0.00	0.00	0.00	0.00
8	0.00	0.00	0.00	0.00	0.00	10.00	0.00	0.00	0.00	0.00	0.00	0.00	0.00	0.00	0.00	0.00
9	0.00	0.00	0.00	0.00	0.00	10.00	0.00	0.00	0.00	0.00	0.00	0.00	0.00	0.00	0.00	0.00
10	0.00	0.00	0.00	0.00	0.00	10.00	0.00	0.00	0.00	0.00	0.00	0.00	0.00	0.00	0.00	0.00
$\mathbf{X}_\mu$	0.00	0.00	0.00	0.00	0.00	10.00	0.00	0.00	0.00	0.00	0.00	0.00	0.00	0.00	0.00	0.00

Table C.6: Detailed results: Noise = 2.0% and 10 Sensors.

Run No.	Identified DI (%) at station No.															
	1	2	3	4	5	6	7	8	9	10	11	12	13	14	15	16
1	0.00	0.00	0.00	0.00	0.00	10.00	0.00	0.00	0.00	0.00	0.00	0.00	0.00	0.00	0.00	0.00
2	0.00	0.00	0.00	0.00	0.00	9.00	1.00	0.00	0.00	0.00	0.00	0.00	0.00	0.00	0.00	0.00
3	0.00	0.00	0.00	0.00	0.00	10.00	0.00	0.00	0.00	0.00	0.00	0.00	0.00	0.00	0.00	0.00
4	0.00	0.00	0.00	0.00	0.00	10.00	0.00	0.00	0.00	0.00	0.00	0.00	0.00	0.00	0.00	0.00
5	0.00	0.00	0.00	0.00	1.00	9.00	0.00	0.00	0.00	0.00	0.00	0.00	0.00	0.00	0.00	0.00
6	0.00	0.00	0.00	0.00	0.00	10.00	0.00	0.00	0.00	0.00	0.00	0.00	0.00	0.00	0.00	0.00
7	0.00	0.00	0.00	0.00	0.00	9.00	0.00	0.00	0.00	0.00	0.00	0.00	0.00	0.00	0.00	0.00
8	0.00	0.00	0.00	0.00	0.00	10.00	0.00	0.00	0.00	0.00	0.00	0.00	0.00	0.00	0.00	0.00
9	0.00	0.00	0.00	0.00	0.00	10.00	0.00	0.00	0.00	0.00	0.00	0.00	0.00	0.00	0.00	0.00
10	0.00	0.00	0.00	0.00	0.00	9.00	0.00	0.00	0.00	0.00	0.00	0.00	0.00	0.00	0.00	0.00
$\mathbf{X}_\mu$	0.00	0.00	0.00	0.00	0.10	9.60	0.10	0.00	0.00	0.00	0.00	0.00	0.00	0.00	0.00	0.00

Table C.7: Detailed results: Noise = 5.0% and 10 Sensors.

Run No.	Identified DI (%) at station No.															
	1	2	3	4	5	6	7	8	9	10	11	12	13	14	15	16
1	0.00	0.00	0.00	0.00	0.00	10.00	0.00	0.00	0.00	0.00	0.00	0.00	0.00	0.00	0.00	0.00
2	0.00	0.00	0.00	0.00	0.00	10.00	0.00	0.00	0.00	0.00	0.00	0.00	0.00	0.00	0.00	0.00
3	0.00	0.00	0.00	0.00	0.00	9.00	0.00	0.00	0.00	0.00	0.00	0.00	0.00	0.00	0.00	0.00
4	0.00	0.00	0.00	1.00	2.00	6.00	0.00	0.00	0.00	0.00	0.00	0.00	0.00	0.00	0.00	0.00
5	0.00	0.00	0.00	0.00	0.00	10.00	0.00	0.00	0.00	0.00	0.00	0.00	0.00	0.00	0.00	0.00
6	0.00	0.00	0.00	0.00	0.00	10.00	0.00	0.00	0.00	0.00	0.00	0.00	0.00	0.00	0.00	0.00
7	0.00	0.00	0.00	0.00	0.00	9.00	0.00	0.00	0.00	0.00	0.00	0.00	0.00	0.00	0.00	0.00
8	0.00	0.00	0.00	0.00	0.00	10.00	0.00	0.00	0.00	0.00	0.00	0.00	0.00	0.00	0.00	0.00
9	0.00	0.00	0.00	0.00	1.00	8.00	2.00	0.00	0.00	0.00	0.00	0.00	0.00	0.00	0.00	0.00
10	0.00	0.00	0.00	1.00	1.00	6.00	2.00	0.00	0.00	0.00	0.00	0.00	0.00	0.00	0.00	0.00
$\mathbf{X}_\mu$	0.00	0.00	0.00	0.20	0.40	8.80	0.40	0.00	0.00	0.00	0.00	0.00	0.00	0.00	0.00	0.00

Table C.8: Detailed results: Noise = 10.0% and 10 Sensors.

Run No.	Identified DI (%) at station No.															
	1	2	3	4	5	6	7	8	9	10	11	12	13	14	15	16
1	0.00	0.00	0.00	0.00	0.00	11.00	0.00	1.00	0.00	0.00	0.00	0.00	0.00	0.00	0.00	0.00
2	0.00	0.00	0.00	0.00	0.00	10.00	0.00	0.00	0.00	0.00	0.00	0.00	0.00	0.00	0.00	0.00
3	0.00	0.00	0.00	0.00	0.00	11.00	0.00	1.00	0.00	0.00	0.00	0.00	0.00	0.00	0.00	0.00
4	0.00	0.00	0.00	1.00	1.00	3.00	0.00	1.00	1.00	0.00	0.00	0.00	0.00	0.00	0.00	0.00
5	0.00	0.00	0.00	0.00	0.00	4.00	0.00	2.00	0.00	0.00	0.00	0.00	0.00	1.00	0.00	0.00
6	0.00	0.00	0.00	0.00	0.00	11.00	0.00	1.00	0.00	0.00	0.00	0.00	0.00	0.00	0.00	0.00
7	0.00	0.00	0.00	0.00	0.00	6.00	1.00	2.00	0.00	0.00	0.00	0.00	0.00	0.00	0.00	0.00
8	0.00	0.00	0.00	0.00	0.00	10.00	0.00	0.00	0.00	0.00	0.00	0.00	0.00	0.00	0.00	0.00
9	0.00	0.00	0.00	0.00	0.00	11.00	1.00	1.00	0.00	0.00	0.00	0.00	0.00	0.00	0.00	0.00
10	0.00	0.00	0.00	0.00	0.00	10.00	1.00	0.00	0.00	0.00	0.00	0.00	0.00	0.00	0.00	0.00
$\mathbf{X}_\mu$	0.00	0.00	0.00	0.10	0.10	8.7	0.30	0.90	0.10	0.00	0.00	0.00	0.00	0.10	0.00	0.00

Table C.9: Detailed results: Noise = 0.0% and 6 Sensors.

Run No.	Identified DI (%) at station No.															
	1	2	3	4	5	6	7	8	9	10	11	12	13	14	15	16
1	0.00	0.00	0.00	0.00	0.00	10.00	0.00	0.00	0.00	0.00	0.00	0.00	0.00	0.00	0.00	0.00
2	0.00	0.00	0.00	0.00	0.00	9.00	0.00	0.00	0.00	0.00	0.00	0.00	0.00	0.00	0.00	0.00
3	0.00	0.00	0.00	0.00	0.00	10.00	0.00	0.00	0.00	0.00	0.00	0.00	0.00	0.00	0.00	0.00
4	0.00	0.00	0.00	1.00	2.00	6.00	0.00	0.00	0.00	0.00	0.00	0.00	0.00	0.00	0.00	0.00
5	0.00	0.00	0.00	0.00	0.00	8.00	0.00	0.00	0.00	0.00	0.00	0.00	0.00	0.00	0.00	0.00
6	0.00	0.00	0.00	0.00	0.00	10.00	0.00	0.00	0.00	0.00	0.00	0.00	0.00	0.00	0.00	0.00
7	0.00	0.00	0.00	0.00	0.00	10.00	0.00	0.00	0.00	0.00	0.00	0.00	0.00	0.00	0.00	0.00
8	0.00	0.00	0.00	0.00	0.00	10.00	0.00	0.00	0.00	0.00	0.00	0.00	0.00	0.00	0.00	0.00
9	0.00	0.00	0.00	0.00	0.00	10.00	0.00	0.00	0.00	0.00	0.00	0.00	0.00	0.00	0.00	0.00
10	0.00	0.00	0.00	0.00	0.00	10.00	0.00	0.00	0.00	0.00	0.00	0.00	0.00	0.00	0.00	0.00
$\mathbf{X}_\mu$	0.00	0.00	0.00	0.10	0.20	9.3	0.00	0.00	0.00	0.00	0.00	0.00	0.00	0.00	0.00	0.00

Table C.10: Detailed results: Noise = 2.0% and 6 Sensors.

Run No.	Identified DI (%) at station No.															
	1	2	3	4	5	6	7	8	9	10	11	12	13	14	15	16
1	0.00	0.00	0.00	1.00	2.00	6.00	0.00	0.00	0.00	0.00	0.00	0.00	0.00	0.00	0.00	0.00
2	0.00	0.00	0.00	0.00	0.00	9.00	0.00	0.00	0.00	0.00	0.00	0.00	0.00	0.00	0.00	0.00
3	0.00	0.00	0.00	0.00	0.00	10.00	0.00	0.00	0.00	0.00	0.00	0.00	0.00	0.00	0.00	0.00
4	0.00	0.00	0.00	1.00	0.00	9.00	1.00	0.00	0.00	0.00	0.00	0.00	0.00	0.00	0.00	0.00
5	0.00	0.00	0.00	0.00	0.00	8.00	0.00	0.00	0.00	0.00	0.00	0.00	0.00	0.00	0.00	0.00
6	0.00	0.00	0.00	0.00	0.00	10.00	0.00	0.00	0.00	0.00	0.00	0.00	0.00	0.00	0.00	0.00
7	0.00	0.00	0.00	0.00	1.00	9.00	1.00	0.00	0.00	0.00	0.00	0.00	0.00	0.00	0.00	0.00
8	0.00	0.00	0.00	0.00	1.00	8.00	2.00	0.00	0.00	0.00	0.00	0.00	0.00	0.00	0.00	0.00
9	0.00	0.00	0.00	0.00	0.00	10.00	0.00	0.00	0.00	0.00	0.00	0.00	0.00	0.00	0.00	0.00
10	0.00	0.00	0.00	0.00	0.00	10.00	1.00	0.00	0.00	0.00	0.00	0.00	0.00	0.00	0.00	0.00
$\mathbf{X}_\mu$	0.00	0.00	0.00	0.20	0.40	8.9	0.50	0.00	0.00	0.00	0.00	0.00	0.00	0.00	0.00	0.00

Table C.11: Detailed results: Noise = 5.0% and 6 Sensors.

Run No.	Identified DI (%) at station No.															
	1	2	3	4	5	6	7	8	9	10	11	12	13	14	15	16
1	0.00	0.00	0.00	1.00	0.00	6.00	1.00	0.00	0.00	0.00	0.00	0.00	0.00	0.00	0.00	0.00
2	0.00	0.00	0.00	1.00	0.00	4.00	2.00	1.00	0.00	0.00	0.00	0.00	0.00	0.00	0.00	1.00
3	0.00	0.00	0.00	1.00	0.00	3.00	1.00	1.00	0.00	0.00	0.00	0.00	0.00	0.00	0.00	0.00
4	0.00	0.00	0.00	0.00	0.00	10.00	0.00	0.00	0.00	0.00	0.00	0.00	0.00	0.00	0.00	0.00
5	0.00	0.00	0.00	0.00	0.00	10.00	0.00	0.00	0.00	0.00	0.00	0.00	0.00	0.00	0.00	0.00
6	0.00	0.00	0.00	0.00	0.00	10.00	2.00	0.00	0.00	0.00	0.00	0.00	0.00	0.00	0.00	0.00
7	0.00	0.00	0.00	0.00	1.00	10.00	0.00	0.00	0.00	0.00	0.00	0.00	0.00	0.00	0.00	0.00
8	0.00	0.00	0.00	0.00	0.00	10.00	0.00	0.00	0.00	0.00	0.00	0.00	0.00	0.00	0.00	0.00
9	0.00	0.00	0.00	1.00	1.00	9.00	1.00	0.00	0.00	0.00	0.00	0.00	0.00	0.00	0.00	0.00
10	0.00	0.00	0.00	1.00	4.00	4.00	2.00	1.00	0.00	0.00	0.00	0.00	0.00	0.00	0.00	1.00
$\mathbf{X}_\mu$	0.00	0.00	0.00	0.50	0.60	7.60	0.90	0.30	0.00	0.00	0.00	0.00	0.00	0.00	0.00	0.20

Table C.12: Detailed results: Noise = 10.0% and 6 Sensors.

Run No.	Identified DI (%) at station No.															
	1	2	3	4	5	6	7	8	9	10	11	12	13	14	15	16
1	0.00	0.00	0.00	1.00	2.00	1.00	0.00	1.00	0.00	0.00	0.00	0.00	0.00	1.00	0.00	0.00
2	0.00	0.00	0.00	0.00	0.00	4.00	0.00	2.00	0.00	0.00	0.00	0.00	0.00	1.00	0.00	0.00
3	0.00	0.00	0.00	1.00	0.00	4.00	0.00	1.00	0.00	0.00	0.00	0.00	0.00	0.00	0.00	0.00
4	0.00	0.00	0.00	0.00	0.00	6.00	0.00	1.00	0.00	0.00	0.00	0.00	0.00	0.00	0.00	0.00
5	0.00	0.00	0.00	0.00	0.00	11.00	0.00	0.00	0.00	0.00	0.00	0.00	0.00	0.00	0.00	0.00
6	0.00	0.00	0.00	0.00	0.00	11.00	0.00	1.00	0.00	0.00	0.00	0.00	0.00	0.00	0.00	0.00
7	0.00	0.00	0.00	0.00	0.00	8.00	0.00	1.00	0.00	0.00	0.00	0.00	0.00	0.00	0.00	0.00
8	0.00	0.00	0.00	0.00	1.00	4.00	0.00	2.00	0.00	0.00	0.00	0.00	0.00	1.00	0.00	0.00
9	0.00	0.00	0.00	1.00	0.00	5.00	1.00	1.00	0.00	0.00	0.00	0.00	0.00	0.00	0.00	0.00
10	0.00	0.00	0.00	0.00	0.00	9.00	1.00	0.00	0.00	0.00	0.00	0.00	0.00	0.00	0.00	0.00
$\mathbf{X}_\mu$	0.00	0.00	0.00	0.30	0.30	6.30	0.20	1.00	0.00	0.00	0.00	0.00	0.00	0.30	0.00	0.00

Table C.13: Detailed results: Noise = 0.0% and 1 Sensors.

Run No.	Identified DI (%) at station No.															
	1	2	3	4	5	6	7	8	9	10	11	12	13	14	15	16
1	0.00	0.00	0.00	0.00	1.00	9.00	1.00	0.00	0.00	0.00	0.00	0.00	0.00	0.00	0.00	1.00
2	0.00	0.00	0.00	0.00	0.00	10.00	0.00	0.00	0.00	1.00	0.00	0.00	0.00	0.00	0.00	0.00
3	0.00	0.00	0.00	0.00	1.00	9.00	1.00	2.00	0.00	0.00	0.00	0.00	0.00	0.00	0.00	0.00
4	0.00	0.00	0.00	0.00	1.00	7.00	2.00	1.00	0.00	0.00	0.00	0.00	0.00	0.00	0.00	0.00
5	0.00	0.00	0.00	0.00	0.00	9.00	0.00	0.00	0.00	0.00	0.00	0.00	0.00	0.00	0.00	0.00
6	0.00	0.00	0.00	2.00	3.00	10.00	0.00	1.00	0.00	0.00	0.00	0.00	0.00	0.00	0.00	1.00
7	0.00	0.00	0.00	1.00	4.00	12.00	0.00	0.00	0.00	1.00	0.00	0.00	0.00	0.00	0.00	0.00
8	0.00	0.00	0.00	2.00	0.00	8.00	1.00	2.00	0.00	0.00	0.00	0.00	0.00	0.00	0.00	0.00
9	0.00	0.00	0.00	0.00	1.00	8.00	0.00	1.00	0.00	0.00	0.00	0.00	0.00	0.00	0.00	0.00
10	0.00	0.00	0.00	0.00	1.00	10.00	1.00	0.00	0.00	0.00	0.00	0.00	0.00	0.00	0.00	0.00
$\mathbf{X}_\mu$	0.00	0.00	0.00	0.50	1.20	9.20	0.60	0.70	0.00	0.20	0.00	0.00	0.00	0.00	0.00	0.20

Table C.14: Detailed results: Noise = 2.0% and 1 Sensors.

Run No.	Identified DI (%) at station No.															
	1	2	3	4	5	6	7	8	9	10	11	12	13	14	15	16
1	0.00	0.00	0.00	0.00	0.00	10.00	0.00	0.00	0.00	0.00	0.00	0.00	0.00	0.00	0.00	0.00
2	0.00	0.00	0.00	1.00	2.00	5.00	0.00	1.00	0.00	0.00	0.00	0.00	0.00	0.00	0.00	0.00
3	0.00	0.00	0.00	1.00	0.00	7.00	0.00	0.00	0.00	0.00	0.00	0.00	0.00	0.00	0.00	3.00
4	0.00	0.00	0.00	1.00	2.00	5.00	0.00	1.00	0.00	0.00	0.00	0.00	0.00	0.00	0.00	0.00
5	0.00	0.00	0.00	0.00	0.00	10.00	0.00	0.00	0.00	0.00	0.00	0.00	0.00	0.00	0.00	0.00
6	0.00	0.00	0.00	0.00	0.00	10.00	0.00	0.00	0.00	0.00	0.00	0.00	0.00	0.00	0.00	0.00
7	0.00	0.00	0.00	0.00	2.00	8.00	0.00	1.00	0.00	0.00	0.00	0.00	0.00	0.00	0.00	0.00
8	0.00	0.00	0.00	0.00	0.00	9.00	0.00	0.00	0.00	0.00	0.00	0.00	0.00	0.00	0.00	3.00
9	0.00	0.00	0.00	1.00	2.00	7.00	0.00	1.00	0.00	0.00	0.00	0.00	0.00	0.00	0.00	0.00
10	0.00	0.00	0.00	0.00	0.00	10.00	0.00	0.00	0.00	0.00	0.00	0.00	0.00	0.00	0.00	0.00
$\mathbf{X}_\mu$	0.00	0.00	0.00	0.40	0.80	8.1	0.00	0.40	0.00	0.00	0.00	0.00	0.00	0.00	0.00	0.60

Table C.15: Detailed results: Noise = 5.0% and 1 Sensors.

Run No.	Identified DI (%) at station No.															
	1	2	3	4	5	6	7	8	9	10	11	12	13	14	15	16
1	0.00	0.00	0.00	2.00	0.00	1.00	0.00	2.00	0.00	0.00	0.00	0.00	0.00	0.00	0.00	2.00
2	0.00	0.00	0.00	1.00	0.00	3.00	1.00	2.00	0.00	0.00	0.00	0.00	0.00	0.00	0.00	0.00
3	0.00	0.00	0.00	1.00	2.00	2.00	1.00	2.00	0.00	0.00	0.00	0.00	0.00	0.00	0.00	0.00
4	0.00	0.00	0.00	1.00	2.00	4.00	0.00	1.00	0.00	0.00	0.00	0.00	0.00	0.00	0.00	0.00
5	0.00	0.00	0.00	1.00	0.00	1.00	0.00	1.00	0.00	0.00	0.00	0.00	0.00	0.00	0.00	0.00
6	0.00	0.00	0.00	0.00	1.00	6.00	0.00	1.00	0.00	0.00	0.00	0.00	0.00	0.00	0.00	0.00
7	0.00	0.00	0.00	2.00	1.00	3.00	1.00	2.00	0.00	0.00	0.00	0.00	0.00	0.00	0.00	0.00
8	0.00	0.00	0.00	2.00	0.00	2.00	1.00	1.00	0.00	0.00	0.00	0.00	0.00	0.00	0.00	0.00
9	0.00	0.00	0.00	1.00	2.00	4.00	0.00	2.00	0.00	0.00	0.00	0.00	0.00	0.00	0.00	0.00
10	0.00	0.00	0.00	1.00	0.00	6.00	0.00	2.00	0.00	0.00	0.00	0.00	0.00	0.00	0.00	2.00
$\mathbf{X}_\mu$	0.00	0.00	0.00	1.20	0.80	3.20	0.40	1.60	0.00	0.00	0.00	0.00	0.00	0.00	0.00	0.40

Table C.16: Detailed results: Noise = 10.0% and 1 Sensors.

Run No.	Identified DI (%) at station No.															
	1	2	3	4	5	6	7	8	9	10	11	12	13	14	15	16
1	0.00	0.00	0.00	0.00	2.00	6.00	0.00	0.00	1.00	0.00	0.00	0.00	0.00	0.00	0.00	0.00
2	0.00	0.00	0.00	1.00	0.00	7.00	0.00	0.00	0.00	0.00	0.00	0.00	0.00	0.00	0.00	0.00
3	0.00	0.00	0.00	1.00	2.00	0.00	1.00	1.00	0.00	2.00	0.00	0.00	0.00	0.00	0.00	0.00
4	0.00	0.00	0.00	0.00	6.00	8.00	0.00	0.00	0.00	0.00	0.00	0.00	0.00	1.00	0.00	0.00
5	0.00	0.00	0.00	1.00	0.00	1.00	1.00	0.00	1.00	0.00	0.00	0.00	0.00	0.00	0.00	1.00
6	0.00	0.00	0.00	0.00	1.00	8.00	1.00	0.00	1.00	0.00	0.00	0.00	0.00	0.00	0.00	1.00
7	0.00	0.00	0.00	1.00	1.00	9.00	0.00	0.00	0.00	0.00	0.00	0.00	0.00	0.00	0.00	0.00
8	0.00	0.00	0.00	1.00	3.00	2.00	0.00	0.00	1.00	1.00	0.00	0.00	0.00	1.00	0.00	0.00
9	0.00	0.00	0.00	1.00	5.00	6.00	1.00	1.00	0.00	1.00	0.00	0.00	0.00	0.00	0.00	0.00
10	0.00	0.00	0.00	0.00	0.00	1.00	0.00	0.00	0.00	0.00	0.00	0.00	0.00	0.00	0.00	0.00
$\mathbf{X}_\mu$	0.00	0.00	0.00	0.60	2.00	4.80	0.40	0.20	0.40	0.40	0.00	0.00	0.00	0.20	0.00	0.20

Appendix D

Detailed Results for Reduced Model

D.1 Validation Results

Table D.1: Detailed validation results: Undamaged case.

Run No.	Identified DI (%) at node No.														
	1	2	3	4	5	6	7	8	9	10	11	12	13	14	15
1	0.00	0.00	0.00	0.00	0.00	0.00	0.00	0.00	0.00	0.00	0.00	0.00	0.00	0.00	0.00
2	0.00	0.00	0.00	0.00	0.00	0.00	0.00	0.00	0.00	0.00	0.00	0.00	0.00	0.00	0.00
3	0.00	0.00	0.00	0.00	0.00	0.00	0.00	0.00	0.00	0.00	0.00	0.00	0.00	0.00	0.00
4	0.00	0.00	0.00	0.00	0.00	0.00	0.00	0.00	0.00	0.00	0.00	0.00	0.00	0.00	0.00
5	0.00	0.00	0.00	0.00	0.00	0.00	0.00	0.00	0.00	0.00	0.00	0.00	0.00	0.00	0.00
6	0.00	0.00	0.00	0.00	0.00	0.00	0.00	0.00	0.00	0.00	0.00	0.00	0.00	0.00	0.00
7	0.00	0.00	0.00	0.00	0.00	0.00	0.00	0.00	0.00	0.00	0.00	0.00	0.00	0.00	0.00
8	0.00	0.00	0.00	0.00	0.00	0.00	0.00	0.00	0.00	0.00	0.00	0.00	0.00	0.00	0.00
9	0.00	0.00	0.00	0.00	0.00	0.00	0.00	0.00	0.00	0.00	0.00	0.00	0.00	0.00	0.00
10	0.00	0.00	0.00	0.00	0.00	0.00	0.00	0.00	0.00	0.00	0.00	0.00	0.00	0.00	0.00
$\mathbf{X}_\mu$	0.00	0.00	0.00	0.00	0.00	0.00	0.00	0.00	0.00	0.00	0.00	0.00	0.00	0.00	0.00

Table D.2: Detailed validation results: Damaged case.

Run No.	Identified DI (%) at node No.														
	1	2	3	4	5	6	7	8	9	10	11	12	13	14	15
1	0.00	0.00	0.00	0.00	9.00	13.00	12.00	0.00	0.00	0.00	0.00	0.00	0.00	0.00	0.00
2	0.00	0.00	0.00	0.00	12.00	8.00	14.00	0.00	0.00	0.00	0.00	0.00	0.00	0.00	0.00
3	0.00	0.00	0.00	0.00	13.00	11.00	10.00	0.00	0.00	0.00	0.00	0.00	0.00	0.00	0.00
4	0.00	0.00	0.00	0.00	9.00	13.00	12.00	0.00	0.00	0.00	0.00	0.00	0.00	0.00	0.00
5	0.00	0.00	0.00	0.00	9.00	13.00	12.00	0.00	0.00	0.00	0.00	0.00	0.00	0.00	0.00
6	0.00	0.00	0.00	0.00	11.00	14.00	11.00	0.00	0.00	0.00	0.00	0.00	0.00	0.00	0.00
7	0.00	0.00	0.00	0.00	10.00	7.00	6.00	0.00	0.00	0.00	0.00	0.00	0.00	0.00	0.00
8	0.00	0.00	0.00	0.00	12.00	8.00	14.00	0.00	0.00	0.00	0.00	0.00	0.00	0.00	0.00
9	0.00	0.00	0.00	0.00	9.00	13.00	15.00	0.00	0.00	0.00	0.00	0.00	0.00	0.00	0.00
10	0.00	0.00	0.00	0.00	9.00	12.00	7.00	0.00	0.00	0.00	0.00	0.00	0.00	0.00	0.00
$\mathbf{X}_\mu$	0.00	0.00	0.00	0.00	10.30	11.20	11.30	0.00	0.00	0.00	0.00	0.00	0.00	0.00	0.00

D.2 Known Mass Identification Results

Table D.3: Detailed results: Known Mass, Noise = 0.0% and 14 Sensors.

Run	Identified DI (%) at node No.															Error	
No.	1	2	3	4	5	6	7	8	9	10	11	12	13	14	15	ϵ_α	ϵ_β
1	0.00	0.00	0.00	0.00	0.00	0.00	0.00	0.00	0.00	0.00	0.00	0.00	0.00	0.00	0.00	0.00	0.00
2	0.00	0.00	0.00	0.00	0.00	0.00	0.00	0.00	0.00	0.00	0.00	0.00	0.00	0.00	0.00	0.00	0.00
3	0.00	0.00	0.00	0.00	0.00	0.00	0.00	0.00	0.00	0.00	0.00	0.00	0.00	0.00	0.00	0.00	0.00
4	0.00	0.00	0.00	0.00	0.00	0.00	0.00	0.00	0.00	0.00	0.00	0.00	0.00	0.00	0.00	0.00	0.00
5	0.00	0.00	0.00	0.00	0.00	0.00	0.00	0.00	0.00	0.00	0.00	0.00	0.00	0.00	0.00	0.00	0.00
6	0.00	0.00	0.00	0.00	0.00	0.00	0.00	0.00	0.00	0.00	0.00	0.00	0.00	0.00	0.00	0.00	0.00
7	0.00	0.00	0.00	0.00	0.00	0.00	0.00	0.00	0.00	0.00	0.00	0.00	0.00	0.00	0.00	0.00	0.00
8	0.00	0.00	0.00	0.00	0.00	0.00	0.00	0.00	0.00	0.00	0.00	0.00	0.00	0.00	0.00	0.00	0.00
9	0.00	0.00	0.00	0.00	0.00	0.00	0.00	0.00	0.00	0.00	0.00	0.00	0.00	0.00	0.00	0.00	0.00
10	0.00	0.00	0.00	0.00	0.00	0.00	0.00	0.00	0.00	0.00	0.00	0.00	0.00	0.00	0.00	0.00	0.00
$\mathbf{X}_\mu$	0.00	0.00	0.00	0.00	0.00	0.00	0.00	0.00	0.00	0.00	0.00	0.00	0.00	0.00	0.00	0.00	0.00

Table D.4: Detailed results: Known Mass, Noise = 2.0% and 14 Sensors.

Run	Identified DI (%) at node No.															Error	
No.	1	2	3	4	5	6	7	8	9	10	11	12	13	14	15	ϵ_α	ϵ_β
1	0.00	0.00	0.00	0.00	0.00	0.00	0.00	0.00	0.00	0.00	0.00	0.00	0.00	0.00	0.00	-0.10	0.00
2	0.00	0.00	0.00	0.00	0.00	0.00	0.00	0.00	0.00	0.00	0.00	0.60	0.90	1.20	0.00	-1.90	-0.80
3	0.00	0.00	0.00	0.00	0.00	0.00	0.00	0.00	0.00	0.00	0.00	0.00	0.00	1.50	0.00	1.00	-0.40
4	0.00	0.00	0.00	0.00	0.00	0.00	0.00	0.00	0.00	0.00	0.00	2.00	0.80	0.70	0.00	2.00	-1.40
5	0.00	0.00	0.00	0.00	0.00	0.00	0.00	0.00	0.00	0.00	0.00	0.00	1.10	2.20	0.00	0.00	0.00
6	0.10	0.00	0.00	0.00	0.00	0.00	0.00	0.00	0.00	0.00	0.00	0.00	0.00	0.00	0.00	0.00	0.10
7	0.00	0.00	0.00	0.00	0.00	0.00	0.00	0.00	0.00	0.00	0.00	0.00	0.00	0.00	0.00	0.00	0.20
8	0.00	0.00	0.00	0.00	0.00	0.00	0.00	0.00	0.00	0.00	0.00	0.00	0.30	0.30	0.00	0.00	-0.20
9	0.00	0.00	0.00	0.00	0.00	0.00	0.00	0.00	0.00	0.00	0.00	0.00	0.00	0.00	0.00	0.00	0.10
10	0.00	0.00	0.00	0.00	0.00	0.00	0.00	0.00	0.00	0.00	0.00	0.00	0.00	0.00	0.00	0.00	0.00
$\mathbf{X}_\mu$	0.01	0.00	0.00	0.00	0.00	0.00	0.00	0.00	0.00	0.00	0.00	0.26	0.31	0.59	0.00	0.10	-0.24

Table D.5: Detailed results: Known Mass, Noise = 5.0% and 14 Sensors.

Run	Identified DI (%) at node No.															Error	
No.	1	2	3	4	5	6	7	8	9	10	11	12	13	14	15	ϵ_α	ϵ_β
1	0.00	0.00	0.00	0.00	0.00	0.00	0.00	0.00	0.00	0.00	0.30	4.00	0.00	0.00	0.00	2.00	-1.30
2	0.00	0.00	0.00	0.00	0.00	0.00	0.00	0.00	0.00	0.00	0.00	0.50	4.20	9.00	0.00	0.00	-5.60
3	0.00	0.00	0.00	0.00	0.00	0.00	0.00	0.00	0.00	0.00	0.00	0.00	0.00	0.00	0.00	0.00	0.00
4	0.00	0.00	0.00	0.00	0.00	0.00	0.00	0.00	0.00	0.00	0.00	0.00	0.00	0.00	0.00	0.00	0.00
5	0.10	0.00	0.00	0.00	0.00	0.00	0.00	0.00	0.00	0.00	0.00	0.00	0.00	0.00	0.00	0.00	1.00
6	0.00	0.00	0.00	0.00	0.00	0.00	0.00	0.00	0.00	0.00	0.00	3.50	1.10	7.10	0.00	-4.40	-3.90
7	0.00	0.00	0.00	0.00	0.00	0.00	0.00	0.00	0.00	0.00	0.00	0.00	0.00	0.00	0.00	0.00	1.00
8	0.00	0.00	0.00	0.00	0.00	0.00	0.00	0.00	0.00	0.00	0.00	0.00	0.00	4.90	0.00	1.00	-0.80
9	0.00	0.00	0.00	0.00	0.00	0.00	0.00	0.00	0.00	0.00	0.00	0.00	0.00	0.00	0.00	0.00	2.00
10	0.00	0.00	0.00	0.00	0.00	0.00	0.00	0.00	0.00	0.00	0.00	2.10	0.70	4.20	0.00	3.00	-2.10
$\mathbf{X}_\mu$	0.01	0.00	0.00	0.00	0.00	0.00	0.00	0.00	0.00	0.00	0.03	1.01	0.60	2.52	0.00	0.16	-0.97

Table D.6: Detailed results: Known Mass, Noise = 10.0% and 14 Sensors.

Run	Identified DI (%) at node No.															Error	
No.	1	2	3	4	5	6	7	8	9	10	11	12	13	14	15	ϵ_α	ϵ_β
1	0.00	0.00	0.00	0.00	0.00	0.00	0.00	0.00	0.00	0.00	0.20	3.60	0.00	0.00	0.00	2.00	-3.50
2	0.00	0.00	0.00	0.00	0.00	0.00	0.00	0.00	0.00	0.00	0.00	0.50	4.70	0.00	0.00	0.00	-4.50
3	0.00	0.00	0.00	0.00	0.10	0.00	0.00	0.00	0.00	0.00	0.00	1.40	0.00	7.70	0.00	-0.40	-6.30
4	0.00	0.00	0.00	0.00	0.00	0.00	0.00	0.00	0.00	0.00	0.00	6.70	1.30	12.20	0.00	-13.40	-9.60
5	0.00	0.00	0.00	0.00	0.00	0.00	0.00	0.00	0.00	0.00	0.00	5.30	7.00	2.00	0.00	-16.90	-11.90
6	0.00	0.00	0.00	0.00	0.00	0.00	0.00	0.00	0.00	0.00	0.00	0.00	0.00	0.00	0.00	1.10	1.50
7	0.00	0.00	0.00	0.00	0.00	0.00	0.00	0.00	0.00	0.00	0.00	0.70	2.10	8.90	0.00	-9.40	-10.00
8	0.40	0.00	0.00	0.00	0.00	0.00	0.00	0.00	0.00	0.00	0.00	0.00	0.00	2.90	0.00	1.40	2.20
9	0.00	0.00	0.00	0.00	0.00	0.00	0.00	0.00	0.00	0.00	0.00	0.00	0.00	0.00	0.00	0.00	1.40
10	0.00	0.00	0.00	0.00	0.00	0.00	0.00	0.00	0.00	0.00	0.00	0.00	0.00	0.00	0.00	-10.80	1.30
$\mathbf{X}_\mu$	0.04	0.00	0.00	0.00	0.01	0.00	0.00	0.00	0.00	0.00	0.02	1.82	1.51	3.37	0.00	-4.64	-3.94

Table D.7: Detailed results: Known Mass, Noise = 0.0% and 7 Sensors.

Run	Identified DI (%) at node No.															Error	
No.	1	2	3	4	5	6	7	8	9	10	11	12	13	14	15	ϵ_α	ϵ_β
1	0.00	0.00	0.00	0.00	0.00	0.00	0.00	0.00	0.00	0.00	0.00	0.00	0.00	0.00	0.00	0.00	0.00
2	0.00	0.00	0.00	0.00	0.00	0.00	0.00	0.00	0.00	0.00	0.00	0.00	0.00	0.00	0.00	0.00	0.00
3	0.00	0.00	0.00	0.00	0.00	0.00	0.00	0.00	0.00	0.00	0.00	0.00	0.00	0.00	0.00	0.00	0.00
4	0.00	0.00	0.00	0.00	0.00	0.00	0.00	0.00	0.00	0.00	0.00	0.00	0.00	0.00	0.00	0.00	0.00
5	0.00	0.00	0.00	0.00	0.00	0.00	0.00	0.00	0.00	0.00	0.00	0.00	0.00	0.00	0.00	0.00	0.00
6	0.00	0.00	0.00	0.00	0.00	0.00	0.00	0.00	0.00	0.00	0.00	0.00	0.00	0.00	0.00	0.00	0.00
7	0.00	0.00	0.00	0.00	0.00	0.00	0.00	0.00	0.00	0.00	0.00	0.00	0.00	0.00	0.00	0.00	0.00
8	0.00	0.00	0.00	0.00	0.00	0.00	0.00	0.00	0.00	0.00	0.00	0.00	0.00	0.00	0.00	0.00	0.00
9	0.00	0.00	0.00	0.00	0.00	0.00	0.00	0.00	0.00	0.00	0.00	0.00	0.00	0.00	0.00	0.00	0.00
10	0.00	0.00	0.00	0.00	0.00	0.00	0.00	0.00	0.00	0.00	0.00	0.00	0.00	0.00	0.00	0.00	0.00
$\mathbf{X}_\mu$	0.00	0.00	0.00	0.00	0.00	0.00	0.00	0.00	0.00	0.00	0.00	0.00	0.00	0.00	0.00	0.00	0.00

Table D.8: Detailed results: Known Mass, Noise = 2.0% and 7 Sensors.

Run	Identified DI (%) at node No.															Error	
No.	1	2	3	4	5	6	7	8	9	10	11	12	13	14	15	ϵ_α	ϵ_β
1	0.00	0.00	0.00	0.00	0.00	0.00	0.10	0.20	0.00	0.00	0.00	0.00	0.00	0.00	0.00	-4.00	0.00
2	0.20	0.00	0.00	0.00	0.00	0.00	0.00	0.00	0.00	0.00	0.00	0.00	0.00	0.00	0.00	5.10	0.00
3	0.00	0.00	0.00	0.00	0.00	0.00	0.00	0.00	0.00	0.00	0.20	1.60	0.40	6.30	0.00	-10.10	-1.20
4	0.10	0.00	0.00	0.00	0.00	0.00	0.00	0.00	0.00	0.00	0.00	0.00	0.00	1.10	0.00	0.00	0.00
5	0.00	0.00	0.00	0.00	0.00	0.00	0.00	0.10	0.10	0.00	0.00	0.00	0.00	0.00	0.00	0.00	0.00
6	0.00	0.00	0.00	0.00	0.00	0.00	0.00	0.00	0.00	0.00	0.20	0.20	0.40	1.70	0.00	-6.40	-0.10
7	0.00	0.00	0.00	0.00	0.00	0.00	0.00	0.00	0.00	0.00	0.00	1.10	0.80	11.20	0.00	-13.20	-2.50
8	0.00	0.00	0.00	0.00	0.00	0.00	0.00	0.00	0.00	0.00	0.00	0.00	0.00	0.00	0.00	0.00	1.40
9	0.00	0.00	0.00	0.00	0.00	0.00	0.00	0.00	0.00	0.00	0.00	0.00	0.00	0.00	0.00	0.00	0.00
10	0.00	0.00	0.10	0.00	0.00	0.00	0.00	0.00	0.00	0.00	0.00	0.00	0.10	2.10	0.00	0.00	0.00
$\mathbf{X}_\mu$	0.03	0.00	0.01	0.00	0.00	0.00	0.01	0.03	0.01	0.00	0.04	0.29	0.17	2.24	0.00	-2.86	-0.24

Table D.9: Detailed results: Known Mass, Noise = 5.0% and 7 Sensors.

Run	Identified DI (%) at node No.															Error	
No.	1	2	3	4	5	6	7	8	9	10	11	12	13	14	15	ϵ_α	ϵ_β
1	0.00	0.00	0.00	0.00	0.00	0.00	0.00	0.00	0.00	0.00	0.30	3.60	1.30	4.10	0.00	-18.40	-1.80
2	0.00	0.00	0.00	0.00	0.10	0.00	0.00	0.00	0.00	0.00	0.00	0.00	0.00	0.00	0.00	0.00	0.00
3	0.00	0.00	0.00	0.00	0.00	0.00	0.00	0.00	0.00	0.00	0.00	0.40	0.00	8.00	0.00	-1.20	-1.80
4	0.00	0.00	0.00	0.00	0.00	0.00	0.00	0.00	0.00	0.00	0.00	0.00	2.40	0.10	0.00	2.30	-0.90
5	0.00	0.00	0.00	0.00	0.10	0.00	0.00	0.00	0.00	0.00	0.00	0.00	0.00	8.90	0.00	-5.50	-1.40
6	0.00	0.00	0.00	0.00	0.00	0.00	0.00	0.00	0.00	0.00	0.00	0.00	0.00	0.00	0.00	0.00	0.00
7	0.00	0.00	0.00	0.00	0.00	0.00	0.00	0.00	0.00	0.00	2.40	0.00	0.00	6.70	0.00	-4.40	-1.60
8	0.00	0.00	0.00	0.00	0.00	0.00	0.00	0.00	0.00	0.00	0.00	0.00	0.00	0.00	0.00	0.00	2.10
9	0.00	0.00	0.00	0.00	0.00	0.00	0.00	0.00	0.00	0.00	0.00	0.00	0.00	1.90	0.00	-4.90	0.00
10	0.00	0.00	0.00	0.00	0.00	0.00	0.00	0.00	0.00	0.00	0.00	0.00	0.00	0.00	0.00	2.40	0.00
$\mathbf{X}_\mu$	0.00	0.00	0.00	0.00	0.02	0.00	0.00	0.00	0.00	0.00	0.27	0.40	0.37	2.97	0.00	-2.97	-0.54

Table D.10: Detailed results: Known Mass, Noise = 10.0% and 7 Sensors.

Run	Identified DI (%) at node No.															Error	
No.	1	2	3	4	5	6	7	8	9	10	11	12	13	14	15	ϵ_α	ϵ_β
1	0.30	0.00	0.00	0.00	0.00	0.00	0.00	0.00	0.00	0.00	0.00	0.00	0.00	0.00	0.00	0.00	0.00
2	0.10	0.00	0.00	0.00	0.00	0.00	0.00	0.00	0.00	0.00	0.00	0.00	0.00	0.00	0.00	0.00	0.00
3	0.00	0.00	0.00	0.00	0.00	0.00	0.00	0.00	0.00	0.00	2.00	2.80	0.00	13.50	0.00	-11.30	-1.10
4	0.00	0.00	0.00	0.00	0.30	0.00	0.00	0.00	0.00	0.00	0.10	1.00	0.00	13.60	0.00	-14.60	-3.60
5	0.50	0.00	0.00	0.00	0.00	0.00	0.00	0.00	0.00	0.00	0.00	0.00	0.00	0.00	0.00	2.20	0.00
6	0.20	0.00	0.00	0.00	0.00	0.00	0.00	0.00	0.00	0.00	0.00	0.00	0.00	0.00	0.00	0.00	4.10
7	0.00	0.00	0.00	0.00	0.00	0.00	0.00	0.00	0.00	0.00	0.30	0.00	11.40	20.00	0.00	-20.00	-10.20
8	0.00	0.00	0.00	0.00	0.00	0.00	0.00	0.00	0.00	0.00	0.00	0.00	0.00	0.00	0.00	0.00	0.10
9	0.00	0.00	0.00	0.00	0.00	0.00	0.00	0.00	0.00	0.00	0.00	0.00	0.00	0.00	0.00	0.00	3.90
10	0.00	0.00	0.00	0.00	0.00	0.00	0.00	0.00	0.00	0.00	0.00	0.00	0.00	0.00	0.00	0.00	0.00
$\mathbf{X}_\mu$	0.11	0.00	0.00	0.00	0.03	0.00	0.00	0.00	0.00	0.00	0.24	0.38	1.14	4.71	0.00	-4.37	-0.68

Table D.11: Detailed results: Known Mass, Noise = 0.0% and 4 Sensors.

Run	Identified DI (%) at node No.															Error	
No.	1	2	3	4	5	6	7	8	9	10	11	12	13	14	15	ϵ_α	ϵ_β
1	0.00	0.00	0.00	0.00	0.00	0.00	0.00	0.00	0.00	0.00	0.00	0.00	0.00	0.00	0.00	0.00	0.00
2	0.00	0.00	0.00	0.00	0.00	0.00	0.00	0.00	0.00	0.00	0.00	0.00	0.00	0.00	0.00	0.00	0.00
3	0.00	0.00	0.00	0.00	0.00	0.00	0.00	0.00	0.00	0.00	0.00	0.00	0.00	0.00	0.00	0.00	0.00
4	0.00	0.00	0.00	0.00	0.00	0.00	0.00	0.00	0.00	0.00	0.00	0.00	0.00	0.00	0.00	0.00	0.00
5	0.00	0.00	0.00	0.00	0.00	0.00	0.00	0.00	0.00	0.00	0.00	0.00	0.00	0.00	0.00	0.00	0.00
6	0.00	0.00	0.00	0.00	0.00	0.00	0.00	0.00	0.00	0.00	0.00	0.00	0.00	0.00	0.00	0.00	0.00
7	0.00	0.00	0.00	0.00	0.00	0.00	0.00	0.00	0.00	0.00	0.00	0.00	0.00	0.00	0.00	0.00	0.00
8	0.00	0.00	0.00	0.00	0.00	0.00	0.00	0.00	0.00	0.00	0.00	0.00	0.00	0.00	0.00	0.00	0.00
9	0.00	0.00	0.00	0.00	0.00	0.00	0.00	0.00	0.00	0.00	0.00	0.00	0.00	0.00	0.00	0.00	0.00
10	0.00	0.00	0.00	0.00	0.00	0.00	0.00	0.00	0.00	0.00	0.00	0.00	0.00	0.00	0.00	0.00	0.00
$\mathbf{X}_\mu$	0.00	0.00	0.00	0.00	0.00	0.00	0.00	0.00	0.00	0.00	0.00	0.00	0.00	0.00	0.00	0.00	0.00

Table D.12: Detailed results: Known Mass, Noise = 2.0% and 4 Sensors.

Run	Identified DI (%) at node No.															Error	
No.	1	2	3	4	5	6	7	8	9	10	11	12	13	14	15	ϵ_α	ϵ_β
1	0.00	0.00	0.00	0.00	0.00	0.00	0.00	0.00	0.00	0.00	0.30	0.90	0.00	4.00	0.00	-1.30	-0.20
2	0.10	0.00	0.00	0.00	0.00	0.00	0.00	0.00	0.00	0.00	0.00	0.00	0.00	0.00	0.00	0.00	0.00
3	0.00	0.00	0.00	0.00	0.00	0.00	0.00	0.00	0.00	0.00	0.00	0.50	0.80	2.70	0.00	-6.00	-1.00
4	0.00	0.00	0.00	0.00	0.00	0.00	0.00	0.00	0.00	0.00	0.00	0.00	0.00	0.00	0.00	0.40	0.00
5	0.00	0.00	0.00	0.00	0.00	0.00	0.00	0.00	0.00	0.00	0.00	3.40	0.00	10.60	0.00	-11.40	-2.20
6	0.00	0.00	0.00	0.00	0.00	0.00	0.00	0.00	0.00	0.00	0.10	1.00	0.60	3.00	0.00	-5.20	-0.70
7	0.00	0.00	0.00	0.00	0.00	0.00	0.00	0.00	0.00	0.00	0.00	0.00	0.00	2.50	0.00	-1.00	-0.40
8	0.00	0.00	0.00	0.00	0.00	0.00	0.00	0.00	0.00	0.00	0.00	0.10	0.00	4.50	0.00	-1.70	-0.70
9	0.00	0.00	0.00	0.00	0.00	0.00	0.00	0.00	0.00	0.00	0.10	1.60	0.00	10.20	0.00	-4.30	-2.00
10	0.00	0.00	0.00	0.00	0.00	0.00	0.00	0.00	0.00	0.00	0.00	0.00	0.00	0.00	0.00	1.40	3.20
$\mathbf{X}_\mu$	0.01	0.00	0.00	0.00	0.00	0.00	0.00	0.00	0.00	0.00	0.05	0.75	0.14	3.75	0.00	-2.91	-0.40

Table D.13: Detailed results: Known Mass, Noise = 5.0% and 4 Sensors.

Run	Identified DI (%) at node No.															Error	
No.	1	2	3	4	5	6	7	8	9	10	11	12	13	14	15	ϵ_α	ϵ_β
1	0.00	0.00	0.00	0.00	0.00	0.00	0.00	0.00	0.00	0.00	0.00	1.10	0.10	11.40	0.00	-0.60	-2.70
2	0.00	0.00	0.00	0.00	0.10	0.00	0.00	0.00	0.00	0.00	0.00	0.10	1.50	1.50	0.00	-5.30	0.00
3	0.00	0.00	0.00	0.00	0.00	0.00	0.00	0.00	0.00	0.00	0.00	0.00	0.00	0.00	0.00	0.00	0.00
4	0.00	0.00	0.00	0.00	0.00	0.00	0.00	0.00	0.00	0.00	2.90	4.50	1.00	20.00	0.00	-20.00	-6.80
5	0.00	0.00	0.00	0.00	0.00	0.00	0.00	0.00	0.00	0.00	0.00	1.00	0.30	9.40	0.00	0.00	-0.80
6	0.00	0.00	0.00	0.00	0.00	0.00	0.00	0.00	0.00	0.00	0.00	0.00	0.00	0.00	0.00	0.00	0.00
7	0.00	0.00	0.00	0.00	0.00	0.00	0.00	0.00	0.00	0.00	0.00	0.00	0.00	1.00	0.00	0.00	-0.30
8	0.00	0.00	0.00	0.00	0.00	0.00	0.00	0.00	0.00	0.00	1.20	1.30	5.70	18.30	0.00	-20.00	-6.40
9	0.10	0.00	0.00	0.00	0.00	0.00	0.00	0.00	0.00	0.00	0.00	0.00	0.00	0.00	0.00	0.00	0.00
10	0.00	0.00	0.00	0.00	0.10	0.00	0.00	0.00	0.00	0.00	0.00	0.20	1.20	8.70	0.00	-6.00	-1.40
$\mathbf{X}_\mu$	0.01	0.00	0.00	0.00	0.02	0.00	0.00	0.00	0.00	0.00	0.41	0.82	0.98	7.03	0.00	-5.19	-1.84

Table D.14: Detailed results: Known Mass, Noise = 10.0% and 4 Sensors.

Run	Identified DI (%) at node No.															Error	
No.	1	2	3	4	5	6	7	8	9	10	11	12	13	14	15	ϵ_α	ϵ_β
1	0.00	0.00	0.00	0.10	0.00	0.00	0.00	0.00	0.00	0.00	0.00	0.00	1.40	13.80	0.00	0.00	-1.50
2	0.00	0.00	0.00	0.00	0.00	0.00	0.00	0.00	0.00	0.00	0.00	3.80	1.40	17.90	0.00	-20.00	-6.00
3	0.00	0.00	0.00	0.00	0.00	0.00	0.00	0.00	0.00	0.00	0.00	0.00	0.00	0.00	0.00	0.00	0.00
4	0.00	0.00	0.00	0.00	0.00	0.00	0.00	0.00	0.00	0.00	0.00	0.00	1.30	12.90	0.00	0.00	0.10
5	0.00	0.00	0.00	0.00	0.00	0.00	0.00	0.00	0.00	0.00	0.40	3.70	2.50	20.00	0.00	-6.60	-3.50
6	0.00	0.00	0.00	0.00	0.00	0.10	0.00	0.00	0.00	0.00	0.00	0.00	0.00	0.00	0.00	-4.10	4.10
7	0.00	0.00	0.00	0.00	0.00	0.00	0.00	0.00	0.00	0.00	1.30	0.40	11.80	20.00	0.00	-17.10	-9.10
8	0.00	0.00	0.00	0.00	0.00	0.00	0.00	0.00	0.00	0.00	0.00	0.00	0.00	0.00	0.00	2.60	0.00
9	0.00	0.00	0.00	0.00	0.00	0.00	0.00	0.00	0.00	0.00	0.00	0.00	12.90	20.00	0.00	0.00	-1.10
10	0.00	0.00	0.00	0.00	0.00	0.00	0.00	0.00	0.00	0.00	2.10	1.80	0.90	20.00	0.00	-20.00	-6.70
$\mathbf{X}_\mu$	0.00	0.00	0.00	0.01	0.00	0.01	0.00	0.00	0.00	0.00	0.38	0.97	3.22	12.46	0.00	-6.52	-2.37

D.3 Unknown Mass Identification Results

Table D.15: Detailed results: Unknown Mass, Noise = 0.0% and 14 Sensors.

Run No.	Identified DI (%) at variable															Error	
	EI_1	EI_2	EI_3	EI_4	EI_5	EI_6	EI_7	EI_8	EI_9	EI_{10}	EI_{11}	EI_{12}	EI_{13}	EI_{14}	EI_{15}	ϵ_α	ϵ_β
	ρ_1	ρ_2	ρ_3	ρ_4	ρ_5	ρ_6	ρ_7	ρ_8	ρ_9	ρ_{10}	ρ_{11}	ρ_{12}	ρ_{13}	ρ_{14}	ρ_{15}		
1	0.10	0.00	0.00	0.00	0.00	0.10	0.00	0.10	0.00	0.10	0.00	0.00	0.00	0.00	0.00	0.00	0.00
	11.90	5.30	0.60	0.30	0.10	0.00	0.00	0.00	0.00	0.10	0.00	0.10	0.00	0.00	0.00		
2	0.00	0.00	0.10	0.10	0.00	0.00	0.00	0.10	0.00	0.10	0.00	0.00	0.00	0.10	0.00	0.00	0.00
	14.30	0.70	0.40	0.60	0.10	0.00	0.10	0.00	0.00	0.00	0.00	0.00	0.10	0.00	0.00		
3	0.10	0.00	0.00	0.00	0.00	0.00	0.00	0.00	0.00	0.10	0.00	0.00	0.00	0.10	0.00	0.00	0.00
	12.30	1.90	0.20	0.00	0.00	0.10	0.00	0.10	0.00	0.00	0.10	0.00	0.00	0.00	0.00		
4	0.20	0.00	0.00	0.00	0.00	0.00	0.00	0.10	0.00	0.00	0.00	0.10	0.00	0.10	0.00	-0.10	0.00
	12.90	0.90	1.20	0.20	0.00	0.00	0.00	0.10	0.10	0.10	0.10	0.00	0.00	0.00	0.00		
5	0.00	0.00	0.00	0.00	0.00	0.10	0.10	0.10	0.00	0.10	0.00	0.00	0.00	0.00	0.00	0.00	0.00
	2.80	5.80	0.10	0.00	0.00	0.00	0.00	0.00	0.10	0.00	0.00	0.00	0.10	0.00	0.00		
6	0.10	0.10	0.00	0.00	0.00	0.10	0.10	0.10	0.00	0.10	0.00	0.00	0.00	0.00	0.00	0.00	0.00
	11.70	0.00	0.00	0.10	0.10	0.10	0.00	0.20	0.10	0.00	0.20	0.00	0.10	0.00	0.00		
7	0.20	0.00	0.00	0.00	0.00	0.00	0.00	0.00	0.10	0.10	0.00	0.00	0.00	0.00	0.00	0.00	0.00
	2.30	1.40	0.10	0.30	0.00	0.10	0.00	0.00	0.10	0.10	0.10	0.00	0.00	0.00	0.00		
8	0.10	0.00	0.00	0.00	0.00	0.10	0.10	0.00	0.10	0.00	0.00	0.10	0.00	0.00	0.00	0.00	0.00
	9.60	1.70	0.20	0.30	0.10	0.10	0.00	0.00	0.00	0.10	0.00	0.10	0.00	0.00	0.00		
9	0.00	0.00	0.00	0.00	0.10	0.00	0.10	0.00	0.10	0.00	0.00	0.00	0.00	0.00	0.00	0.00	0.00
	8.00	1.60	0.20	0.10	0.10	0.00	0.00	0.10	0.00	0.00	0.00	0.10	0.00	0.00	0.00		
10	0.00	0.10	0.00	0.00	0.00	0.00	0.00	0.00	0.00	0.00	0.10	0.00	0.10	0.00	0.00	0.00	0.00
	0.90	3.00	0.20	0.30	0.00	0.10	0.00	0.00	0.10	0.00	0.00	0.10	0.00	0.00	0.00		
$\mathbf{X}_\mu$	0.08	0.02	0.01	0.01	0.01	0.04	0.04	0.05	0.03	0.07	0.01	0.03	0.02	0.02	0.00	-0.01	0.00
	8.67	2.23	0.32	0.22	0.05	0.05	0.01	0.05	0.05	0.04	0.05	0.05	0.03	0.00	0.00		

Table D.16: Detailed results: Unknown Mass, Noise = 2.0% and 14 Sensors.

Run No.	Identified DI (%) at variable															Error	
	EI_1	EI_2	EI_3	EI_4	EI_5	EI_6	EI_7	EI_8	EI_9	EI_{10}	EI_{11}	EI_{12}	EI_{13}	EI_{14}	EI_{15}	ϵ_α	ϵ_β
	ρ_1	ρ_2	ρ_3	ρ_4	ρ_5	ρ_6	ρ_7	ρ_8	ρ_9	ρ_{10}	ρ_{11}	ρ_{12}	ρ_{13}	ρ_{14}	ρ_{15}		
1	8.00	1.00	0.30	0.00	0.10	0.10	0.00	0.20	0.60	0.40	0.70	2.10	0.70	5.20	0.00	0.00	-0.10
	9.40	15.20	4.50	1.60	0.40	2.90	0.60	0.90	1.30	0.40	1.30	0.80	0.00	3.50	0.00		
2	0.00	0.00	0.00	0.00	0.00	0.00	0.00	0.10	0.00	0.00	0.00	0.00	0.00	0.00	0.00	0.00	0.00
	16.90	4.80	0.00	0.40	0.00	0.10	0.10	0.00	0.00	0.00	0.10	0.00	0.00	0.00	0.00		
3	0.20	0.00	0.00	0.00	0.00	0.00	0.00	0.00	0.00	0.00	0.00	0.00	0.00	0.00	0.00	0.00	0.00
	12.10	2.30	0.00	0.00	0.20	0.00	0.00	0.00	0.00	0.10	0.00	0.00	0.00	0.00	0.00		
4	0.00	0.00	0.00	0.00	0.00	0.00	0.00	0.00	0.00	0.00	0.00	0.00	0.00	0.00	0.00	0.00	0.00
	19.50	2.20	0.50	0.00	0.00	0.00	0.00	0.00	0.00	0.00	0.00	0.00	0.10	0.00	0.00		
5	5.80	4.40	1.00	0.50	2.00	0.10	2.60	0.90	1.50	4.00	0.60	0.90	1.50	6.80	0.00	0.00	-0.60
	10.00	5.60	6.00	1.00	2.60	5.20	1.30	2.50	1.90	3.20	1.90	1.50	0.40	6.30	0.00		
6	0.10	0.00	0.00	0.00	0.00	0.00	0.00	0.00	0.00	0.00	0.00	0.00	0.00	0.00	0.00	0.00	0.00
	19.90	6.70	0.50	0.10	0.10	0.00	0.00	0.00	0.00	0.00	0.00	0.00	0.00	0.00	0.00		
7	0.00	0.00	0.00	0.00	0.00	0.00	0.10	0.00	0.00	0.00	0.00	0.00	0.30	0.30	0.00	0.00	0.00
	15.00	11.80	2.70	0.70	0.00	0.10	0.00	0.00	0.00	0.00	0.00	0.00	0.00	0.00	0.00		
8	0.00	0.00	0.00	0.00	0.00	0.00	0.00	0.00	0.00	0.00	0.10	0.00	0.00	0.00	0.00	0.00	0.00
	2.00	1.30	0.70	0.10	0.20	0.10	0.00	0.00	0.00	0.00	0.00	0.00	0.00	0.00	0.00		
9	0.10	0.20	1.40	1.10	1.50	1.70	0.70	0.10	0.90	1.80	1.60	0.00	0.30	1.70	0.00	-1.30	0.00
	7.70	16.40	2.50	0.10	2.00	0.30	0.30	0.70	0.20	2.70	0.40	1.30	0.10	1.90	0.00		
10	2.20	1.50	0.60	0.00	0.20	0.40	0.00	0.20	0.20	0.40	0.80	0.00	0.20	2.10	0.00	-0.10	-0.10
	13.90	15.40	14.90	0.40	0.10	0.60	0.20	0.10	1.50	0.40	0.90	0.20	0.10	2.10	0.00		
$\mathbf{X}_\mu$	1.64	0.71	0.33	0.16	0.38	0.23	0.34	0.15	0.32	0.66	0.38	0.30	0.30	1.61	0.00	-0.14	-0.08
	12.64	8.17	3.23	0.44	0.56	0.93	0.25	0.42	0.49	0.68	0.46	0.39	0.06	1.38	0.00		

Table D.17: Detailed results: Unknown Mass, Noise = 5.0% and 14 Sensors.

Run No.	Identified DI (%) at variable															Error	
	EI_1	EI_2	EI_3	EI_4	EI_5	EI_6	EI_7	EI_8	EI_9	EI_{10}	EI_{11}	EI_{12}	EI_{13}	EI_{14}	EI_{15}	ϵ_α	ϵ_β
	ρ_1	ρ_2	ρ_3	ρ_4	ρ_5	ρ_6	ρ_7	ρ_8	ρ_9	ρ_{10}	ρ_{11}	ρ_{12}	ρ_{13}	ρ_{14}	ρ_{15}		
1	5.00	5.80	4.20	10.50	6.50	9.60	3.80	3.80	5.20	6.90	7.30	3.20	3.50	9.20	0.00	-5.40	-0.80
	2.10	10.30	8.30	2.50	3.00	3.80	8.40	4.60	6.20	8.80	6.10	7.60	0.60	15.20	0.00		
2	0.00	0.00	0.00	0.00	0.00	0.00	0.00	0.00	0.10	0.10	0.00	0.00	0.00	0.00	0.00	0.00	0.00
	12.20	6.90	1.10	0.00	0.00	0.00	0.00	0.00	0.00	0.00	0.00	0.00	0.00	0.00	0.00		
3	6.50	1.80	1.90	5.30	3.50	5.90	4.90	1.00	6.90	3.60	2.20	1.10	2.20	6.40	0.00	-1.20	-0.80
	1.00	11.20	3.10	0.40	5.10	2.00	5.00	2.60	5.30	2.20	3.00	3.80	1.60	9.30	0.00		
4	11.40	4.80	0.40	0.70	2.80	1.50	2.20	3.20	0.90	4.40	4.70	1.10	0.00	10.30	0.00	-1.30	-0.30
	8.10	15.80	3.00	1.20	3.50	1.20	6.40	6.10	3.70	1.20	5.20	2.10	0.00	8.60	0.00		
5	6.60	1.10	0.00	0.20	1.00	0.70	0.10	0.00	0.10	0.40	2.60	0.50	0.90	3.40	0.00	0.00	-0.10
	17.00	11.80	2.60	4.30	1.40	0.20	0.10	0.70	2.70	0.80	0.40	1.20	0.10	3.10	0.00		
6	0.20	0.00	0.00	0.00	0.00	0.00	0.00	0.00	0.00	0.10	0.10	0.00	0.10	2.60	0.00	0.00	0.00
	11.00	3.90	0.30	0.20	0.00	0.00	0.00	0.10	0.00	0.00	0.00	0.00	0.00	0.00	0.00		
7	7.30	1.10	1.50	2.20	0.00	1.10	0.30	0.30	3.10	2.80	1.40	0.40	0.60	5.50	0.00	0.00	-0.60
	18.00	11.90	3.00	2.30	2.40	1.20	3.60	1.90	3.30	2.30	2.10	0.80	0.00	4.70	0.00		
8	0.10	0.00	0.00	0.00	0.00	0.00	0.10	0.00	0.00	0.00	0.00	0.00	0.00	0.00	0.00	0.00	0.00
	4.00	0.50	0.20	0.00	0.00	0.10	0.00	0.00	0.10	0.00	0.00	0.00	0.00	0.00	0.00		
9	0.00	0.00	0.00	0.20	0.50	2.20	1.40	1.40	0.40	0.00	0.00	0.00	0.00	0.00	0.00	-7.30	0.00
	5.50	4.50	0.00	0.20	0.10	0.00	0.20	0.40	1.20	0.90	0.80	1.90	0.10	0.00	0.00		
10	2.40	6.80	8.10	7.10	0.20	5.30	6.70	3.10	6.90	8.60	3.40	3.00	5.70	11.40	0.00	-3.50	-0.40
	6.10	8.70	4.80	6.20	3.10	1.10	7.70	10.60	3.40	5.60	5.20	5.40	1.50	13.60	0.00		
$\mathbf{X}_\mu$	3.95	2.14	1.61	2.62	1.45	2.63	1.95	1.28	2.36	2.69	2.17	0.93	1.30	4.88	0.00	-1.87	-0.30
	8.50	8.55	2.64	1.73	1.86	0.96	3.14	2.70	2.59	2.18	2.28	2.28	0.39	5.45	0.00		

Table D.18: Detailed results: Unknown Mass, Noise = 10.0% and 14 Sensors.

Run No.	Identified DI (%) at variable															Error	
	EI_1	EI_2	EI_3	EI_4	EI_5	EI_6	EI_7	EI_8	EI_9	EI_{10}	EI_{11}	EI_{12}	EI_{13}	EI_{14}	EI_{15}	ϵ_α	ϵ_β
	ρ_1	ρ_2	ρ_3	ρ_4	ρ_5	ρ_6	ρ_7	ρ_8	ρ_9	ρ_{10}	ρ_{11}	ρ_{12}	ρ_{13}	ρ_{14}	ρ_{15}		
1	0.00	0.00	0.00	0.10	0.00	0.00	0.00	0.00	0.00	0.00	0.00	0.00	0.00	0.00	0.00	0.00	0.00
	9.90	4.90	0.50	0.30	0.10	0.00	0.00	0.00	0.00	0.00	0.00	0.00	0.00	0.00	0.00		
2	12.60	4.90	0.60	3.90	3.50	0.20	1.40	3.10	3.00	5.50	5.10	0.10	0.70	5.40	0.00	-6.20	0.00
	9.10	10.90	12.40	15.60	0.30	1.10	0.50	5.30	5.80	5.40	8.60	2.40	0.50	7.90	0.00		
3	0.00	0.10	0.00	0.00	0.00	0.00	0.00	0.00	0.00	0.00	0.00	0.00	0.00	0.00	0.00	0.00	0.00
	6.40	3.30	1.70	0.10	0.10	0.10	0.00	0.00	0.00	0.00	0.00	0.00	0.00	0.00	0.00		
4	8.10	17.00	16.80	17.70	18.10	2.10	6.40	11.30	18.30	10.10	12.80	4.50	18.30	20.00	0.00	0.00	-6.00
	15.10	5.70	5.70	6.30	5.90	19.90	14.20	11.60	13.00	19.80	12.90	13.30	19.90	20.00	0.00		
5	0.00	0.00	0.00	0.00	0.20	0.40	0.00	0.00	0.00	0.00	0.00	0.00	0.00	0.00	0.00	-0.20	5.10
	5.50	1.20	1.50	0.30	0.10	0.00	0.00	0.40	0.80	0.30	0.00	0.00	0.00	0.00	0.00		
6	0.00	0.00	0.10	0.00	0.10	2.00	1.50	0.00	0.20	0.00	0.00	0.00	0.00	0.00	0.00	-3.20	1.10
	5.30	1.80	0.30	0.20	0.00	0.00	0.00	0.00	0.10	1.20	1.70	0.60	0.00	0.00	0.00		
7	0.00	0.00	0.10	0.10	0.00	2.40	0.80	0.70	0.00	0.00	0.00	0.00	0.00	0.00	0.00	-2.30	1.20
	9.70	0.60	1.40	0.10	0.00	0.00	0.00	0.00	0.00	1.70	1.60	0.30	0.00	0.00	0.00		
8	18.90	14.20	19.60	18.40	1.50	0.50	10.30	18.10	6.90	4.10	6.20	14.20	20.00	19.90	0.00	-0.10	-6.10
	16.70	2.50	7.90	8.20	15.50	15.50	10.80	19.10	11.20	6.40	15.80	13.20	19.40	20.00	0.00		
9	0.10	0.00	0.20	0.70	1.30	3.80	2.10	0.90	0.30	1.50	0.10	1.50	2.50	2.50	0.00	4.60	-0.40
	2.20	1.60	0.00	0.00	0.00	1.20	0.70	0.10	0.00	0.10	0.20	0.70	0.00	3.40	0.00		
10	20.00	17.90	0.00	1.20	7.70	4.70	1.00	2.00	9.70	12.00	2.50	2.90	12.10	19.60	0.00	-0.10	-2.40
	8.20	6.40	5.50	7.40	10.80	9.60	12.00	10.30	7.60	6.00	13.40	1.30	5.20	20.00	0.00		
$\mathbf{X}_\mu$	5.97	5.41	3.74	4.21	3.24	1.61	2.35	3.61	3.84	3.32	2.67	2.32	5.36	6.74	0.00	-0.75	-0.75
	8.81	3.89	3.69	3.85	3.28	4.74	3.82	4.68	3.85	4.09	5.42	3.18	4.50	7.13	0.00		

Table D.19: Detailed results: Unknown Mass, Noise = 0.0% and 7 Sensors.

Run No.	Identified DI (%) at variable															Error	
	EI_1	EI_2	EI_3	EI_4	EI_5	EI_6	EI_7	EI_8	EI_9	EI_{10}	EI_{11}	EI_{12}	EI_{13}	EI_{14}	EI_{15}	ϵ_α	ϵ_β
	ρ_1	ρ_2	ρ_3	ρ_4	ρ_5	ρ_6	ρ_7	ρ_8	ρ_9	ρ_{10}	ρ_{11}	ρ_{12}	ρ_{13}	ρ_{14}	ρ_{15}		
1	0.10	0.00	0.00	0.00	0.00	0.00	0.00	0.10	0.00	0.00	0.20	0.00	0.00	0.10	0.00	0.00	0.00
	13.90	4.70	0.30	0.10	0.00	0.00	0.10	0.00	0.10	0.00	0.10	0.00	0.00	0.00	0.00		
2	0.20	0.00	0.00	0.00	0.00	0.00	0.10	0.00	0.00	0.00	0.00	0.00	0.00	0.00	0.00	-0.10	0.00
	9.90	0.40	0.40	0.00	0.00	0.00	0.00	0.10	0.10	0.00	0.00	0.00	0.10	0.00	0.00		
3	0.10	0.00	0.00	0.00	0.00	0.10	0.10	0.10	0.00	0.10	0.00	0.10	0.00	0.00	0.00	0.00	0.00
	18.50	0.10	0.80	0.00	0.00	0.20	0.00	0.00	0.10	0.00	0.00	0.10	0.10	0.00	0.00		
4	0.00	0.10	0.00	0.00	0.00	0.00	0.00	0.20	0.00	0.00	0.00	0.00	0.00	0.10	0.00	0.00	0.00
	13.80	3.30	0.50	0.00	0.10	0.00	0.00	0.00	0.10	0.10	0.00	0.10	0.00	0.00	0.00		
5	0.00	0.00	0.00	0.00	0.10	0.00	0.10	0.10	0.00	0.00	0.00	0.10	0.00	0.20	0.00	0.00	0.00
	5.90	6.90	1.60	0.00	0.00	0.10	0.00	0.00	0.00	0.10	0.00	0.00	0.10	0.00	0.00		
6	0.00	0.00	0.10	0.00	0.00	0.00	0.00	0.10	0.00	0.00	0.00	0.00	0.00	0.10	0.00	0.00	0.00
	1.20	1.70	0.40	0.30	0.00	0.00	0.00	0.00	0.00	0.10	0.00	0.10	0.00	0.00	0.00		
7	0.10	0.10	0.00	0.00	0.00	0.00	0.10	0.00	0.00	0.00	0.00	0.10	0.00	0.00	0.10	0.00	0.00
	18.30	0.40	0.00	0.60	0.00	0.00	0.10	0.10	0.00	0.00	0.00	0.10	0.10	0.00	0.00		
8	0.10	0.10	0.00	0.00	0.00	0.00	0.10	0.00	0.00	0.00	0.00	0.00	0.10	0.00	0.00	-0.20	0.00
	18.90	4.90	0.10	0.00	0.00	0.00	0.10	0.00	0.10	0.10	0.00	0.00	0.10	0.00	0.00		
9	0.00	0.00	0.10	0.00	0.00	0.10	0.00	0.00	0.00	0.10	0.00	0.00	0.00	0.10	0.00	-0.10	0.00
	5.10	4.90	1.00	0.10	0.00	0.00	0.00	0.00	0.00	0.00	0.10	0.00	0.10	0.00	0.00		
10	0.00	0.00	0.00	0.00	0.00	0.00	0.10	0.10	0.00	0.00	0.10	0.00	0.00	0.00	0.00	0.00	0.00
	16.10	2.60	0.30	0.00	0.10	0.00	0.10	0.10	0.00	0.10	0.00	0.00	0.00	0.00	0.00		
$\mathbf{X}_\mu$	0.06	0.03	0.02	0.00	0.01	0.02	0.06	0.07	0.01	0.01	0.04	0.02	0.02	0.06	0.00	-0.04	0.00
	12.16	2.99	0.54	0.11	0.02	0.03	0.04	0.03	0.05	0.05	0.02	0.04	0.06	0.00	0.00		

Table D.20: Detailed results: Unknown Mass, Noise = 2.0% and 7 Sensors.

Run No.	Identified DI (%) at variable															Error	
	EI_1	EI_2	EI_3	EI_4	EI_5	EI_6	EI_7	EI_8	EI_9	EI_{10}	EI_{11}	EI_{12}	EI_{13}	EI_{14}	EI_{15}	ϵ_α	ϵ_β
	ρ_1	ρ_2	ρ_3	ρ_4	ρ_5	ρ_6	ρ_7	ρ_8	ρ_9	ρ_{10}	ρ_{11}	ρ_{12}	ρ_{13}	ρ_{14}	ρ_{15}		
1	0.00	0.00	0.00	0.00	0.00	0.00	0.00	0.10	0.10	0.10	0.00	0.20	0.00	0.60	0.00	0.00	0.00
	9.30	1.70	0.80	0.20	0.00	0.10	0.00	0.00	0.00	0.00	0.10	0.00	0.00	0.00	0.00		
2	4.60	4.30	0.00	0.10	0.00	0.10	0.00	0.10	0.00	0.70	1.50	0.60	0.70	12.80	0.00	0.00	-0.40
	9.10	6.40	1.50	4.00	1.80	3.60	1.60	0.90	2.40	0.30	0.00	2.30	3.30	1.10	0.00		
3	0.20	3.70	4.50	2.30	3.40	0.90	3.60	4.00	0.60	0.50	4.30	0.00	1.60	11.50	0.00	-1.80	-0.20
	13.60	1.30	4.80	3.20	0.50	5.00	3.90	0.90	1.10	5.30	0.00	3.30	6.40	3.10	0.00		
4	0.80	0.60	0.30	0.80	0.70	0.10	2.30	1.20	1.40	0.10	0.30	0.00	0.70	2.90	0.00	-1.00	0.00
	5.00	17.20	7.80	0.40	1.50	0.40	0.50	1.00	0.70	0.50	0.00	0.00	3.00	0.30	0.00		
5	3.00	0.00	0.00	0.00	0.00	0.00	0.00	0.00	0.00	0.10	0.00	0.40	0.50	3.20	0.00	0.00	0.00
	4.00	3.20	0.10	0.00	0.00	0.10	1.40	0.30	0.00	0.10	0.10	0.10	1.20	0.00	0.00		
6	11.40	4.30	2.30	6.50	1.70	3.70	1.20	4.20	3.70	1.10	2.10	1.10	2.30	19.10	0.00	-0.40	-0.80
	13.80	6.30	11.90	9.60	0.80	3.70	4.80	7.30	2.50	3.80	2.10	3.90	10.60	4.50	0.00		
7	0.20	0.00	0.00	0.00	0.00	0.00	0.00	0.00	0.00	0.00	0.00	0.00	0.10	2.90	0.00	0.00	0.00
	12.60	4.00	0.70	0.00	0.30	0.00	0.00	0.00	0.00	0.00	0.00	0.00	0.00	0.00	0.00		
8	0.00	0.00	0.00	0.00	0.00	0.00	0.10	0.00	0.00	0.00	0.00	0.00	0.00	0.00	0.00	0.00	1.40
	13.40	2.80	1.10	0.20	0.00	0.00	0.00	0.10	0.10	0.00	0.00	0.00	0.00	0.00	0.00		
9	0.00	0.00	0.00	0.00	0.10	0.00	0.00	0.00	0.00	0.00	0.00	0.00	0.00	0.40	0.00	2.00	0.00
	15.90	0.20	0.10	0.30	0.30	0.00	0.10	0.00	0.00	0.00	0.00	0.00	0.00	0.00	0.00		
10	0.70	1.30	1.00	0.10	1.10	2.40	1.10	0.80	0.20	0.00	0.70	0.40	0.40	5.80	0.00	-0.70	-0.10
	13.00	0.40	0.10	0.30	0.60	3.50	0.10	0.10	0.80	0.30	0.00	1.90	2.60	0.80	0.00		
$\mathbf{X}_\mu$	2.09	1.42	0.81	0.98	0.70	0.72	0.83	1.04	0.60	0.26	0.89	0.27	0.63	5.92	0.00	-0.19	-0.01
	10.97	4.35	2.89	1.82	0.58	1.64	1.24	1.06	0.76	1.03	0.23	1.15	2.71	0.98	0.00		

Table D.21: Detailed results: Unknown Mass, Noise = 5.0% and 7 Sensors.

Run No.	Identified DI (%) at variable															Error	
	EI_1	EI_2	EI_3	EI_4	EI_5	EI_6	EI_7	EI_8	EI_9	EI_{10}	EI_{11}	EI_{12}	EI_{13}	EI_{14}	EI_{15}	ϵ_α	ϵ_β
	ρ_1	ρ_2	ρ_3	ρ_4	ρ_5	ρ_6	ρ_7	ρ_8	ρ_9	ρ_{10}	ρ_{11}	ρ_{12}	ρ_{13}	ρ_{14}	ρ_{15}		
1	0.20	0.00	0.00	0.10	0.00	0.00	0.00	0.00	0.00	0.00	0.10	0.00	0.00	0.00	0.00	0.00	0.00
	12.60	0.60	1.60	0.10	0.10	0.10	0.00	0.00	0.00	0.00	0.00	0.00	0.00	0.00	0.00		
2	0.00	0.00	0.00	0.00	0.00	0.00	0.00	0.00	0.00	0.10	0.00	0.00	0.00	0.00	0.00	0.00	0.00
	18.90	9.80	2.40	0.40	0.10	0.00	0.00	0.00	0.00	0.00	0.00	0.00	0.00	0.00	0.00		
3	0.00	0.00	0.50	4.60	6.80	12.00	1.50	0.70	7.10	2.40	0.30	0.10	0.20	1.90	0.00	-5.50	0.00
	14.00	4.00	3.40	0.30	0.20	1.00	0.90	5.60	0.30	3.10	2.70	1.50	7.30	4.40	0.00		
4	9.80	3.40	3.30	6.20	3.60	3.20	8.00	6.70	5.10	0.60	2.90	3.50	2.80	19.30	0.00	-0.20	-1.00
	7.30	12.20	17.80	11.00	10.60	2.80	7.80	5.50	3.50	3.70	1.70	4.10	12.60	5.20	0.00		
5	19.30	2.90	3.00	2.80	4.30	1.10	0.20	2.10	4.10	1.70	1.30	4.20	0.40	18.70	0.00	-0.20	-0.60
	12.20	0.50	3.80	11.30	1.30	1.20	6.20	6.40	4.10	5.70	3.30	2.50	8.60	5.80	0.00		
6	1.10	0.00	0.10	0.10	0.00	0.00	0.30	0.20	0.20	0.10	0.00	0.00	0.00	0.00	0.00	-2.00	0.00
	16.50	19.10	12.50	0.20	0.00	0.10	0.00	0.00	0.00	0.60	0.20	0.10	0.40	0.00	0.00		
7	0.20	0.10	0.00	0.00	0.00	0.10	0.00	0.00	0.00	0.00	0.00	0.00	0.00	0.00	0.00	0.00	0.00
	2.10	1.00	0.50	0.20	0.00	0.10	0.00	0.00	0.00	0.00	0.00	0.00	0.00	0.00	0.00		
8	0.10	0.00	0.00	0.00	0.10	0.00	0.00	0.00	0.00	0.00	0.00	0.00	0.00	0.00	0.00	0.00	0.00
	7.40	1.10	0.40	0.10	0.10	0.00	0.10	0.00	0.00	0.00	0.00	0.00	0.00	0.00	0.00		
9	0.00	0.00	0.00	0.00	0.00	0.00	0.00	0.00	0.00	0.00	0.00	0.00	0.00	0.00	0.00	0.00	0.00
	16.70	4.80	1.10	0.00	0.10	0.00	0.10	0.00	0.00	0.00	0.00	0.00	0.00	0.00	0.00		
10	0.00	0.00	0.00	0.10	0.00	0.00	0.00	0.00	0.00	0.00	0.00	0.00	0.00	0.00	0.00	0.00	0.00
	3.90	2.10	0.50	1.40	0.00	0.00	0.00	0.00	0.00	0.00	0.00	0.00	0.00	0.00	0.00		
$\mathbf{X}_\mu$	3.07	0.64	0.69	1.39	1.48	1.64	1.00	0.97	1.65	0.49	0.46	0.78	0.34	3.99	0.00	-0.79	-0.16
	11.16	5.52	4.40	2.50	1.25	0.53	1.51	1.75	0.79	1.31	0.79	0.82	2.89	1.54	0.00		

Table D.22: Detailed results: Unknown Mass, Noise = 10.0% and 7 Sensors.

Run No.	Identified DI (%) at variable															Error	
	EI_1	EI_2	EI_3	EI_4	EI_5	EI_6	EI_7	EI_8	EI_9	EI_{10}	EI_{11}	EI_{12}	EI_{13}	EI_{14}	EI_{15}	ϵ_α	ϵ_β
	ρ_1	ρ_2	ρ_3	ρ_4	ρ_5	ρ_6	ρ_7	ρ_8	ρ_9	ρ_{10}	ρ_{11}	ρ_{12}	ρ_{13}	ρ_{14}	ρ_{15}		
1	0.10	0.00	0.00	0.10	8.10	5.70	4.20	0.90	5.10	0.10	0.10	0.00	0.00	0.00	0.00	-14.10	0.00
	14.70	0.00	1.10	0.30	0.10	0.40	0.60	0.80	3.30	0.30	0.10	0.00	10.80	0.00	0.00		
2	0.00	0.00	0.10	0.10	0.00	0.00	0.00	0.10	0.00	0.00	0.00	0.00	0.00	0.00	0.00	0.00	-14.00
	13.20	2.00	1.40	10.70	13.10	17.10	18.40	19.60	8.20	4.00	17.70	20.00	9.70	20.00	0.00		
3	7.00	4.80	7.80	14.90	14.90	7.00	6.00	13.90	9.50	6.50	4.30	2.00	10.10	20.00	0.00	-1.90	-3.10
	11.50	0.80	8.60	14.50	8.70	4.70	2.90	11.70	6.50	11.00	2.50	11.90	12.80	16.00	0.00		
4	0.00	0.00	0.10	0.10	0.00	0.00	0.00	0.10	0.00	0.00	0.00	0.00	0.00	0.00	0.00	-0.10	0.00
	7.10	1.00	0.20	0.10	0.10	0.00	0.00	0.00	0.00	0.10	0.10	0.00	0.00	0.00	0.00		
5	0.00	0.00	0.10	0.00	0.00	0.00	0.00	0.00	0.20	0.30	1.10	0.10	0.00	0.00	0.00	0.00	0.00
	1.90	0.30	0.20	0.00	0.00	0.00	0.00	0.00	0.00	0.10	0.00	0.00	0.00	0.00	0.00		
6	0.00	0.10	0.00	0.00	0.00	0.00	0.00	0.00	1.70	0.00	0.00	0.00	0.00	0.00	0.00	0.00	-5.60
	7.50	10.40	4.40	8.50	14.00	10.60	6.60	10.80	14.30	3.20	1.40	19.70	0.30	20.00	0.00		
7	0.00	0.00	0.10	0.10	0.00	0.00	0.00	0.10	0.00	0.00	0.00	0.00	0.00	0.00	0.00	0.00	-11.40
	12.70	4.00	12.40	9.60	14.40	13.30	17.60	15.80	10.40	0.50	19.60	20.00	7.70	20.00	0.00		
8	7.50	0.00	0.00	1.50	3.20	0.00	0.00	0.00	0.00	1.00	2.30	0.00	0.00	0.00	0.00	-2.70	0.00
	1.60	0.70	0.60	0.10	0.20	0.00	0.30	0.50	4.30	5.90	0.00	0.20	3.90	0.00	0.00		
9	0.00	0.10	0.00	0.00	0.00	0.00	0.00	0.00	1.70	0.00	0.00	0.00	0.00	0.00	0.00	-0.40	0.00
	12.20	0.40	1.70	0.30	0.00	0.00	0.00	0.00	0.00	0.00	0.10	0.40	0.10	0.00	0.00		
10	0.00	0.00	0.10	0.00	0.10	0.40	1.80	10.20	0.40	0.00	0.00	0.00	0.00	0.00	0.00	-2.70	0.00
	11.10	15.80	8.00	3.40	2.50	3.80	2.00	0.70	3.00	0.50	0.00	0.00	2.30	0.00	0.00		
$\mathbf{X}_\mu$	1.46	0.50	0.83	1.68	2.63	1.31	1.20	2.53	1.86	0.79	0.78	0.21	1.01	2.00	0.00	-2.19	-3.41
	9.35	3.54	3.86	4.75	5.31	4.99	4.84	5.99	5.00	2.56	4.15	7.22	4.76	7.60	0.00		

Table D.23: Detailed results: Unknown Mass, Noise = 0.0% and 4 Sensors.

Run No.	Identified DI (%) at variable															Error	
	EI_1	EI_2	EI_3	EI_4	EI_5	EI_6	EI_7	EI_8	EI_9	EI_{10}	EI_{11}	EI_{12}	EI_{13}	EI_{14}	EI_{15}	ϵ_α	ϵ_β
	ρ_1	ρ_2	ρ_3	ρ_4	ρ_5	ρ_6	ρ_7	ρ_8	ρ_9	ρ_{10}	ρ_{11}	ρ_{12}	ρ_{13}	ρ_{14}	ρ_{15}		
1	0.20	0.00	0.00	0.00	0.00	0.00	0.00	0.00	0.20	0.00	0.00	0.00	0.00	0.00	0.00	0.00	0.00
	9.10	5.20	0.10	0.10	0.10	0.00	0.10	0.10	0.10	0.10	0.10	0.00	0.00	0.00	0.00		
2	0.10	0.00	0.00	0.00	0.00	0.10	0.00	0.10	0.10	0.00	0.00	0.00	0.00	0.00	0.00	0.00	0.00
	5.90	0.30	0.70	0.40	0.00	0.10	0.10	0.00	0.00	0.00	0.10	0.10	0.00	0.00	0.00		
3	0.10	0.00	0.10	0.00	0.00	0.00	0.00	0.00	0.00	0.00	0.10	0.00	0.10	0.00	0.00	0.00	0.00
	11.80	2.80	1.10	0.20	0.00	0.00	0.00	0.00	0.00	0.00	0.00	0.10	0.00	0.10	0.00	0.00	
4	0.10	0.10	0.00	0.00	0.00	0.10	0.00	0.00	0.10	0.00	0.10	0.00	0.10	0.00	0.00	0.00	0.00
	17.10	5.80	0.70	0.30	0.00	0.10	0.00	0.20	0.00	0.00	0.20	0.10	0.00	0.00	0.00		
5	0.00	0.10	0.00	0.00	0.00	0.10	0.00	0.10	0.00	0.00	0.00	0.00	0.10	0.00	0.00	0.00	0.00
	9.90	4.20	0.40	0.10	0.10	0.00	0.00	0.10	0.00	0.10	0.00	0.00	0.00	0.10	0.00	0.00	
6	0.10	0.00	0.00	0.00	0.00	0.00	0.00	0.00	0.10	0.00	0.00	0.00	0.10	0.10	0.00	0.00	0.00
	0.60	6.30	0.60	0.20	0.00	0.00	0.00	0.00	0.10	0.10	0.00	0.00	0.00	0.00	0.00		
7	0.20	0.00	0.10	0.00	0.00	0.00	0.10	0.00	0.10	0.00	0.00	0.00	0.00	0.10	0.00	0.00	0.00
	7.80	4.00	0.20	0.10	0.00	0.10	0.10	0.10	0.10	0.00	0.00	0.00	0.20	0.00	0.00		
8	0.20	0.10	0.00	0.00	0.00	0.00	0.00	0.00	0.10	0.00	0.00	0.00	0.00	0.00	0.00	0.00	0.00
	3.00	5.90	0.50	0.00	0.00	0.20	0.00	0.10	0.00	0.00	0.10	0.20	0.00	0.00	0.00		
9	0.20	0.00	0.10	0.00	0.00	0.00	0.00	0.00	0.00	0.00	0.10	0.00	0.10	0.00	0.00	0.00	0.00
	6.10	4.60	0.10	0.30	0.10	0.00	0.00	0.00	0.00	0.10	0.10	0.00	0.00	0.10	0.00		
10	0.10	0.00	0.00	0.00	0.10	0.00	0.00	0.00	0.10	0.00	0.00	0.10	0.00	0.00	0.00	0.00	0.00
	8.90	4.40	0.10	0.00	0.00	0.00	0.00	0.00	0.00	0.10	0.00	0.10	0.00	0.00	0.00		
$\mathbf{X}_\mu$	0.13	0.03	0.03	0.00	0.01	0.03	0.01	0.02	0.08	0.01	0.02	0.02	0.04	0.02	0.00	0.00	0.00
	8.02	4.35	0.45	0.17	0.03	0.05	0.03	0.06	0.03	0.05	0.07	0.05	0.04	0.01	0.00		

Table D.24: Detailed results: Unknown Mass, Noise = 2.0% and 4 Sensors.

Run No.	Identified DI (%) at variable															Error	
	EI_1	EI_2	EI_3	EI_4	EI_5	EI_6	EI_7	EI_8	EI_9	EI_{10}	EI_{11}	EI_{12}	EI_{13}	EI_{14}	EI_{15}	ϵ_α	ϵ_β
	ρ_1	ρ_2	ρ_3	ρ_4	ρ_5	ρ_6	ρ_7	ρ_8	ρ_9	ρ_{10}	ρ_{11}	ρ_{12}	ρ_{13}	ρ_{14}	ρ_{15}		
1	0.00	0.00	0.00	0.00	0.10	0.00	0.00	0.00	0.00	0.00	0.00	0.00	0.00	0.00	0.00	0.00	0.00
	9.20	1.70	0.90	0.20	0.20	0.00	0.10	0.00	0.00	0.00	0.00	0.00	0.00	0.00	0.00		
2	0.50	0.20	0.10	0.80	0.80	2.10	2.30	0.10	0.20	0.90	0.20	0.00	0.00	0.00	0.00	-1.20	0.00
	9.60	4.50	6.50	0.90	0.30	0.00	0.10	0.10	2.10	0.60	0.80	0.10	2.60	0.00	0.00		
3	0.00	0.00	0.00	0.00	0.00	0.00	0.10	0.00	0.10	0.00	0.00	0.00	0.00	0.00	0.00	0.00	0.00
	2.90	3.10	0.60	0.10	0.20	0.10	0.10	0.00	0.00	0.00	0.00	0.00	0.00	0.00	0.00		
4	1.10	1.70	1.20	3.30	0.50	2.40	0.30	1.90	0.40	1.00	0.00	0.50	0.50	8.30	0.00	0.00	-0.20
	16.30	13.00	10.10	2.60	1.40	0.50	0.70	2.60	0.60	1.20	0.20	0.10	6.40	0.70	0.00		
5	3.10	1.20	0.40	0.20	0.00	0.00	0.00	0.00	0.00	0.00	0.00	0.00	0.90	6.80	0.00	-0.10	0.00
	12.70	15.40	2.60	3.60	0.50	0.20	0.40	0.90	0.00	0.10	0.00	0.70	2.60	0.20	0.00		
6	0.20	0.10	0.00	0.00	0.00	0.00	0.10	0.00	0.10	0.00	0.00	0.00	0.00	0.00	0.00	0.00	0.00
	5.40	0.80	0.20	0.00	0.20	0.00	0.00	0.00	0.10	0.00	0.00	0.00	0.00	0.00	0.00		
7	4.80	0.20	0.00	0.00	0.00	0.00	0.00	0.00	0.00	0.00	0.10	0.00	0.80	5.50	0.00	0.00	-0.10
	11.60	2.60	0.10	1.00	0.60	0.50	0.70	2.40	0.50	0.10	0.00	0.10	2.10	0.10	0.00		
8	0.00	0.00	0.00	0.00	0.00	0.00	0.00	0.00	0.00	0.10	0.00	0.00	0.00	0.00	0.00	0.00	0.00
	18.20	7.40	0.30	0.40	0.10	0.00	0.00	0.00	0.00	0.10	0.00	0.00	0.00	0.00	0.00		
9	2.50	5.70	3.40	2.70	0.10	2.00	1.10	2.70	0.50	1.50	0.50	0.20	1.90	16.30	0.00	0.00	-0.70
	4.70	13.50	10.80	3.70	2.80	0.00	3.20	3.20	3.90	0.50	0.50	0.80	10.60	1.70	0.00		
10	0.00	0.00	0.00	0.00	0.00	0.00	0.10	0.00	0.00	0.00	0.00	0.00	0.00	0.00	0.00	0.00	0.00
	15.90	1.10	1.10	0.00	0.30	0.00	0.10	0.10	0.00	0.00	0.00	0.00	0.00	0.00	0.00		
$\mathbf{X}_\mu$	1.22	0.91	0.51	0.70	0.15	0.65	0.40	0.47	0.13	0.35	0.08	0.07	0.41	3.69	0.00	-0.13	-0.10
	10.65	6.31	3.32	1.25	0.66	0.13	0.54	0.93	0.72	0.26	0.15	0.18	2.43	0.27	0.00		

Table D.25: Detailed results: Unknown Mass, Noise = 5.0% and 4 Sensors.

Run	Identified DI (%) at variable															Error	
No.	EI_1	EI_2	EI_3	EI_4	EI_5	EI_6	EI_7	EI_8	EI_9	EI_{10}	EI_{11}	EI_{12}	EI_{13}	EI_{14}	EI_{15}	ϵ_α	ϵ_β
	ρ_1	ρ_2	ρ_3	ρ_4	ρ_5	ρ_6	ρ_7	ρ_8	ρ_9	ρ_{10}	ρ_{11}	ρ_{12}	ρ_{13}	ρ_{14}	ρ_{15}		
1	0.10	0.00	0.00	0.00	0.00	0.00	0.00	0.00	0.00	0.00	0.00	0.00	0.00	0.00	0.00	0.00	0.00
	18.80	12.40	3.30	1.10	0.00	0.10	0.00	0.00	0.00	0.00	0.00	0.00	0.00	0.00	0.00		
2	5.60	2.90	7.10	5.80	0.60	4.20	0.80	1.30	0.80	8.20	1.70	0.60	0.70	14.20	0.00	-0.10	-1.20
	0.90	6.70	9.80	5.40	4.50	2.30	0.30	3.30	7.20	5.20	1.70	2.20	11.40	2.60	0.00		
3	9.20	1.60	2.50	1.80	7.70	9.10	6.50	0.50	4.20	5.10	4.50	0.60	2.60	13.50	0.00	-4.80	-0.10
	9.90	13.70	7.50	5.00	7.70	2.80	4.70	0.60	6.20	8.10	3.10	1.90	10.10	5.10	0.00		
4	5.60	0.40	0.00	0.00	0.00	0.00	0.00	0.00	0.00	0.00	0.00	0.10	0.90	7.60	0.00	0.00	-0.10
	13.00	0.70	0.40	0.00	0.30	1.90	0.80	0.50	1.20	0.40	0.10	0.10	2.30	0.40	0.00		
5	7.20	4.90	4.30	11.30	2.00	3.50	10.80	3.00	6.80	7.70	3.70	0.10	3.10	19.40	0.00	0.00	-1.30
	10.20	11.50	11.60	0.80	12.80	4.20	4.50	10.30	6.70	5.10	4.80	0.40	13.70	8.30	0.00		
6	9.80	4.70	0.70	1.70	1.80	1.70	2.90	0.00	0.80	2.40	1.40	0.20	1.20	20.00	0.00	0.00	-1.00
	10.70	6.40	13.00	7.30	3.30	0.50	4.00	6.00	4.10	0.10	0.00	1.80	11.50	1.00	0.00		
7	19.10	8.90	0.50	0.60	0.10	0.10	0.00	0.00	0.50	0.10	0.10	0.00	11.70	20.00	0.00	0.00	-1.40
	12.70	14.70	14.50	18.40	6.80	2.90	1.30	9.40	0.30	0.00	0.00	8.20	7.80	6.00	0.00		
8	0.20	0.00	0.00	0.10	0.00	0.00	0.00	0.00	0.00	0.00	0.00	0.00	0.00	0.00	0.00	0.00	0.00
	14.00	9.30	0.50	0.10	0.00	0.00	0.00	0.10	0.10	0.00	0.00	0.00	0.00	0.00	0.00		
9	0.00	0.10	0.00	0.00	0.10	0.00	0.00	0.00	0.00	0.00	0.00	0.00	0.00	0.00	0.00	0.00	0.20
	12.00	5.70	0.10	0.60	0.00	0.00	0.00	0.00	0.00	0.10	0.00	0.00	0.00	0.00	0.00		
10	0.10	0.00	0.00	0.10	0.00	0.00	0.00	0.00	0.00	0.00	0.10	0.00	0.00	0.00	0.00	0.10	0.00
	5.20	3.00	0.90	0.10	0.00	0.00	0.00	0.00	0.00	0.00	0.00	0.00	0.00	0.00	0.00		
$\mathbf{X}_\mu$	5.69	2.35	1.51	2.14	1.23	1.86	2.10	0.48	1.31	2.35	1.15	0.16	2.02	9.47	0.00	-0.48	-0.49
	10.74	8.41	6.16	3.88	3.54	1.47	1.56	3.02	2.58	1.90	0.97	1.46	5.68	2.34	0.00		

Table D.26: Detailed results: Unknown Mass, Noise = 10.0% and 4 Sensors.

Run	Identified DI (%) at variable															Error	
No.	EI_1	EI_2	EI_3	EI_4	EI_5	EI_6	EI_7	EI_8	EI_9	EI_{10}	EI_{11}	EI_{12}	EI_{13}	EI_{14}	EI_{15}	ϵ_α	ϵ_β
	ρ_1	ρ_2	ρ_3	ρ_4	ρ_5	ρ_6	ρ_7	ρ_8	ρ_9	ρ_{10}	ρ_{11}	ρ_{12}	ρ_{13}	ρ_{14}	ρ_{15}		
1	12.00	10.80	3.40	5.70	4.00	13.20	11.60	4.90	5.90	8.20	6.00	1.10	1.50	16.00	0.00	-14.50	-0.90
	0.20	18.80	8.10	16.60	8.60	0.40	6.60	8.50	17.00	6.20	7.10	1.20	17.40	10.70	0.00		
2	0.00	0.00	0.00	0.10	0.00	0.20	1.30	0.00	0.00	0.00	0.00	0.00	0.00	0.00	0.00	-0.10	0.00
	6.50	5.10	4.20	0.00	0.00	0.00	0.10	0.00	1.00	0.00	0.00	0.10	0.20	0.00	0.00		
3	8.90	5.30	8.50	5.30	1.80	2.90	12.50	5.40	2.50	10.00	1.90	0.30	9.60	20.00	0.00	0.00	-1.80
	7.70	18.10	10.20	18.30	8.10	5.70	7.80	7.70	4.70	3.80	0.10	4.70	11.50	11.40	0.00		
4	0.10	0.10	0.00	0.10	0.00	0.00	0.10	0.00	0.00	0.00	0.00	0.00	0.00	0.00	0.00	0.00	0.00
	5.80	2.00	1.10	0.80	0.00	0.00	0.00	0.00	0.10	0.00	0.00	0.00	0.00	0.00	0.00		
5	0.00	0.00	0.00	0.00	0.00	0.00	0.00	0.00	0.00	0.00	0.00	0.00	0.00	0.00	0.00	0.00	0.00
	6.70	2.20	0.20	0.10	0.00	0.00	0.00	0.10	0.20	0.10	0.10	0.00	0.00	0.00	0.00		
6	0.00	0.10	0.00	0.10	0.00	0.00	0.00	0.00	0.00	0.00	0.00	0.00	0.00	0.00	0.00	0.00	0.00
	5.00	7.20	0.30	0.00	0.00	0.10	0.10	0.10	0.00	0.00	0.00	0.00	0.00	0.00	0.00		
7	1.00	4.20	5.50	3.80	0.10	0.40	3.70	5.10	1.80	0.50	2.00	0.60	2.10	12.30	0.00	-4.20	0.00
	10.00	3.70	1.70	6.50	2.00	0.70	1.60	1.10	7.70	4.30	1.50	1.70	7.00	3.30	0.00		
8	0.30	0.00	0.00	0.00	0.00	0.00	0.00	0.00	0.10	0.00	1.40	0.80	2.00	4.80	0.00	0.00	0.00
	5.90	1.10	0.00	0.00	0.00	0.00	0.00	0.00	0.00	0.10	0.00	0.40	0.10	0.00	0.00		
9	0.00	0.00	0.10	0.20	0.60	0.10	0.00	0.00	0.00	0.00	0.00	0.00	0.00	0.00	0.00	0.00	0.00
	11.90	2.30	1.50	0.50	0.20	0.40	0.30	0.70	0.30	0.00	0.00	0.00	0.00	0.00	0.00		
10	0.10	0.00	0.00	0.00	0.00	0.00	0.10	0.00	0.00	0.00	0.00	0.00	0.00	0.00	0.00	0.00	0.00
	16.70	9.50	4.90	0.00	0.00	0.20	0.00	0.00	0.00	0.00	0.00	0.00	0.00	0.00	0.00		
$\mathbf{X}_\mu$	2.24	2.05	1.75	1.53	0.65	1.68	2.93	1.54	1.03	1.87	1.13	0.28	1.52	5.31	0.00	-1.88	-0.27
	7.64	7.00	3.22	4.28	1.89	0.75	1.65	1.82	3.10	1.45	0.88	0.81	3.62	2.54	0.00		

D.4 Known Mass Damage Detection Results

Table D.27: Detailed Damage Detection: Noise = 0.0% and 14 Sensors.

Run	Identified DI (%) at node No.															Error	
No.	1	2	3	4	5	6	7	8	9	10	11	12	13	14	15	ϵ_α	ϵ_β
1	0.00	0.00	0.00	0.30	0.90	7.90	0.80	0.00	0.00	0.00	0.00	0.00	0.00	0.00	0.00	-0.10	0.00
2	0.10	0.00	0.00	0.00	1.40	7.50	1.00	0.00	0.00	0.00	0.00	0.00	0.10	0.00	0.00	-0.10	0.00
3	0.00	0.00	0.00	0.00	2.40	6.10	1.40	0.00	0.00	0.00	0.00	0.00	0.10	0.00	0.00	-0.20	0.00
4	0.10	0.00	0.00	0.00	0.60	8.90	0.40	0.00	0.00	0.00	0.00	0.00	0.00	0.00	0.00	0.00	0.00
5	0.00	0.00	0.00	0.10	0.70	8.60	0.60	0.00	0.00	0.00	0.00	0.00	0.00	0.00	0.00	-0.10	0.00
6	0.00	0.00	0.00	0.00	2.10	6.50	1.30	0.00	0.00	0.00	0.00	0.00	0.00	0.00	0.00	-0.10	0.00
7	0.00	0.00	0.00	0.00	1.90	6.70	1.40	0.00	0.00	0.00	0.00	0.00	0.00	0.00	0.00	0.00	0.00
8	0.00	0.00	0.00	0.00	0.70	8.90	0.30	0.10	0.00	0.00	0.00	0.00	0.00	0.00	0.00	-0.10	0.00
9	0.00	0.10	0.00	0.00	0.40	9.20	0.20	0.00	0.00	0.00	0.00	0.00	0.00	0.00	0.00	0.10	0.00
10	0.00	0.00	0.00	0.00	0.90	8.50	0.50	0.10	0.00	0.00	0.00	0.00	0.00	0.00	0.00	0.50	0.00
$\mathbf{X}_\mu$	0.02	0.01	0.00	0.04	1.20	7.88	0.79	0.02	0.00	0.00	0.00	0.00	0.02	0.00	0.00	-0.01	0.00

Table D.28: Detailed Damage Detection: Noise = 2.0% and 14 Sensors.

Run	Identified DI (%) at node No.															Error	
No.	1	2	3	4	5	6	7	8	9	10	11	12	13	14	15	ϵ_α	ϵ_β
1	0.10	0.00	0.00	0.00	4.30	4.90	0.30	0.00	0.00	0.00	0.00	1.10	0.50	2.40	0.00	0.00	-0.40
2	0.00	0.10	0.30	0.40	2.30	5.90	0.10	0.00	0.00	0.00	0.00	0.00	0.00	0.00	0.00	0.00	0.00
3	3.00	0.20	0.30	1.40	2.10	8.40	3.00	0.00	0.00	0.00	0.00	0.00	0.00	0.00	0.00	0.00	0.00
4	0.00	0.00	0.00	0.00	2.50	5.70	1.60	0.00	0.00	0.00	0.00	0.00	0.00	0.00	0.00	-1.90	1.30
5	0.00	0.00	0.00	0.00	1.80	7.60	2.00	0.00	0.00	0.00	0.60	0.90	3.20	0.80	0.00	-9.00	-2.00
6	0.10	0.00	0.30	0.00	5.30	13.70	0.40	0.00	0.10	0.10	0.70	0.50	0.00	0.00	0.00	0.00	-0.40
7	0.00	0.00	0.00	0.00	2.40	6.80	0.30	0.10	0.10	0.00	0.00	0.90	0.10	1.10	0.00	-2.30	-0.80
8	0.00	0.00	0.00	0.00	4.20	4.60	1.50	0.10	0.00	0.00	0.10	1.60	1.40	0.00	0.00	1.50	-2.10
9	0.00	0.00	0.00	0.00	1.70	7.80	0.30	0.00	0.00	0.00	0.20	0.20	0.00	0.10	0.00	-0.50	-0.10
10	3.70	0.50	0.20	0.20	3.70	11.90	4.10	0.00	0.00	0.00	0.00	0.00	0.00	0.00	0.00	0.00	0.70
$\mathbf{X}_\mu$	0.69	0.08	0.11	0.20	3.03	7.73	1.36	0.02	0.02	0.01	0.16	0.52	0.52	0.44	0.00	-1.22	-0.38

Table D.29: Detailed Damage Detection: Noise = 5.0% and 14 Sensors.

Run	Identified DI (%) at node No.															Error	
No.	1	2	3	4	5	6	7	8	9	10	11	12	13	14	15	ϵ_α	ϵ_β
1	1.60	1.40	2.90	0.00	0.20	0.10	9.00	0.00	0.00	0.00	0.00	0.00	0.00	0.00	0.00	0.00	0.00
2	0.00	0.00	0.00	0.00	5.70	7.30	6.70	0.00	0.00	0.10	0.10	0.00	0.00	0.00	0.00	-11.60	-0.10
3	5.20	1.70	0.10	0.00	0.20	11.70	0.00	0.00	0.00	0.00	0.00	0.00	0.00	0.00	0.00	0.00	1.80
4	0.00	0.00	0.00	0.00	4.90	2.90	6.00	0.00	0.00	0.00	1.60	1.50	0.00	3.10	0.00	-8.20	-2.60
5	0.20	1.40	4.00	0.00	6.00	6.60	0.00	0.00	0.00	0.00	0.00	0.00	0.00	3.00	0.00	1.90	0.00
6	0.00	0.00	0.00	0.00	0.50	7.50	0.10	0.00	0.00	0.00	0.50	5.20	0.00	1.10	0.00	-7.10	-5.30
7	0.00	0.00	0.00	0.00	2.20	5.10	0.00	0.00	0.00	0.10	1.40	2.10	2.60	0.70	0.00	1.60	-4.00
8	0.00	0.00	0.10	0.10	0.20	15.00	5.10	0.10	0.00	0.00	0.00	0.00	0.00	0.00	0.00	-1.70	0.40
9	0.00	0.00	0.00	0.00	2.50	10.40	0.10	0.00	0.00	0.00	1.60	1.00	0.00	0.00	0.00	1.30	-1.80
10	0.00	0.00	0.00	0.00	5.70	9.50	0.00	0.00	0.00	0.00	0.00	2.40	3.20	0.00	0.00	0.00	-3.00
$\mathbf{X}_\mu$	0.70	0.45	0.71	0.01	2.81	7.61	2.70	0.01	0.00	0.02	0.52	1.22	0.58	0.79	0.00	-2.38	-1.46

Table D.30: Detailed Damage Detection: Noise = 10.0% and 14 Sensors.

Run	Identified DI (%) at node No.															Error	
No.	1	2	3	4	5	6	7	8	9	10	11	12	13	14	15	ϵ_α	ϵ_β
1	0.00	0.00	0.00	0.00	0.10	8.30	0.90	0.00	0.00	1.20	0.80	0.80	3.10	0.00	0.00	-16.40	-0.80
2	6.20	0.60	0.80	0.20	0.00	11.40	9.00	0.00	0.00	0.00	0.00	0.00	0.00	0.00	0.00	0.00	0.00
3	0.00	0.00	0.00	0.00	0.00	4.20	6.00	0.50	0.00	0.10	2.00	3.10	0.00	0.00	0.00	0.50	-9.80
4	0.00	0.00	0.90	0.70	3.90	2.50	0.50	0.00	0.00	0.00	0.00	0.00	0.00	0.00	0.00	0.00	0.00
5	2.00	3.10	0.60	0.00	0.00	11.20	0.00	0.00	0.00	0.00	0.00	0.00	0.00	0.00	0.00	0.00	0.00
6	0.00	0.00	0.00	0.10	6.70	8.70	0.00	0.00	0.00	0.00	0.20	1.60	0.00	1.00	0.00	-1.20	-2.20
7	6.20	0.10	0.10	1.70	0.50	6.70	0.00	0.00	0.00	0.00	0.00	0.00	0.00	4.70	0.00	0.00	4.70
8	2.40	2.90	0.30	0.10	1.30	6.60	0.00	0.00	0.00	0.00	0.00	0.00	0.00	0.00	0.00	0.00	0.00
9	4.80	1.40	0.40	0.60	8.70	8.10	0.00	0.00	0.00	0.00	0.00	0.00	0.00	0.00	0.00	0.00	0.00
10	0.00	0.00	0.00	0.00	0.20	4.30	6.50	1.20	0.00	0.00	0.00	0.00	0.00	0.00	0.00	-13.00	0.00
$\mathbf{X}_\mu$	2.16	0.81	0.31	0.34	2.14	7.20	2.29	0.17	0.00	0.13	0.30	0.55	0.31	0.57	0.00	-3.01	-0.81

Table D.31: Detailed Damage Detection: Noise = 0.0% and 7 Sensors.

Run	Identified DI (%) at node No.															Error	
No.	1	2	3	4	5	6	7	8	9	10	11	12	13	14	15	ϵ_α	ϵ_β
1	0.00	0.00	0.00	0.00	1.50	7.60	0.80	0.00	0.00	0.00	0.10	0.00	0.00	0.00	0.00	-0.10	0.00
2	0.00	0.00	0.00	0.00	2.30	6.00	1.60	0.00	0.00	0.00	0.10	0.00	0.00	0.00	0.00	-0.10	0.00
3	0.00	0.00	0.00	0.00	1.20	8.00	0.80	0.00	0.00	0.00	0.00	0.00	0.00	0.10	0.00	-0.10	0.00
4	0.00	0.00	0.00	0.10	0.30	9.40	0.10	0.10	0.00	0.00	0.00	0.00	0.00	0.00	0.00	0.00	0.00
5	0.00	0.00	0.00	0.00	1.80	7.00	1.10	0.00	0.00	0.00	0.00	0.10	0.00	0.00	0.00	-0.10	0.00
6	0.00	0.00	0.00	0.00	1.00	8.30	0.60	0.10	0.00	0.00	0.00	0.00	0.00	0.00	0.00	0.00	0.00
7	0.00	0.00	0.00	0.10	0.90	8.30	0.70	0.00	0.00	0.00	0.00	0.00	0.00	0.00	0.00	0.00	0.00
8	0.00	0.00	0.00	0.00	0.90	8.50	0.60	0.00	0.00	0.00	0.00	0.00	0.00	0.00	0.00	-0.10	0.00
9	0.00	0.00	0.00	0.00	2.40	5.80	1.80	0.00	0.00	0.00	0.00	0.00	0.00	0.10	0.00	-0.10	0.00
10	0.10	0.00	0.00	0.00	0.90	8.40	0.60	0.00	0.00	0.00	0.00	0.00	0.00	0.10	0.00	0.00	0.00
$\mathbf{X}_\mu$	0.01	0.00	0.00	0.02	1.32	7.73	0.87	0.02	0.00	0.00	0.02	0.01	0.01	0.02	0.00	-0.06	0.00

Table D.32: Detailed Damage Detection: Noise = 2.0% and 7 Sensors.

Run	Identified DI (%) at node No.															Error	
No.	1	2	3	4	5	6	7	8	9	10	11	12	13	14	15	ϵ_α	ϵ_β
1	1.30	0.80	3.10	0.20	1.00	0.20	0.00	0.00	0.00	0.00	0.00	0.00	0.00	0.00	0.00	0.00	0.00
2	0.00	0.00	0.00	0.00	3.10	6.00	0.10	0.00	0.00	0.00	0.40	1.70	0.30	1.70	0.00	-6.30	-0.30
3	0.00	0.00	0.00	0.10	3.70	4.80	0.40	0.10	0.10	0.00	0.00	1.50	0.00	0.00	0.00	-2.60	-1.20
4	0.00	0.00	0.00	0.00	0.40	9.20	0.10	0.00	0.00	0.10	0.60	0.30	1.00	0.40	0.00	-7.60	-0.30
5	0.60	0.80	0.10	0.10	3.20	3.50	0.10	0.00	0.00	0.00	0.00	0.00	0.00	0.00	0.00	0.00	1.70
6	0.00	0.00	0.00	0.10	7.20	13.30	0.00	0.00	0.00	0.00	0.00	1.40	0.10	0.00	0.00	-2.90	-1.60
7	1.10	0.90	0.20	0.40	2.20	3.60	0.00	0.00	0.00	0.00	0.00	0.00	0.00	0.00	0.00	0.70	2.90
8	0.00	0.00	0.00	0.00	0.50	8.10	1.60	0.00	0.00	0.00	0.10	0.90	0.10	0.60	0.00	-4.50	-0.20
9	1.20	1.60	1.40	0.40	1.50	8.60	0.00	0.00	0.00	0.00	0.00	0.00	0.00	0.00	0.00	0.00	0.00
10	0.30	1.60	3.40	0.20	0.20	15.00	11.00	0.00	0.00	0.00	0.00	0.00	0.00	0.00	0.00	0.00	0.00
$\mathbf{X}_\mu$	0.45	0.57	0.82	0.15	2.30	7.23	1.33	0.01	0.01	0.01	0.11	0.58	0.15	0.27	0.00	-2.32	0.10

Table D.33: Detailed Damage Detection: Noise = 5.0% and 7 Sensors.

Run	Identified DI (%) at node No.															Error	
No.	1	2	3	4	5	6	7	8	9	10	11	12	13	14	15	ϵ_α	ϵ_β
1	0.00	0.00	0.00	0.00	5.30	5.10	0.00	0.00	0.00	0.00	0.00	1.40	0.00	0.20	0.00	-7.20	-2.10
2	0.00	0.00	0.90	1.60	3.50	1.30	1.60	0.00	0.00	0.10	0.10	0.00	0.00	0.00	0.00	0.00	0.00
3	4.30	0.40	1.40	1.00	0.50	3.30	0.00	0.00	0.00	0.00	0.00	0.00	0.00	0.00	0.00	1.40	0.00
4	1.00	0.00	0.00	0.00	5.80	6.70	0.10	0.00	0.00	0.00	0.80	0.40	0.20	1.40	0.00	0.10	0.00
5	2.10	0.10	0.00	0.10	5.40	7.40	0.00	0.00	0.00	0.00	0.00	0.00	0.20	2.00	0.00	0.00	0.00
6	0.00	0.00	0.00	0.00	7.70	6.30	0.00	0.00	0.00	0.20	2.00	1.90	0.20	0.00	0.00	-13.60	-3.00
7	2.60	1.80	1.70	0.30	0.00	9.00	7.60	0.00	0.00	0.00	0.00	0.00	0.00	0.00	0.00	0.00	0.00
8	1.80	0.50	0.00	0.10	3.90	8.10	0.10	0.00	0.00	0.00	0.00	0.00	0.00	0.00	0.00	0.00	1.70
9	0.00	0.00	0.00	0.00	7.20	11.30	7.10	0.00	0.00	0.00	0.60	4.70	0.00	0.90	0.00	-18.00	-2.10
10	2.10	1.20	0.20	1.70	1.90	11.70	0.00	0.00	0.00	0.00	0.00	0.00	0.00	0.00	0.00	0.00	0.00
$\mathbf{X}_\mu$	1.39	0.40	0.42	0.48	4.12	7.02	1.65	0.00	0.00	0.03	0.35	0.84	0.06	0.45	0.00	-3.73	-0.55

Table D.34: Detailed Damage Detection: Noise = 10.0% and 7 Sensors.

Run	Identified DI (%) at node No.															Error	
No.	1	2	3	4	5	6	7	8	9	10	11	12	13	14	15	ϵ_α	ϵ_β
1	0.00	0.00	0.00	1.40	4.00	1.70	0.00	0.00	0.00	0.00	0.00	0.00	0.00	0.00	0.00	0.00	0.00
2	0.00	0.00	0.00	0.00	4.40	2.60	0.00	0.00	0.00	1.60	6.80	0.10	3.70	0.00	0.00	-9.70	-5.10
3	0.00	0.00	0.00	0.00	0.00	8.60	1.20	0.10	0.00	0.00	0.00	0.00	0.00	0.00	0.00	-20.00	0.00
4	0.10	1.10	4.00	0.00	0.00	7.00	0.00	0.00	0.00	0.00	0.00	0.00	0.00	3.10	0.00	0.00	0.00
5	2.40	0.10	0.00	0.00	3.70	2.70	0.20	0.00	0.00	0.00	0.00	0.00	0.00	0.00	0.00	0.00	0.00
6	0.00	0.10	0.00	0.00	6.20	4.90	0.00	0.00	0.00	0.00	0.00	0.00	0.00	0.00	0.00	0.00	0.00
7	0.00	0.00	0.00	0.00	0.00	8.70	1.10	0.10	0.60	0.00	0.00	0.00	0.00	0.00	0.00	-6.60	0.00
8	0.00	0.00	0.00	0.00	2.20	7.60	1.10	2.70	0.00	0.00	3.00	4.10	0.20	1.40	0.00	-18.90	0.00
9	1.60	3.30	0.40	0.00	0.00	5.20	0.00	0.00	0.00	0.00	0.00	0.00	0.00	0.00	0.00	0.00	0.00
10	0.00	0.00	0.00	0.00	0.00	7.30	9.80	0.10	0.20	0.00	0.00	0.00	0.00	0.00	0.00	-20.00	0.00
$\mathbf{X}_\mu$	0.41	0.46	0.44	0.14	2.05	5.63	1.34	0.30	0.08	0.16	0.98	0.42	0.39	0.45	0.00	-7.52	-0.51

Table D.35: Detailed Damage Detection: Noise = 0.0% and 4 Sensors.

Run	Identified DI (%) at node No.															Error	
No.	1	2	3	4	5	6	7	8	9	10	11	12	13	14	15	ϵ_α	ϵ_β
1	0.00	0.00	0.00	0.00	1.30	7.80	0.90	0.00	0.00	0.00	0.00	0.00	0.00	0.10	0.00	0.00	0.00
2	0.10	0.00	0.00	0.30	0.40	8.70	0.40	0.00	0.00	0.00	0.00	0.10	0.00	0.00	0.10	0.00	0.00
3	0.10	0.00	0.00	0.00	2.90	5.00	1.90	0.00	0.00	0.00	0.00	0.00	0.00	0.00	0.10	-0.10	0.00
4	0.00	0.00	0.00	0.00	1.90	6.80	1.20	0.10	0.00	0.00	0.00	0.00	0.00	0.00	0.00	-0.20	0.00
5	0.10	0.00	0.00	0.00	2.10	6.30	1.50	0.00	0.00	0.10	0.00	0.00	0.00	0.00	0.00	-0.20	0.00
6	0.00	0.00	0.00	0.00	1.80	6.90	1.30	0.00	0.00	0.00	0.00	0.00	0.00	0.00	0.00	-0.20	0.00
7	0.10	0.00	0.00	0.20	0.60	8.70	0.30	0.00	0.00	0.00	0.00	0.00	0.00	0.00	0.00	-0.10	0.00
8	0.10	0.00	0.00	0.00	1.60	7.20	1.10	0.00	0.00	0.00	0.00	0.00	0.00	0.00	0.00	-0.10	0.00
9	0.10	0.00	0.00	0.10	0.40	9.00	0.40	0.00	0.00	0.00	0.00	0.00	0.00	0.00	0.00	-0.10	0.00
10	0.00	0.00	0.00	0.00	2.60	5.60	1.60	0.10	0.00	0.00	0.00	0.10	0.00	0.00	0.10	-0.10	0.00
$\mathbf{X}_\mu$	0.06	0.00	0.00	0.06	1.56	7.20	1.06	0.02	0.00	0.01	0.00	0.02	0.00	0.01	0.03	-0.11	0.00

Table D.36: Detailed Damage Detection: Noise = 2.0% and 4 Sensors.

Run	Identified DI (%) at node No.															Error	
No.	1	2	3	4	5	6	7	8	9	10	11	12	13	14	15	ϵ_α	ϵ_β
1	0.00	0.00	0.00	0.00	1.70	6.30	1.80	0.00	0.10	0.70	0.10	0.00	0.00	0.00	0.00	-8.30	0.00
2	0.20	0.20	0.00	0.00	3.60	3.70	1.60	0.00	0.00	0.00	0.00	0.00	0.00	0.00	0.00	0.00	0.00
3	1.80	1.40	0.70	1.90	0.20	5.70	0.00	0.00	0.00	0.00	0.00	0.00	0.00	0.00	0.00	0.00	0.00
4	0.00	0.00	0.00	0.00	2.30	6.80	0.00	0.00	0.00	0.10	0.90	1.10	0.60	2.80	0.00	-6.10	-0.50
5	0.00	0.00	0.00	0.00	3.20	5.90	0.10	0.00	0.00	0.70	0.50	0.50	0.00	5.70	0.00	-0.60	-0.60
6	2.20	2.10	1.80	0.10	0.00	7.70	0.00	0.00	0.00	0.00	0.00	0.00	0.00	0.00	0.00	0.00	0.00
7	2.40	1.20	1.90	0.70	0.30	11.30	0.00	0.00	0.00	0.00	0.00	0.00	0.00	0.00	0.00	0.00	0.00
8	0.10	0.10	0.00	0.00	1.00	7.40	1.40	0.00	0.00	0.00	0.00	0.50	0.00	0.80	0.00	0.00	-0.20
9	3.20	1.10	0.00	0.00	2.50	13.30	0.10	0.00	0.00	0.00	0.00	0.00	0.00	0.00	0.00	0.00	0.00
10	2.10	1.00	0.30	0.10	4.20	9.40	0.00	0.00	0.00	0.00	0.00	0.00	0.00	0.00	0.00	0.00	0.00
$\mathbf{X}_\mu$	1.20	0.71	0.47	0.28	1.90	7.75	0.50	0.00	0.01	0.15	0.15	0.21	0.06	0.93	0.00	-1.50	-0.13

Table D.37: Detailed Damage Detection: Noise = 5.0% and 4 Sensors.

Run	Identified DI (%) at node No.															Error	
No.	1	2	3	4	5	6	7	8	9	10	11	12	13	14	15	ϵ_α	ϵ_β
1	0.00	0.00	0.00	0.00	1.00	9.20	1.00	0.00	0.00	0.00	0.00	0.00	0.00	0.00	0.00	-12.20	-1.40
2	4.30	0.80	1.50	0.60	0.00	0.10	0.00	0.00	0.00	0.00	0.00	0.00	0.00	0.00	0.00	0.00	0.00
3	3.70	1.30	1.60	0.20	0.20	0.00	0.00	0.00	0.00	0.00	0.00	0.00	0.00	0.00	0.00	0.00	0.00
4	4.20	1.20	1.00	1.10	0.00	0.00	0.00	0.00	0.00	0.00	0.00	0.00	0.00	0.00	0.00	0.00	0.00
5	0.00	0.00	0.00	0.00	0.60	9.00	0.00	0.00	0.00	0.00	1.10	4.20	0.00	0.00	0.00	-19.70	-0.80
6	0.00	0.00	0.00	0.00	2.10	8.70	0.50	0.00	0.00	0.00	1.70	0.70	0.00	2.40	0.00	-14.70	-2.60
7	0.00	0.00	0.00	0.00	3.10	5.10	1.00	0.00	0.00	0.00	3.60	0.10	1.10	0.70	0.00	-15.40	-6.40
8	0.00	0.00	0.00	0.00	1.00	8.80	0.00	0.00	0.00	0.00	0.00	0.00	0.00	0.00	0.00	0.00	0.00
9	2.60	1.30	1.50	1.10	0.10	11.40	0.00	0.00	0.00	0.00	0.00	0.00	0.00	0.00	0.00	0.00	0.00
10	0.90	0.40	0.20	5.00	2.01	0.00	0.00	0.00	0.00	0.00	0.00	0.90	0.60	0.40	0.00	0.00	-0.20
$\mathbf{X}_\mu$	1.57	0.50	0.58	0.80	1.01	5.23	0.25	0.00	0.00	0.00	0.64	0.59	0.17	0.35	0.00	-6.20	-1.14

Table D.38: Detailed Damage Detection: Noise = 10.0% and 4 Sensors.

Run	Identified DI (%) at node No.															Error	
No.	1	2	3	4	5	6	7	8	9	10	11	12	13	14	15	ϵ_α	ϵ_β
1	0.00	0.00	0.00	2.70	4.00	0.00	0.00	0.00	0.00	0.20	4.10	0.60	0.00	0.90	0.00	-7.20	-3.70
2	0.00	0.00	0.00	0.20	6.60	0.00	0.00	0.00	0.00	0.00	0.00	0.00	0.00	3.30	0.00	0.00	-11.80
3	0.20	1.70	0.00	0.00	7.80	0.00	0.00	0.00	0.00	0.00	0.00	0.00	0.00	0.00	0.00	0.00	0.00
4	0.00	0.00	0.00	0.20	0.90	8.80	0.10	0.00	0.00	0.00	0.00	0.00	0.00	0.00	0.00	0.00	0.00
5	0.00	0.00	0.00	0.00	3.80	4.20	0.00	0.00	0.00	0.00	0.00	0.00	0.70	0.00	0.00	-18.50	-1.80
6	0.30	1.40	0.00	0.00	4.50	1.30	0.00	0.00	0.00	0.00	0.00	0.00	0.00	0.00	0.00	0.00	0.00
7	0.00	0.00	0.00	0.10	7.70	0.00	0.00	0.00	0.00	0.20	0.80	0.00	0.50	0.10	0.00	-9.50	-10.40
8	0.00	0.00	0.00	3.60	2.50	0.00	0.00	0.20	3.40	0.00	0.00	1.30	1.10	1.60	0.00	-7.10	0.00
9	0.30	4.80	0.10	0.10	8.90	0.00	0.00	0.00	0.00	0.00	0.00	0.00	0.00	0.00	0.00	0.00	0.00
10	0.00	0.00	0.00	0.00	7.90	0.00	0.00	0.00	0.00	0.00	3.60	0.00	2.10	1.70	0.00	-17.90	-14.40
$\mathbf{X}_\mu$	0.08	0.79	0.01	0.69	5.46	1.43	0.01	0.02	0.34	0.04	0.85	0.19	0.44	0.76	0.00	-6.02	-4.21

D.5 Output-Only Results

Table D.39: Detailed results: Output-only, Noise = 0.0% and 16 Sensors.

Run	Identified DI (%) at node No.															Error	
No.	1	2	3	4	5	6	7	8	9	10	11	12	13	14	15	ϵ_α	ϵ_β
1	0.00	0.00	0.00	0.00	0.00	0.00	0.00	0.00	0.00	0.00	0.00	0.00	0.00	0.00	0.00	-0.20	0.00
2	0.00	0.00	0.00	0.00	0.00	0.00	0.00	0.00	0.00	0.00	0.00	0.00	0.00	0.00	0.00	-0.70	0.00
3	0.00	0.00	0.00	0.00	0.00	0.00	0.00	0.00	0.00	0.00	0.00	0.20	0.00	0.10	0.00	-1.70	0.00
4	0.00	0.00	0.00	0.00	0.00	0.00	0.00	0.00	0.00	0.00	0.00	0.00	0.00	0.00	0.00	-0.30	0.00
5	0.00	0.00	0.00	0.00	0.00	0.00	0.00	0.00	0.00	0.00	0.00	0.00	0.00	0.00	0.00	-0.20	0.00
6	0.00	0.00	0.00	0.00	0.00	0.00	0.00	0.00	0.00	0.00	0.00	0.00	0.00	0.00	0.00	-0.70	0.00
7	0.00	0.00	0.00	0.00	0.00	0.00	0.00	0.00	0.00	0.00	0.00	0.00	0.00	0.00	0.00	-0.50	0.00
8	0.00	0.00	0.00	0.00	0.00	0.00	0.00	0.00	0.00	0.00	0.00	0.00	0.00	0.00	0.00	-0.30	0.00
9	0.00	0.00	0.00	0.00	0.00	0.00	0.00	0.00	0.00	0.00	0.00	0.00	0.00	0.00	0.00	-0.20	0.00
10	0.00	0.00	0.00	0.00	0.00	0.00	0.00	0.00	0.00	0.00	0.00	0.00	0.00	0.00	0.00	-1.00	0.00
$\mathbf{X}_\mu$	0.00	0.00	0.00	0.00	0.00	0.00	0.00	0.00	0.00	0.00	0.00	0.02	0.00	0.01	0.00	-0.58	0.00

Table D.40: Detailed results: Output-only, Noise = 2.0% and 16 Sensors.

Run	Identified DI (%) at node No.															Error	
No.	1	2	3	4	5	6	7	8	9	10	11	12	13	14	15	ϵ_α	ϵ_β
1	0.00	0.00	0.00	0.00	0.00	0.00	0.00	0.00	0.00	0.00	0.00	0.10	0.00	0.00	0.00	-1.00	0.00
2	0.00	0.00	0.00	0.00	0.00	0.00	0.00	0.20	0.00	0.00	0.00	0.10	0.00	0.20	0.00	-3.70	0.00
3	0.00	0.00	0.00	0.00	0.00	0.00	0.00	0.00	0.00	0.00	0.20	0.10	0.10	0.10	0.00	-2.20	0.00
4	0.00	0.00	0.00	0.10	0.00	0.00	0.00	0.00	0.00	0.00	0.00	0.00	0.00	0.00	0.00	-0.90	0.00
5	0.00	0.00	0.00	0.00	0.00	0.00	0.00	0.00	0.00	0.00	0.00	0.00	0.00	0.00	0.00	-1.00	0.00
6	0.10	0.00	0.00	0.00	0.10	0.00	0.00	0.00	0.00	0.00	0.00	0.00	0.00	0.10	0.00	-1.30	0.00
7	0.00	0.00	0.00	0.00	0.00	0.00	0.00	0.10	0.10	0.00	0.00	0.00	0.10	0.20	0.00	-3.10	0.00
8	0.00	0.00	0.00	0.00	0.00	0.00	0.00	0.10	0.00	0.00	0.00	0.00	0.00	0.00	0.00	0.00	0.00
9	0.00	0.00	0.20	0.00	0.00	0.00	0.00	0.00	0.10	0.00	0.00	0.00	0.00	0.10	0.00	-1.00	0.00
10	0.00	0.00	0.00	0.00	0.00	0.00	0.00	0.00	0.00	0.00	0.00	0.00	0.00	0.00	0.00	-0.50	0.00
$\mathbf{X}_\mu$	0.01	0.00	0.02	0.01	0.01	0.00	0.00	0.04	0.02	0.00	0.02	0.03	0.02	0.07	0.00	-1.47	0.00

Table D.41: Detailed results: Output-only, Noise = 5.0% and 16 Sensors.

Run	Identified DI (%) at node No.															Error	
No.	1	2	3	4	5	6	7	8	9	10	11	12	13	14	15	ϵ_α	ϵ_β
1	0.00	0.00	0.00	0.00	0.00	0.00	0.00	0.00	0.00	0.00	0.00	0.20	0.10	0.00	0.00	-3.50	0.00
2	0.00	0.00	0.00	0.00	0.00	0.00	0.00	0.00	0.00	0.00	0.00	0.00	0.10	0.00	0.00	0.00	0.00
3	0.00	0.00	0.00	0.40	0.00	0.00	0.00	0.00	0.00	0.00	0.00	0.00	0.10	0.00	0.00	-1.20	0.00
4	0.00	0.00	0.00	0.00	0.00	0.00	0.00	0.00	0.00	0.00	0.00	0.00	0.00	0.20	0.00	-4.80	0.00
5	0.00	0.00	0.00	0.00	0.20	0.10	0.10	0.10	0.30	0.00	0.20	0.10	0.00	0.20	0.10	-2.10	0.00
6	0.10	0.00	0.00	0.00	0.00	0.00	0.00	0.00	0.00	0.00	0.00	0.00	0.00	0.10	0.00	-1.70	0.00
7	0.00	0.00	0.00	0.00	0.00	0.00	0.00	0.00	0.00	0.00	0.10	0.00	0.00	0.00	0.10	-4.10	0.00
8	0.00	0.00	0.00	0.00	0.00	0.00	0.00	0.00	0.00	0.00	0.00	0.00	0.10	0.00	0.00	-0.80	0.00
9	0.00	0.00	0.00	0.00	0.00	0.00	0.00	0.00	0.10	0.30	0.10	0.20	0.40	0.10	0.20	-0.40	0.00
10	0.00	0.00	0.00	0.20	0.00	0.00	0.00	0.00	0.00	0.00	0.00	0.00	0.00	0.00	0.00	-0.60	0.00
$\mathbf{X}_\mu$	0.01	0.00	0.00	0.06	0.02	0.01	0.01	0.01	0.04	0.03	0.04	0.05	0.08	0.06	0.04	-1.92	0.00

Table D.42: Detailed results: Output-only, Noise = 10.0% and 16 Sensors.

Run	Identified DI (%) at node No.															Error	
No.	1	2	3	4	5	6	7	8	9	10	11	12	13	14	15	ϵ_α	ϵ_β
1	0.00	0.00	0.00	0.00	0.00	0.00	0.00	0.00	0.00	0.00	0.00	0.30	0.20	0.00	0.00	-6.50	0.00
2	0.00	0.00	0.00	0.00	0.00	0.00	0.00	0.00	0.00	0.00	0.00	0.00	0.20	0.20	0.00	-3.50	0.00
3	1.30	0.00	0.00	0.00	0.00	0.00	0.00	0.00	0.00	0.00	0.00	0.00	0.00	0.20	0.00	-3.40	0.00
4	0.00	0.00	0.00	0.40	0.00	0.00	1.10	0.10	0.00	0.00	0.00	0.00	0.50	1.10	0.00	-18.10	0.00
5	0.00	0.00	0.00	0.00	0.00	1.20	0.10	0.00	0.00	0.00	0.00	0.00	0.00	0.30	0.10	0.00	0.00
6	0.00	0.10	0.00	0.00	0.00	0.10	0.30	0.60	0.00	0.00	0.00	0.10	0.00	0.00	0.10	-0.10	0.00
7	0.00	0.00	0.00	0.00	0.10	0.50	0.00	0.00	0.00	0.00	1.20	0.10	0.00	0.00	0.10	0.00	0.00
8	0.00	0.00	0.00	1.60	0.00	0.00	0.00	0.00	0.00	0.00	0.00	0.40	0.80	0.80	0.00	-0.70	0.00
9	1.00	0.00	0.00	0.00	0.00	0.00	0.00	0.00	0.00	0.00	0.00	0.00	0.00	0.40	0.00	-2.30	0.00
10	0.00	0.00	0.00	0.00	0.00	0.00	0.00	0.00	0.00	0.00	0.00	0.00	0.00	0.00	0.10	-15.90	0.00
$\mathbf{X}_\mu$	0.23	0.01	0.00	0.20	0.01	0.18	0.15	0.07	0.00	0.00	0.12	0.09	0.17	0.30	0.04	-5.05	0.00

Table D.43: Detailed results: Output-only, Noise = 0.0% and 10 Sensors.

Run	Identified DI (%) at node No.															Error	
No.	1	2	3	4	5	6	7	8	9	10	11	12	13	14	15	ϵ_α	ϵ_β
1	0.00	0.00	0.00	0.00	0.00	0.00	0.00	0.00	0.00	0.00	0.00	0.00	0.00	0.00	0.00	-0.20	0.00
2	0.00	0.00	0.00	0.00	0.00	0.00	0.00	0.00	0.00	0.00	0.00	0.10	0.00	0.10	0.00	-1.70	0.00
3	0.00	0.00	0.00	0.00	0.00	0.00	0.00	0.00	0.00	0.10	0.00	0.00	0.00	0.00	0.00	-0.40	0.00
4	0.00	0.00	0.00	0.00	0.00	0.00	0.00	0.00	0.00	0.00	0.00	0.00	0.00	0.00	0.00	0.00	0.00
5	0.00	0.00	0.00	0.00	0.00	0.00	0.00	0.00	0.00	0.00	0.00	0.00	0.00	0.00	0.00	-0.10	0.00
6	0.00	0.00	0.00	0.00	0.00	0.00	0.00	0.00	0.00	0.00	0.00	0.00	0.00	0.00	0.00	-0.40	0.00
7	0.00	0.00	0.00	0.00	0.00	0.00	0.00	0.00	0.00	0.00	0.00	0.00	0.00	0.00	0.00	-0.10	0.00
8	0.00	0.00	0.00	0.00	0.00	0.00	0.00	0.00	0.00	0.00	0.00	0.00	0.00	0.00	0.00	-0.20	0.00
9	0.00	0.00	0.00	0.00	0.00	0.00	0.00	0.00	0.00	0.00	0.10	0.00	0.00	0.10	0.00	-1.70	0.00
10	0.00	0.00	0.00	0.00	0.00	0.00	0.00	0.00	0.00	0.00	0.00	0.00	0.00	0.00	0.00	-0.90	0.00
$\mathbf{X}_\mu$	0.00	0.00	0.00	0.00	0.00	0.00	0.00	0.00	0.00	0.01	0.01	0.01	0.00	0.02	0.00	-0.57	0.00

Table D.44: Detailed results: Output-only, Noise = 2.0% and 10 Sensors.

Run	Identified DI (%) at node No.															Error	
No.	1	2	3	4	5	6	7	8	9	10	11	12	13	14	15	ϵ_α	ϵ_β
1	0.00	0.00	0.00	0.00	0.00	0.00	0.00	0.00	0.00	0.00	0.00	0.00	0.00	0.00	0.00	-0.30	0.00
2	0.00	0.00	0.20	0.00	0.00	0.00	0.00	0.00	0.10	0.00	0.00	0.00	0.00	0.00	0.10	-1.50	0.00
3	0.00	0.00	0.00	0.00	0.30	0.00	0.00	0.00	0.00	0.00	0.00	0.20	0.00	0.10	0.00	-2.00	0.00
4	0.00	0.00	0.00	0.00	0.00	0.00	0.00	0.00	0.00	0.00	0.10	0.00	0.10	0.20	0.00	-1.30	-0.10
5	0.00	0.00	0.00	0.10	0.00	0.00	0.00	0.00	0.00	0.00	0.00	0.00	0.10	0.20	0.00	-3.90	0.00
6	0.20	0.00	0.00	0.00	0.00	0.00	0.00	0.00	0.00	0.00	0.10	0.00	0.00	0.00	0.00	-0.10	0.00
7	0.00	0.00	0.00	0.00	0.00	0.00	0.00	0.00	0.00	0.00	0.00	0.10	0.00	0.00	0.00	-0.20	0.00
8	0.00	0.00	0.00	0.00	0.00	0.00	0.00	0.00	0.00	0.10	0.10	0.40	0.10	0.30	0.00	-5.60	0.00
9	0.00	0.00	0.00	0.00	0.00	0.10	0.10	0.00	0.00	0.00	0.00	0.20	0.00	0.10	0.00	-0.10	0.00
10	0.10	0.00	0.00	0.00	0.00	0.00	0.00	0.00	0.00	0.00	0.00	0.00	0.00	0.10	0.00	-1.90	0.00
$\mathbf{X}_\mu$	0.03	0.00	0.02	0.01	0.03	0.01	0.01	0.00	0.01	0.01	0.03	0.09	0.03	0.10	0.01	-1.69	-0.01

Table D.45: Detailed results: Output-only, Noise = 5.0% and 10 Sensors.

Run	Identified DI (%) at node No.															Error	
No.	1	2	3	4	5	6	7	8	9	10	11	12	13	14	15	ϵ_α	ϵ_β
1	0.00	0.00	0.00	0.00	0.00	0.00	0.00	0.00	0.00	0.00	0.00	0.00	0.20	0.00	0.00	-0.50	0.00
2	0.00	0.00	0.00	0.10	0.00	0.00	0.00	0.00	0.00	0.00	0.00	0.10	0.10	0.00	0.00	0.00	0.00
3	0.00	0.00	0.00	0.20	0.00	0.00	0.00	0.00	0.00	0.00	0.20	0.00	0.40	0.00	0.00	-0.10	0.00
4	0.00	0.00	0.00	0.00	0.20	0.00	0.00	0.00	0.00	0.00	0.40	0.60	0.40	0.40	0.00	0.00	0.00
5	0.00	0.00	0.00	0.00	0.00	0.00	0.00	0.00	0.10	0.00	0.00	0.00	0.00	0.10	0.00	-4.60	0.00
6	0.10	0.00	0.00	0.00	0.00	0.00	0.00	0.00	0.00	0.00	0.10	0.10	0.30	0.00	0.00	-3.80	0.00
7	0.30	0.00	0.00	0.00	0.00	0.00	0.00	0.00	0.00	0.00	0.00	0.30	0.00	0.00	0.00	-6.00	0.00
8	0.00	0.00	0.00	0.00	0.30	0.00	0.00	0.00	0.00	0.00	0.00	0.30	0.10	0.00	0.10	-0.20	0.00
9	0.00	0.00	0.00	0.00	0.00	0.00	0.00	0.00	0.00	0.00	0.00	0.00	0.60	0.10	0.00	-0.80	0.00
10	0.00	0.00	0.00	0.00	0.00	0.00	0.00	0.00	0.00	0.00	0.00	0.70	0.00	0.10	0.00	0.00	0.00
$\mathbf{X}_\mu$	0.04	0.00	0.00	0.03	0.05	0.00	0.00	0.00	0.01	0.00	0.07	0.21	0.21	0.07	0.01	-1.60	0.00

Table D.46: Detailed results: Output-only, Noise = 10.0% and 10 Sensors.

Run	Identified DI (%) at node No.															Error	
No.	1	2	3	4	5	6	7	8	9	10	11	12	13	14	15	ϵ_α	ϵ_β
1	0.00	0.00	0.00	0.00	0.00	0.00	0.00	0.00	0.00	0.00	0.00	0.00	0.20	0.00	0.00	-0.10	0.00
2	0.00	0.00	0.00	0.00	0.00	0.00	0.30	0.50	0.00	0.00	0.00	0.50	0.20	0.00	0.00	-8.40	0.00
3	0.00	0.00	0.00	0.00	0.00	0.00	0.00	0.00	0.00	0.00	0.00	0.00	0.00	0.50	0.30	-10.30	0.00
4	1.30	0.00	0.00	0.00	0.00	0.00	0.00	0.00	0.00	0.00	0.00	0.60	0.00	1.20	0.00	-19.80	0.00
5	0.00	0.00	0.00	0.00	0.00	0.00	0.00	0.00	0.00	0.00	0.00	0.00	0.30	0.00	0.00	-0.10	0.00
6	0.00	0.00	0.00	0.00	0.00	0.00	0.50	0.00	0.00	0.00	0.40	1.00	0.20	0.30	0.00	-3.40	-0.10
7	0.00	0.00	0.00	0.00	0.00	0.00	0.00	0.00	0.00	0.00	0.00	0.00	0.00	0.00	0.30	-5.60	0.00
8	0.00	0.00	0.00	0.70	1.20	0.00	0.40	0.00	0.00	0.00	0.00	0.90	0.00	0.80	0.40	-0.30	-0.20
9	0.00	0.00	0.00	0.00	0.00	0.00	0.00	0.00	0.00	0.00	0.10	0.40	0.30	0.10	0.00	-0.10	0.00
10	0.00	0.00	0.00	0.00	0.00	0.00	0.00	0.00	0.00	0.00	0.00	0.00	0.00	0.80	0.00	-18.00	0.00
$\mathbf{X}_\mu$	0.13	0.00	0.00	0.07	0.12	0.00	0.12	0.05	0.00	0.00	0.05	0.34	0.12	0.37	0.10	-6.61	-0.03

Table D.47: Detailed results: Output-only, Noise = 0.0% and 6 Sensors.

Run	Identified DI (%) at node No.															Error	
No.	1	2	3	4	5	6	7	8	9	10	11	12	13	14	15	ϵ_α	ϵ_β
1	0.00	0.00	0.00	0.00	0.00	0.00	0.00	0.00	0.00	0.00	0.00	0.00	0.00	0.00	0.00	-0.30	0.00
2	0.00	0.00	0.00	0.00	0.00	0.00	0.00	0.00	0.00	0.00	0.00	0.00	0.00	0.00	0.00	-0.30	0.00
3	0.00	0.00	0.00	0.00	0.00	0.00	0.00	0.00	0.00	0.00	0.00	0.10	0.00	0.00	0.00	-0.70	0.00
4	0.00	0.00	0.00	0.00	0.00	0.00	0.00	0.00	0.00	0.00	0.00	0.00	0.00	0.00	0.00	-0.20	0.00
5	0.00	0.00	0.00	0.00	0.10	0.00	0.00	0.00	0.00	0.00	0.00	0.00	0.00	0.00	0.00	-0.50	0.00
6	0.00	0.00	0.00	0.00	0.00	0.00	0.00	0.00	0.00	0.00	0.00	0.10	0.00	0.00	0.00	-0.20	0.00
7	0.00	0.00	0.00	0.00	0.10	0.00	0.00	0.00	0.00	0.00	0.00	0.00	0.00	0.00	0.00	-0.60	0.00
8	0.00	0.00	0.00	0.00	0.00	0.00	0.00	0.00	0.00	0.00	0.00	0.00	0.00	0.00	0.00	-0.40	0.00
9	0.00	0.00	0.00	0.00	0.00	0.00	0.00	0.00	0.00	0.00	0.00	0.00	0.00	0.00	0.00	-0.60	0.00
10	0.00	0.00	0.00	0.00	0.00	0.00	0.00	0.00	0.00	0.00	0.00	0.00	0.00	0.00	0.00	-0.10	0.00
$\mathbf{X}_\mu$	0.00	0.00	0.00	0.00	0.02	0.00	0.00	0.00	0.00	0.00	0.00	0.02	0.00	0.00	0.00	-0.39	0.00

Table D.48: Detailed results: Output-only, Noise = 2.0% and 6 Sensors.

Run	Identified DI (%) at node No.															Error	
No.	1	2	3	4	5	6	7	8	9	10	11	12	13	14	15	ϵ_α	ϵ_β
1	0.00	0.00	0.00	0.00	0.00	0.00	0.00	0.00	0.00	0.00	0.00	0.10	0.10	0.00	0.00	-0.40	0.00
2	0.00	0.00	0.00	0.10	0.10	0.00	0.00	0.00	0.00	0.00	0.00	0.00	0.00	0.10	0.00	-1.10	0.00
3	0.00	0.00	0.00	0.00	0.00	0.00	0.00	0.00	0.00	0.00	0.00	0.50	0.00	0.10	0.00	-1.10	0.00
4	0.00	0.00	0.00	0.00	0.00	0.00	0.10	0.00	0.00	0.00	0.00	0.40	0.00	0.20	0.00	-4.30	0.00
5	0.00	0.00	0.00	0.00	0.10	0.00	0.00	0.00	0.00	0.00	0.10	0.00	0.10	0.10	0.00	-1.10	0.00
6	0.00	0.00	0.00	0.00	0.00	0.00	0.10	0.10	0.00	0.00	0.00	0.40	0.00	0.10	0.00	-0.70	0.00
7	0.00	0.00	0.00	0.00	0.00	0.00	0.00	0.00	0.00	0.00	0.10	0.20	0.00	0.00	0.00	-0.10	0.00
8	0.00	0.00	0.00	0.00	0.20	0.00	0.00	0.00	0.00	0.00	0.10	0.10	0.00	0.00	0.10	-0.60	0.00
9	0.00	0.00	0.10	0.10	0.00	0.00	0.00	0.00	0.00	0.00	0.00	0.10	0.00	0.00	0.00	-0.10	0.00
10	0.00	0.00	0.00	0.00	0.00	0.00	0.00	0.00	0.00	0.00	0.00	0.00	0.00	0.10	0.00	-1.60	0.00
$\mathbf{X}_\mu$	0.00	0.00	0.01	0.02	0.04	0.00	0.02	0.01	0.00	0.00	0.03	0.18	0.02	0.07	0.01	-1.11	0.00

Table D.49: Detailed results: Output-only, Noise = 5.0% and 6 Sensors.

Run	Identified DI (%) at node No.															Error	
No.	1	2	3	4	5	6	7	8	9	10	11	12	13	14	15	ϵ_α	ϵ_β
1	0.00	0.00	0.00	0.00	0.00	0.30	0.00	0.00	0.00	0.00	0.00	0.20	0.40	0.00	0.00	-0.10	0.00
2	0.10	0.00	0.00	0.00	0.00	0.90	0.00	0.00	0.00	0.10	0.40	0.00	0.00	0.30	0.00	0.00	0.00
3	0.00	0.00	0.00	0.00	0.50	0.80	0.00	0.00	0.00	0.00	0.00	0.00	0.00	0.40	0.00	-4.70	0.00
4	0.00	0.00	0.00	0.20	0.00	0.00	0.00	0.00	0.00	0.00	0.00	0.00	0.10	0.10	0.00	-1.40	0.00
5	0.00	0.00	0.00	0.00	0.60	0.00	0.00	0.00	0.00	0.00	0.00	0.00	0.10	0.20	0.00	-5.00	-0.10
6	0.00	0.00	0.00	0.00	0.00	0.00	0.00	0.00	0.00	0.00	0.00	0.60	0.10	0.90	0.00	-11.30	0.00
7	0.00	0.00	0.00	0.10	0.10	0.00	0.00	0.00	0.00	0.00	0.00	0.00	0.00	0.00	0.00	-0.80	0.00
8	0.00	0.00	0.00	0.00	0.60	0.00	0.00	0.00	0.00	0.00	0.00	0.30	0.00	0.00	0.10	0.00	0.00
9	0.00	0.00	0.00	0.00	0.00	0.00	0.00	0.00	0.00	0.00	0.00	0.00	0.00	0.40	0.00	-0.30	0.00
10	0.00	0.00	0.00	0.00	0.00	0.00	0.00	0.00	0.00	0.00	0.00	0.00	0.20	0.00	0.00	0.00	0.00
$\mathbf{X}_\mu$	0.01	0.00	0.00	0.03	0.18	0.20	0.00	0.00	0.00	0.01	0.04	0.11	0.09	0.23	0.01	-2.36	-0.01

Table D.50: Detailed results: Output-only, Noise = 10.0% and 6 Sensors.

Run	Identified DI (%) at node No.															Error	
No.	1	2	3	4	5	6	7	8	9	10	11	12	13	14	15	ϵ_α	ϵ_β
1	0.00	0.00	0.00	0.00	0.00	0.60	0.00	0.00	0.00	0.00	0.00	0.40	0.70	0.00	0.00	0.00	0.00
2	0.00	0.00	0.00	0.00	0.00	0.00	0.00	0.00	0.10	0.00	0.00	0.90	0.80	0.30	0.00	-9.30	-0.10
3	0.00	0.00	0.00	0.00	0.00	0.10	1.50	0.00	0.00	0.00	0.00	0.80	0.00	0.50	0.50	-7.90	0.00
4	0.00	0.00	0.20	0.10	0.20	0.00	0.00	0.00	0.00	0.00	1.90	0.00	0.00	0.40	0.00	0.00	0.00
5	0.00	0.00	0.00	0.70	0.00	0.00	0.00	0.00	0.00	0.00	0.00	0.00	0.00	0.60	0.20	-17.20	0.00
6	0.00	0.00	0.00	0.00	0.00	0.00	0.00	0.00	0.00	0.00	0.00	0.00	0.00	0.30	0.10	-2.90	0.00
7	0.00	0.00	0.00	0.90	0.00	0.00	0.00	0.00	0.00	0.00	0.00	0.00	0.00	0.00	0.10	-2.90	0.00
8	0.00	0.00	0.00	0.00	0.00	0.00	0.00	0.00	0.00	0.00	0.00	0.00	0.00	0.00	0.00	-5.20	0.00
9	0.00	0.00	0.00	0.00	0.00	0.00	0.00	0.00	0.00	0.00	0.40	0.80	0.00	0.60	0.00	-4.00	0.00
10	0.00	0.00	0.00	0.00	0.00	0.00	0.00	0.00	0.00	0.00	0.00	0.50	0.00	0.00	0.00	-7.70	0.00
$\mathbf{X}_\mu$	0.00	0.00	0.02	0.17	0.02	0.07	0.15	0.00	0.01	0.00	0.23	0.34	0.15	0.27	0.09	-5.71	-0.01

Appendix E

Detailed Results for Experimental Tripile Structure

A laboratory test model of a scaled wind turbine tower supported by a tripile foundation was tested at the Institute of Structural Analysis (Institut für Statik und Dynamik - ISD) at Leibniz Universität Hannover (LUH). These results are used to perform structural identification for both undamaged and damaged cases of the tripile. Damage was induced via loosening the bolts in a flange installed in one of the tripile legs. Detailed results are presented in this appendix.

E.1 Results for Undamaged Tripile

Table E.1: Detailed results for experimental undamaged tripile.

Run No.	Identified DI (%) at variable															
	E_1	E_2	E_3	E_4	E_5	E_6	E_7	E_8	E_9	E_{10}	E_{11}	E_{12}	E_{13}	E_{14}	E_{15}	ζ_1
	G_1	G_2	G_3	G_4	G_5	G_6	G_7	G_8	G_9	G_{10}	G_{11}	G_{12}	G_{13}	G_{14}	G_{15}	ζ_2
1	0.0	0.0	2.0	2.0	0.0	0.0	0.0	0.0	0.0	0.0	0.0	0.0	0.0	0.0	0.0	0.0020
	0.0	0.0	0.0	0.0	0.0	0.0	0.0	0.0	2.0	1.0	0.0	0.0	0.0	0.0	0.0	0.0020
2	0.0	0.0	2.0	2.0	0.0	0.0	0.0	0.0	0.0	0.0	0.0	0.0	0.0	0.0	0.0	0.0020
	0.0	0.0	0.0	0.0	0.0	0.0	0.0	0.0	2.0	1.0	0.0	0.0	0.0	0.0	0.0	0.0020
3	0.0	0.0	2.0	1.5	0.0	0.0	0.0	0.0	0.0	0.0	0.0	0.0	0.0	0.0	0.0	0.0020
	0.0	0.0	0.0	0.0	0.0	0.0	0.0	0.0	2.0	1.0	0.0	0.0	0.0	0.0	0.0	0.0020
4	0.0	0.0	2.0	2.0	0.0	0.0	0.0	0.0	0.0	0.0	0.0	0.0	0.0	0.0	0.0	0.0020
	0.0	0.0	0.0	0.0	0.0	0.0	0.0	0.0	2.0	1.0	0.0	0.0	0.0	0.0	0.0	0.0020
5	0.0	0.0	1.5	2.0	0.0	0.0	0.0	0.0	0.0	0.0	0.0	0.0	0.0	0.0	0.0	0.0020
	0.0	0.0	0.0	0.0	0.0	0.0	0.0	0.0	2.0	1.0	0.0	0.0	0.0	0.0	0.0	0.0020
6	0.0	0.0	2.0	2.0	0.0	0.0	0.0	0.0	0.0	0.0	0.0	0.0	0.0	0.0	0.0	0.0020
	0.0	0.0	0.0	0.0	0.0	0.0	0.0	0.0	2.0	1.0	0.0	0.0	0.0	0.0	0.0	0.0020
7	0.0	0.0	1.0	2.5	0.0	0.0	0.0	0.0	0.0	0.0	0.0	0.0	0.0	0.0	0.0	0.0020
	0.0	0.0	0.0	0.0	0.0	0.0	0.0	0.0	2.0	1.0	0.0	0.0	0.0	0.0	0.0	0.0020
8	0.0	0.0	2.0	2.0	0.0	0.0	0.0	0.0	0.0	0.0	0.0	0.0	0.0	0.0	0.0	0.0020
	0.0	0.0	0.0	0.0	0.0	0.0	0.0	0.0	2.0	1.0	0.0	0.0	0.0	0.0	0.0	0.0020
9	0.0	0.0	2.5	2.0	0.0	0.0	0.0	0.0	0.0	0.0	0.0	0.0	0.0	0.0	0.0	0.0020
	0.0	0.0	0.0	0.0	0.0	0.0	0.0	0.0	2.0	1.0	0.0	0.0	0.0	0.0	0.0	0.0020
10	0.0	0.0	2.0	2.0	0.0	0.0	0.0	0.0	0.0	0.0	0.0	0.0	0.0	0.0	0.0	0.0020
	0.0	0.0	0.0	0.0	0.0	0.0	0.0	0.0	2.0	1.0	0.0	0.0	0.0	0.0	0.0	0.0020
$\mathbf{X}_\mu$	0.0	0.0	1.9	2.0	0.0	0.0	0.0	0.0	0.0	0.0	0.0	0.0	0.0	0.0	0.0	0.0020
	0.0	0.0	0.0	0.0	0.0	0.0	0.0	0.0	2.0	1.0	0.0	0.0	0.0	0.0	0.0	0.0020

Table E.2: Detailed results for experimental damaged tripile.

Run No.	Identified DI (%) at variable															
	E_1	E_2	E_3	E_4	E_5	E_6	E_7	E_8	E_9	E_{10}	E_{11}	E_{12}	E_{13}	E_{14}	E_{15}	ζ_1
	G_1	G_2	G_3	G_4	G_5	G_6	G_7	G_8	G_9	G_{10}	G_{11}	G_{12}	G_{13}	G_{14}	G_{15}	ζ_2
1	0.0	16.5	0.5	0.0	0.0	18.5	3.0	0.0	18.5	62.0	26.0	0.5	0.0	0.0	0.0	0.2166
	0.0	19.5	11.5	28.5	0.0	20.0	25.5	8.0	40.0	82.0	24.0	20.5	0.0	0.0	0.0	0.0020
2	0.0	0.0	9.5	0.5	0.0	2.0	19.5	0.0	42.5	54.5	2.0	0.0	0.0	0.0	0.0	0.2347
	0.0	24.5	5.5	13.5	0.0	31.5	7.0	16.0	50.5	59.0	43.5	64.50	0.0	0.0	0.0	0.0013
3	0.0	0.0	0.0	0.0	0.0	0.0	3.5	0.5	35.0	65.0	2.0	0.0	0.0	0.0	0.0	0.2318
	0.0	2.0	0.5	18.0	0.0	4.0	8.0	9.0	70.5	42.5	10.5	14.5	0.0	0.0	0.0	0.0015
4	0.0	0.0	3.5	2.0	0.0	14.5	14.5	0.0	26.5	67.0	0.0	0.0	0.0	0.0	0.0	0.2309
	0.0	49.5	13.0	0.0	0.0	44.5	38.5	28.0	3.5	44.5	77.0	42.0	0.0	0.0	0.0	0.0011
5	0.0	0.0	0.0	0.0	0.0	0.0	3.5	0.5	35.0	65.0	2.0	0.0	0.0	0.0	0.0	0.2318
	0.0	2.0	0.5	18.0	0.0	4.0	8.0	9.0	70.5	42.5	10.5	14.5	0.0	0.0	0.0	0.0015
6	0.0	0.0	9.5	0.5	0.0	2.0	19.5	0.0	42.5	54.5	2.0	0.0	0.0	0.0	0.0	0.2347
	0.0	24.5	5.5	13.5	0.0	31.5	7.0	16.0	50.5	59.0	43.5	64.50	0.0	0.0	0.0	0.0013
7	0.0	0.0	0.0	0.0	0.0	0.0	3.5	0.5	35.0	65.0	2.0	0.0	0.0	0.0	0.0	0.2318
	0.0	2.0	0.5	18.0	0.0	4.0	8.0	9.0	70.5	42.5	10.5	14.5	0.0	0.0	0.0	0.0015
8	0.0	13.0	5.0	0.0	0.0	6.0	1.5	2.0	41.5	50.0	10.5	0.0	0.0	0.0	0.0	0.2185
	0.0	84.5	23.0	3.0	0.0	60.0	0.5	5.0	20.5	55.5	62.5	7.5	0.0	0.0	0.0	0.0020
9	0.0	0.0	0.0	0.0	0.0	0.0	3.5	0.5	35.0	65.0	2.0	0.0	0.0	0.0	0.0	0.2318
	0.0	2.0	0.5	18.0	0.0	4.0	8.0	9.0	70.5	42.5	10.5	14.5	0.0	0.0	0.0	0.0015
10	0.0	0.5	15.0	1.0	0.0	18.5	5.5	0.0	44.0	33.5	10.0	1.0	0.0	0.0	0.0	0.2375
	0.0	2.0	0.5	18.0	0.0	4.0	8.0	9.0	70.5	42.5	10.5	14.5	0.0	0.0	0.0	0.0012
μ	0.0	3.0	4.3	0.4	0.0	6.15	7.75	0.4	35.55	58.15	5.85	0.15	0.0	0.0	0.0	0.2300
	0.0	26.8	6.35	13.85	0.0	25.6	14.65	11.55	52.2	47.85	35.4	32.15	0.0	0.0	0.0	0.0025

Curriculum Vitae

Personal Information

Name: Mahmoud M. Jahjouh

Date of birth: 18.03.1988

Place of birth: Darmstadt, Germany

Address: Hemelingstr. 16, 30419 Hannover, Germany

Mobile: +4917672334782

E-mail: eng.m.jahjouh@hotmail.com

Education

09/2005–08/2006	General Secondary Education Examination / Scientific Stream. Percentage Average = 98.4%.
09/2006–06/2010	Bachelor of Science in Civil Engineering, Islamic University of Gaza. Cumulative Grade Point Average = 95.5%.
09/2010–04/2012	Master of Science in Civil Engineering – Design and Rehabilitation of Structures, Islamic University of Gaza. Cumulative Grade Point Average = 92.7%.

Professional Experience

08/2013–present	Research Assistant at Institute of Mechanics and Computational Mechanics, Leibniz Universität Hannover, Germany
11/2012–03/2013	Senior Design and Assessment Engineer at ENFRA Consultants.
06/2012–01/2013	Lecturer at the civil engineering department of the Islamic University of Gaza.

11/2011–03/2013	Civil Engineer at the department of scientific research of the Ministry of Public Works and Housing.
11/2010–10/2011	Civil Engineer at the department of training of the General Personnel Council.

Language Skills

Arabic: Native language.

English: Excellent.

German: Very Good.

Awards and Achievements

04/2013-06/2016	Research Grant for Doctoral Candidates and Young Academics, DAAD.
01/2007–06/2010	Islamic University's Scholarship for Talented Students.
08/2006	Prime Minister's Scholarship for Talented Students.
07/2003–01/2005	MSP/ACCESS English Language Scholarship, AMIDEAST Gaza.

March 30, 2016

Forschungs- und Seminarberichte

Institut für Baumechanik und Numerische Mechanik
Gottfried Wilhelm Leibniz Universität Hannover

Bisher in dieser Schriftenreihe erschienene Berichte:

S 73/1	Seminar über Thermodynamik und Kontinuumsmechanik, Hannover 1973
F 75/1	"Die Spannungsberechnung im Rahmen der Finite–Element–Methode", R. Ahmad, Dissertation, April 1975
F 76/1	"Zur Theorie und Anwendung der Stoffgleichungen elastisch–plastisch–viskoser Werkstoffe", H. Mentlein, Dissertation, April 1976
F 77/1	Seminar über lineare und geometrisch nichtlineare Schalentheorie einschließlich Stabilitätstheorie, Hannover 1978
F 77/2	"Beitrag zur Berechnung von Gründungsplatten mit Hilfe der Finite–Element–Methode", H. Meyer, Dissertation, Juli 1977
F 77/3	"Zur Berechnung der Eigenfrequenzen und Eigenschwingungsformen räumlich vorgekrümmter und vorverwundener Stäbe" J. Möhlenkamp, Dissertation, Dezember 1977
F 77/4	"Zur Theorie und Berechnung geometrisch und physikalisch nichtlinearer Kontinua mit Anwendung der Methode der finiten Elemente", J. Paulun, Dissertation, Dezember 1977
F 78/1	2. Seminar über Thermodynamik und Kontinuumsmechanik, Hannover 1978
F 79/1	"Theoretische und numerische Behandlung geometrisch nichtlinearer viskoplastischer Kontinua", K.–D. Klee, Dissertation, Februar 1979
F 79/2	"Zur Konstruierbarkeit von Variationsfunktionalen für nichtlineare Probleme der Kontinuumsmechanik", J. Siefer, Dissertation, Oktober 1979

F 80/1 “Theoretische und numerische Behandlung gerader Stäbe mit endlichen Drehungen”,
M. Kessel, Dissertation, Februar 1980

F 81/1 “Zur Berechnung von Kontakt– und Stoßproblemen elastischer Körper mit Hilfe der Finite–Element–Methode”,
P. Wriggers, Dissertation, Januar 1981

F 81/2 “Stoffgleichungen für Steinsalze unter mechanischer und thermischer Beanspruchung”,
J. Olschewski, E. Stein, W. Wagner, D. Wetjen, geänderte Fassung eines Zwischenberichtes zum BMFT–Forschungsvorhaben KWA 1608/5

F 82/1 “Konvergenz und Fehlerabschätzung bei der Methode der Finiten Elemente”,
R. Rohrbach, E. Stein, Abschlußbericht eines VW–Forschungsvorhabens, Februar 1982

F 82/2 “Alternative Spannungsberechnung in Finite–Element–Verschiebungsmodellen”,
C. Klöhn, Dissertation, November 1982

F 83/1 Seminar über nichtlineare Stabtheorie,
Hannover 1983

F 83/2 “Beiträge zur nichtlinearen Theorie und inkrementellen Finite–Element–Berechnung dünner elastischer Schalen”,
A. Berg, Dissertation, Juli 1983

F 83/3 “Elastoplastische Plattenbiegung bei kleinen Verzerrungen und großen Drehungen”,
J. Paulun, Habilitation, September 1983

F 83/4 “Geometrisch nichtlineare FE–Berechnung von Faltwerken mit plastisch / viskoplastischem Deformationsverhalten”,
M. Krog, Dissertation, Dezember 1983

F 85/1 Verleihung der Ehrendoktorwürde des Fachbereichs Bauingenieur– und Vermessungswesen der Universität Hannover an die Herren Prof. Dr. Drs. h.c. J.H. Argyris, Dr.–Ing. H. Wittmeyer

F 85/2 “Eine geometrisch nichtlineare Theorie schubelastischer Schalen mit Anwendung auf Finite–Element–Berechnungen von Durchschlag– und Kontaktproblemen”,
W. Wagner, Dissertation, März 1985

F 85/3 “Geometrisch/physikalisch nichtlineare Probleme – Struktur und Algorithmen – ”,
GAMM–Seminar im Februar 1985 in Hannover

F 87/1 “Finite–Elemente-Berechnungen ebener Stabtragwerke mit Fließgelenken und großen Verschiebungen”,
R. Kahn, Dissertation, Oktober 1987

F 88/1 “Theorie und Numerik schubelastischer Schalen mit endlichen Drehungen unter Verwendung der Biot–Spannungen”,
F. Gruttmann, Dissertation, Juni 1988

F 88/2 “Optimale Formgebung von Stabtragwerken mit Nichtlinearitäten in der Zielfunktion und in den Restriktionen unter Verwendung der Finite–Element–Methode”,
V. Berkhahn, Dissertation, Oktober 1988

F 88/3 “Beiträge zur Theorie und Numerik großer plastischer und kleiner elastischer Deformationen mit Schädigungseinfluß”,
R. Lammering, Dissertation, November 1988

F 88/4 “Konsistente Linearisierungen in der Kontinuumsmechanik und ihrer Anwendung auf die Finite–Elemente–Methode”,
P. Wriggers, Habilitation, November 1988

F 88/5 “Mathematische Formulierung und numerische Methoden für Kontaktprobleme auf der Grundlage von Extremalprinzipien”,
D. Bischoff, Habilitation, Dezember 1988

F 88/6 “Zur numerischen Behandlung thermomechanischer Prozesse”,
C. Miehe, Dissertation, Dezember 1988

F 89/1 “Zur Stabilität und Konvergenz gemischter finiter Elemente in der linearen Elastizitätstheorie”,
R. Rolfes, Dissertation, Juni 1989

F 89/2 “Traglastberechnungen von Faltwerken mit elastoplastischen Deformationen”,
K.–H. Lambertz, Dissertation, November 1989

F 89/3 “Transientes Kriechen und Kriechbruch im Steinsalz”,
U. Heemann, Dissertation, November 1989

F 89/4 “Materialgesetze zum Verhalten von Betonkonstruktionen bei harten Stößen”,
E. Stein, P. Wriggers, T. Vu Van & T. Wedemeier, Dezember 1989

F 89/5 “Lineare Konstruktion und Anwendungen von Begleitmatrizen”,
C. Carstensen, Dissertation, Dezember 1989

F 90/1 “Zur Berechnung prismatischer Stahlbetonbalken mit verschiedenen Querschnittformen für allgemeine Beanspruchungen”,
H. N. Lucero–Cimas, Dissertation, April 1990

F 90/2 “Zur Behandlung von Stoß– Kontaktproblemen mit Reibung unter Verwendung der Finite–Element–Methode”,
T. Vu Van, Dissertation, Juni 1990

F 90/3 “Netzadaption und Mehrgitterverfahren für die numerische Behandlung von Faltwerken”,
L. Plank, Dissertation, September 1990

F 90/4 “Beiträge zur Theorie und Numerik finiter inelastischer Deformationen”,
N. Müller–Hoeppe, Dissertation, Oktober 1990

F 90/5 “Beiträge zur Theorie und Numerik von Materialien mit innerer Reibung am Beispiel des Werkstoffes Beton”,
T. Wedemeier, Dissertation, Oktober 1990

F 91/1 “Zur Behandlung von Stabilitätsproblemen der Elastostatik mit der Methode der Finiten Elemente”,
W. Wagner, Habilitation, April 1991

F 91/2 “Mehrgitterverfahren und Netzadaption für lineare und nichtlineare statische Finite–Elemente–Berechnungen von Flächentragwerken”,
W. Rust, Dissertation, Oktober 1991

F 91/3 “Finite Elemente Formulierung im Trefftzschen Sinne für dreidimensionale anisotrop–elastische Faserverbundstrukturen”,
K. Peters, Dissertation, Dezember 1991

F 92/1 “Einspielen und dessen numerische Behandlung von Flächentragwerken aus ideal plastischem bzw. kinematisch verfestigendem Material”, G. Zhang, Dissertation, Februar 1992

F 92/2 “Strukturoptimierung stabilitätsgefährdeter Systeme mittels analytischer Gradientenermittlung”, A. Becker, Dissertation, April 1992

F 92/3 “Duale Methoden für nichtlineare Optimierungsprobleme in der Strukturmechanik”, R. Mahnken, Dissertation, April 1992

F 93/1 “Kanonische Modelle multiplikativer Elasto–Plastizität. Thermodynamische Formulierung und numerische Implementation”, C. Miehe, Habilitation, Dezember 1993

F 93/2 “Theorie und Numerik zur Berechnung und Optimierung von Strukturen aus isotropen, hyperelastischen Materialien”, F.–J. Barthold, Dissertation, Dezember 1993

F 94/1 “Adaptive Verfeinerung von Finite–Element–Netzen für Stabilitätsprobleme von Fläschentragwerken”, E. Stein, B. Seifert, W. Rust, Forschungsbericht, Oktober 1994

F 95/1 “Adaptive Verfahren für die Formoptimierung von Flächentragwerken unter Berücksichtigung der CAD–FEM–Kopplung”, A. Falk, Dissertation, Juni 1995

F 96/1 “Theorie und Numerik dünnwandiger Faserverbundstrukturen”, F. Gruttmann, Habilitation, Januar 1996

F 96/2 “Zur Theorie und Numerik finiter elastoplastischer Deformationen von Schalenstrukturen”, B. Seifert, Dissertation, März 1996

F 96/3 “Theoretische und algorithmische Konzepte zur phänomenologischen Beschreibung anisotropen Materialverhaltens”, J. Schröder, Dissertation, März 1996

F 96/4 “Statische und dynamische Berechnungen von Schalen endlicher elastischer Deformationen mit gemischten finiten Elementen”, P. Betsch, Dissertation, März 1996

F 96/5 “Kopplung von Finiten Elementen und Randelementen für ebene Elastoplastizität mit Impelementierung auf Parallelrechnern”, M. Kreienmeyer, Dissertation, März 1996

F 96/6 “Theorie und Numerik dimensions– und modeladaptiver Finite–Elemente–Methoden von Fläschentragwerken”, S. Ohnimus, Dissertation, Juni 1996

F 96/7 “Adaptive Finite Elemente Methoden für MIMD-Parallelrechner zur Behandlung von Strukturproblemen mit Anwendung auf Stabilitätsprobleme”, O. Klaas, Dissertation, Juli 1996

F 96/8 “Institutsbericht 1971–1996 aus Anlaß des 25–jährigen Dienstjubiläums von Prof. Dr.–Ing. Dr.–Ing. E.h. Dr. h.c. mult. Erwin Stein”, Dezember 1996

F 97/1 “Modellierung und Numerik duktiler kristalliner Werkstoffe”, P. Steinmann, Habilitation, August 1997

F 97/2 “Formoptimierung in der Strukturdynamik”,
L. Meyer, Dissertation, September 1997

F 97/3 “Modellbildung und Numerik für Versagensprozesse in Gründungen von Caisonwellenbrechern”,
M. Lengnick, Dissertation, November 1997

F 98/1 “Adaptive gemischte finite Elemente in der nichtlinearen Elastostatik und deren Kopplung mit Randelementen”,
U. Brink, Dissertation, Februar 1998

F 98/2 “Theoretische und numerische Aspekte zur Parameteridentifikation und Modellierung bei metallischen Werkstoffen”,
R. Mahnken, Habilitation, Juli 1998

F 98/3 “Lokalisierung und Stabilität der Deformation wassergesättigter bindiger und granularer Böden”,
J. M. Panesso, Dissertation, August 1998

F 98/4 “Theoretische und numerische Methoden in der angewandten Mechanik mit Praxisbeispielen”,
R. Mahnken (Hrsg.), Festschrift anlässlich der Emeritierung von Prof. Dr.–Ing. Dr.–Ing. E.h. h.c. mult. Erwin Stein, November 1998

F 99/1 “Eine h–adaptive Finite–Element–Methode für elasto–plastische Schalenproblem in unilateralem Kontakt”,
C.–S. Han, Dissertation, Juli 1999

F 00/1 “Ein diskontinuierliches Finite–Element-Modell für Lokalisierungsversagen in metallischen und granularen Materialien”,
C. Leppin, Dissertation, März 2000

F 00/2 “Untersuchungen von Strömungen in zeitlich veränderlichen Gebieten mit der Methode der Finiten Elementen”,
H. Braess, Dissertation, März 2000

F 00/3 “Theoretische und algorithmische Beiträge zur Berechnung von Faserverbundschalen”,
J. Tessmer, Dissertation, März 2000

F 00/4 “Theorie und Finite–Element–Methode für die Schädigungsbeschreibung in Beton und Stahlbeton”,
D. Tikhomirov, Dissertation, August 2000

F 01/1 “A C1 - continuous formulation for finite deformation contact”,
L. Krstulovic–Opara, Dissertation, Januar 2001

F 01/2 “Strain Localisation Analysis for Fully and Partially Saturated Geomaterials”,
H. Zhang, Dissertation, Januar 2001

F 01/3 “Meso–makromechanische Modellierung von Faserverbundwerkstoffen mit Schädigung”,
C. Döbert, Dissertation, April 2001

F 01/4 “Thermomechanische Modellierung gummiartiger Polymerstrukturen”,
S. Reese, Habilitation, April 2001

F 01/5 “Thermomechanisches Verhalten von Gummimaterialien während der Vulkanisation – Theorie und Numerik –”,
M. André, Dissertation, April 2001

F 01/6 "Adaptive FEM für elastoplastische Deformationen – Algorithmen und Visualisierung",
M. Schmidt, Dissertation, Juni 2001

F 01/7 "Verteilte Algorithmen für h–, p– und d–adaptive Berechnungen in der nichtlinearen Strukturmechanik",
R. Niekamp, Dissertation, Juni 2001

F 01/8 "Theorie und Numerik zur Berechnung und Optimierung von Strukturen mit elastoplastischen Deformationen",
K. Wiechmann, Dissertation, Juli 2001

F 01/9 "Direct Computation of Instability Points with Inequality using the Finite Element Method",
H. Tschöpe, Dissertation, September 2001

F 01/10 "Theorie und Numerik residualer Fehlerschätzer für die Finite–Elemente–Methode unter Verwendung äquilibrierter Randspannungen",
S. Ohnimus, Habilitation, September 2001

F 02/1 "Adaptive Algorithmen für thermo–mechanisch gekoppelte Kontaktprobleme",
A. Rieger, Dissertation, August 2002

F 02/2 "Consistent coupling of shell– and beam–models for thermo–elastic problems",
K. Chavan, Dissertation, September 2002

F 03/1 "Error–controlled adaptive finite element methods in large strain hyperelasticity and fracture mechanics",
M. Rüter, Dissertation, Mai 2003

F 03/2 "Formulierung und Simulation der Kontaktvorgänge in der Baugrund–Tragwerks–Interaktion",
A. Haraldsson, Dissertation, Juni 2003

F 03/3 "Concepts for Nonlinear Orthotropic Material Modeling with Applications to Membrane Structures",
T. Raible, Dissertation, Juni 2003

F 04/1 "On Single– and Multi–Material arbitrary Lagrangian–Eulerian Approaches with Application to Micromechanical Problems at Finite Deformations",
D. Freßmann, Dissertation, Oktober 2004

F 04/2 "Computational Homogenization of Microheterogeneous Materials at Finite Strains Including Damage",
S. Löhnert, Dissertation, Oktober 2004

F 05/01 "Numerical Micro–Meso Modeling of Mechanosensation driven Osteonal Remodeling in Cortical Bone",
C. Lenz, Dissertation, Juli 2005

F 05/02 "Mortar Type Methods Applied to Nonlinear Contact Mechanics",
K.A. Fischer, Dissertation, Juli 2005

F 05/3 "Models, Algorithms and Software Concepts for Contact and Fragmentation in Computational Solid Mechanics",
C. Hahn, Dissertation, November 2005

F 06/1 "Computational Homogenization of Concrete",
S. Moftah, Dissertation, Januar 2006

F 06/2 Reduction Methods in Finite Element Analysis of Nonlinear Structural Dynamics",
H. Spiess, Dissertation, Februar 2006

F 06/3 "Theoretische und algorithmische Konzepte zur Beschreibung des beanspruchungsadaptiven Knochenwachstums",
B. Ebbecke, Dissertation, März 2006

F 06/4 "Experimentelle Untersuchungen an elastomeren Werkstoffen",
M. Dämgen, Dissertation, Dezember 2006

F 07/1 "Numerische Konzepte zur Behandlung inelastischer Effekte beim reibungsbehafteten Rollkontakt",
M. Ziefle, Dissertation, Februar 2007

F 07/2 "Begleitbuch zur Leibniz–Ausstellung",
Hrsg: E. Stein, P. Wriggers, 2007

F 07/3 "Modellierung und Simulation der hochfrequenten Dynamik rollender Reifen",
M. Brinkmeier, Dissertation, Juni 2007

F 07/4 "Computational Homogenization of micro–structural Damage due to Frost in Hardened Cement Paste",
M. Hain, Dissertation, Juli 2007

F 07/5 "Elektromechanisch gekoppelte Kontaktmodellierung auf Mikroebene",
T. Helmich, Dissertation, August 2007

F 07/6 "Dreidimensionales Diskretes Elemente Modell für Superellipsoide",
C. Lillie, Dissertation, Oktober 2007

F 07/7 "Adaptive Methods for Continuous and Discontinuous Damage Modeling in Fracturing Solids",
S.H. Reese, Dissertation, Oktober 2007

F 08/1 "Student Projects of Micromechanics",
Hrsg: U. Nackenhorst, August 2008

F 09/1 "Theory and Computation of Mono– and Poly– crystalline Cyclic Martensitic Phase Transformations",
G. Sagar, Dissertation, August 2009

F 09/2 "Student projects of Micromechanics",
D. Balzani and U. Nackenhorst, Course Volume, Oktober 2009

F 09/3 "Multiscale Coupling based on the Quasicontinuum Framework, with Application to Contact Problems",
W. Shan, Dissertation, November 2009

F 10/1 "A Multiscale Computational Approach for Microcrack Evolution in Cortical Bone and Related Mechanical Stimulation of Bone Cells",
D. Kardas, Dissertation, September 2010

F 12/1 "Ein physikalisch motiviertes Reifen–Fahrbahnmodell für die Gesamtfahrzeugsimulation",
R. Chiarello, Dissertation, Februar 2012

F 13/1 "Thermomechanical Analysis of Tire Rubber Compounds in Rolling Contact",
A. Suwannachit, Dissertation, September 2012

F 13/2 "Towards a Finite Element Model for Fluid Flow in the Human Hip Joint",
K. Fietz, Dissertation, September 2013

F 14/1 “Micro-Mechanically Based Damage Analysis of Ultra High Performance Fibre Reinforced Concrete Structures with Uncertainties”,
A. Hürkamp, Dissertation, Dezember 2013

F 14/2 “Numerical Solution of High–Dimensional Fokker–Planck Equations with Discontinuous Galerkin Methods”,
F. Loerke, Dissertation, Dezember 2013

F 14/3 “Numerische Simulation probabilistischer Schädigungsmodelle mit der Stochastischen Finite Elemente Methode”,
P. Jablonski, Dissertation, September 2014

F 15/1 “On a Finite Element Approach for the Solution of a Mechanically Stimulated Biochemical Fracture Healing Model”,
A. Sapotnick, Dissertation, November 2015.

F 15/2 “Simulation of Elastic-Plastic Material Behaviour with Uncertain Material Parameters. A Spectral Stochastic Finite Element Method Approach”,
S. Fink, Dissertation, November 2015.

F 15/3 “A Fully Micro-mechanically Motivated Material Law for Filled Elastomer”,
O. Stegen, Dissertation, Februar 2016.